UNIVERSIDADE DE BRASÍLIA

FACULDADE DE TECNOLOGIA

DEPARTAMENTO DE ENGENHARIA CIVIL E AMBIENTAL

PERSPECTIVA GEOTÉCNICA DO USO DE RESÍDUOS INDUSTRIAIS DO ESPÍRITO SANTO EM ATERROS E PAVIMENTOS

JOÃO RENATO REMEDE PRANDINA

ORIENTADOR: MARCIO MUNIZ DE FARIAS, PhD

TESE DE DOUTORADO EM GEOTECNIA

PUBLICAÇÃO: G.TD-217/2026

BRASÍLIA-DF: MAIO/2026

UNIVERSIDADE DE BRASÍLIA

FACULDADE DE TECNOLOGIA

DEPARTAMENTO DE ENGENHARIA CIVIL E AMBIENTAL

PERSPECTIVA GEOTÉCNICA DO USO DE RESÍDUOS INDUSTRIAIS DO ESPÍRITO SANTO EM ATERROS E PAVIMENTOS

JOÃO RENATO REMEDE PRANDINA

ORIENTADOR: MARCIO MUNIZ DE FARIAS, PhD

TESE DE DOUTORADO EM GEOTECNIA

PUBLICAÇÃO: G.TD-217/2026

BRASÍLIA / DF: MAIO / 2026

UNIVERSIDADE DE BRASÍLIA

FACULDADE DE TECNOLOGIA

DEPARTAMENTO DE ENGENHARIA CIVIL E AMBIENTAL

PERSPECTIVA GEOTÉCNICA DO USO DE RESÍDUOS INDUSTRIAIS DO ESPÍRITO SANTO EM ATERROS E PAVIMENTOS

JOÃO RENATO REMEDE PRANDINA

TESE DE DOUTORADO SUBMETIDA AO DEPARTAMENTO DE ENGENHARIA CIVIL E AMBIENTAL DA UNIVERSIDADE DE BRASÍLIA COMO PARTE DOS REQUISITOS NECESSÁRIOS PARA A OBTENÇÃO DO GRAU DE DOUTOR.

APROVADA POR:

MARCIO MUNIZ DE FARIAS, PhD
ORIENTADOR

RAFAEL CERQUEIRA SILVA, PhD
EXAMINADOR INTERNO

GILSON DE FARIAS NEVES GITIRANA JÚNIOR, PhD (UFG)
EXAMINADOR EXTERNO

TIAGO DE JESUS SOUZA, PhD (UFSCar)
EXAMINADOR EXTERNO

DATA: BRASÍLIA/DF, 21 DE MAIO DE 2026.

FICHA CATALOGRÁFICA

PRANDINA, JOÃO RENATO REMEDE
Perspectiva geotécnica do uso de resíduos industriais do Espírito Santo em aterros e pavimentos [Distrito Federal] (2026)
A4, 303 p., 297 mm (ENC/FT/UnB, Doutorado, Geotecnia, 2026)
Tese de Doutorado - Universidade de Brasília. Faculdade de Tecnologia. Departamento de Engenharia Civil e Ambiental
1. Geotecnia 2. Resíduos industriais 3. Infraestrutura 4. Espírito Santo I. ENC/FT/UnB II. Doutor

REFERÊNCIA BIBLIOGRÁFICA

PRANDINA, J. R. R. (2026). Perspectiva geotécnica do uso de resíduos industriais do Espírito Santo em em aterros e pavimentos. Tese de Doutorado, Publicação (G.TD-217/2026), Departamento de Engenharia Civil e Ambiental, Universidade de Brasília, Brasília, DF, 303 p.

CESSÃO DE DIREITOS

NOME DO AUTOR: João Renato Remede Prandina
TÍTULO DA TESE DE DOUTORADO: Geotechnical Perspective of the Espírito Santo Industrial Waste Applications in Infrastructure
GRAU: Doutor / ANO: 2026

É concedida à Universidade de Brasília a permissão para reproduzir cópias desta tese de doutorado e para emprestar ou vender tais cópias somente para propósitos acadêmicos e científicos. O autor reserva outros direitos de publicação e nenhuma parte desta tese de doutorado pode ser reproduzida sem autorização por escrito do autor.

João Renato Remede Prandina
Av. Nossa Senhora da Penha, 1495 / 504-A
Vitória-ES. 29.056-905

UNIVERSITY OF BRASÍLIA
SCHOOL OF TECHNOLOGY
DEPARTMENT OF CIVIL AND ENVIRONMENTAL ENGINEERING

GEOTECHNICAL PERSPECTIVE OF THE ESPIRITO SANTO INDUSTRIAL WASTE APPLICATIONS IN EMBANKMENTS AND PAVEMENTS

JOÃO RENATO REMEDE PRANDINA

ADVISOR: MARCIO MUNIZ DE FARIAS, PhD

PH.D. THESIS IN GEOTECHNICAL ENGINEERING
PUBLICATION: G.TD-217/2026

BRASILIA/DF: MAY/2026

UNIVERSITY OF BRASÍLIA

SCHOOL OF TECHNOLOGY

DEPARTMENT OF CIVIL AND ENVIRONMENTAL ENGINEERING

GEOTECHNICAL PERSPECTIVE OF THE ESPIRITO SANTO INDUSTRIAL WASTE APPLICATIONS IN EMBANKMENTS AND PAVEMENTS

JOÃO RENATO REMEDE PRANDINA

A PH.D. THESIS SUBMITTED TO THE DEPARTMENT OF CIVIL AND ENVIRONMENTAL ENGINEERING OF THE UNIVERSITY OF BRASILIA AS PARTIAL FULFILLMENT OF THE REQUIREMENTS FOR THE DEGREE OF DOCTOR OF PHILOSOPHY.

APPROVED BY:

_____

MARCIO MUNIZ DE FARIAS, PhD
ADVISOR

_____

RAFAEL CERQUEIRA SILVA, PhD
INTERNAL EXAMINER

_____

GILSON DE FARIAS NEVES GITIRANA JÚNIOR, PhD (UFG)
EXTERNAL EXAMINER

_____

TIAGO DE JESUS SOUZA, PhD (UFSCar)
EXTERNAL EXAMINER

DATE: BRASILIA/DF, BRAZIL, MAY 21st, 2026.

CATALOGING-IN-PUBLICATION

PRANDINA, JOÃO RENATO REMEDE
Geotechnical Perspective of the Espírito Santo Industrial Waste Applications in Embankments and Pavements [Distrito Federal] (2026)
A4, 303 p., 297 mm (ENC/FT/UnB, Ph.D., Geotechnical Engineering, 2026)
Ph.D. Thesis - University of Brasília. School of Technology. Department of Civil and Environmental Engineering
1. Geotechnical Engineering 2. Industrial Waste 3. Infrastructure 4. Espírito Santo I. ENC/FT/UnB II. Ph.D.

BIBLIOGRAPHIC REFERENCE

PRANDINA, J. R. R. (2026). Geotechnical Perspective of the Espírito Santo Industrial Waste Applications in Embankments and Pavements. Ph.D. Thesis, Publication (G.TD-217/2026), Department of Civil and Environmental Engineering, University of Brasília, Brasília, DF, 303 p.

COPYRIGHT

AUTHOR'S NAME: João Renato Remede Prandina
TITLE OF THE PH.D. THESIS: Geotechnical Perspective of the Espírito Santo Industrial Waste Applications in Infrastructure
DEGREE: Ph.D. / YEAR: 2026

Permission is hereby granted to the University of Brasília to reproduce copies of this doctoral thesis and to lend or sell such copies for academic and scientific purposes only. The author reserves other publication rights and no part of this doctoral thesis may be reproduced without the written permission of the author.

João Renato Remede Prandina
Av. Nossa Senhora da Penha, 1495 / 504-A
Vitória-ES. 29.056-905

DECLARAÇÃO DE ISENÇÃO DE RESPONSABILIDADE

É importante ressaltar que o presente trabalho tem como único objetivo ampliar o entendimento sobre a representatividade de modelos numéricos na simulação do fenômeno da liquefação estática. O estudo não tem a intenção, em nenhum momento, de determinar a causa da ruptura do caso utilizado como base, nem de questionar ou revisar as análises realizadas por painéis de especialistas que avaliaram o evento, incluindo as publicações de Arroyo e Gens (2021) e Robertson et al. (2019). Além disso, não visa definir se seria possível realizar intervenções para evitar a ruptura. Os autores não fazem qualquer julgamento sobre a representatividade dos modelos apresentados em relação às condições reais da barragem antes ou durante o evento de ruptura. Este estudo deve ser entendido exclusivamente como uma investigação acadêmica e educacional, sem qualquer intenção de emitir declarações ou considerações sobre a responsabilidade ou as causas da ruptura da barragem. O trabalho não deve ser interpretado como base para qualquer tipo de investigação sobre a responsabilidade pelo ocorrido. Os modelos numéricos e os resultados apresentados neste estudo são de natureza teórica e devem ser considerados exclusivamente dentro do contexto acadêmico proposto. Não devem ser utilizados por terceiros como fundamento para decisões práticas, políticas, jurídicas ou de engenharia, sem a devida avaliação de especialistas ou sem considerar o contexto real e técnico completo do evento. Em caso de qualquer uso indevido ou interpretação além do escopo acadêmico, os autores não se responsabilizam pelas consequências práticas ou jurídicas que possam decorrer dessa interpretação.

DISCLAIMER

It is important to emphasize that this work has the sole purpose of expanding the understanding of the representativeness of numerical models in simulating the phenomenon of static liquefaction. The study does not, at any point, aim to determine the cause of the failure of the case used as the basis, nor to question or review the analyses carried out by expert panels who evaluated the event, including the publications by Arroyo and Gens (2021) and Robertson et al. (2019). Furthermore, it does not aim to define whether interventions could have been made to prevent the failure. The authors make no judgment regarding the representativeness of the models presented in relation to the actual conditions of the dam before or during the failure event. This study should be understood exclusively as an academic and educational investigation, with no intention of making any statements or considerations about the responsibility or causes of the dam failure. The work should not be interpreted as the basis for any investigation into the responsibility for the event. The numerical models and results presented in this study are theoretical in nature and should be considered exclusively within the proposed academic context. They should not be used by third parties as the basis for practical, political, legal, or engineering decisions without the proper evaluation of experts or without considering the full real and technical context of the event. In the case of any misuse or interpretation beyond the academic scope, the authors do not assume responsibility for any practical or legal consequences that may arise from such interpretation.

To my wife Jucélia,
for her love, unwavering support, and grace.

ACKNOWLEDGMENTS

To God, first and foremost, for His Grace.

To my advisor, Prof. Dr. Márcio Muniz de Farias, for his brilliant guidance of this research, for his trust in me, and for all the knowledge shared throughout this doctoral program.

To my wife, flesh of my flesh, Jucélia C. Prandina, I thank you for your companionship and patience throughout this entire process.

To my family: father, João Prandina, I offer my deepest reverence. Thank you for your unconditional support, for the tireless errands that made so many stages of this work possible, and, above all, for your true friendship. To my son, Davi Prandina, for being the 'nicest boy in the world' and the wisest I have ever known. To my brother, André Prandina, for his constant companionship, words of encouragement, and the strong friendship. To the memory of my mother, Maria Lilia, who would have been so happy and proud of all these achievements.

To the CEO of PROPAV, Eduardo Luis Silva, for his unprecedented in-kind contributions and the extensive logistical support that enabled the execution of the complex resilient modulus and permanent deformation tests. Eduardo's vision reaches far beyond the immediate scope of this research; he has been a silent yet pivotal contributor to pavement innovation in the state of Espírito Santo, providing the essential means for virtually every significant investigation into alternative geomaterials over the last decade. From the studies on REVSOL and Kambara Slag (KR) to the current research on OSR, his commitment to scientific development has been unparalleled.

To the DNIT Transport Infrastructure Analyst, Renan Ribeiro Guzzo, for his essential support provided at the very beginning of this scientific journey.

To Igor Cuzzuol, for his constant support and partnership throughout the various stages of this research. I am grateful for your loyal partnership and the encouragement during this entire scientific journey.

To the distinguished professors of the Postgraduate Program in Geotechnics (PPGG) at the University of Brasília, for all the knowledge imparted and their continuous dedication to academic excellence.

To the internal and external examiners of my qualification exam, for their valuable critiques, insights, and contributions that elevated the technical rigor of this work.

To the employees of PROPAV, for their valuable competence, continuous dedication to management, and precision in executing various characterization tests of soils and geomaterials of this research.

To the late Engineer Ronaldo Lacourt Mendonça (in memoriam), whose pioneering work in the technique of applying steelmaking slags in geotechnics paved the way for many. I am grateful for his generous sharing of vast experiences.

To my colleagues at UnB, for their pleasant company, rich intellectual exchanges, and the sincere friendships built throughout the Ph.D.

To Vitória Stone, especially Eng. Adriano Alves and Sandro Verzola, a company that welcomed me with open doors on countless visits to collect ornamental stone residue samples and made either in-kind contributions trough their granite slabs.

To ArcelorMittal, for providing essential granular materials from the pig iron and

steelmaking processes (KRS, LD-SS, GBF), as well as sharing valuable CBR test results and some technical data available from their archives.

To Yohanan Shori, kindly represented by Mr. João Batista da Vitória, for the invaluable supply of part of the soils from its borrow pit used in this research.

To Levantina Natural Stone, particularly Mr. Gesiel, for the excellent reception on the several occasions I needed to collect ornamental stone residue samples at their facilities.

To my current supervisor, DNIT Transport Infrastructure Analyst, Bruno Barbiero Moraes, for granting the leave of absence necessary for 3 months to complete this research, honoring the fair principle of isonomy.

To Prof. Patrício Pires, of the Federal University of Espírito Santo (UFES), for the authorization to use the laboratory facilities and technical staff to perform some characterization and compaction tests of the Espírito Santo soil of this research, in compliance with the legal principles of public access to laboratories in federal research and educational institutions.

To SENAI and its laboratory team in Vila Velha-ES, represented by Mr. Mateus Alves of FINDES, for providing the infrastructure required to perform the tests with slabs that were part of this research.

To God, once again and finally, the Alpha and Omega of all things, for the immense grace of crossing my path with all these extraordinary people.

RESUMO

PRANDINA, J. R. R. (2026). **Perspectiva geotécnica do uso de resíduos industriais do Espírito Santo em aterros e pavimentos**. Tese de Doutorado, Publicação G.TD-217/2026, Depart. de Engenharia Civil e Ambiental, Universidade de Brasília, Brasília, DF, 300 p.

Resíduos industriais, que apresentam elevado desempenho geotécnico, reconhecidos publicamente por usuários e autoridades, podem ser denominados materiais sustentáveis (MS). No entanto, são utilizados apenas esporadicamente em projetos de infraestrutura no Brasil, em obras de aterros e pavimentos. São conhecidos desde a década de 80; diversas normas técnicas preveem o seu uso e, atualmente, o Brasil passa por uma transição do dimensionamento empírico de pavimentos para o Mecânistico-Empírico (M-E), liderada pela implementação e padronização do método MeDiNa (Método de Dimensionamento Nacional). Notavelmente, no estado do Espírito Santo (ES), a coexistência de dois grandes polos industriais — rochas ornamentais e siderurgia — apresenta uma oportunidade única para a sinergia entre as obras de infraestrutura e estas cadeias produtivas. Esta tese de doutorado investiga a viabilidade geotécnica da utilização do Resíduo de Rochas Ornamentais (RRO) e da Escória de Reator Kambara (KRS) como componentes sinérgicos em camadas estruturais de pavimentos e na construção de aterros. Apesar da abundância desses resíduos e sua utilização hoje no ES, sua adoção é dificultada pela alta variabilidade física, pela falta de transparência metodológica e pela escassez da adoção de parâmetros de rigidez, como o Módulo Resiliente (MR). Para preencher essas lacunas, foi conduzido um programa experimental em múltiplas escalas. Primeiro, uma abrangente e fundamental revisão da literatura consolidou as tendências geomecânicas, comprovando um significativo vácuo de conhecimento em relação às misturas ternárias (Solo-RRO-KRS). As fases experimentais avaliaram misturas solo-resíduo binárias (2 materiais) e ternárias (3 materiais) por meio de ensaios de compactação, Índice de Suporte Califórnia (CBR), Resistência à Compressão Simples (RCS) e Ensaios Triaxiais de Cargas Cíclicas. A pesquisa investigou solos tropicais regionais em duas etapas: misturas binárias para avaliação do MR; uma avaliação pioneira de sistemas ternários com foco nos efeitos de cura em função do tempo e na cinética química. Os resultados demonstram que, embora o RRO melhore a resistência estática por meio do preenchimento de vazios, seu impacto na resposta elástica exige avaliações M-E rigorosas, porque este desempenho depende das proporções das misturas função das características geotécnicas do solo melhorado. Em contrapartida, o KRS transforma argilas de baixa qualidade em matrizes de alta rigidez, com comportamento de ganho de ridez sob elevação das tensões desviadoras. Em sistemas ternários, o RRO atua como corretor granulométrico que supre fisicamente o período de latência pozolânica da escória, garantindo estabilidade mecânica imediata enquanto a KRS desenvolve ligações cimentícias permanentes. Além disso, esta pesquisa estabelece inovações quanto aos modelos de Teor Ótimo de Resíduo (ORC) e Teor Máximo de Resíduo (MRC), definindo um estado de equilíbrio granular que resulta em um comportamento previsível e independente do estado de tensões. A tese conclui que a combinação tecnológica de RRO e KRS transforma passivos ambientais em ativos geotécnicos de alto desempenho, fornecendo um caminho metodologico sólido e alinhado ao MeDiNa para avançar do processo empírito de tentativa e erro rumo a uma engenharia mecanicista racional, em prol de uma infraestrutura de transporte sustentável em todo Brasil.

Palavras-chave: Resíduo de Rocha Ornamental; Escória de Aciaria; Sinergia Industrial; Módulo de Resiliência; MeDiNa; Framework ORC/MRC.

ABSTRACT

PRANDINA, J. R. R. (2026). **Geotechnical Perspective of the Espírito Santo Industrial Waste Applications in Embankments and Pavements**. Ph.D. Thesis, Publication G.TD-217/2026, Depart. of Civil and Environmental Engineering, University of Brasília, Brasília, DF, 300 p.

Industrial residues, which exhibit high geotechnical performance and are publicly recognized by users and authorities in some specific applications, can be classified as sustainable materials (SM). However, these SM, known since the 1980s, are utilized only sporadically in embankments and pavements of infrastructure projects nationwide. Several technical standards have been issued to provide for their use. Brazil is undergoing a transition from empirical to Mechanistic-Empirical (M-E) pavement design, spearheaded by the implementation and standardization of the MeDiNa method. Notably, in the state of Espírito Santo (ES), the coexistence of two major industrial hubs—ornamental stones and steelmaking, the sources of the aforementioned SM—presents a unique opportunity for synergy between infrastructure works and these production chains. This doctoral thesis investigates the geotechnical feasibility of using Ornamental Stone Residue (OSR) and Kambara Reactor Slag (KRS) as synergistic components in structural pavement layers and embankment construction. Despite the abundance of these residues and their successful track record in empirical applications within ES, their formal and widespread adoption is hindered by high physical variability, a lack of methodological transparency, and the scarcity of adopting stiffness parameters, such as the Resilient Modulus (RM). To address these gaps, a multi-scale experimental program was conducted. First, a comprehensive and fundamental literature review consolidated geomechanical trends, demonstrating a significant knowledge vacuum regarding ternary mixtures (Soil-OSR-KRS). The core experimental phases evaluated binary (2-material) and ternary (3-material) soil-residue mixtures using compaction, California Bearing Ratio (CBR), Unconfined Compressive Strength (UCS), and Cyclic Load Triaxial Tests (CLTT). The research investigated regional tropical soils across two stages: binary mixtures assessing the RM; and a pioneering evaluation of ternary systems focusing on time-dependent curing effects and chemical kinetics. The results demonstrate that while OSR effectively improves static resistance via void-filling and particle packing, its impact on elastic response necessitates rigorous M-E evaluations, because this performance depends on the mixture proportions as a function of the upgraded soil's geotechnical characteristics. Conversely, KRS fundamentally transforms poor-quality clays into high-stiffness matrices with increasing stiffness behavior with increasing deviatoric stresses. In ternary systems, OSR acts as a granulometric corrector that physically bridges the pozzolanic latency period of the slag, ensuring immediate mechanical stability while KRS develops permanent cementitious bonds. Furthermore, this research establishes innovations regarding the Optimum Residue Content (ORC) and Maximum Residue Content (MRC) models, defining a state of granular equilibrium that yields highly predictable and stress-independent behavior. The thesis concludes that the technological combination of OSR and KRS transforms environmental liabilities into high-performance geotechnical assets, providing a methodologically sound, MeDiNa-aligned path to advance from the empirical trial-and-error process toward a rational mechanistic engineering, in favor of a sustainable transportation infrastructure.

Keywords: Dimension Stone Residue; Steel Slag; Industrial Synergy; Resilient Modulus; MeDiNa; ORC/MRC Framework.

TABLE OF CONTENTS

1 INTRODUCTION **1**

1.1 Motivation 1

1.2 Context and Justification 4

1.3 Problem 5

1.4 Objectives 7

2 LITERATURE REVIEW **11**

2.1 Roadway Residue Utilization in Espírito Santo 11

2.1.1 Regulatory Overview on the Use of Residues in Embankments and Pavements 14

2.1.2 Regulatory Limitation on the Use of Residues in Embankments and Pavements 16

2.1.3 Proposal for Future Research: The ES Open Laboratory 17

2.2 Design Criteria (or lack thereof): Soil-Residue Content (SRC) 17

2.3 Reality: Still in Transition from CBR to MeDiNa 21

2.3.1 Mechanical Stabilization and Normative Criteria 23

2.3.2 The Obsolescence of Prescriptive Rigidity: The Espírito Santo Case Study 25

2.3.3 Mechanistic Characterization of Pavements: Resilient Modulus (M_R) . 25

2.3.4 Permanent Deformation and the Shakedown Theory 32

2.3.4.1 Multistage Testing and Shakedown Thresholds 36

2.4 The Waste Materials of the Doctoral Thesis 39

2.4.1 LD-SS: Physical, Chemical and Mineralogical (XRD/XRF) Analysis . 39

2.4.2 KRS: Physical, Chemical, and Mineralogical (XRD/XRF) Analysis 44

2.4.3 OSR: Physical, Chemical, and Mineralogical Analysis (XRD/XRF) 47

2.5 Stabilization of Soils with Residues 53

2.5.1 Soil Mixtures with SS-LD: Historical Use and Strength Gains 53

2.5.1.1 Historical Evolution of LD-SS Availability 56

2.5.1.2 Historical Impact of Expansion on LD-SS Reputation 57

2.5.1.3 Geotechnical Strength Gains with LD-SS 58

2.5.1.4 The Paradox of High-Performance Matrices: Analyzing the Structural Inversion in Santos (2024) 63

2.5.2 Soil Mixtures with KRS: Potential for Chemical Stabilization and Pozzolanic Reactions . . . 66
2.5.2.1 Chemical Mechanisms and Cation Exchange . . . 67
2.5.2.2 Formation of Cementitious Compounds . . . 68
2.5.2.3 Resilient Modulus (MR) of KRS-Soil Mixtures . . . 73
2.5.2.4 Permanent Deformation of KRS-Soil Mixtures . . . 76
2.5.2.5 Novel Stress-Dependent Anthropogenic Geomaterial . . . 81
2.6 Potential: Soil Stabilization with OSR . . . 82
2.6.1 The Implementation Gap: OSR vs. Steel Slag . . . 84
2.6.2 Typical Grain Size Distribution (GSD) of OSR . . . 85
2.6.3 Implications for Geotechnical Stabilization . . . 87
2.6.4 OSR Maximum Dry Density (MDD) and OMC . . . 91
2.6.5 Atterberg Limits and OSR-soil Classification . . . 92
2.6.6 Unconfined Compressive Strength (UCS) . . . 93
2.6.7 California Bearing Ratio (CBR) of/with OSR . . . 97
2.6.7.1 The Paradox of Performance Degradation: The Case of Dias (2024) . . . 100
2.6.7.2 High Potential for Lateritic A-4 Soil Stabilization . . . 102
2.6.8 Resilient Modulus of OSR-Soil Mixtures . . . 103

3 MATERIALS AND METHODS 108
3.1 Binary OSR-Soil Mixtures for Subbase Applications . . . 109
3.1.1 Mixture Proportions and Dosage Rationale . . . 110
3.1.2 Caramuru Region Soil (Santa Leopoldina, ES) . . . 111
3.1.3 SG-12 Soil from UnB Experimental Site (Brasília, DF) . . . 112
3.1.4 The OSR Applied and Its Source . . . 114
3.2 OSR on Binary KRS-SOIL Mixtures . . . 116
3.2.1 Soil Selection: Non-Lateritic Behavior . . . 117
3.2.2 Kambara Reactor Slag (KRS) . . . 117
3.2.3 OSR for Ternary Systems . . . 117
3.2.4 Dosage Design and Mixture Proportions . . . 118
3.2.5 Curing Protocol and Testing Matrix for Binary Soil-KRS Mixtures . . . 119
3.3 OSR for Upgrading Rejected Marginal Soils for Final Embankment Layers . . . 119
3.3.1 Geotechnical Threshold and Soil Rejection . . . 119

3.3.2 Advanced Characterization for MeDiNa Modeling 120
3.4 Behavior of Soils from Espírito Santo - Barreiras Formation 121
3.4.1 Classification Using the Laterization Index (L) 122
3.5 Testing Protocol 123

4 RESULTS AND MECHANISTIC-EMPIRICAL DISCUSSION 125
4.1 OSR Mixed with a Lateritic Soil of Espírito Santo 125
4.1.1 Basic Classification of Geomaterials 126
4.1.2 Strategies for Discurssions of CLTT on Vitória Soil and OSR Mixtures 133
4.1.3 Evaluation of Reference Resilient Behavior Vitória Soil - 0% OSR Content 136
4.1.4 Evaluation of Raw Data and Quality Control Impact Vitória Soil - 0% OSR Content 140
4.1.4.1 Unfiltered 3D Individual Modeling 140
4.1.4.2 Average Unfiltered Surface and Stress Sensitivities 141
4.1.5 Evaluation of Resilient Behavior: Vitória Soil - 5% OSR Content 142
4.1.6 Evaluation of Resilient Behavior: Vitória Soil - 10% OSR Content . . . 145
4.1.7 Evaluation of Resilient Behavior: Vitória Soil - 15% OSR Content 148
4.1.8 Strategic Reevaluation of 30% OSR: From Structural Failure to Infrastructure Viability 152
4.2 OSR Mixed with a Lateritic Soil of Brasilia 155
4.2.1 Evaluation of Reference Resilient Behavior Brasília Soil - 0% OSR Content 155
4.2.2 Evaluation of Resilient Behavior: Brasília Soil - 5% OSR Content . . . 163
4.2.3 Evaluation of Resilient Behavior: Brasília Soil - 10% OSR Content . . 166
4.2.4 Evaluation of Resilient Behavior: Brasília Soil - 15% OSR Content . . 169
4.2.5 Saturation Threshold and Infrastructure Performance: 30% OSR 172
4.2.6 Summary of Constitutive Parameters 175
4.2.7 UCS Tests: Results on Specimens after CLTT 176
4.3 Espírito Santo KRS-SOIL Mixtures: Establishing the Chemical Baseline 183
4.3.1 Soil Selection (S1): Non-Lateritic Behavior 183
4.3.2 The Kambara Reactor Slag (KRS) 184
4.3.3 The Ornamental Stone Residue (OSR) 185

4.4 Phase I: Binary Baseline Analysis (The Chemical Phase) 188
4.4.1 Structural Benchmark, Data Curation, and Curing Protocol 188
4.4.2 Evolution of Confining Sensitivity and Early-Age Structural Transition 192
4.4.3 Three-Dimensional Resilient Response and Model Validation 192
4.4.4 Comparative Stress-State Cross-Sections 196
4.5 Ternary Baseline Analysis (Physical-Chemical Synergy) 200
4.5.1 Experimental Design, Dosages, and Testing Protocol 200
4.5.2 The Filler Effect and OSR Content Optimization 200
4.5.3 Comparative Analysis of Residue-Slag Interaction 201
4.5.4 Evolution of Resilient Modulus (M_R) and 3D Response Surfaces 202
4.5.5 Microstructural Densification and Stress Sensitivity 203
4.5.6 Optimum Residue Content (ORC) as a Pavement Design Criterion . . . 210
4.5.7 Partial Conclusions on Ternary Stabilization 213

5 CONCLUSIONS **215**
5.1 State of the Art of OSR Utilization 215
5.2 State of the Art of KRS Utilization 216
5.3 Mechanistic Behavior of OSR in Lateritic Clays 216
5.4 Mechanistic Behavior of KRS in Non-Lateritic Clays 217
5.5 Influence of OSR on the Mechanistic Behavior of Ternary Mixtures (Non-Lateritic Clays and KRS) 218
5.6 ORC and MRC Concepts as Design Criteria for Binary and Ternary Mixtures Based on Resilient Modulus 218
5.7 Recommendations for Future Research 219

ANNEX 1
Raw Data Records of Resilient Modulus Tests **245**

ANNEX 2
Photographic Report: Selected Research Records **262**

LIST OF FIGURES

1.1 Typical polished slabs from the Ornamental Stone Industry (OSI) at a processing plant in Espírito Santo, Brazil (Photo: Prandina, 2015) 2

2.1 Age 0 (1 week) of an "unpaved" rural roadway (ES-346, km 5) with SS-soil mixture. Picture data: may/2025 11

2.2 Age 1.5 year of an "unpaved" rural roadway (BR-342/ES) with SS-soil mixture. Picture data: out/2024 12

2.3 Effect of OSR-M content on the MR of an A-6 soil (from Jaffar et al., 2022). . 20

2.4 Hypothetical curve of OSR content effect on the MR to present the design concepts of soil-residue content (SRC): ORC, MRC, Zero-E, and SRC-0. . . . 21

2.5 Geomechanical response to cyclic loading: (a) Theoretical behavior of unbound materials under repeated cyclic load (modified from Erlingsson, Rahman, & Salour, 2017); (b) Typical behaviors of the permanent deformation (PD) curve of soils (from Rahman, Erlingsson, & Ahmed, 2023) 34

2.6 Permanent deformation behavior models for soils (from DNIT, 2018b). 36

2.7 Full sample of a LD-SS from Espírito Santo industrial plant (from Izoton, 2020) 39

2.8 320,000 m$^2 Residue Stockpile Area of the Steelmaking Industrial Processing Plant in Vitria,$ I

2.9 The CSN slag stockpile yards illustrate the true scale of the waste management challenge posed by continuous steel production (Foco Regional, 2019). 41

2.10 Scanning Electron Microscopy (SEM) micrographs of LD-SS samples: (a) hydrated calcium ferrite (1–3); (b) portlandite (1–2); (c) dicalcium silicate (1, 3) and tricalcium silicate (2); (d) calcium carbonate (1) and hydrated calcium ferrite (2); (e) calcium phosphate (1); and (f) calcium carbonate (1) and calcium ferro-silicate (2). Adapted from Polese et al. (2006). 41

2.11 Scanning Electron Microscopy (SEM) micrograph of fresh LD-SS at age zero, highlighting clean and highly reactive mineral surfaces (Modified from Yildirim & Prezzi, 2011) 42

2.12 Scanning Electron Microscopy (SEM) micrograph of aged LD-SS, illustrating the surface covered by rhombohedral calcite ($CaCO_3$) crystals resulting from atmospheric carbonation (Modified from Yildirim & Prezzi, 2015) 43

2.13 Description of sample A. 45

2.14 Description of sample B. 45

2.15 X-ray diffraction (XRD) pattern of typical soils from Espírito Santo (different CH and SC) and KRS, highlighting the following mineral phases: (H) Portlandite – $Ca(OH)_2$; (I) Calcite – $CaCO_3$; (B) Quartz – SiO_2; (A) Gibbsite – $Al(OH)_3$; (C) Kaolinite – $Al_2Si_2O_5(OH)_4$; (E) Silicon Oxide – SiO_2; (J) Ettringite – $Ca_6Al_2(SO_4)_3(OH)_{12} \cdot 26H_2O$; (D) Magnesium Aluminum Hydroxide – $Mg_6Al_2(OH)_{18} \cdot 4H_2O$; (F) Sodium Iron Oxide Silicate – $NaFeSi_2O_6$; (K) Magnesioferrite – $MgFe_2O_4$; and (G) Sodium Aluminium Silicate – $NaAlSi_3O_8$ (from Oliveira, 2018). 47

2.16 Genesis of the OSR: (A) detail of the micro-abrasion area where the cutting mechanism via diamond wire sawing acts; (B) solid part of the block left uncut due to irregularities (Photo: Prandina, 2015) 48

2.17 XRD pattern of OSR mixtures identifying mineral phases: quartz, kaolinite, and calcite (modified Lunz, 2021) 52

2.18 Scanning Electron Microscopy (SEM) images: (a) Pure soil sample showing aggregated structure; (b) OSRs sample showing fine discrete particles. 53

2.19 CBR vs LD-SS and gravel percentages in A-4 soil mixtures (from Santos, 2024) 59

2.20 Continuous CBR growth for A-4 soil stabilized with LD-SS (modified from Silva, 2021) 60

2.21 CBR vs LD-SS percentage for CH lateritic soil mixtures (modified from Boldrini & Pacheco, 2022) 61

2.22 1089 stake MR of LD-SS and 1090 stake LD-SS/soil mixture (modified from Resende, 2010) 62

2.23 Back analysis of different pavement layers and different base layers materials including a 80% LD-SS mixed with 20% clayey soil (modified from Resende, 2010) 63

2.24 CBR inversion at high replacement ratios in A-4 lateritic soil (modified from Santos, 2024) 64

2.25 Physical states of soil-aggregate mixtures and the filler effect (modified from Yoder and Witczak, 1975; Yildirim, 2023) 66

2.26 Performance indicators for ORC of soil/LD-SS and soil/KRS: variation of CBR (a), Plasticity index (b), CBR sensitivity to moisture (c), and OMC (d), at different LD slag (LD-SS, open symbols) and KR slag (KRS, solid symbols) contents (Modified from Gomes, Magalhães, Rocha, & Fonseca, 2021) 71

2.27 Resilient Modulus (M_R) vs. deviator stress (σ_d) for natural soils and the AE + 20% KRS mixture, highlighting the shift to stiffness-increasing behavior (Modified from Bastos, 2022) 74

2.28 Log-log regression analysis of Resilient Modulus (M_R) versus confining and deviatoric stresses for pure and KRS-stabilized soil specimens (Adapted Mendoza, 2023; Fardim, 2024). 75

2.29 Consolidated 3D Resilient Modulus surfaces representing the composite MeDiNa model ($M_R = k_1 \cdot \sigma_3^{k_2} \cdot \sigma_d^{k_3}$). The 3% KRSP surface fades out above 600 MPa to enhance the visualization of the lower-stress boundaries. 76

2.30 Accumulated permanent strain (ϵ_p) for KRSP3 mixture (adapted from Mendoza, 2023). 78

2.31 Accumulated permanent strain (ϵ_p) for KRSP5 mixture (adapted from Mendoza, 2023). 78

2.32 Behavioral analysis of the material based on permanent deformation — KRSP3 (from Mendoza, 2023). 79

2.33 Behavioral analysis of the material based on permanent deformation — KRSP5 (from Mendoza, 2023). 79

2.34 Grain Size Distribution (GSD) of OSR samples compared to Type I Portland cement and Canadian Granular A (Gran A) limits (Modified from Prandina, Fall, & Sedano, 2017). 85

2.35 Methodology for evaluation of OSR beneficial use in geotechnical fills, following the USEPA framework (Adapted from Lohar & Shrivastava, 2025). . 90

2.36 Standard Proctor compaction curves for soil-OSR mixtures: contrasting gradation optimization in clayey soil (BR-120) and the excess filler effect in sandy soil (VILA) (Adapted from Lunz, 2021). 92

2.37 Variation of Liquid Limit (LL), Plastic Limit (PL), and Plasticity Index (PI) across different soil-OSR mixtures as reported in literature (Prandina & Farias, 2026). 93

2.38 Unconfined Compressive Strength (UCS) test on A2-5 soil and soil-OSR specimens compacted on Modified energy (Adapted from Cardoso, 2019). . . . 94

2.39 Tensile strength by diametral compression – Standard Proctor energy (Brazilian Test) A2-5 soil and soil-OSR specimens (Adapted Cardoso, 2019). 95

2.40 UCS function of OSR content (Modified Lunz, 2021) 96

2.41 CBR and expansion function of OSR content (Modified Lunz, 2021) 99

2.42 General view of the soil deposit utilized for the study (Source: Author, 2026). . 101

2.43 CBR losses and expansion in different contents of soil-OSR mixtures, (Adapted from Dias, 2024). 101

2.44 Professional dual-panel synchronized bar chart visualizing the pronounced CBR increase and low expansion in soil-OSR mixtures, with annotation explaining the cationic shock mechanism in lateritic A-4 soil (Adapted from Farias et al., 2018). 102

2.45 Resilient Modulus (M_R) of an A-2-4 soil mixed with OSR (modified from Dias, 2024). 104

2.46 MR results of: i) ORC of OSR-M added to A-6 soil; ii) Optimum proportion of sand added to the same A-6 soil (modified from Jaffar et al., 2022). 105

2.47 Comparison of 3D Resilient Modulus response surfaces for BR-120 soil and OSR mixture. Note the inversion of the σ_d axis in the mixture plot (b) (modified from Lunz, 2021). 106

2.48 M_R graphs obtained from the models for the first mix (5% OSR, 40% RAP, 55% gravel): (i) Simplified Model θ (Bulk stress); (ii) Composite Model (modified from A. S. Santos & Leandro, 2017). 106

3.1 Location of the Caramuru borrow pit and delimitation of sampling areas (GEOBASES, 2026). 112

3.2 Regional map of the Santa Leopoldina region (IDAF, 2026). 113

3.3 General view of the Geotechnical Experimental Site at the University of Brasília (UnB), near the SG-12 sampling area (Geotecnia UnB, 2026). 114

3.4 OSR recovery system at the Vitória Stone facility: (a) overview of the automated filter press; (b) extraction of the solid residue after the pressing cycle. 114

3.5 Consolidated particle size distribution (GSD) curves for the baseline materials evaluated in Section 3.1: Caramuru soil, natural SG-12 soil, and pure OSR Q-16 mineral filler. 115

3.6 Comparative particle size distribution (GSD) curves for the raw materials utilized in Section 3.2 (Soil, KRS, and aggregated OSR) classified under standard geotechnical fractions. 118

4.1 Grain size distribution of OSR-Q (2016), Caramuru soil (also called Vitória soil), SG-12 UnB site soil (Brasília) with and without deflocculant, and reference OSR from Bacarji et al. (2013). 126

4.2 Collection of the Brasília (SG-12 UnB site) soil; (center) Soil and OSR transport for drying; (right) Hydrometeer test for grain size analysis. 126

4.3 Grain size distribution of OSR-Q (2016) with and without deflocculant. 127

4.4 WL and PI of Brasília (SG-12 UnB site) and Espírito Santo (ES) soils mixed with different percentages of OSR-Q 128

4.5 WP and PI of Brasília (SG-12 UnB site) and Espírito Santo (ES) soils mixed with different percentages of OSR-Q. 128

4.6 Compaction curves of Espírito Santo (Vitória-ES) soil with the 3 different energies 129

4.7 Compaction curves of Espírito Santo (Vitória-ES) soil with the 3 different energies 129

4.8 Compaction curves of OSR with different energies 130

4.9 Close view of the mixed OSR (white particles) in the soil matrix (yellow partciles) 131

4.10 Compaction and moisture parameters for the soil-OSR blends: (a) superimposed compaction curves, and (b) Optimum Moisture Content (OMC) evaluation as a function of the OSR content. 132

4.11 Compaction and saturation matrix for the Brasília (SG-12) soil-OSR systems: (a) natural soil (0% OSR), (b) 5% OSR, (c) 10% OSR, (d) 15% OSR, (e) 30% OSR mixtures, and (f) pure rock residue (100% OSR) mapped against their respective 80% and 100% (ZAV) saturation lines. 132

4.12 Advanced mechanical and density characterization for the soil-waste geomaterials: (a) Maximum Dry Density (MDD) trends under intermediate compaction, and (b) California Bearing Ratio (CBR) performance mapping across distinct residue substitution rates. 133

4.13 3D Resilient Modulus models comparison for Vitória soil (0% OSR): (a) specimen CP1; (b) specimen CP2. 137

4.14 Average Resilient Modulus 3D surface for Vitória soil (0% OSR) including MeDiNa and MEPDG model parameters. 137

4.15 Evaluation of the Vitória soil (0% OSR) stiffness sensitivity to stress changes at low ($\sigma_3 = 0.02$ MPa) and structural ($\sigma_3 = 0.07$ MPa) confinement levels. . . . 138

4.16 1D Bivariate sensitivity models for Vitória soil (0% OSR): (left) confinement effect ($M_R \times \sigma_3$); (right) shear effect ($M_R \times \sigma_d$). 139

4.17 3D Models Impact Without QC for Vitória soil (0% OSR): (a) unfiltered specimen CP1; (b) unfiltered specimen CP2. 141

4.18 Evaluation of impact without QC on the Vitória soil (0% OSR) stiffness sensitivity to stress changes at low and structural confinement levels. 141

4.19 1D Bivariate Models [UNFILTERED]: (left) confinement effect; (right) shear effect. 142

4.20 3D Resilient Modulus models comparison for Vitória soil (5% OSR): (a) specimen CP1; (b) specimen CP2. 143

4.21 Average Resilient Modulus 3D surface for Vitória soil (5% OSR) including MeDiNa and MEPDG model parameters. 143

4.22 Evaluation of the Vitória soil (5% OSR) stiffness sensitivity to stress changes at low ($\sigma_3 = 0.02$ MPa) and structural ($\sigma_3 = 0.07$ MPa) confinement levels. . . . 144

4.23 1D Bivariate sensitivity models for Vitória soil (5% OSR): (left) confinement effect ($M_R \times \sigma_3$); (right) shear effect ($M_R \times \sigma_d$). 144

4.24 3D Resilient Modulus models comparison for Vitória soil (10% OSR): (a) specimen CP1; (b) specimen CP2. 145

4.25 Average Resilient Modulus 3D surface for Vitória soil (10% OSR) including MeDiNa and MEPDG model parameters. 146

4.26 Evaluation of the Vitória soil (10% OSR) stiffness sensitivity to stress changes at low ($\sigma_3 = 0.02$ MPa) and structural ($\sigma_3 = 0.07$ MPa) confinement levels. . . 147

4.27 1D Bivariate sensitivity models for Vitória soil (10% OSR): (left) confinement effect ($M_R \times \sigma_3$); (right) shear effect ($M_R \times \sigma_d$). 147

4.28 3D Resilient Modulus models comparison for Vitória soil (15% OSR): (a) specimen CP1; (b) specimen CP2. 149

4.29 Average Resilient Modulus 3D surface for Vitória soil (15% OSR) including MeDiNa and MEPDG model parameters. 150

4.30 Evaluation of the Vitória soil (15% OSR) stiffness sensitivity to stress changes at low ($\sigma_3 = 0.02$ MPa) and structural ($\sigma_3 = 0.07$ MPa) confinement levels. . . 151

4.31 1D Bivariate sensitivity models for Vitória soil (15% OSR): (left) confinement effect ($M_R \times \sigma_3$); (right) shear effect ($M_R \times \sigma_d$). 151

4.32 3D Resilient Modulus model for Vitória soil (30% OSR) demonstrating highly predictable structural behavior. 152

4.33 Evaluation of the Vitória soil (30% OSR) stiffness sensitivity to stress changes showcasing pronounced MR increasing under structural confinement. 153

4.34 1D Bivariate sensitivity models for Vitória soil (30% OSR) confirming positive correlation with both confining and deviatoric stresses. 153

4.35 3D Resilient Modulus models comparison for natural Brasília soil (0% OSR): (a) specimen CP1; (b) specimen CP2. 156

4.36 Visual inspection of natural SG-12 soil specimens (0% OSR) after cyclic loading triaxial testing, prior to the unconfined compression test. 156

4.37 Average Resilient Modulus 3D surface for natural Brasília soil (0% OSR) including MeDiNa and MEPDG model parameters. 157

4.38 Evaluation of the natural Brasília soil (0% OSR) stiffness sensitivity to stress changes at low ($\sigma_3 = 0.02$ MPa) and structural ($\sigma_3 = 0.07$ MPa) confinement levels. 157

4.39 Log-Log evaluation of the natural Brasília soil (0% OSR) stiffness sensitivity to stress changes at 0.02 MPa and 0.07 MPa confining pressures. 158

4.40 1D Bivariate sensitivity models for natural Brasília soil (0% OSR): (left) confinement effect ($M_R \times \sigma_3$); (right) shear effect ($M_R \times \sigma_d$). 159

4.41 Filtered 3D Resilient Modulus models ($\sigma_d \geq \sigma_3$) for natural Brasília soil (0% OSR): (a) specimen CP1; (b) specimen CP2. 161

4.42 Filtered Average Resilient Modulus 3D surface for natural Brasília soil (0% OSR). 161

4.43 Filtered 1D Bivariate sensitivity models for natural Brasília soil (0% OSR) demonstrating data scatter under realistic shear conditions. 163

4.44 Filtered 3D Resilient Modulus models ($\sigma_d \geq \sigma_3$) for Brasília soil with 5% OSR: (a) specimen CP1; (b) specimen CP2; (c) specimen CP3 (6-month storage). . . 164

4.45 Average Resilient Modulus 3D surface for Brasília soil (5% OSR) demonstrating a high coefficient of determination ($R^2 = 0.8710$). 164

4.46 Linear evaluation of the Brasília soil-OSR mixture (5% OSR) stiffness sensitivity to stress changes at low (0.02 MPa) and structural (0.07 MPa) confinement levels. 165

4.47 1D Bivariate sensitivity models for Brasília soil (5% OSR) confirming strong correlation with shear and confinement in the logarithmic domain. 165

4.48 Filtered 3D Resilient Modulus models ($\sigma_d \geq \sigma_3$) for Brasília soil with 10% OSR: (a) specimen CP1; (b) specimen CP2; (c) specimen CP3. 166

4.49 Average Resilient Modulus 3D surface for Brasília soil (10% OSR) demonstrating sustained statistical reliability ($R^2 = 0.8231$). 167

4.50 Linear evaluation of the Brasília soil-OSR mixture (10% OSR) stiffness sensitivity to stress changes at low (0.02 MPa) and structural (0.07 MPa) confinement levels. 168

4.51 1D Bivariate sensitivity models for Brasília soil (10% OSR) under realistic shear conditions. 168

4.52 Filtered 3D Resilient Modulus models ($\sigma_d > \sigma_3$) for Brasília soil with 15% OSR: (a) specimen CP1; (b) specimen CP2. 169

4.53 Average Resilient Modulus 3D surface for Brasília soil (15% OSR) demonstrating the structural compromise of the mixture. 170

4.54 Revised linear decreasing (MR) stiffness analysis for Brasília soil (15% OSR) demonstrating the divergent behavior of the specimens. 171

4.55 1D Bivariate sensitivity models for Brasília soil (15% OSR) illustrating the breakdown of structural correlation. 172

4.56 3D Resilient Modulus surface for BSB soil at 30% OSR: The disintegration of the cohesive matrix leads to the "Floating Soil" phenomenon, with stiffness values stabilized at a lower baseline. 173

4.57 Mechanistic diagnostic of the 30% OSR BSB matrix: (left) Transition to increasing (MR) stiffness in 2D slices; (right) Bivariate Log-Log trends showing the dominant influence of stress states on the frictional matrix. 174

4.58 Post-cyclic UCS test results for the Vitória soil mixtures (Set 1). 178

4.59 Post-cyclic UCS test results for the Vitória soil mixtures (Set 2). 179

4.60 Set 1 of post-cyclic UCS trends for the Brasília soil with varying OSR percentages (0%, 5%, 10%, and 15%). 180

4.61 Set 2 of post-cyclic UCS trends for the Brasília soil with varying OSR percentages (0%, 5%, 10%, and 15%). 181

4.62 Grain size distribution (GSD) curves of the natural soil matrix (S1), the evaluated Steel Slag (KRS), binary baselines (85/15 and 80/20), and the reference KRS from Fardin (2024), highlighting the physical-chemical influence on the sedimentation tails. 184

4.63 Grain size distribution (GSD) comparison of pure OSR: deflocculation sensitivity and particle aggregation analysis. 185

4.64 Collection of the Ornamental Stone Residue (OSR) at the industrial plant: (a) general view of the filter press equipment; and (b) detail of the fresh residue discharge. 186

4.65 Resilient Modulus (M_R) of Binary 85/15 (Soil-KRS) mixture at 0 days of curing (immediate state). 189

4.66 Refined Resilient Modulus (M_R) of Binary 85/15 mixture at 0 days. The average trendline is established excluding CP01 based on geotechnical consistency criteria ($R^2 > 0.90$). 191

4.67 Resilient Modulus (M_R) as a function of confining pressure (σ_3) for binary baselines at 4 days: (a) 85/15 mixture; and (b) 80/20 mixture. 192

4.68 Temporal evolution of the 3D Resilient Modulus (M_R) response for the 85/15 Binary Mixture (0 vs. 28 days). 193

4.69 Temporal evolution of the 3D Resilient Modulus (M_R) response for the 80/20 Binary Mixture (0 vs. 28 days). 194

4.70 3D Resilient Modulus (M_R) surface comparison between Binary 85/15 and 80/20 mixtures at advanced maturity (28 days). 195

4.71 Comparative Resilient Modulus cross-sections at fixed confining pressures: (a) $\sigma_3 = 0.02$ MPa and (b) $\sigma_3 = 0.07$ MPa. 196

4.72 Temporal evolution of the Resilient Modulus (M_R) as a function of confining pressure (σ_3) for binary baselines at 0, 4, and 28 days: (a) 85/15 mixture; and (b) 80/20 mixture. 197

4.73 Temporal evolution of the 3D Resilient Modulus response for the 85/15 Binary Mixture. 198

4.74 Temporal evolution of the 3D Resilient Modulus response for the 80/20 Binary Mixture. 199

4.75 Resilient Modulus (M_R) optimization through Ornamental Stone Residue (OSR) addition at 4 days of curing: (a) 85/15 matrix showing an optimum at 5% OSR; and (b) 80/20 matrix achieving peak stiffness at 10% OSR. The dashed blue line represents the reference binary baseline. 201

4.76 3D Resilient Modulus maturation for Ternary Optimum Residue Content (ORC) at 4 days: (a) 85/15 + 5% OSR matrix; and (b) 80/20 + 10% OSR matrix. Comparison between MeDiNa (Composite) and MEPDG (Universal) models. . 202

4.77 Cross-sectional analysis of M_R vs. deviatoric stress (σ_d) at 4 days: (a) low confinement ($\sigma_3 = 0.02$ MPa) and (b) high confinement ($\sigma_3 = 0.07$ MPa). The plots illustrate the stiffness gap and the stress-independence threshold. 204

4.78 Effect of OSR on soil-KRS mixtures: 3D response surfaces comparing the 85/15 binary matrix maturation (4 vs. 28 days) against the immediate structural gain of the ternary mixture with 5% OSR at 4 days. 205

4.79 Effect of OSR: 3D response surfaces comparing the 85/15 binary matrix maturation against the immediate structural stability of the ternary mixture with 10% OSR at 4 days. 206

4.80 Effect of OSR on soil-KRS mixtures: 3D response surfaces comparing the 80/20 binary matrix maturation against the immediate Granular Equilibrium achieved by the ternary mixture with 10% OSR at 4 days. 207

4.81 The Power of OSR: 3D comparative analysis for the 80/20 matrix. The orange surface (5% OSR ternary at 4 days) rivals the 28-day chemical maturation of the 0% OSR binary baseline (dark red surface). 208

4.82 Projected maturation of the 80/20 + 5% OSR ternary system. 209

4.83 Residue Content Optimization and Pavement Design Criteria for the 85/15 Soil-KRS Matrix at 4 days ($\sigma_3 = 50$ kPa, $\sigma_d = 50$ kPa). 211

4.84 Universal Geotechnical Evaluation Framework: ORC and MRC mapping for multiple soil-KRS matrices. 213

5.1 External view of the Infrastructure Laboratory (Infralab) at the University of Brasília (UnB). 262
5.2 Espírito Santo (ES) soil specimens wrapped in plastic film for moisture content preservation during the curing period. 263
5.3 Detail of soil samples prepared in metallic rings for physical characterization and moisture control tests. 264
5.4 Unconfined Compressive Strength (UCS) test setup for a natural Brasília soil specimen (SG-12, 0% OSR). 264
5.5 General view of failed specimens after testing, showcasing the contrast between Brasília (SG-12) and Vitória soil matrices with varying OSR dosages. 265
5.6 Specimen preparation for advanced geotechnical testing (Resilient Modulus) involving 30% OSR content. 265
5.7 Identification and storage of stabilized specimens for the study of 5% and 10% OSR mixture maturation. 266
5.8 Initial stage of manual mixing: Ornamental Stone Residue (white powder) being integrated into the Brasília (SG-12) red soil matrix. 266
5.9 Homogenization and moisture adjustment for the 10% OSR-soil mixture in the preparation tray. 267
5.10 Specimen molding phase using a Proctor mold for the 30% OSR-SG12 soil mixture. 268
5.11 Set of cylindrical specimens molded in 2019, ready for basic geotechnical characterization tests. 268
5.12 Molded specimen (5% OSR-SG12) positioned on the triaxial base for Resilient Modulus (MR) testing. 269

LIST OF TABLES

1.1 Primary acronyms and definitions for core research materials and industrial byproducts. 9

1.2 Secondary list of acronyms for geotechnical, pavement engineering, and characterization terms. 10

2.1 Main milestones and case studies of SS applications in Brazil (prepared by the authors) 13

2.2 Comparative summary of geotechnical properties and compaction behavior of soils and OSR-Soil Mixtures. 19

2.3 Consolidated minimum performance requirements for roadway layers according to DNIT standards. 22

2.4 Consolidated granulometric requirements for Base layers (Natural Soil, Acerita®, and Açobrita®). 24

2.5 Comparison of Resilient Modulus (M_R) Models: International Literature vs. MeDiNa Simplifications 30

2.6 Models and their formulations for predicting permanent deformation 35

2.7 Chemical composition of LD-SS from Brazilian industrial plants (Adapted from Oliveira, 2016) 40

2.8 Main Chemical Composition of KRS (Pires et al., 2019). 45

2.9 Chemical composition of KRS and LD-SS (% by mass) 46

2.10 Chemical composition of the OSR in percentages 49

2.11 Chemical composition of the samples (Oxides %). 50

2.12 Chemical composition of the marble slurry reordered by concentration. 51

2.13 Comparative of OSR-G and OSR-M Summarized Chemical Profiles Galetakis and Soultana (2016). 52

2.14 Table 6. Geotechnical properties of the steelmaking slag (LD slag) (Adapted from Gomes et al., 2021) 54

2.15 Physical Characterization of the REVSOL Material (ArcelorMittal, 2016) . . . 55

2.16 Commercial blends made available by the industry of steelmaking slags and recommended applications (ArcelorMittal, 2016) 57

2.17 MG-232 road CBR test on classified construction materials (from Resende, 2010) 59

2.18 Chemical Mechanisms of KRS-Soil Interaction 68

2.19 Microstructural and Long-Term Cementitious Mechanisms of KRS-Soil Stabilization 69

2.20 Comparison of CBR, MDD, and OMC for 70% Slag and 30% Non-Lateritic Soil (S2) mixtures under different compaction energies (Adapted from A. J. Magalhães, Gomes, & Pires, 2022) 70
2.21 CBR results for natural soils and stabilized mixtures based on laboratory characterization (Adapted from Bridi, 2020; Furieri, 2019; Nepomuceno, 2019) 72
2.22 Monismith model parameters for SKRSP mixtures (adapted from Mendoza, 2023). 77
2.23 Summary of Mechanical Characterization and Mechanistic Performance Parameters for Granular and Stabilized Materials 80
2.24 Connection between Brazilian research and international peer-reviewed literature (from Prandina & Farias, 2026) 83
2.25 Geotechnical characterization and classification of OSR: Summary of national and international findings (from Prandina & Farias, 2026). 86
2.26 Properties of Soils Stabilized with OSR from granite Summary of Research Findings (from Prandina & Farias, 2025a) 88
2.27 Properties of Soils Stabilized with OSR from marble Summary of Key Research Findings (from Prandina & Farias, 2025a) 89
2.28 CBR values for Sample M1 under different compaction and saturation conditions (Adapted from Barrientos et al., 2010). 98
2.29 CBR and Expansion results for soil-OSR mixtures (Adapted from Farias, Fernandes, & Espíndola, 2018a). 99
2.30 Mechanisms and geotechnical effects of OSR addition to cohesive soils 103

3.1 Summary of the investigated tropical soils, geological origins, and associated waste stabilization systems. 108
3.2 Experimental matrix for the Brasília soil (SG-12) stabilized with OSR. 111
3.3 Experimental matrix for the Santa Leopoldina soil (Caramuru) stabilized with OSR. 111
3.4 Geotechnical properties of the natural soils from Brasília (SG-12 EGS) and from Caramuru Borrow Pit, later tested in Vitória, state capital of Espírito Santo (from Prandina, 2019). 116
3.5 Revised experimental matrix: Soil-KRS binary bases and OSR additive variations. 119
3.6 Experimental matrix for binary Soil-KRS mixtures: Curing periods and testing protocols. 119
3.7 Technical specifications of the data acquisition system transducers. 120
3.8 Classification of tropical behavior based on the Laterization Index. 123
3.9 Geotechnical and pavement testing program summary. 124

4.1 Compaction parameters of soil-OSR mixtures with different percentage rates . 130
4.2 Summary of Non-Linear Parameters - Composite Model (MeDiNa/DNIT) . . . 175

4.3 Summary of Non-Linear Parameters - Universal Model (MEPDG) 176
4.4 Unconfined compressive strength test results for the ES Soil 182
4.5 Comprehensive geotechnical characterization, compaction parameters, and mechanical performance (CBR and Expansion) for raw materials, binary baselines, and ternary mixtures. 187
4.6 Experimental matrix: Curing periods and testing protocols. 188
4.7 Individual specimen molding parameters and regression constants for binary mixtures at 0 days. 190
4.8 Dixon's Q-Test for outlier identification (k_1 values) at a 90% confidence level. . 190
4.9 Revised experimental matrix: Soil-KRS binary bases and OSR additive variations. 200
4.10 Calculated Resilient Modulus (M_R) values for ternary mixtures at 4 days of curing 203

5.1 Resilient Modulus Test Data - Vitória Soil 0% OSR (CP1) 246
5.2 Resilient Modulus Test Data - Vitória Soil 0% OSR (CP2) 246
5.3 Full test sequences for Vitória Soil CP1 (0% OSR) - December 2018 Data. . . . 247
5.4 Full test sequences for Vitória Soil CP2 (0% OSR) - December 2018 Data. . . . 247
5.5 M_R Test Results for Vitória Soil CP1 (0% OSR). 248
5.6 M_R Test Results for Vitória Soil CP2 (0% OSR). 248
5.7 Resilient Modulus Test Data - Vitória Soil 5% OSR (CP1) 249
5.8 Resilient Modulus Test Data - Vitória Soil 5% OSR (CP2) 249
5.9 Resilient Modulus Test Data - Vitória Soil 10% OSR (CP1) 250
5.10 Resilient Modulus Test Data - Vitória Soil 10% OSR (CP2) 250
5.11 Resilient Modulus Test Data - Vitória Soil 15% OSR (CP1) 251
5.12 Resilient Modulus Test Data - Vitória Soil 15% OSR (CP2) 251
5.13 Resilient Modulus Test Data - Vitória Soil 30% OSR (CP2) 252
5.14 Resilient Modulus Test Data - Vitória Soil 30% OSR (CP2) 252
5.15 Resilient Modulus Test Data - Vitória Soil 30% OSR (CP1 - Retest) 253
5.16 Composite Model (DNIT) Parameters for Vitória Soil (VIX) with varying OSR contents 253
5.17 Resilient Modulus Test Data - BSB Soil 0% OSR (CP1) 254
5.18 Resilient Modulus Test Data - BSB Soil 0% OSR (CP2) 254
5.19 Resilient Modulus Test Data - BSB Soil 5% OSR (CP1) 255
5.20 Resilient Modulus Test Data - BSB Soil 5% OSR (CP1) 255
5.21 Resilient Modulus Test Data - BSB Soil 5% OSR (CP2) 256
5.22 Resilient Modulus Test Data - BSB Soil 5% OSR (CP2) 256

5.23 Integral Resilient Modulus Test Data - BSB Soil 5% OSR (CP3 - Materials Stored for 6 Months) 257
5.24 Resilient Modulus Test Data - BSB Soil 10% OSR (CP1) 257
5.25 Resilient Modulus Test Data - BSB Soil 10% OSR (CP2) 258
5.26 Integral Resilient Modulus Test Data - BSB Soil 10% OSR (CP3 - Materials Stored for 6 Months) 258
5.27 Integral Resilient Modulus Test Data - BSB Soil 15% OSR (Specimen 1) . . . 259
5.28 Resilient Modulus Test Data - BSB Soil 15% OSR (CP2) 259
5.29 Integral Resilient Modulus Test Data - BSB Soil 15% OSR (Specimen 2) . . . 260
5.30 Integral Resilient Modulus Test Data - BSB Soil 30% OSR (Specimen 1) . . . 261
5.31 Summary of Non-Linear Parameters - Composite Model (MeDiNa/DNIT) . . . 270

LIST OF SYMBOLS

a, b	Experimental parameters for permanent strain models
A, B	Experimental parameters for Monismith and Resende models
E_c, E_d	Elastic moduli during loading and unloading
h	Pavement layer thickness
k_1, k_2, k_3, k_4	Mechanistic model regression constants (MeDiNa / Universal)
M_R	Resilient Modulus
N	Number of load repetitions or cycles
P_a	Reference Atmospheric Pressure (0.101325 MPa)
R^2	Coefficient of Determination
S_f	Stress function or stress parameter
w	Moisture Content
α, μ	Material parameters for Uzan's permanent strain model
β, ρ, ϵ_0	Material properties for the Tseng and Lytton model
γ_d	Dry Unit Weight (Dry Density)
$\delta_p(N)$	Permanent deformation of the layer after N cycles
ϵ_p	Accumulated permanent specific strain (plastic strain)
ϵ_p^{esp}	Specific permanent strain percentage
ϵ_r	Recoverable or resilient axial strain
ϵ_v	Average resilient vertical strain
$\hat{\epsilon}_p^{5000} - \hat{\epsilon}_p^{3000}$	Rate of strain increment between cycles 3,000 and 5,000
θ	Bulk Stress / First Stress Invariant
σ_1	Major principal axial stress
σ_3	Confining Pressure
σ_d	Deviatoric Stress
τ_{oct}	Octahedral Shear Stress
$\Psi_1, \Psi_2, \Psi_3, \Psi_4$	Regression parameters for the Guimarães (DNIT) model
CBR	California Bearing Ratio
CLTT	Cyclic Load Triaxial Test
GBF-S	Granulated Blast Furnace Slag
GSD	Grain Size Distribution
KRS	Kambara Reactor Slag (also KR-SS)
MDD	Maximum Dry Density
MeDiNa	National Pavement Design Method
MRC	Maximum Residue Content
OMC	Optimum Moisture Content
ORC	Optimum Residue Content
OSR	Ornamental Stone Residue
PD	Permanent Deformation
SRC	Soil-Residue Content
SRC-0	Soil-Residue Content Zero
UCS	Unconfined Compressive Strength
Zero-E	Zero-Equivalent Residue Content

1 - INTRODUCTION

This introductory chapter establishes the research framework by detailing the background and the underlying motivation for the study. It identifies the primary challenges addressed, defines the specific research objectives, and provides a structural roadmap for the remaining sections of the thesis.

1.1 - MOTIVATION

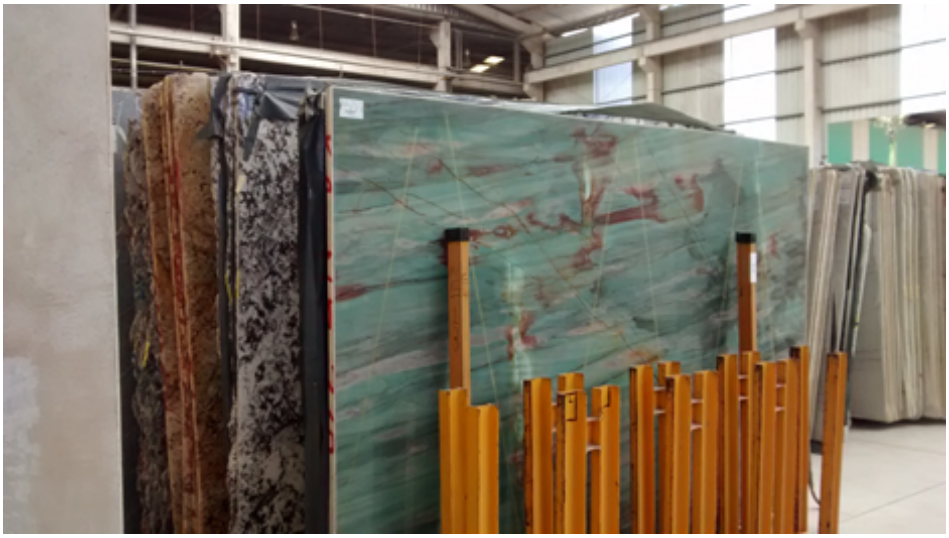
Infrastructure works, which encompass the design and construction of embankments, pavements, and other projects where the field of geotechnical engineering is the primary provider of knowledge, are fundamental to economic development for any country or region.

For at least a decade, various residues from the steelmaking industry (SIND) in Espírito Santo, particularly steelmaking slag from Linz-Donawitz (SS-LD), also known as Basic Oxygen Furnace (BOF), and pig-iron slag generated in the desulfurization process in the Kambara Reactor (KRS), have been increasingly employed in the construction of such works throughout the state, reaching more than 6 million metric tons aplayed in roadways in the last 10 years (ArcelorMittal, 2025). According to Polese et al. (2006), based on an average generation of 120 kg of steelmaking slag per tonne of crude steel, a total of 4 million tonnes of slag was generated, positioning this byproduct as one of the highest-volume wastes in the steel industry. Given that Brazilian crude steel production reached 33.3 million tonnes in 2025 (IAB, 2026), the estimated annual slag generation remains at levels equivalent to those observed two decades ago ($\approx$ 4.0 Mt), highlighting the persistent magnitude of this environmental and geotechnical challenge.

Another important and prevalent industrial cluster is the dimension stone industry (DSI) — as typically called in North America, and locally referred to as the Ornamental Stone Industry (OSI). Brazil's global prominence in this sector is evidenced by official U.S. trade data, which indicates that 41% of all dimension stones imported by the United States originate from Brazil. These exports are predominantly composed of polished slabs (Figure 1.1a and 1.1) used for high-end residential finishes. The global production of this industry has shown significant expansion. Total gross extraction increased from 252 million tonnes in 2013 to approximately 318 Mt in 2020 (Montani, 2021), representing a 26% growth. This study focuses on industrial processing residue, specifically that generated during the transformation of raw blocks into slabs. This waste volume totaled 63.5 Mt in 2020 (Montani, 2021), corresponding to a consistent loss of approximately 41% of the mass of blocks entering the processing phase. Global ornamental stone production remains concentrated within a limited number of countries, China as the undisputed global leader in extraction volume ($\approx$ 98 million metric ton), followed

by India (≈ 44 Mt), Turkey (≈ 28 Mt), and Brazil (≈ 19 Mt), among others. Bringing to Espírito Santo, only 15 municipalities produced 71,200 t (Centrorochas, 2025) of finished slab, leading to 29,000 t of OSR in the last year.

Consequently, this investigation concentrates on the residue generated during this second phase, which occurs after the extracted blocks are transported to processing facilities—typically located in urban areas. In these facilities, the blocks are sawed into slabs with thicknesses ranging from 8 to 30 mm (Fig. 2.16), primarily intended for architectural and building finishes.



(a) Detail of a high-gloss polished exotic so-called commercially “quartzite slab” displayed vertically.



(b) Finished stone slabs, commercially known as granite, stored for export

Figure 1.1: Typical polished slabs from the Ornamental Stone Industry (OSI) at a processing plant in Espírito Santo, Brazil (Photo: Prandina, 2015)

This doctoral research proposes to evaluate the properties of these two primary materials from a geotechnical engineering perspective, focusing on their application in

embankment and pavement layers, including the subgrade, subbase, and base course. The literature review indicates, for example, that the residues of the cutting of marble blocks increase the stiffness and mechanical properties of clayey soils, while the residues of the cutting of granite blocks effectively reduce the spaces in the soil mixtures, improving their bearing capacity and the stability of the original soil. Key parameters such as Optimum Moisture Content (OMC) and Maximum Dry Density (MDD) exhibit favorable trends, suggesting enhanced compaction characteristics when using Ornamental Stone Residue (Prandina & Farias, 2026).

It is important to emphasize the potential of using Espírito Santo industrial residues to promote environmentally efficient construction practices, addressing theoretical and engineering challenges in predicting the behavior of works when applying OSR and steel slag in infrastructure projects such as embankments and pavements. This investigation examines the utilization of OSR from stone processing as a viable material for the construction of roadway infrastructure (embankments and pavements), whose results and conclusions might extend to dams, landfills, and tailings dams, among other geotechnical structures, comparing it with other residues, especially steel slag (SS), from a geotechnical standpoint.

The research in this doctoral thesis addresses the current gap in comprehensive data on the behavior of OSR in embankments and pavement layers and outlines a methodology to evaluate its mechanical properties mixed with different soils adopted in these projects. The mechanical behavior of soil mixtures containing OSR, SS-LD and KRS for use in embankments, subgrades, subbases, and base course layers is analyzed. This analysis employs a suite of laboratory tests to characterize the samples physically, geotechnically, mechanically, and to evaluate how the properties and behavior of the original soil are altered by mixing these residues.

The testing program included geotechnical characterization, featuring compaction tests, specifically analyzing Maximum Dry Density (MDD) and Optimum Moisture Content (OMC), and the California Bearing Ratio (CBR), as well as mechanical evaluations through Cyclic Loading Triaxial Tests (CLTT) and Unconfined Compression Strength (UCS). The addition of SS-LD, KRS, and OSR to soils produced a range of different mechanical behaviors in the resulting composite materials, which can be referred to as geomaterials.

These findings may stimulate the commercial use of OSR in pavements in Espírito Santo and other Brazilian states, particularly in urban and rural areas near these industrial centers. This is supported by Brazilian environmental regulations, which have established provisions for the utilization of recycled aggregates—especially non-toxic materials such as the different combinations of LD-SS, KRS, and OSR mixed with natural soils in infrastructure projects.

At the core of this research is the provision of a comprehensive vision of how OSR and

the steel slags affect the geotechnical properties of soil mixtures—such as density, plasticity, strength, and stiffness—and their performance as chemical binders for soil mixtures and fillers.

By synthesizing current knowledge and practical applications, this study aims to demonstrate the technical feasibility and engineering relevance of integrating OSR into road construction, mirroring the successful global adoption of steel slag. Beyond immediate waste management and resource conservation, this research advocates for a fundamental shift in pavement engineering: the transition from traditional empirical metrics, such as the California Bearing Ratio (CBR), toward the mechanistic-empirical (M-E) paradigm established by the MeDiNa framework. While this transition imposes a higher degree of scientific complexity—demanding a robust understanding of the resilient behavior of non-traditional geomaterials—it represents a necessary evolution in infrastructure design. This effort is empowered by the widespread availability of advanced computational tools, including machine learning and artificial intelligence, which facilitate the handling of complex material characterization and performance prediction, aligning sustainable development with modern engineering precision

1.2 - CONTEXT AND JUSTIFICATION

The growing demand for infrastructure in Brazil, coupled with the necessity for more sustainable construction practices, drives the search for alternative materials with lower environmental impacts. The state of Espírito Santo, home to prominent SIND and OSI hubs, generates a significant volume of industrial processing waste. If not managed properly, these residues represent environmental liabilities and a significant waste of resources. Steelmaking slags already have a proven track record of successful application in geotechnical works within the state—particularly SS-LD, whose various commercial names are linked to specific treatments for volumetric expansion control—demonstrating both technical and economic feasibility (Prandina & Farias, 2025a). OSR, conversely, shows similar potential but remains largely underutilized.

This research builds upon three primary pillars:

Sustainability and Circular Economy: Incorporating OSR, SS-LD, and KRS into pavement and embankment projects transforms an environmental liability into an engineering asset. This practice reduces the demand for non-renewable natural resources, such as sand and gravel, lessens the pressure on sanitary landfills and industrial waste sites, and aligns with circular economy principles, where the byproduct of one industry serves as the raw material for another.

Economic and Technical Feasibility: The procurement and transportation of natural aggregates constitute a significant portion of infrastructure budgets. The abundant local

availability of OSR, SS-LD, and KRS in Espírito Santo presents a clear opportunity for cost reduction, especially for projects located near industrial generation hubs. From a technical standpoint, different studies as demonstrated by Prandina & Farias (2025a)—including the preliminary results conducted within the scope of this research—indicate that these residues can significantly improve the geotechnical properties of local soils. These enhancements include increased bearing capacity—evidenced by higher Maximum Dry Density (MDD) and California Bearing Ratio (CBR) values—and improved stiffness (Resilient Modulus), rendering them technically competent materials for various applications.

Innovation and Regional Development: Comprehensive research into the behavior of these geomaterials, including novel mixtures never designed or tested, and their integration into modern mechanistic-empirical design methodologies, such as MeDiNa, addresses a crucial knowledge gap. Generating technical data and proposing constitutive models for these non-conventional mixtures fosters innovation in geotechnical and pavement engineering, empowering engineers to design more optimized, safe, and cost-effective solutions. Furthermore, validating the use of these materials promotes a regional production chain, adding value to waste products and encouraging industrial symbiosis.

Therefore, this thesis addresses the urgent need to develop and validate engineering solutions that are simultaneously economically viable, technically robust, and environmentally responsible, utilizing the resources and byproducts available within the regional context of Espírito Santo.

1.3 - PROBLEM

Despite the evident potential of Ornamental Stone Residue (OSR) and the increasing application of steelmaking slags, their systematic and optimized utilization in geotechnical works—particularly in structural pavement layers—faces significant hurdles that constitute the central problem of this research. This problem can be decomposed into the following interconnected issues:

I. Lack of a Systematized Approach for Waste-Based Design: A gap exists in systematized knowledge regarding how to approach and test OSR and steelmaking slag for geotechnical applications. According to Prandina & Farias (2025a), several strategies can integrate these residues into projects, expressed by the following concepts for minimum, optimum, and maximum waste content:

(a) Soil-Residue Content Zero (SRC-0): a minimum residue content, which does not change the engineering parameter for less than 5% from the natural condition, or the minimum waste content that causes no alteration in performance or the primary studied parameter.

(b) Optimum Residue Content (ORC): The optimum residue content that maximizes positive performance alterations relative to the primary studied parameter.

(c) Maximum Residue Content (MRC): The maximum residue content that maximizes residue utilization at the limit of performance alteration relative to the primary studied parameter.

(d) Zero-Equivalent Residue Content (Zero-E): The amount of residue content, which can be greater or smaller than MRC, which takes the geotechnical parameter to the performance of the natural soil present in the mixture.

II. **Incomplete Parametric Mapping within Standardized Geotechnical Frameworks:** Standardized geotechnical protocols and testing methods are well-established for conventional paving materials; however, their systematic application to interpret the mechanistic behavior of alternative geomaterials, specifically OSR and steelmaking slag blended with regional soils, remains fragmented. The existing standardized frameworks have not been deployed to map the high inherent variability of these industrial residues stemming from diverse geological origins and processing phases in Espírito Santo. Consequently, there is a scarcity of regional baseline parameters required for modern pavement design, such as the Resilient Modulus (M_R) and permanent deformation trends under varying moisture and compaction states. Without this targeted application of standard testing protocols, the use of these coproducts remains tied to local empiricism rather than a fully quantified, standardized geotechnical response.

III. **Lack of Model Calibration and Parameterization for Mechanistic-Empirical (M-E) Design:** Modern mechanistic-empirical pavement design frameworks, such as MeDiNa (Método de Dimensionamento Nacional), rely on pre-existing constitutive equations to simulate structural performance. The critical gap lies not in the absence of mathematical models, but in the fact that these established behavioral models have not yet been calibrated or validated for non-conventional mixtures incorporating OSR and steelmaking slag from Espírito Santo. This lack of specific statistical parameterization (the regression k-coefficients) prevents engineers from rationally integrating these alternative materials into the MeDiNa workflow. As a result, their application is frequently restricted to legacy empirical methods (such as the CBR method) that fail to capture or exploit the true structural and resilient potential of the developed mixtures.

IV. **Uncertainty Regarding Interaction and Synergy Between Different Residues:** While steelmaking slag is already in use and OSR is studied in isolation, there is a lack of investigation into the behavior of mixtures that combine both residues with local soils. The synergistic or antagonistic interaction between the physicochemical properties of OSR (fine-grained, siliceous/calcareous) and slag

(granular, cementitious) remains unknown. Therefore, the problem also lies in the inability to design optimized "geomaterials" that combine different residues to achieve superior mechanical properties or to meet diverse engineering requirements (e.g., a high-stiffness base course versus a subbase with filter/drainage functions).

V. **Absence of a Mandatory System and Regulation for the Compulsory Use of Viable Industrial Waste** No institutionalized legal system currently mandates or incentivizes through regulations the use of residues, such as SS and OSR, in infrastructure projects.

Ultimately, the research addresses the lack of a techno-scientific framework for the safe, predictable, and optimized utilization of SS-LD, KRS, and OSR of Espírito Santo most prevalent industrial clusters. By focusing on mechanistic-empirical principles, this study seeks to bridge the gap between comprehensive geotechnical characterization and the practical integration of these residues into modern pavement and embankment design.

Given the context outlined above, the primary questions this work seeks to address are:

- **Question 1:** To what extent can the proposed framework of specific thresholds—namely Optimum Residue Content (ORC) and Maximum Residue Content (MRC)—be validated as a reliable methodology for the design of soil mixtures using SS-LD, KRS, and OSR?
- **Question 2:** How do the inherent variability and the physicochemical interactions between different industrial residues (granular slags and silty OSR) influence the constitutive parameters required for Mechanistic-Empirical (M-E) design, such as Resilient Modulus (M_R) and Permanent Deformation?
- **Question 3:** Is it possible to develop optimized "geomaterials" by combining synergistic residues that outperform traditional natural aggregates while remaining compliant with the performance requirements of the MeDiNa design workflow?
- **Question 4:** How can a geotechnically "inert" and non-cohesive silty residue (classified as A-4 by TRB) act as a performance enhancer when integrated into binary or ternary mixtures of SS-LD, KRS, and regional soils?
- **Question 5:** To what extent does the methodological focus on determining the **Optimum Residue Content (ORC)** reveal synergistic interactions between industrial residues from distinct clusters that are not predictable by traditional empirical characterization methods?

1.4 - OBJECTIVES

General Objective: To develop a robust technical-scientific framework for the sustainable utilization of Ornamental Stone Residues (OSR)—categorized by mineralogical and geological

origin—and steel industry slags (SS-LD and KRS) as high-performance geomaterials for infrastructure. This framework integrates advanced geotechnical characterization with mechanistic-empirical (M-E) modeling for pavement design and an optimization methodology for embankments and final layers. By applying the Optimum Residue Content (ORC) approach, the research aims to meet and exceed existing regulatory requirements while leveraging the technical autonomy granted by modern infrastructure standards.

Specific Objectives:

I. **Conduct a Comprehensive Literature Review:** Systematize the state-of-the-practice and state-of-the-art regarding the geotechnical application of OSR and steelmaking slags. This review focuses on the physical, chemical, and environmental characterization of these residues, synthesizing data from recently performed laboratory tests to establish a robust performance baseline. This review introduces a pioneering classification of OSR into marble-based (OSR-M) and granitic/siliceous-based (OSR-G) categories (including Granite, Gabbro, and Gneiss). It further examines Brazilian standards, specifically DNIT 108/2009-ES , and incorporates the critical updates from Errata 1/2025 regarding designer autonomy in embankment layer thickness. The study also examines other current Brazilian standards, regional residue characteristics from Espírito Santo, and critical pavement design parameters—such as OMC, MDD, CBR, Resilient Modulus (M_R), and permanent deformation— of different soil-residue mixtures.

II. **Develop and Validate the ORC Optimization Framework:** Analyze the experimental results through the lens of the Optimum Residue Content (ORC). This objective aims to demonstrate that a specific, ideal blending ratio exists for each residue type that maximizes soil performance. This framework provides a standardized methodology to predict the "optimal point" for enhancing any soil type using these three industrial residues, transitioning from empirical trial-and-error to a rational engineering approach.

III. **Establish the ORC Framework for Embankments and Final Layers:** Develop the Optimum Residue Content (ORC) framework to optimize the use of OSR as a primary material. This objective seeks to demonstrate that OSR, particularly in its pure or highly concentrated form, can significantly exceed the minimum requirements of DNIT 108/2009-ES—which mandates $CBR \geq 2\%$ for embankment bodies and $CBR \geq 6\%$ for final layers.

IV. **Evaluate the Mechanical Behavior of Binary Soil-Residue Mixtures:** Execute a laboratory testing program on typical regional soils blended with varying concentrations of individual residues (OSR, or steelmaking slag). This phase aims to

quantify the isolated influence of each residue on the soil's hydro-mechanical response through compaction, California Bearing Ratio (CBR), cyclic loading triaxial tests, Unconfined Compressive Strength (UCS) to characterize resilient modulus (M_R) and permanent deformation.

V. **Assess the Curing Effect on Geomechanical Properties:** Investigate the time-dependent mechanical strength and stiffness evolution of the stabilized mixtures. This involves performing resilient modulus (M_R), at different curing intervals (e.g., 0, 7, and 28 days) to evaluate the progression of pozzolanic or cementitious reactions driven by the incorporated residue KRS, a subject with a scarse number of studies, if none.

VI. **Characterize the Synergistic Behavior of Ternary Mixtures:** Formulate and test ternary blends combining soil, steelmaking slag (KRS) and OSR. This objective focuses on identifying optimum mixture proportions and evaluating their comprehensive hydro-mechanical performance—via compaction, CBR, and advanced cyclic triaxial testing—to determine the combined structural benefits and potential material optimization for pavement layers.

To ensure conceptual clarity and streamline the reading of the experimental program, the primary acronyms and technical abbreviations utilized throughout this research are systematically defined below. Table 1.1 outlines the core non-conventional geomaterials and industrial byproducts investigated in this study, whereas Table 1.2 details the specialized geotechnical, pavement engineering, and microstructural characterization terms.

Table 1.1: Primary acronyms and definitions for core research materials and industrial byproducts.

Acronym	Full Definition and Technical Description
OSR	Ornamental Stone Residue (Resíduo de Rochas Ornamentais)
KRS	Kambara Reactor Slag (Escória do Reator Kambara)
LD-SS	Linze-Donawitz Steelmaking Slag (Escória de Aciaria LD)

To bridge the gap between experimental characterization and practical application, the fulfillment of these objectives will provide a rigorous technical pathway for integrating regional industrial residues into critical infrastructure projects.

Table 1.2: Secondary list of acronyms for geotechnical, pavement engineering, and characterization terms.

Acronym	Full Definition and Technical Description
MeDiNa	Método de Dimensionamento Nacional (Brazilian National Pavement Design Software)
M-E	Mechanistic-Empirical (Methodology for pavement analysis)
M_R	Resilient Modulus (Módulo de Resiliência)
PD	Permanent Deformation (Deformação Permanente)
CBR	California Bearing Ratio (Índice de Suporte Califórnia)
GSD	Grain Size Distribution (Granulometria / Curva Granulométrica)
ORC	Optimum Residue Content (Teor Ótimo de Resíduo)
XRF	X-ray Fluorescence (Fluorescência de Raios-X)
XRD	X-ray Diffraction (Difração de Raios-X)
UCS	Unconfined Compressive Strength (Resistência à Compressão Simples)

By transitioning from traditional empirical methods to the proposed ORC and mechanistic-empirical frameworks, this research establishes the scientific basis required to validate OSR and steelmaking slag as viable, high-performance geomaterials. This approach directly supports the technical autonomy provided by recent regulatory updates, allowing for the design of more resilient and sustainable embankments and pavement structures. To establish the theoretical and regulatory foundation for this investigation, the following chapter provides a comprehensive literature review, detailing the mineralogical, environmental, and geotechnical evolution of these materials.

2 - LITERATURE REVIEW

2.1 - ROADWAY RESIDUE UTILIZATION IN ESPÍRITO SANTO

Across the state of Espírito Santo, Steel Slag (SS) is frequently blended with local soils in proportions ranging from 15% to 80% to pave rural road networks as a low-cost wearing course surface, locally known in Portuguese as "revestimento primário", or literally translated as "primary surfacing". Figure 2.1 illustrates a recently completed roadway segment (as of June 2025) constructed with these specific SS and local soil mixtures. Due to chemical reactions and pozzolanic activity, particularly when interacting with clayey soils, this primary surfacing solution has established itself as an effective alternative for unpaved roads. It has gained widespread popularity for its efficacy in erosion control and high-quality roadbed regularization, achieving performance levels that approach those of conventional asphalt-surfaced pavements. Consequently, there is significant interest among municipal governments in adopting this solution, driving the substantial utilization rates of steelmaking slag currently observed in Espírito Santo.

Since the program's inception, a strategic public-private partnership between the regional steel industry and the state government has facilitated the application of more than 6 million metric tons of SS (Figure 2.1).



Figure 2.1: Age 0 (1 week) of an "unpaved" rural roadway (ES-346, km 5) with SS-soil mixture. Picture data: may/2025

According to ArcelorMittal (2025), this volume has improved approximately 2,000 kilometers of rural and local infrastructure, encompassing nearly 5,000 separate roadways across 60 of the 88 municipalities in Espírito Santo. This initiative has gained significant

momentum in recent years, with record material donations of 1.1 million metric tons in 2022 and 1.24 metric million tons in 2023 (SEAG, 2025). The current regulatory framework establishes municipal-led public works as the primary consumers of the distributed SS. This high utilization rate is driven by the enhanced perception of quality of rural unpaved roads which wearing course have been transformed to ones with acceptable performance (Figure 2.2), leveling paved asphalt wearing courses.



Figure 2.2: Age 1.5 year of an "unpaved" rural roadway (BR-342/ES) with SS-soil mixture. Picture data: out/2024

Furthermore, contemporary state-of-the-practice identifies SS as a high-performance material characterized by exceptional mechanical strength (Kabeta & Lemma, 2023; Zumrawi & Babikir, 2017). Consequently, while its use for soil stabilization is technically effective, higher-value applications such as integration into structural pavement layers- have emerged as more economically and technically attractive engineering alternatives.

The following Table 2.1 consolidates the main milestones and case studies of slag applications in Brazilian roads, going from geotechnical applications of soft soil improvement in subgrades, primary surfacing with SS-soil mixtures of rural unpaved roads, to unbound base layers of highway pavements. The Table 1 offers a synoptic view of the journey of using steel slag aggregates in Brazilian paving.

In the state of Espírito Santo, a historical sequence of SS relevant applications is presented by DER-ES (2019), using the previous technical name of the Linz-Donawitz steelmaking slag (LD-SS) byproduct as "Acerita" (ArcelorMittal, 2016), later named REVSOL (Mendonça & Rodrigues, 2010); several projects have already been carried out using it, including:

- LD-SS applied in 105.3 km (pavement base layer) of the Transcol Project/1983;
- LD-SS applied in 8.6 km (pavement base layer) TIMS/1995;

Table 2.1: Main milestones and case studies of SS applications in Brazil (prepared by the authors)

Location (City/State)	Associated Company / Inst.	Slag Type	Application or Study Focus	Year / Period	Reference
São Domingos do Prata, MG	N/A	N/A	First paving application in Brazil	1978	Souza et al. (2017)
4 cities of ES	CST	Steel	105 km of urban paving (base/subbase)	1983	(DER-ES, 2019)
Ipatinga, MG	Usiminas, DERMG	Steel	"Caminhos do Vale" program, rural roads	2000, 2017, 2021	(Rohde, 2002)
Sapucaia do Sul, RS	UFRGS	Steel (Electric)	Study for base and subbase	2002, 2013	Pinheiro et al. (2015)
Maracanaú, CE	Gerdau, UFC	Steel (EAF)	Soil-slag mixtures (base); Asphalt mixtures	2003, 2004	Pinheiro et al. (2015)
Santa Cruz, RJ	Gerdau-Cosigua	Steel	Study for triple surface treatment	2005	Lanzellotti et al. (2005)
Linhares, ES	Local Steel Mill	Blast Furnace (Raw)	Base and drainage layer on soft soil (5.6 km)	2007	Silva et al. (2007)
Cariacica, ES	ArcelorMittal, Kaeme Consulting	Steel (LD)	"Novos Caminhos" program in urban area, primary surfacing	2010	(Mendonça & Rodrigues, 2010)
Pindamonhangaba, SP	USP	Steel	Study for base and subbase	2013	Pinheiro et al. (2015)
Barro Alto, GO	Anglo American, Ecovias	Iron-Nickel	Test in base of federal highways (BR-153/414/080)	2022	(Anglo American, 2022)
Curvelo, MG	DER-MG	Steel	Recovery of unpaved highway (MG-164)	2022	(SEINFRA, 2025)
Eco 101 Highway, ES	ArcelorMittal, UFES	Steel (Sidercal®)	Use in subbase for highway duplication	2013–2022	(J. E. Teixeira, 2022)

- LD-SS applied in 6.0 km (pavement base and HMA) in the Access to Praia Mole Port/2001;
- pavement 46.0 km (pavement base layer) in streets and avenues of the city of Vila Velha/1989;
- 80.0 km (pavement base layer) in the streets and avenues of Serra/2006;
- Initial drainage layer in the duplication works of Rodovia do Sol (1999-2001);
- Pavement base layer in the Vitória Airport runway (2003-2015);

- Pavement subbase layer and 20 cm base (90% Acerita and 10% clay) for the internal roads of the Serra Multimodal Industrial Terminal (2004);
- Subgrade reinforcement (50% Acerita and 50% clay), 20 cm subbase (Acerita), and 20 cm base (Acerita) at the Steel Products Terminal - ArcelorMittal;
- Pavement base layer (70% Acerita and 30% gravel), subbase layer with 30% Acerita and 70% clayey sand base on highway ES-446, Colatina - Acampamento section, among others.

Even though the majority of the SS volume applied has been in soil mixtures for the purpose of surfacing layer of rural unpaved roads, called in the Brazilian technical terminology as primary surfacing, basically defined as an improved soil layer on the top of an unpaved road (DNIT, 2005) serving as wearing course, in recent years different SS has been researched and applied in this top layer (DNIT, 2023) and in the structural layers of rural and urban road, highway pavements, granting a more appropriate engineering use for a high strength geomaterial.

2.1.1 - REGULATORY OVERVIEW ON THE USE OF RESIDUES IN EMBANKMENTS AND PAVEMENTS

The state-of-the-practice (SOP) is defined as the set of methods, techniques, and standards widely accepted and implemented in the market, proven to be both safe and viable. Geotechnical and pavement engineering SOP in Brazil has undergone a significant evolution, recently transitioning from purely empirical design methods to more robust mechanistic-empirical (M-E) approaches.

Historically, the California Bearing Ratio (CBR) method, developed around 1930, served as the primary tool for flexible pavement design. Consolidated in standards from the former DNER and subsequently DNIT, this method replaces older specifications and establishes systematic procedures for road platform execution.

The CBR method for pavement design relies on empirical correlations that fail to fully capture material behavior under complex traffic loading and environmental variations, although it remains a critical parameter for evaluating subgrades and granular layers within the embankment structure.

The test, standardized by DNIT-ME 172/2016, compares the penetration resistance of a soil to that of a standard crushed stone—theoretically the strongest reference material—to provide a bearing capacity index. From a regulatory and normative perspective, several Brazilian standards address the use of various Steel Slags (SS), primarily focusing on LD Steelmaking Slag (SS-LD) as noted by Prandina (2018a), who presented the list of standardized DNIT guidelines for SS utilization in geotechnical works:

- 113/2009: Artificial Aggregate – Evaluation of SS expansion potential;
- 114/2009: Granular-stabilized subbase with SS - ACERITA®;
- 115/2009: Granular-stabilized base with SS - ACERITA®;
- 406/2017: Granular-stabilized base with Açobrita®;
- 407/2017: Granular-stabilized subbase with Açobrita®;
- NBR 16.364/2015: Execution of granular-stabilized subbase and base with steel aggregate for road pavement.

The commercial names are retained as they appear in the official standards. However, considering the full spectrum of SS types and potential mixtures currently in practice, existing standards cover only a limited range. This suggests a deficient regulatory system that must evolve to ensure the safety of the SOP regarding SS in geotechnical applications. Regarding residue utilization regulations, Brazil possesses a normative framework supporting such applications. The National Solid Waste Policy (Law No. 12,305/2010) establishes shared responsibility and incentivizes waste reduction, reuse, and recycling. Specifically for civil construction, CONAMA Resolution No. 307/2002 (and its updates) classifies waste and sets management guidelines, facilitating the use of materials like recycled aggregates.

Furthermore, ABNT standards such as NBR 15116 specify requirements for recycled aggregates from construction waste for use in concrete pavements. Older DNIT standards, such as DNER ES-303/97 for stabilized bases, already contemplated mixture possibilities, allowing the incorporation of alternative materials provided once they met performance criteria. Finally, in terms of historical records, the first mention of waste in national regulations occurred via IPR (1988), which noted the use of steelmaking slags since the 1970s. Modern updates to these standards, such as the Errata 1/2025 for DNIT 108/2009-ES, now grant designers greater autonomy in determining layer thicknesses based on specific techno-economic and geotechnical performance.

Building upon this regulatory landscape, the code DNIT 108/2009-ES (DNIT, 2025) serves as the definitive standard for the execution of highway embankments, establishing the systematic requirements for materials, quality control, and performance criteria. This regulation specifies that all materials must be characterized and selected through detailed engineering studies, generally prioritizing 1st and 2nd category soils, a group classification for excavable soils with manual or mechanical equipment. According to the standard, the embankment body must maintain a California Bearing Ratio (CBR) of at least 2% and a maximum expansion of 4%. For the final layer, the regulation demands the best possible bearing capacity with expansion limited to 2%, specifically requiring the analysis of at least one design alternative utilizing material with a CBR of 6% or higher.

While these requirements were traditionally prescriptive, Subclause 5.1(e) provides a critical opening for innovation by permitting the use of 3rd category rock materials when

explicitly specified in the engineering project, thereby establishing a legal foundation for the application of high-strength industrial residues. The recent publication of the DNIT 108/2009-ES standard represents a pivotal advancement in this framework, prompted by technical reviews regarding embankment execution over rocky materials. This update modifies Subclause 5.3.12 DNIT 108/2009-ES (DNIT, 2025) to replace rigid thickness constraints with a mandate for professional autonomy. Crucially, the norma DNIT 108/2009-ES stipulates that the total thickness of the final layer must now be determined by the designer through a technical-economic analysis, considering the unique geotechnical conditions of the embankment. This shift toward performance-based design grants engineers the necessary authority to justify the use of OSR and steelmaking slag based on their superior mechanical properties, allowing for the integration of the ORC framework (Prandina & Farias, 2026) into modern, sustainable infrastructure projects.

2.1.2 - REGULATORY LIMITATION ON THE USE OF RESIDUES IN EMBANKMENTS AND PAVEMENTS

A significant technical gap persists within the current regulatory framework, as existing standards (DNIT 114/2009-ES, 115/2009-ES, 406/2017-ES, and 407/2017-ES) provide no specific protocols for the environmental characterization of soil-residue mixtures. While Section 6 of these documents focuses on site-level management—such as covering stockpiles to prevent rainwater interaction—they omit mandatory laboratory testing to evaluate the chemical safety of the final geomaterial.

Nevertheless, this lack of prescriptive testing requirements introduces a high degree of technical subjectivity into the licensing process, leaving environmental assessments open to inconsistent interpretations by regulatory agencies. Because the interaction between residues and regional soils can alter leaching characteristics, pH levels, and pozzolanic reactions, evaluating the resulting compacted mixture is essential for ensuring long-term environmental integrity. Consequently, transitioning from administrative compliance to standardized, performance-based environmental testing of the geomaterial is necessary to mitigate these regulatory shortcomings and provide a reliable scientific basis for large-scale infrastructure applications.

The state of Espírito Santo represents a unique, large-scale "open laboratory" for the longitudinal assessment of leaching behavior in steelmaking slag-soil mixtures. While the current regulatory framework—governed by standards such as DNIT 108/2009-ES, DNIT 114/2009-ES, and DNIT 406/2017-ES—focuses primarily on administrative licensing and operational management, it lacks prescriptive laboratory protocols for the chemical characterization of the final engineered geomaterial.

This gap highlights the scientific importance of the extensive field data available in

the region.The scale of application in Espírito Santo provides an unprecedented dataset for environmental monitoring:Massive Deployment: Since the inception of regional public-private partnerships, over 6 million tons of steelmaking slag (SS) have been applied.Geographical Breadth: The utilization of commercial blends, such as REVSOL (comprising LD-SS and KRS), extends across 60 of the 88 municipalities in the state (ArcelorMittal, 2025). Infrastructure Footprint: Approximately 2,000 kilometers of rural and local roads serve as active leaching sites, providing real-world exposure to diverse climatic and geological conditions.

This "open laboratory" allows for the evaluation of the long-term status of environmental interactions that laboratory leaching tests (such as DNIT 113/2009-ME, which focuses solely on physical expansion) cannot fully replicate. As time passes, the surrounding soil and water tables in these monitored areas offer a definitive assessment of how these geomaterials behave under continuous rainwater interaction and mechanical stress.

By analyzing these in-situ results, researchers can bridge the "regulatory blackout" found in current DNIT and ABNT standards, transitioning from subjective environmental assessments to a data-driven, performance-based understanding of steel slag sustainability in civil infrastructure. Consequently, Espírito Santo's roadways do not merely serve as infrastructure but as a critical scientific baseline for validating the safe, large-scale integration of industrial byproducts into the environment.

2.1.3 - PROPOSAL FOR FUTURE RESEARCH: THE ES OPEN LABORATORY

The extensive application of SS across Espírito Santo—exceeding 6 million tons and covering over 2,000 km of roadways—presents a unique opportunity for a longitudinal *in-situ* environmental study. Current standards, such as DNIT 108/2009-ES and 407/2017-ES, establish protocols for licensing but lack prescriptive testing for the chemical safety of the final soil-residue geomaterial. Future research should utilize this "open laboratory" to:

- Analyze the long-term leaching behavior of **REVSOL** blends (LD-SS and KRS) under real-world climatic conditions.
- Bridge the current regulatory gap by proposing standardized laboratory protocols that characterize the environmental interaction of the mixture rather than the isolated residue.
- Validate the **Optimum Residue Content (ORC)** framework as a predictive tool for both mechanical performance and environmental stability, providing designers with the scientific evidence required to exercise the autonomy granted by **Errata 1/2025**.

2.2 - DESIGN CRITERIA (OR LACK THEREOF): SOIL-RESIDUE CONTENT (SRC)

One of the most significant challenges identified in the current state-of-the-practice is the lack of a systematized approach to mixture design using residues. Traditional design relies

on fixed proportions (e.g., 90/10 mixtures), which fail to account for the inherent variability of industrial byproducts. To address this, current research proposes a performance-based framework centered on specific content thresholds.

The concept of Optimum Residue Content (ORC) is defined as the specific percentage of residue that maximizes a target geotechnical parameter, such as the Resilient Modulus (M_R) or Maximum Dry Density (MDD). Conversely, the Maximum Residue Content (MRC) represents the highest proportion of residue that can be incorporated while still meeting the minimum engineering criteria for a specific pavement layer. This differentiation is critical for project economic viability; if the goal is to maximize waste diversion (e.g., for environmental credits or landfill reduction), the designer seeks the MRC. If the goal is superior performance for heavy loads, the ORC is targeted.

The BR-262 duplication project in the mountainous region of Espírito Santo serves as a contemporary case study for the necessity of these criteria. This R$ 8.6 billion project involves 180 kilometers of road, 50 viaducts, and 4 tunnels through challenging terrain. The scale of this project requires substantial volumes of stable fill material. Utilizing SS-LD, KRS, and OSR in these embankments—leveraging their high mechanical strength and durability—could significantly reduce the need for rock blasting and natural soil borrow pits. However, without standardized ORC and MRC guidelines, the risk of non-uniform behavior in these complex mountainous stretches remains a barrier to full-scale adoption.

The transition from traditional empirical metrics toward the performance-based paradigm of the National Pavement Design Method (MeDiNa) requires a shift in how alternative materials are evaluated. For unbound layers, the Resilient Modulus (M_R) replaces the CBR as the primary input for characterizing structural response. However, a meta-analysis of current literature reveals a significant inconsistency in the results of waste-soil stabilization.

Variations in MDD and OMC are directly related to OSR proportions and the inherent properties of both soil and residue (Teixeira et al., 2017; Mello, 2019). When OSR provides particle size gradation complementation, MDD increases and OMC decreases (Sivrikaya et al., 2014). However, a systematic review synthesized in Table 2.2 indicates that only 8 out of the 14 analyzed studies (57%) report immediate mechanical gains in the MDD parameter, which indicates CBR gains. This apparent lack of consensus stems from a frequently overlooked nonlinear behavior, confirming that the effective use of OSR depends on a judicious adjustment of the residue-to-soil ratio and the selection of compaction energy (Aguiar, 2019; Nascimento, 2019). It is argued that the absence of improvement in the remaining 43% of cases is typically due to testing residue proportions situated outside the “performance window”. Conversely, the adoption of a strategy that systematically seeks the Optimum Residue Content (ORC) ensures mechanical gains in 100% of applications by optimizing particle packing and void filling (M. B. O. Dias, 2024; L. A. Silva & Isewaki, 2018).

Table 2.2: Comparative summary of geotechnical properties and compaction behavior of soils and OSR-Soil Mixtures.

#	OSR Type / Study Reference	Comp. Energy	Soil MDD	Soil OMC (%)	Soil Type	OSR %	Mixture MDD	MDD Gain (%)
1	Aguiar (2019) OSR Paulista-PE	S	15.5	22.0	High-plasticity Clay (CH/A-7-5)	30, 40, 50	N/A	N/A
2	Araújo (2018) OSR-M Caraúbas/RN	S, I, M	17.6	15.6	Clayey Sand (SC/A-2-6)	2, 5	19.5 (at 2% OSR, M.E.)	11
3	Araújo (2018) OSR Parnamirim/RN	S	15.4	22.0	High-plasticity Clay (CH/A-7-6)	11.1, 25, 42.8	16.2 (at 42.8% OSR)	5
4	Braz (2024) OSR, Vitória ES	S	20.5	8.7	Silty Sand (SM/A-2-4)	10, 20, 30, 50	20.35 (at 10% OSR)	-1
5	Jaffar et al. (2022) OSR-M Pakistan	S	17.1	14.5	Low-plasticity Clay (CL/A-6)	3, 5, 7, 9, 11, 13	18.8 (at 9% OSR)	10
6	Braz (2024) OSR, Vitória ES	S	17.3	19.0	High-plasticity Silt (MH)	25, 50, 75	16.7 (at 25% OSR)	-3
7	Lunz (2021)	S	20.5	10.0	Clayey Sand (SC)	25, 50, 75	18.9 (at 25% OSR)	-7
8	Marques, Costa Farias, & Moraes Garcia (2019) OSR Maceió, AL	S	19.1	12.0	Sandy Soil (A-2-4)	5, 10	N/A	N/A
9	Mello (2019) OSR-M Cajazeiras, PB	S	18.5	14.5	Silty Sand (SM/A-2-4)	5, 10, 15, 20, 25	18.2 (at 5% OSR)	-2
10	Nascimento (2019) OSR Campina Gr., PB	S	17.2	17.5	Silty Sand (SM/A-2-4)	5, 10, 15, 20, 25	18.1 (at 20% OSR)	5
11	T. Oliveira (2015) OSR São Paulo	S	16.5	19.0	Clayey Sand (SC/A-2-6)	10, 20, 30, 50	17.5 (at 50% OSR)	6
12	A. Cardoso (2019a) OSR Paraná	S	14.4	28.1	High-plasticity Clay (CH/A-7-5)	3, 5, 7, 9	15.2 (at 7% OSR)	6
13	Farias et al. (2018a) OSR, Maceió AL	S	19.4	10.7	Sandy Soil (A-2-4)	20, 30, 40, 50	20.96 (at 50% OSR)	8
14	Pequeno (2020) OSR Campina Gr., PB	S	14.8	24.6	Bentonite Clay (CH/A-7-5)	10, 20, 30	15.5 (at 30% OSR)	5

Note: MDD units are in kN/m^3. $Abbreviations for compaction energies: S = Standard; I = Intermediate; M = Modified.$

This non-linear relationship is clearly evidenced in the study by Jaffar et al. (2022), who investigated an A-6 clay soil mixed with **OSR-M** (3% to 13% by dry weight). Their results showed that the M_R increased progressively from 270 MPa at a 3% addition rate to a

pronounced peak of 546 MPa at a 9% addition rate—effectively doubling the stiffness. Beyond this threshold, the stiffness declined to 384 MPa at 13% content.

As shown in Figure 2.3, this "bell-curve" behavior, or a non-linear parabolic trend, confirms that **OSR** improvement is driven by a chemical and physical optimization: the calcium-rich residue induces flocculation of clay particles and promotes cementitious bonds, but an excess of fine particles eventually compromises the granular skeleton.

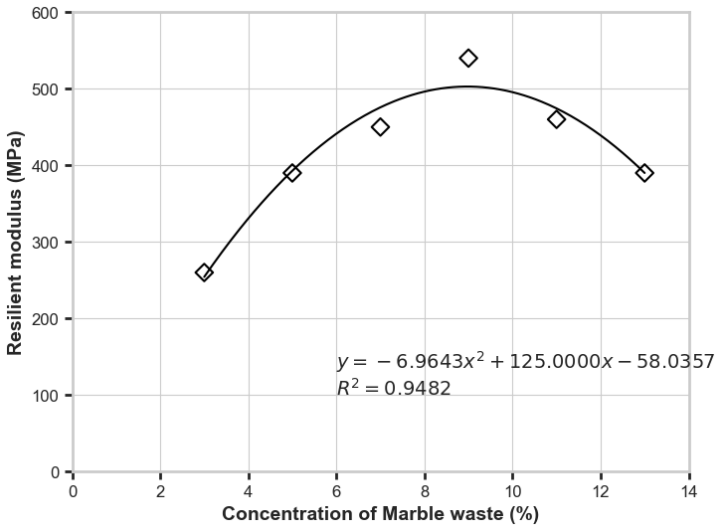


Figure 2.3: Effect of OSR-M content on the MR of an A-6 soil (from Jaffar et al., 2022).

To formalize this behavior into a design tool, the research introduces a comprehensive Soil-Residue Content (SRC) framework. The thresholds are defined as follows:

- SRC-0: The natural soil condition with no residue.
- Minimum Residue Content (MiRC): The lowest percentage of residue that produces a change in the engineering parameter of less than 5% relative to the natural condition.
- Optimum Residue Content (ORC): The specific percentage that maximizes the target parameter, such as M_R or MDD.
- Maximum Residue Content (MRC): The highest proportion of residue that can be incorporated while still meeting the minimum engineering criteria for a specific pavement layer.
- Zero-Equivalent Residue Content (Zero-E): The residue content that takes the geotechnical parameter to the performance level of the natural soil present in the mixture.

As illustrated in Figure 2.4, for the M_R data from Jaffar et al. (2022), the ORC is identified at 8.23%, the MRC at 14.9%, and the Zero-E at 17.4%. This behavior is consistent with the findings of Eltwati et al. (2020), who stabilized high-plasticity clay with granite dust and identified a clear peak at approximately 8.6% **OSR**.

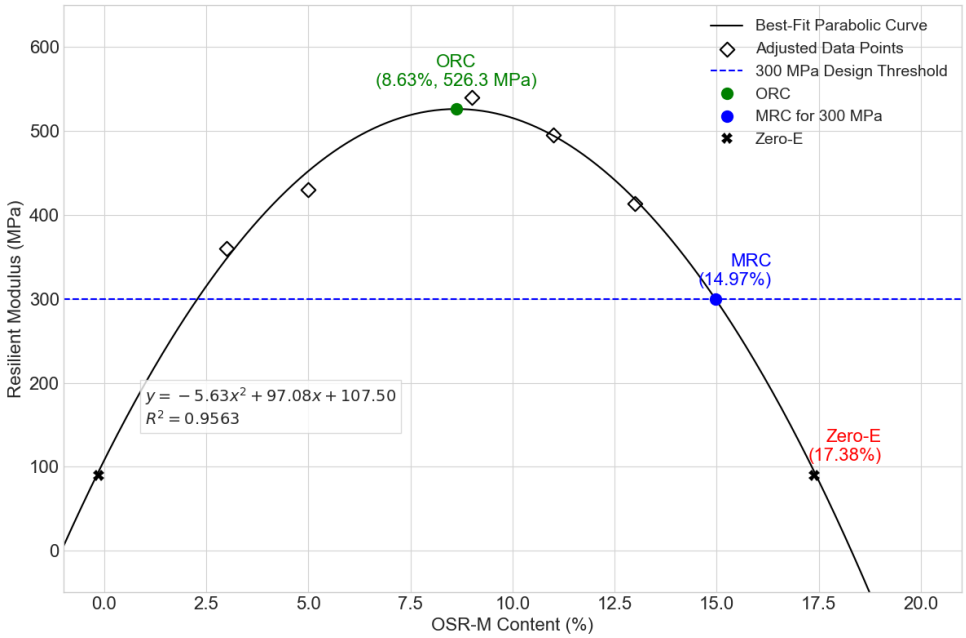


Figure 2.4: Hypothetical curve of OSR content effect on the MR to present the design concepts of soil-residue content (SRC): ORC, MRC, Zero-E, and SRC-0.

This differentiation is critical for project economic viability. If the primary goal is environmental—maximizing waste diversion—the designer seeks the MRC. However, if the goal is superior structural performance for heavy traffic loads, the ORC must be the target. By defining these thresholds, the "model blackout" is replaced by a rational engineering approach that supports predictable performance gains across the evaluated applications.

2.3 - REALITY: STILL IN TRANSITION FROM CBR TO MEDINA

The Brazilian paving industry is in the midst of its most significant technological shift in seventy years: the move from the empirical **California Bearing Ratio (CBR)** method to the mechanistic-empirical **National Pavement Design Method (MeDiNa)** (Prandina & Farias, 2025). Historically, CBR (developed c. 1930) was the primary metric for defining the quality of subgrades and bases. It is a simple penetration test that provides an index of resistance compared to standard crushed stone. However, the CBR is a static test and cannot predict the elastic response or the accumulation of plastic strain under millions of dynamic wheel load repetitions (Souza et al., 2022). MeDiNa models the pavement as a multi-layer elastic system where the fundamental material input is the **Resilient Modulus** (M_R). The M_R is defined by the ratio of cyclic deviator stress (σ_d) to the recoverable axial strain (ϵ_r).

For industrial residues, this transition is particularly impactful. Research shows that mixtures of soil and slag can exhibit “stiffness-increasing” behavior, where the material becomes stiffer as confining pressure increases, a phenomenon that the CBR test cannot capture (Magalhaes et al., 2017). The transition to MeDiNa allows engineers to accurately account for

the superior stiffness (M_R) of KRS and SS-LD mixed with Espírito Santo soils, which often outperform traditional cement-stabilized solutions in terms of fatigue resistance (Pires et al., 2019).

Table 2.3 consolidates the minimum performance requirements for the primary geomaterials employed in roadway infrastructure, as established by current DNIT standards. The data is hierarchically organized by pavement layer—moving from the upper to the lower structural components (**Base** $\rightarrow$ **Subbase** $\rightarrow$ **Primary Coating** $\rightarrow$ **Subgrade Improvement** $\rightarrow$ **Embankment**)—and further categorized within each group by material origin, following the sequence: **Natural Materials** $\rightarrow$ **Acerita®** $\rightarrow$ **Açobrita®** $\rightarrow$ **Processed Mixtures**.

Historically, DNIT normalized the use of LD (Linz-Donawitz) steelmaking slags under the commercial designations of Acerita® and Açobrita®. These materials are specifically treated to mitigate their expansive potential, addressing the volumetric instability inherent in raw, untreated LD slag.

Table 2.3: Consolidated minimum performance requirements for roadway layers according to DNIT standards.

DNIT Standard	**Layer**	**Material**	**CBR (%)**	**Exp. (%)**	**MR (MPa)**
141/2022-ES	Base	Natural Soil	$\geq 80^a$	≤ 0.5	Charact.
115/2009-ES	Base	Acerita®	> 60	$< 1.5^*$	≥ 300
406/2017-ES	Base	Açobrita®	≥ 80	$< 3.0^\dagger$	≥ 300
142/2022-ES	Base	Soil-Cement	$\geq 20^b$	≤ 1.0	Charact.
139/2010-ES	Subbase	Natural Soil	≥ 20	≤ 1.0	Charact.
114/2009-ES	Subbase	Acerita®	> 20	$< 1.5^*$	Charact.
407/2017-ES	Subbase	Açobrita®	≥ 20	$< 3.0^\dagger$	Charact.
140/2010-ES	Subbase	Soil-Cement	$\geq 20^b$	≤ 1.0	Charact.
445/2023-ES	Primary Coat.	Natural/Rec.	≥ 20	≤ 2.0	N/A
422/2019-ES	Subgrade Imp.	Soil-Lime	Designer^c	$\leq 2.0^d$	Designer^c
108/2009-ES	Final Layer	Soil 1st/2nd Cat	≥ 6	≤ 2.0	N/A
108/2009-ES	Emb. Body	Soil 1st/2nd Cat	≥ 2	≤ 4.0	N/A

Note:
^{a} For low traffic volume ($N \leq 5 \times 10^6$), a minimum CBR of 60% is permitted.
^{b} Value for natural soil before cement addition. Final mixture evaluated by UCS and durability.
^{c} Parameters defined by the designer; no fixed minimum for the mixture. UCS testing is mandatory.
^{d} Refers to the natural soil before lime addition (Item 5.1.1).
* Expansion by DNIT 113/2009-ME. Standard also limits DNER-ME 129/94 expansion to 0.5% (Base) and 1.0% (Subbase).
† Potential expansion average of 3 specimens (DNIT 113/2009-ME).
Charact. = MR determination is mandatory for mechanistic-empirical characterization.

Notably, however, Acerita® has largely fallen into disuse in recent years. This technological shift occurred as the generating plant transitioned from original stabilization

methods to a contemporary mitigation strategy. This current approach involves managing the expansive behavior of untreated LD slag by blending it with a specialized set of other industrial residues, most notably KRS, leading to the development of modern hybrid recycled aggregates.

The interpretation of Table 2.3 highlights a transitional phase in Brazilian roadway regulations, exposing what can be characterized as a "hybrid system" of technical compliance. Although the country has advanced toward mechanistic-empirical (M-E) design with the implementation of the MeDiNa method, DNIT service specifications (ES) maintain a profound reliance on the CBR as the primary parameter for material acceptance.

From the embankment body to the base layer, the **CBR** remains the absolute technical "gatekeeper". Even for modern industrial residues such as Acerita® and Açobrita®, field viability is not initially dictated by elastic or resilient performance, but rather by meeting a minimum **CBR** threshold (ranging from $\geq$ 80% for bases to $\geq$ 2% for embankments). This regulatory persistence creates a paradox: the material is designed based on its **Resilient Modulus (**M_R**)**, yet its "birth certificate" at the construction site and subsequent contractual measurement still depend on a static penetration test developed in the 1920s.

The analysis of all standards consolidated in Table 2.3 reveals a complete absence of performance references regarding **permanent deformation (PD)** for materials individually. While M_R is now featured as a mandatory characterization item in recent standards—such as DNIT 141/2022 and 142/2022—there are no established cutoff values, performance classes, or "shakedown" criteria to limit the propensity of the material to accumulate plastic strain under cyclic loading.

This gap indicates that current normalization delegates the control of rutting exclusively to the structural analysis of the entire pavement within the design software. Consequently, the material as an isolated input is not strictly tested for its long-term mechanical stability. For academic research and the large-scale use of steelmaking slags and OSR, this scenario underscores a critical opportunity: the need to characterize these materials beyond standard requirements, bridging the void between static resistance (**CBR**) and accumulated deformation to ensure that high support capacity does not mask a vulnerability to permanent deformation.

2.3.1 - MECHANICAL STABILIZATION AND NORMATIVE CRITERIA

According to DNIT 141/2022–ES, mechanical stabilization (*estabilização granulométrica*) is defined as the "process of improving the characteristics of *in-natura* soils by adding one or more materials to achieve a final mixture with adequate stability and durability properties." It is essential to emphasize the technical choice of the term *mixture* (*mistura*) to describe the blend of materials. In this research, the terms "mixture" and "mixed" are used extensively to maintain terminological alignment with Brazilian technical standards while avoiding literal translations

that might fail to reflect the engineering context of soil-residue blending.

The normative framework for natural soils (DNIT 141/2022) establishes a significant precedent regarding material acceptance: performance criteria—specifically CBR and expansion—take precedence over rigid grain-size distribution limits. In practice, a soil mixture that falls outside the standardized gradation ranges (A through F) may still be approved for construction, provided it demonstrates compliance with the required mechanical thresholds. The comparative granulometric requirements and the specific envelopes for natural soils and treated slags are detailed in Table 2.4.

However, a comparative analysis reveals a clear regulatory inconsistency when dealing with industrial by-products. While natural soil standards prioritize performance, the specifications for steelmaking slags, such as Acerita® (DNIT 115/2009) and Açobrita® (DNIT 406/2017), appear to strictly mandate obedience to the established granulometric envelopes.

Table 2.4: Consolidated granulometric requirements for Base layers (Natural Soil, Acerita®, and Açobrita®).

Sieve (mm)	**DNIT 141/2022 (Soil Mixture)**		**DNIT 115/2009 (Acerita)**		**DNIT 406/2017 (Açobrita)**	
	Ranges A-D	**Ranges E-F**	**Range A**	**Range B**	**Range A**	**Range B**
50.8 (2")	100	100	—	—	100	100
25.4 (1")	75 – 100	100	100	100	100	100
9.5 (3/8")	30 – 100	100	50 – 85	60 – 100	30 – 65	40 – 75
4.8 (Nº 4)	25 – 85	85 – 100	35 – 65	50 – 85	25 – 55	30 – 60
2.0 (Nº 10)	15 – 70	75 – 100	25 – 50	40 – 70	15 – 40	20 – 50
0.42 (Nº 40)	8 – 45	40 – 100	15 – 30	25 – 45	8 – 20	10 – 30
0.074 (Nº 200)	2 – 25	10 – 45	5 – 15	10 – 25	2 – 8	4 – 12

Notes: DNIT 141 (Soil) ranges A-D refer to traffic $N > 5 \times 10^6$ and E-F to $N \leq 5 \times 10^6$. For Acerita (115) and Açobrita (406), the values represent the final stabilized mixture as specified in the service standards.

This rigid requirement might pose a significant barrier to the optimization of new geomaterials. As demonstrated in this study, the incorporation of KRS dust acted as a "performance champion," elevating the Resilient Modulus (M_R) to levels exceeding 500 MPa. Such high-performance results were achieved through the chemical and physical interaction within the mixture, regardless of whether the final gradation strictly aligned with traditional soil envelopes. This evidence suggests that the "performance-over-gradation" logic applied to natural soils should be extended to industrial residues, fostering a more technical and less

prescriptive approach to sustainable pavement engineering.

2.3.2 - THE OBSOLESCENCE OF PRESCRIPTIVE RIGIDITY: THE ESPÍRITO SANTO CASE STUDY

The transition of DNIT standards toward obsolescence was primarily accelerated by the excessive industrial control required for specific granulometric parameters. These requirements demanded prohibitive investments in particle separation and processing, creating a disconnect between regulatory theory and economic reality. In the State of Espírito Santo, however, engineering practice effectively superseded national regulations. Over the past decade, more than 6 million tons of steelmaking and ironmaking by-products—specifically LD and KR slags—were successfully deployed as primary surface wearing courses for rural roads.

This widespread application exposed a significant regulatory paradox. While DNIT provides minimal normative requirements for primary surfacing, lacking both mechanistic analysis and strict layer thickness control, the field performance of these developed slag mixtures earned the trust of the local population and consecutive state administrations. For over ten years, these materials were applied based on "good engineering practice," rooted in an empirical approach that, demonstrating substantial practical efficacy in regional corridor stabilization.

The success of this empirical implementation is corroborated by current evidence, including 2025 and 2026 media reports and recent public tenders exceeding R$ 40 million earmarked for the maintenance of these primary wearing courses. This scenario demonstrates that field-proven performance has effectively marginalized the existing prescriptive framework, highlighting a critical need for a performance-based regulatory update that acknowledges the structural contribution of industrial by-products even in lower-requirement applications.

2.3.3 - MECHANISTIC CHARACTERIZATION OF PAVEMENTS: RESILIENT MODULUS (M_R)

The transition to a mechanistic design philosophy requires a thorough understanding of the stress-dependent behavior of geomaterials (Prandina & Farias, 2026). State-of-the-art pavement design has consolidated the use of the **Resilient Modulus (M_R)** to characterize the elastic response of road layers; and laboratory determination through **Cyclic Load Triaxial Tests (CLTT)** allows for the calibration of constitutive models such as the "Universal Model" (Ooi et al., 2004):

$$M_R = k_1 \cdot p_a \cdot \left(\frac{\theta}{p_a}\right)^{k_2} \cdot \left(\frac{\tau_{oct}}{p_a} + 1\right)^{k_3} \tag{2.1}$$

Where θ is the bulk stress, τ_{oct} is the octahedral shear stress, and p_a is the atmospheric pressure (reference stress).

With the advancement of pavement mechanics, the Resilient Modulus (M_R) has emerged as a fundamental parameter, as it measures the elastic stiffness of the material under cyclic loading, simulating traffic action in a more realistic manner. The M_R is a critical input for mechanistic-empirical (M-E) models, which serve as the foundation for computational design tools such as AASHTOWare Pavement ME Design and MeDiNa, aiming to predict pavement performance over time (Prandina, 2025).

The Brazilian standard DNIT 134/2018-ME establishes the procedure for laboratory M_R determination, aligning national practices with international standards such as AASHTO T 307-99. A comparative analysis of these protocols (Prandina, 2025) reveals philosophical differences in the applied stress sequences. The Brazilian standard specifies a conditioning phase with significant deviatoric stresses, whereas the AASHTO standard begins with a pure confinement condition ($\sigma_3 > 0, \sigma_d \approx 0$). This distinction is pivotal, as low deviatoric stress states in the AASHTO protocol are especially important for isolating the effect of confining stress on stiffness and for the robust calibration of constitutive models.

M_R values are utilized in structural analysis models to calculate pavement response under wheel loads and within pavement design procedures. The test facilitates the characterization of pavement construction geomaterials under various environmental and physical conditions (e.g., moisture content and density). Furthermore, the standard distinguishes between **Type 1 Material**—generally comprising granular base/subbase materials and subgrade soils with low fines content and low plasticity index—and **Type 2 Material**, a distinction that directly influences the required specimen dimensions. The present research studies soil mixtures with different residues for base, subbase, and subgrade applications, therefore encompassing both groups of geomaterials.

A precise definition of the stress states within the triaxial apparatus is required to analyze the test sequence and develop accurate constitutive models:

- **Confining Stress** (σ_3): The constant pressure applied in all radial directions to the specimen inside the triaxial chamber, simulating geostatic or overburden pressure.
- **Axial Stress** (σ_1): The total vertical stress applied to the specimen, calculated as:

$$\sigma_1 = \sigma_3 + \sigma_d \tag{2.2}$$

- **Deviatoric Stress** (σ_d): This parameter is defined as the difference between the total axial stress and the confining stress ($\sigma_1 - \sigma_3$). Within the AASHTO T 307 protocol, this stress is applied cyclically—typically using a 0.1s haversine load pulse followed by a

0.9s rest period—to simulate the transient nature of moving wheel loads. The Resilient Modulus (M_R) is subsequently determined as the ratio of the applied cyclic deviatoric stress amplitude (σ_d) to the resulting recoverable axial strain (ϵ_r):

$$M_R = \frac{\sigma_d}{\epsilon_r} \tag{2.3}$$

- **Bulk Stress (θ)**: This parameter represents the sum of the principal stresses ($\sigma_1+\sigma_2+\sigma_3$). In standard triaxial tests, the intermediate and minor principal stresses are assumed to be equal to the confining stress ($\sigma_2 = \sigma_3$). Consequently, the expression simplifies to:

$$\theta = \sigma_1 + 2\sigma_3 \tag{2.4}$$

By substituting the relation $\sigma_1 = \sigma_3 + \sigma_d$, the bulk stress is defined as:

$$\theta = (\sigma_3 + \sigma_d) + 2\sigma_3 = \sigma_d + 3\sigma_3 \tag{2.5}$$

Bulk stress is a critical parameter in numerous constitutive models for granular materials.

- **Octahedral Shear Stress (τ_{oct})**: A measure of the three-dimensional shear state, frequently utilized in universal constitutive models, defined as:

$$\tau_{oct} = \frac{\sqrt{2}}{3}\sigma_d \tag{2.6}$$

The milestone of this evolution in Brazil is the development of the National Pavement Design Method (MeDiNa). This method utilizes M_R and permanent deformation models as primary input parameters, enabling a more rational analysis of pavement layer behavior. The incorporation of non-conventional materials, such as industrial residues, into MeDiNa requires the experimental determination of these parameters and the development of constitutive models—such as the Composite Model (Equation 2.7)—to describe their specific behavior:

$$M_R = k_1 \cdot \sigma_3^{k_2} \cdot \sigma_d^{k_3} \tag{2.7}$$

Where:

- M_R is the resilient modulus;
- σ_3 is the minor principal stress (confining stress);
- σ_d is the variable deviatoric stress ($\sigma_1 - \sigma_3$); and
- $k_1, k_2,$ and k_3 are experimental parameters.

It is essential to clarify the relationship between σ_1 and σ_3 within the context of the stress discrepancies between AASHTO and DNIT standards. Test sequences where the confining stress (σ_3) appears to be "greater than" the vertical stress (σ_1) are, in fact, those where the cyclic deviatoric stress ($\sigma_d = \sigma_1 - \sigma_3$) is zero or negligible. By definition, $\sigma_1 = \sigma_3 + \sigma_d$. If $\sigma_d = 0$, then $\sigma_1 = \sigma_3$. If σ_d is a small positive value, then σ_1 is slightly higher than σ_3. In conventional compression tests, the major principal axial stress (σ_1) is always greater than or equal to the minor principal stress (σ_3). Confusion may arise from interpreting the σ_3 and σ_d columns in the standard's table separately, without applying the fundamental definition that relates them to σ_1.

Untreated granular materials (typical of base/subbase layers, classified as Type 1 materials) generally exhibit an **increasing stiffness** behavior. This implies that their resilient modulus (M_R) tends to increase with increments in confining stress (σ_3) and/or bulk stress (θ). Certain constitutive models also incorporate dependence on deviatoric stress or octahedral shear stress. In contrast, fine-grained soils often exhibit **decreasing stiffness**, characteristically resulting in lower M_R values as the deviatoric stress increases.

According to the standard protocol for determining the Resilient Modulus (M_R) of pavement geomaterials (AASHTO T307), soils and aggregate mixtures are rigorously categorized into two primary types based on their physical, grain-size, and plastic properties. This classification dictates both the laboratory testing stress states and the governing constitutive behavior under cyclic loading:

- **Type 1 Materials (Unbound Granular Materials):** This category encompasses all unbound granular base and subbase materials, as well as coarse-grained subgrade soils. Structurally, they are defined as materials with less than 70% passing the No. 200 (75 μm) sieve and a Plasticity Index (PI) of 10 or less. Mechanically, Type 1 materials characteristically display an **increasing stiffness** behavior, where the resilient modulus significantly increases as a function of the confining pressure (σ_3) and bulk stress (θ) due to particle interlocking and confinement densification.

- **Type 2 Materials (Fine-Grained Cohesive Soils):** This group includes all subgrade soils and fine-grained matrices that do not meet the criteria for Type 1 (i.e., soils featuring more than 70% passing the No. 200 sieve or a PI greater than 10). From a mechanistic standpoint, Type 2 materials typically exhibit a **decreasing stiffness** response under traffic loading, meaning that their M_R values tend to decrease as the deviatoric stress (σ_d) increases, a phenomenon driven by shear strain amplification in the cohesive structure.

In 2004, the National Cooperative Highway Research Program (NCHRP, 2004) continued a 1997 study (Project 1-28) through Project 1-28A. This research, led by the University of Maryland (USA), focused on developing methods for determining the resilient

modulus of both granular base and subbase materials as well as hot-mix asphalt (HMA). The proposed methodology for granular materials consists of subjecting a soil specimen to cyclic loading tests at pre-established levels. Subsequently, the test results are processed using non-linear regression techniques to calculate the modulus value, according to the constitutive equation developed within the project.

During the same period, Ooi et al. (2004) emphasized the importance of incorporating soil characteristics—such as type, structure, and physical properties—into mathematical models to describe the variation in the resilient modulus. The authors observed that many existing models failed to simultaneously account for these three parameters. Aiming to develop a new generation of models for low-plasticity silts under confinement and repeated loading, the researchers conducted tests on several fine-grained soil specimens from Hawaii. They subsequently evaluated different explanatory variables to fit three-parameter regression models, building upon previous work by Uzan (1985), Witczak & Uzan (1988), and Pezo (1993), culminating in the proposal of the Universal Model (Equation 2.8):

$$M_R = k_1 \cdot P_a \cdot \left(\frac{\theta}{P_a}\right)^{k_2} \cdot \left(\frac{\tau_{oct}}{P_a} + 1\right)^{k_3} \tag{2.8}$$

Where:

- P_a is the normalization pressure (typically atmospheric pressure, ≈ 0.101 MPa);
- θ is the bulk stress ($\sigma_1 + 2\sigma_3$);
- τ_{oct} is the octahedral shear stress, defined for triaxial conditions as:

$$\tau_{oct} = \frac{\sqrt{2}}{3}\sigma_d \approx 0.471 \cdot \sigma_d \tag{2.9}$$

- $k_1, k_2,$ and k_3 are regression constants.

The k_2 exponent specifically governs the sensitivity of M_R to the bulk stress (θ), which, in turn, is heavily influenced by the confining stress (σ_3), given that $\theta = \sigma_d + 3\sigma_3$. Without data points spanning a range of σ_3 values, including those where $\sigma_d = 0$ (where $\theta = 3\sigma_3$ and $\tau_{oct} = 0$), the reliable determination of the k_2 parameter becomes difficult. These $\sigma_d = 0$ points serve as essential numerical anchors for model calibration.

The mechanical behavior was quantified through Resilient Modulus (M_R) tests following the DNIT 134/2018-ME standard. Specimens were tested under varying stress states to determine the parameters for the unified prediction model adopted by the MeDiNa software (Equation 2.10):

$$M_R = k_1 \cdot \sigma_3^{k_2} \cdot \sigma_d^{k_3} \cdot \theta^{k_4} \tag{2.10}$$

Where:

- M_R is the resilient modulus (MPa);
- σ_3 is the confining stress (MPa);
- σ_d is the deviatoric stress (MPa);
- θ is the first stress invariant (MPa);
- k_1, k_2, k_3, k_4 are regression constants.

Table 2.5 summarizes these approaches, comparing the mathematical framework of the classical models, the composite approach, the MEPDG international standard, and the simplified unified formulation adopted by the current Brazilian pavement design method.

Table 2.5: Comparison of Resilient Modulus (M_R) Models: International Literature vs. MeDiNa Simplifications

Behavior Model	**Analysis Focus**	**Mathematical Expression**	**Origin**	**MeDiNa (2025)** $M_R = k_1\sigma_3^{k_2}\sigma_d^{k_3}\theta^{k_4}$
$M_R \times \sigma_3$	Influence of confinement and intergranular friction.	$M_R = k_1 P_a \left(\frac{\sigma_3}{P_a}\right)^{k_2}$	Dunlap (1963)	$M_R = k_1\sigma_3^{k_2}$ $(k_3 = 0, k_4 = 0)$
$M_R \times \sigma_d$	Sensitivity to shear and reducing stiffness of the matrix.	$M_R = k_1\sigma_d^{k_2}$	Hicks (1970)	$M_R = k_1\sigma_d^{k_3}$ $(k_2 = 0, k_4 = 0)$
Composite Model	Evaluation of both confinement and deviation.	$M_R = k_1 P_a \left(\frac{\sigma_3}{P_a}\right)^{k_2} \left(\frac{\sigma_d}{P_a}\right)^{k_3}$	Pezo (1993)	$M_R = k_1\sigma_3^{k_2}\sigma_d^{k_3}$ $(k_4 = 0)$
Universal (MEPDG)	International reference via stress invariants.	$M_R = k_1 P_a \left(\frac{\theta}{P_a}\right)^{k_2} \left(\frac{\tau_{oct}}{P_a} + 1\right)^{k_3}$	Witczak & Uzan (1988)	N/A[a]

[a] N/A: Not applicable; the MeDiNa unified equation does not explicitly incorporate the τ_{oct} term.

A primary objective of this research is to verify the behavioral shift in soil mixtures following the integration of industrial residues from Espírito Santo. In geotechnical practice, this transition is characterized by the migration from a **decreasing stiffness** regime—typical of unstable fine-grained soils—to a **increasing stiffness** behavior, characteristic of high-quality granular materials.

In the decreasing stiffness regime, the resilient modulus (M_R) decreases as the deviatoric stress (σ_d) increases, indicating a sensitivity to shear-induced structural degradation. By introducing KRS (steelmaking slag) and OSR (ornamental stone residue), the mixture undergoes a dual transformation:

1. **Matrix Lithification**: The high alkalinity and pozzolanic potential of the KRS promote chemical cementation, bonding the fine particles into a rigid matrix;

2. **Skeleton Reinforcement**: The OSR acts as a mineral filler that optimizes the particle size distribution, establishing a robust intergranular skeleton.

The verification of this "behavioral jump" is empirically demonstrated through the calibration of the constitutive parameters $k_1, k_2,$ and k_3. A successful stabilization is marked by a transition toward positive k_2 and k_3 values in the Composite Model (Equation 2.7), signifying that the newly formed geomaterial gains stiffness under increased confining and bulk stresses (σ_3 and θ). This shift is fundamental for the implementation of these residues in the MeDiNa framework, as it ensures the structural longevity and performance of the pavement layers under heavy traffic loading.

Stress states where $\sigma_d = 0$ are particularly significant as they allow for a direct assessment of the material's stiffness response to variations in confining pressure (hydrostatic stress), effectively isolating this effect from the influence of cyclic deviatoric/shear stress. These points provide essential data for calibrating the parameters (k_1, k_2, k_3) in constitutive models that describe the relationship between M_R and the stress state.

The integration of binary mixtures (a mixture with 2 materials), one a natural soil and the second a residue, by a soil-residue content (SRC); or ternary mixtures—which mixes natural soil, KRS, and OSR—presents a hybrid behavior. While the chemical reaction induces cementation promoted by the slag creates a rigid cohesive structure, the ornamental stone residue (OSR) reinforces the granular mineral skeleton.

Therefore, utilizing mathematical models of different natures, including the composite model similar to the one proposed by Pezo (1993), and the universal model adopted in the MEPDG (Mechanistic-Empirical Pavement Design Guide), provides the scientific basis for the transition from empirical CBR designs to modern mechanistic-empirical frameworks. This multi-criteria approach aims to mitigate the technical data gap—the so-called "model blackout"—that currently limits the systematic use of industrial residues in Brazilian infrastructure (Carvalho, 2023).

2.3.4 - PERMANENT DEFORMATION AND THE SHAKEDOWN THEORY

This section presents the literature on a critical mechanical parameter for predicting the service life and structural integrity of road pavements: permanent deformation (PD). Permanent deformation in flexible pavements arises from the progressive accumulation of instant, non-recoverable strains induced by repetitive traffic loading. Macroscopically, this phenomenon manifests as wheel track rutting or shear-induced mass displacement within the asphalt surface layer.

The accumulation of permanent deformation in unbound aggregate materials is governed by a complex interplay of factors, as identified in seminal studies by Thom & Brown (1988) and Lekarp et al. (2000). These variables encompass loading conditions—such as applied stress levels, stress history, and the rotation of principal stress axes under moving wheel loads—as well as intrinsic material properties, including shear strength, mineralogy, gradation, and the content and plasticity of fines (Tutumluer et al., 2018).

Furthermore, the physical state of the material, specifically its dry density and degree of saturation, significantly dictates its deformational response. Notably, several prevalent predictive frameworks, including the AASHTO Pavement ME Design software, utilize resilient strain levels as a primary indicator for modeling the accumulation of permanent deformation in unbound pavement layers.

Despite being a highly detrimental condition, rutting remains one of the most prevalent structural distresses across the Brazilian highway network, not incorporated into the Maintenance Condition Index (ICM; DNIT, 2022), which currently serves as the primary state-of-the-practice methodology for assessing highway maintenance requirements. As discussed by Prandina (2018a), the current exclusion of this parameter from the index's framework represents a significant methodological gap. This limitation may result in an underestimation of localized operational hazards, particularly regarding hydroplaning risks and reduced surface drainage efficiency during periods of high precipitation.

A common axiom within the highway engineering community suggests that approximately 70% of surface distresses originate within the subgrade layer. As elucidated by Bastos (2022), the geometric distortion caused by these depressions severely compromises the pavement's surface drainage capacity, thereby exacerbating moisture-induced damage. Furthermore, the localized thinning of the asphalt layer directly beneath the wheel paths significantly amplifies the structure's susceptibility to fatigue cracking. Beyond accelerating structural degradation, the resulting surface irregularities and water ponding severely impair vehicle drivability and safety, creating hazardous traffic conditions such as hydroplaning.

Consequently, this proportion often extends to differential deformations, which catalyze even more severe structural failures. When moving traffic loads encounter these

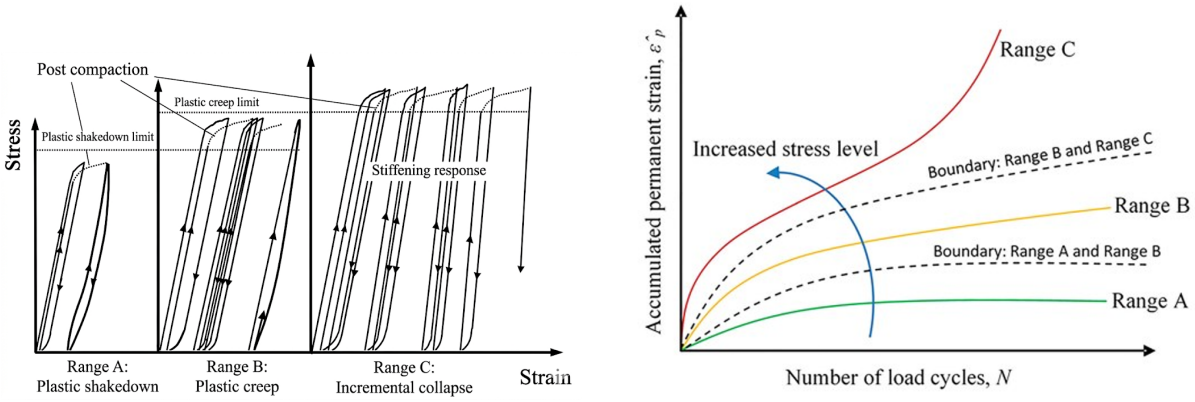
surface irregularities, they induce both horizontal and vertical dynamic impact loads that significantly exceed the magnitudes of standard rolling loads observed on even surfaces (Rith et al., 2017; Wang et al., 2022). Notwithstanding these dynamic effects, contemporary design frameworks—such as the MeDiNa multilayer elastic analysis—predominantly consider only vertical loading for pavement structural dimensioning.

The state-of-the-art in **MeDiNa**, therefore, requires the prediction of **Permanent Deformation (PD)** due to vertical trafficking loads, which leads to rutting. The model by Guimarães (2009), adopted by **DNIT 179/2018-IE**, correlates accumulated plastic strain (ϵ_p) with the number of cycles (N) and the stress state. The Brazilian standard, DNIT 179/2018-IE, establishes a single-stage, long-duration testing procedure. The method consists of molding one specimen for each stress pair (σ_3 and σ_d) to be investigated. Each specimen is then subjected to a minimum of 150,000 loading cycles, maintaining the stress state constant throughout the entire test. The standard suggests a matrix of nine typical stress pairs for a complete characterization.

Practical and economic implications constitute the main disadvantage of the MeDiNa's segment for DP assessment, as it requires time- and resource-consuming efforts at a scale seldom encountered in routine pavement engineering. Performing a test with 150,000 cycles at a frequency of 1 Hz takes approximately 42 hours per specimen (5 h for 5 Hz). To characterize a single material across the nine recommended stress pairs, about 378 hours—or nearly 16 days of continuous testing—would be required. This extensive time severely limits the routine application of the test in commercial projects and quality control programs, restricting it primarily to academic research and high scale well-funded projects. Beyond equipment time, there is a significant consumption of material and specialized labor for molding multiple specimens.

Residues like **KRS** and **SS-LD** often exhibit "Shakedown Type A" behavior, where the plastic strain rate diminishes to zero, ensuring long-term structural stability (Cabral, 2021) for typically unbound pavement layers of base, subbases, and subgrade, which extend its postive influence in the pavement performance when used in the wearing course asphalt layer (Rondón-Quintana et al., 2018). This resistance to rutting is significantly superior to that of natural clayey soils, allowing, for example, to thinner asphalt surface layers.

The accumulation of PD in the lower layers, particularly the subgrade, is the primary driver of wheel track rutting on the asphalt surface. Under the action of traffic-induced cyclic loads, the evolution of strain (Figure 2.5a) is intrinsically linked to the applied stress level and can be categorized into three response regimes—known as Ranges—based on Shakedown Theory (Dawson & Wellner, 1999); (Werkmeister et al., 2001); (Rahman et al., 2023):



(a) (b)

Figure 2.5: Geomechanical response to cyclic loading: (a) Theoretical behavior of unbound materials under repeated cyclic load (modified from Erlingsson et al., 2017); (b) Typical behaviors of the permanent deformation (PD) curve of soils (from Rahman et al., 2023)

- **Range A (Plastic Shakedown):** The specimen stabilizes after a finite number of load applications. Permanent strain accumulation ceases, and the material transitions to a strictly resilient (elastic) response.
- **Range B (Plastic Creep):** The strain rate decreases rapidly during initial cycles but does not fully stabilize, continuing to accumulate plastic deformation at a slow and constant rate.
- **Range C (Incremental Collapse):** Permanent strain accumulation accelerates with each cycle, preventing structural stabilization and leading the material to rapid failure.

To categorize the types of behavior of unbound materials under cyclic loading, as illustrated in Figure 2.5b, the criteria established by Guimarães (2009) present in the DNIT code define four distinct response modes based on the accumulation of permanent strain:

Type I – Plastic Shakedown: Characterized by a rapid stabilization of permanent deformation within a small number of load cycles for a given stress state.

Type II – Stable Shakedown with High Initial Strain: The material eventually reaches stabilization; however, it accumulates a significant magnitude of permanent displacement before the deformation rate subsides.

Type III – Continuous Plastic Accumulation (Plastic Creep): The material fails to reach an equilibrium state, exhibiting a persistent and nearly constant increase in permanent strain as the number of cycles progresses.

Type IV – Incremental Collapse: A critical failure mode where the material undergoes rapid and accelerating strain accumulation, leading to structural rupture at a very low number of load repetitions.

Table 2.6: Models and their formulations for predicting permanent deformation

Model	**Equation and Parameters**	**Development**
Barksdale (1972)	$\epsilon_{1,p} = a + b \cdot \log(N)$ $\epsilon_{1,p}$: Plastic specific strain a, b: Constants for a given stress level N: Number of load repetitions	Triaxial repeated load tests for more than 100,000 loading cycles.
Monismith et al. (1975)	$\epsilon_p = A \cdot N^B$ ϵ_p: Plastic specific strain A, B: Experimental parameters N: Number of load repetitions	Triaxial load tests for up to 100,000 loading cycles.
Uzan (1982)	$\frac{\epsilon_p(N)}{\epsilon_r} = \mu \cdot N^{-\alpha}$ $\epsilon_p(N)$: Plastic strain for the n-th layer ϵ_r: Resilient strain μ, α: Material parameters N: Number of load repetitions	Based on the differentiation of Monismith's equation. During loading and unloading, elastic moduli E_c and E_d are distinct, and the stress-strain relationship is considered linear.
Tseng & Lytton (1989)	$\delta_p(N) = \left(\frac{\epsilon_0}{\epsilon_r}\right) \cdot e^{-(\frac{\rho}{N})^\beta} \cdot \epsilon_v \cdot h$ $\delta_p(N)$: Permanent deformation of the layer ϵ_0, ρ, β: Material properties ϵ_v: Average resilient vertical strain ϵ_r: Resilient strain h: Layer thickness N: Number of load repetitions	From the application of multiple regression on a database of repeated load permanent deformation tests. Parameters are estimated according to their application: subgrade, base, and subbase.
M. H. Resende (1999)	$\epsilon_p = A \cdot N^B \cdot \sigma_d$ ϵ_p: Plastic specific strain A, B: Experimental parameters σ_d: Deviator stress N: Number of load repetitions	Proposed the differentiation of Monismith's equation by incorporating the deviator stress.
Guimarães (2009)	$\epsilon_p^{esp}(\%) = \Psi_1 \cdot (\sigma_3)^{\Psi_2} \cdot (\sigma_d)^{\Psi_3} \cdot (N)^{\Psi_4}$ ϵ_p^{esp}: Specific permanent strain (%) $\Psi_1, \Psi_2, \Psi_3, \Psi_4$: Model parameters N: Number of load cycles	Through multiple non-linear regression analysis of permanent deformation test results.

The integration of the previous four categories with Shakedown Theory, these four types of behavior are mechanistically grouped into the three Ranges of the Shakedown Theory commonly used in modern pavement design frameworks:

Range A (Types I and II): Represents the plastic shakedown limit, where the material

is considered stable for long-term performance.

Range B (Type III): Represents the plastic creep limit, where deformation continues but at a controlled rate.

Range C (Type IV): Represents the incremental collapse limit, indicating a stress state that exceeds the material's structural capacity.

To mathematically model these responses within the framework of the National Pavement Design Method (MeDiNa), various empirical formulations are adopted. For tropical soils, the formulation proposed by Guimarães (2009) is particularly significant, alongside other classic models from the literature (Table 2.6). To evaluate the occurrence of shakedown, a graphical analysis was conducted based on the Dawson & Wellner (1999) model, utilizing the permanent strain accumulation rates specified in the DNIT 179/2018 standard. Figure 2.6 illustrates the four soil behavior models employed for the shakedown analysis.

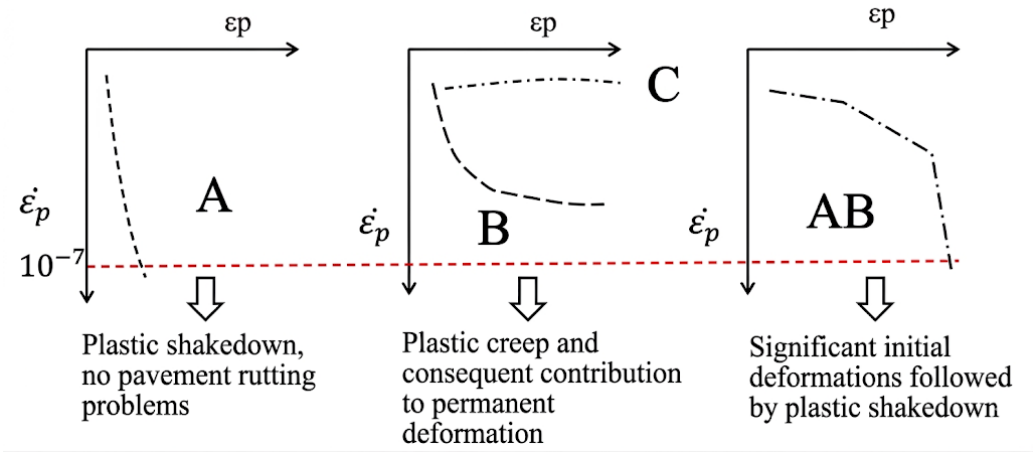


Figure 2.6: Permanent deformation behavior models for soils (from DNIT, 2018b).

2.3.4.1 Multistage Testing and Shakedown Thresholds

Historically, single-stage permanent deformation tests required a high volume of specimens and significant laboratory time. As an optimized alternative, multistage protocols—supported by standards such as EN 13286-7—subject a single specimen to sequentially increasing stress states, according to CEN (2004) and Lima et al. (2021). This methodology allows for the rapid identification of shakedown thresholds in granular materials and recycled mixtures.

To mechanistically distinguish between tolerable behavior and failure, mathematical criteria of Rahman et al. (2023) are applied to evaluate the rate of strain increment between cycles 3,000 and 5,000 of the triaxial test, according to the following equations:

Range A: $$(\hat{\epsilon}_p^{5000} - \hat{\epsilon}_p^{3000}) < 0.045 \times 10^{-3} \tag{2.11}$$

Range B: $$0.045 \times 10^{-3} < (\hat{\epsilon}_p^{5000} - \hat{\epsilon}_p^{3000}) < 0.4 \times 10^{-3} \tag{2.12}$$

Range C: $$(\hat{\epsilon}_p^{5000} - \hat{\epsilon}_p^{3000}) > 0.4 \times 10^{-3} \tag{2.13}$$

Where:

$\hat{\epsilon}_p^{5000}$ is the accumulated permanent strain (plastic strain) measured at 5,000 loading cycles;

$\hat{\epsilon}_p^{3000}$ is the accumulated permanent strain measured at 3,000 loading cycles;

$(\hat{\epsilon}_p^{5000} - \hat{\epsilon}_p^{3000})$ represents the rate of permanent strain increment (or the slope of the deformation curve) between these two specific loading stages.

Consistent with the accumulated strain rate, the material may exhibit one of four macroscopic responses: pure elasticity (fully recoverable strain), plastic shakedown, plastic creep, or incremental collapse (Figure 2.6). From a structural design perspective, only responses within Ranges A and B are acceptable for pavement foundations, ensuring the prevention of premature infrastructure failure.

The transition from single-stage to multistage (MS) testing requires enhanced analytical sophistication to account for the effects of stress history. At an advanced stage of an MS test, the material has already undergone densification and a progressive increase in stiffness during previous loading stages; consequently, its mechanical response differs from that of a virgin specimen subjected to the same stress level. To address this history-dependent behavior in cumulative permanent deformation modeling, analytical strain-shifting formulations, such as the strain-hardening or time-hardening hypotheses, are traditionally required.

The strain-hardening technique facilitates the construction of a continuous permanent deformation curve from discontinuous multistage data. Its fundamental principle states that the material's future permanent strain accumulation depends strictly on the current level of accumulated plastic strain, regardless of the specific stress path that led to that state.

The mathematical formulation for the accumulated permanent strain ϵ_p after N total cycles can be expressed through fitted empirical models. One of the most prominent models is the one proposed by Rahman & Erlingsson (2015), which integrates the number of cycles and the stress state through a stress function S_f:

$$\epsilon_p(N) = aN^b S_f \tag{2.14}$$

Where:

- a and b are material fitting parameters;
- S_f is the stress parameter, often defined as $S_f = (\sigma_d/p_a)/(\sigma_1/p_a)^{\alpha}$;
- σ_d is the deviator stress, σ_1 is the major principal stress, and p_a is the reference atmospheric pressure.

Recent advancements in pavement geotechnics strongly support the multistage (MS) approach as a scientifically robust and computationally efficient alternative to the exhaustive 150,000-cycle single-stage tests. The validity of this optimized methodology is demonstrated across varying granular and cohesive materials, significantly reducing laboratory effort while maintaining predictive reliability.

For instance, Erlingsson et al. (2017) demonstrated that applying a reduced sequence of 10,000 load cycles per stress step is sufficient to accurately characterize the permanent deformation properties and successfully identify the Shakedown ranges of unbound granular materials. By applying the time-hardening procedure to compensate for the stress history of the specimen, their multistage protocol consolidates both resilient modulus and permanent strain evaluations into a single, time-efficient test.

Corroborating these findings within the Brazilian mechanistic-empirical context, Ben et al. (2023) evaluated the permanent deformation of lateritic clayey subgrade soils using MS methodologies. Their research verified that MS protocols utilizing 10,000 cycles per stage yielded predictive permanent deformation curves highly consistent with those obtained from the conventional single-stage 150,000-cycle protocol. This adaptation not only preserved the accuracy of the regression parameters required by the MeDiNa design software but also significantly reduced the total testing time and material consumption.

In conclusion, the integration of multistage testing—guided by Shakedown thresholds and time-hardening mathematical models, represents a viable evolution in modern pavement engineering. It effectively mitigates the severe practical and economic constraints of current standards like DNIT 179/2018-IE, bridging the gap between advanced mechanistic-empirical modeling and routine commercial laboratory applications.

2.4 - THE WASTE MATERIALS OF THE DOCTORAL THESIS

The residues under investigation represent the three most voluminous and geotechnically promising streams in the Espírito Santo industrial ecosystem.

2.4.1 - LD-SS: PHYSICAL, CHEMICAL AND MINERALOGICAL (XRD/XRF) ANALYSIS

Linz-Donawitz slag (LD-SS) is a granular byproduct of the conversion of pig-iron to steel (A. D. d. Resende, 2010). It features high angularity and a rough surface texture, which promotes exceptional interparticle interlocking (Boldrini & Pacheco, 2022). Figure 2.7 illustrates a typical sample of LD-SS. Figure 2.8 presents the local area of the LD-SS stockpiles at the industrial level in Vitória, ES.



Figure 2.7: Full sample of a LD-SS from Espírito Santo industrial plant (from Izoton, 2020)

The generation of this material is inherently linked to several operational phases, starting with the precise positioning and tilt of the converter, followed by the introduction of solid scrap and the subsequent pouring of molten pig iron. These production stages are critical to the formation of LD-SS, which emerges through complex chemical reactions and phase separations occurring within the refining vessel (Resende, 2010; Izoton, 2020). The CSN slag stockpile yards, illustrated in Figure 2.9, demonstrate the true scale of the waste management challenge posed by continuous steel production.

The chemical profiles of LD-SS from various Brazilian industrial facilities, updated with their current corporate ownership, are summarized in Table 2.7. The physico-chemical properties of LD-SS are fundamentally dictated by the quality of the raw materials and the specific thermodynamic conditions of the steelmaking cycle. Characterized as a granular and heterogeneous material, LD-SS is primarily composed of calcium, silicon, iron, and magnesium



Figure 2.8: 320,000 m^2 *ResidueStockpileAreaoftheSteelmakingIndustrialProcessingPlantinVitria*

Table 2.7: Chemical composition of LD-SS from Brazilian industrial plants (Adapted from Oliveira, 2016)

Plants	**CaO**	**MgO**	**Al_2O_3**	**SiO_2**	**MnO**	**Fe (total)**	**S**	**P_2O_5**
ArcelorMittal - Vitória	45.20	5.50	0.80	12.20	7.10	18.80	0.07	2.75
Aperam South America	44.81	7.32	2.42	15.47	02.09	14.06	0.06	1.18
ArcelorMittal - João Monlevade	47.00	8.00	1.50	15.00	3.00	19.00	–	–
Usiminas	41.40	6.20	1.40	11.00	6.30	22.00	–	1.80
Gerdau - Ouro Branco	45.58	9.48	0.75	12.01	6.59	16.71	–	2.23
Gedau Cocais	36.20	12.50	0.93	15.40	5.80	21.00	0.04	01.01
Vallourec	43.00	7.00	0.80	15.00	3.00	22.00	0.20	1.60
CSN	35.00	6.00	4.00	15.00	3.50	19.70	0.34	0.70
Usiminas - Cubatão	38.69	9.76	1.29	11.17	6.42	22.29	0.06	1.44

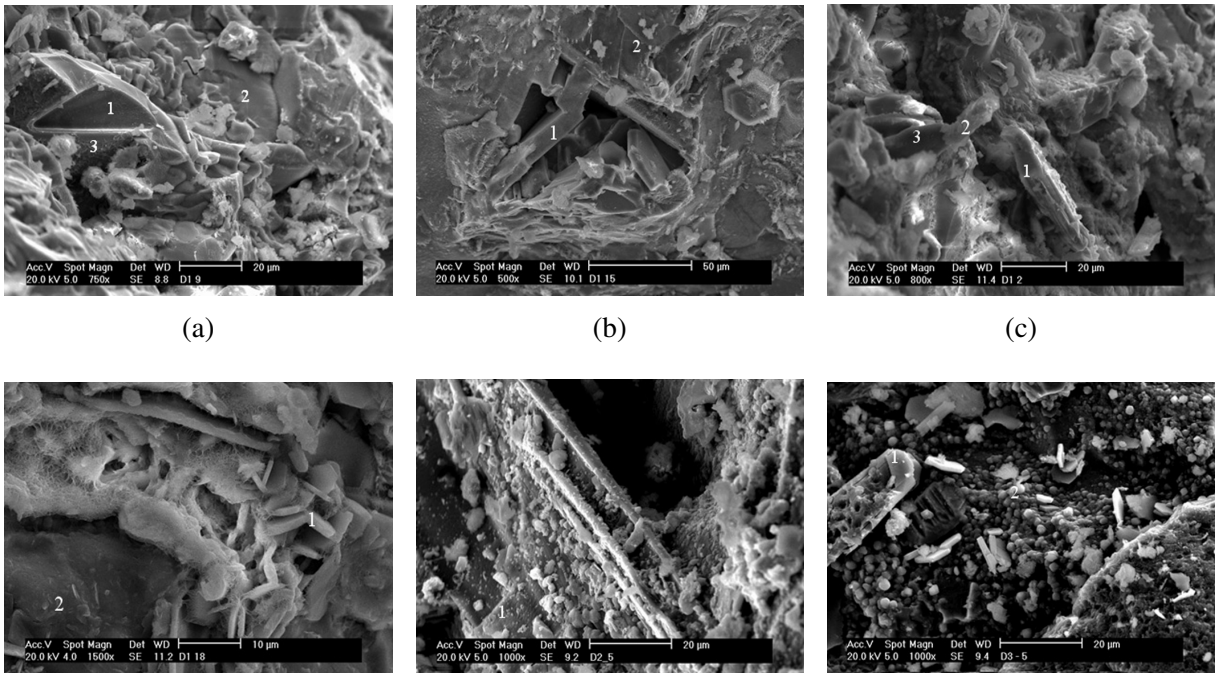
oxides.

A defining challenge of LD-SS is its inherent expansive potential, which stems largely from the presence of uncombined (free) lime and periclase. This volumetric instability is a critical parameter for its application as a construction aggregate. Unless properly stabilized, such expansion can compromise the integrity of geotechnical structures, requiring standardized assessment methods, such as autoclave expansion tests, to validate the material's engineering suitability (Resende, 2010; Raposo, 2005). The stabilization and reduction of this expansive behavior are paramount to ensuring the structural durability and geotechnical reliability of infrastructure projects utilizing LD-SS.

According to the microstructural analysis conducted by Polese et al. (2006),



Figure 2.9: The CSN slag stockpile yards illustrate the true scale of the waste management challenge posed by continuous steel production (Foco Regional, 2019).



(a) (b) (c)

(d) (e) (f)

Figure 2.10: Scanning Electron Microscopy (SEM) micrographs of LD-SS samples: (a) hydrated calcium ferrite (1–3); (b) portlandite (1–2); (c) dicalcium silicate (1, 3) and tricalcium silicate (2); (d) calcium carbonate (1) and hydrated calcium ferrite (2); (e) calcium phosphate (1); and (f) calcium carbonate (1) and calcium ferro-silicate (2). Adapted from Polese et al. (2006).

the morphological features of LD-SS evidence a highly reactive mineralogical assemblage dominated by calcium silicates (alite and larnite) and free lime (CaO). Upon exposure to moisture, these phases undergo intense hydration and carbonation, leading to the precipitation of portlandite, calcium carbonates, and hydrated calcium ferrites, as clearly identified in the micrographs. While this intrinsic chemical reactivity is the primary driver of the slag's volumetric instability (expansion) in its pure state, it becomes a critical stabilizing mechanism when integrated with geomaterials. In a soil-slag matrix, the continuous dissolution of calcium ions (Ca^{2+}) and the resulting high-alkalinity environment not only trigger immediate cation exchange and flocculation in clayey soils but also provide the essential chemical precursors for long-term pozzolanic reactions, ultimately cementing the stabilized infrastructure layer.

The temporal evolution of these mineralogical phases is further elucidated by the morphological comparison between "fresh" and "aged" samples. While Figure 2.10 details the specific hydration products, Figure 2.11 and Figure 2.12 capture the macroscopic result of the atmospheric exposure described by (Polese, Carreiro, & Silva, 2006). In its fresh state (Figure 2.8a), the LD-SS displays a clean, highly reactive surface where free lime and silicates are directly exposed, representing the material at "age zero" with maximum expansion potential. Conversely, the aged sample (Figure 2.8b) reveals a surface extensively covered by rhombohedral calcite ($CaCO_3$) crystals. This precipitated layer confirms the advanced stage of carbonation and serves as a physical evidence of chemical "passivation". This process is the fundamental mechanism behind industrial treatments like humidification cycles, which aim to "pre-expand" the material and stabilize its volumetric behavior before its application as a geomaterial.

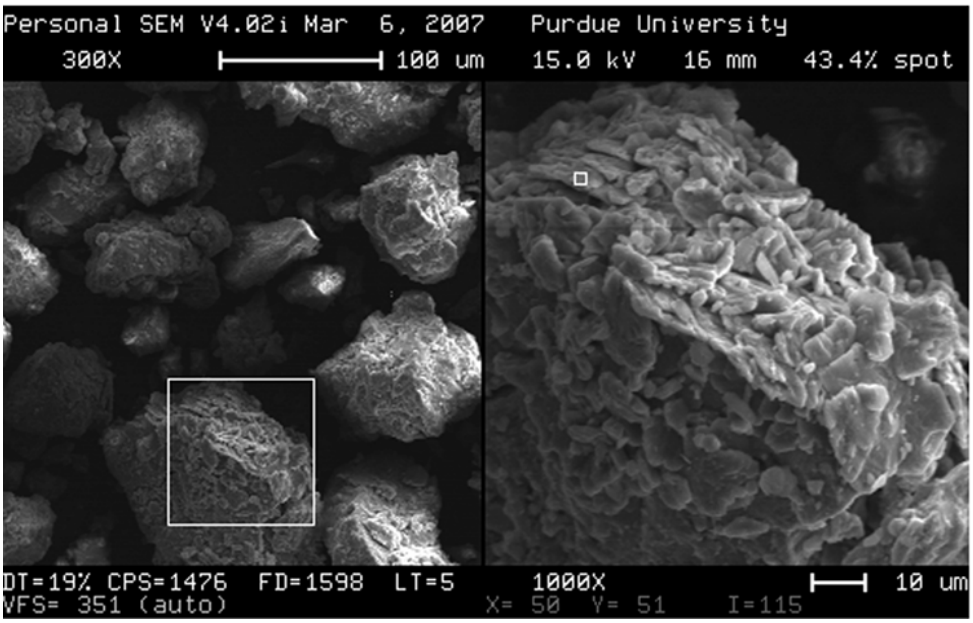


Figure 2.11: Scanning Electron Microscopy (SEM) micrograph of fresh LD-SS at age zero, highlighting clean and highly reactive mineral surfaces (Modified from Yildirim & Prezzi, 2011)

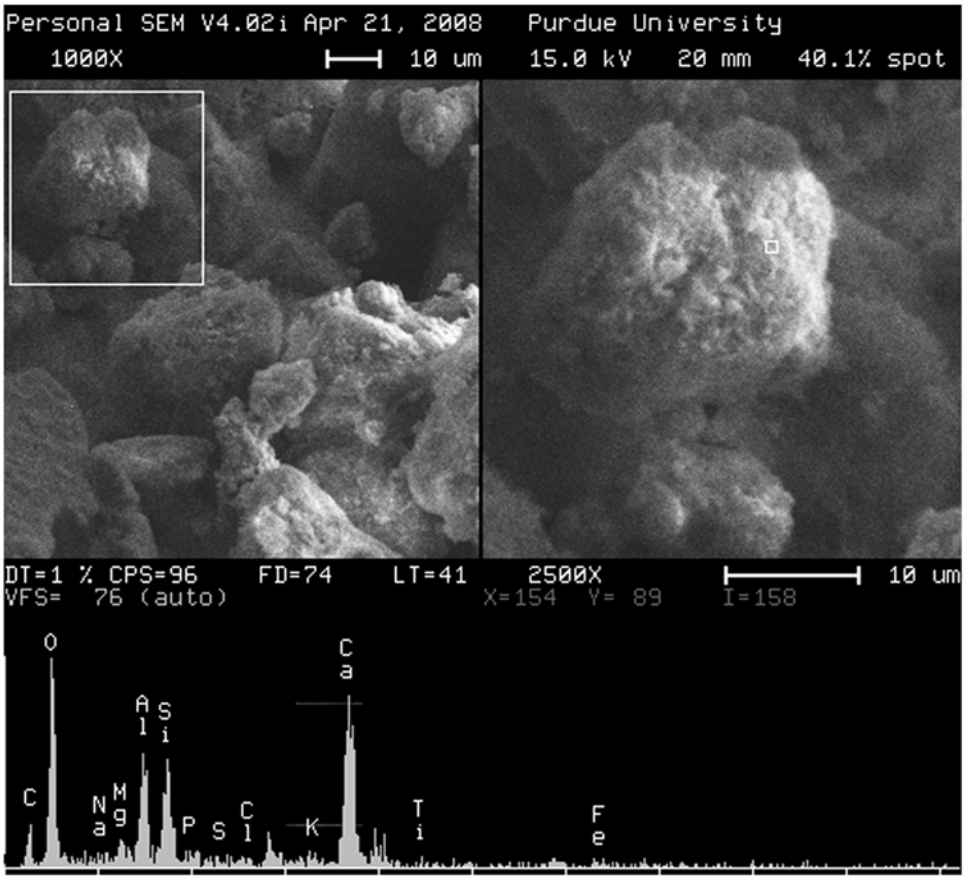


Figure 2.12: Scanning Electron Microscopy (SEM) micrograph of aged LD-SS, illustrating the surface covered by rhombohedral calcite ($CaCO_3$) crystals resulting from atmospheric carbonation (Modified from Yildirim & Prezzi, 2015)

The mineralogical characterization of LD-SS is further substantiated by the findings of Yildirim & Prezzi (2015), who identified the predominant phases through X-ray diffraction (XRD) and corroborated them with SEM imaging.

According to their analysis, the "fresh" slag is characterized by a high concentration of larnite (β-Ca_2SiO_4), srebrodolskite ($Ca_2Fe_2O_5$), wüstite (FeO), and reactive portlandite ($Ca(OH)_2$). However, the transition to the "aged" state involves a significant mineralogical shift.The rhombohedral crystals clearly observed in the aged sample (Figure 2.12) are identified as calcite ($CaCO_3$), a secondary precipitate resulting from the carbonation of free lime and portlandite upon exposure to atmospheric CO_2. While Polese et al. (2006) detailed the presence of silicates and ferrites, Yildirim and Prezzi (2015) provide the temporal link: the clean surfaces of the fresh slag (Figure 2.11) represent the highly unstable age-zero state, whereas the calcite-covered surfaces of the aged slag represent a passivated, more volumetrically stable geomaterial. This mineralogical evolution is the scientific basis for the industrial "curing" processes, such as those used for Acerita and Revsol, turning a potentially deleterious waste into a reliable infrastructure material.

The mineralogical characterization of LD-SS is further supported by the X-ray

diffraction (XRD) analysis conducted by Yildirim and Prezzi (2015). Their findings corroborate the presence of complex phases such as larnite (β-Ca_2SiO_4), srebrodolskite ($Ca_2Fe_2O_5$), and portlandite ($Ca(OH)_2$). Notably, the comparison between fresh and aged slag highlights the transformation of free lime (CaO) into calcium carbonate ($CaCO_3$), a process visually documented in the SEM micrographs previously discussed. This mineralogical transition confirms that the carbonation layer observed on the aged slag surfaces is not merely a morphological change but a chemical stabilization of the reactive phases, which directly influences the volumetric behavior of the slag when used as a pavement geomaterial.

2.4.2 - KRS: PHYSICAL, CHEMICAL, AND MINERALOGICAL (XRD/XRF) ANALYSIS

Kambara Reactor (KR) slag (KRS) is a byproduct generated from the desulfurization of hot metal (pig iron) in a Kambara Reactor. This slag is characterized by its unique chemical and mineralogical composition, which is influenced by the operational parameters of the Kambara Reactor and the raw materials used. The KR process involves the agitation of the molten iron with a desulfurizing agent to reduce impurities like sulfur, which results in the formation of the slag byproduct (Medina, 2024). KRS is distinct from other steelmaking slags such as LD-SS due to its distinct chemical composition and mineralogical characteristics, which are a direct consequence of the desulfurization reactions and the specific fluxes employed in the process (Bridi, 2020; Meneguete, 2018).

The primary function of the slag-forming agents in the desulfurization process is to capture and remove sulfur from molten iron, typically through the addition of lime-based materials and other fluxes that promote the formation of stable sulfide phases. The chemical composition of desulfurization slag is characterized by elevated contents of CaO and, to a lesser extent, magnesium oxide (MgO), both of which are essential for the efficient removal of sulfur from the metal bath (Meneguete, 2018).

The pig-iron industrial production process generates two fundamental types of KRS: Type I, characterized by a coarse-grained distribution with little to no fines passing the #200 sieve; and Type II, produced in powdered form, with nearly 100% of the material passing the #200 sieve.

Figure 2.13 presents the Scanning Electron Microscopy (SEM) image of a KRS sample from Espírito Santo (augmented 100 times), in two different scales, providing a detailed view of the particle morphology and surface texture (Figure 2.13 1000 times). This microstructural analysis is essential for understanding the physical interlocking potential and the surface area available for chemical reactions when these residues are integrated into soil matrices.

The chemical composition of KRS (Table 2.9) typically reveals high CaO content, often exceeding 40%, which is a key driver for cementitious reactions when mixed with clayey

soils Sant'Ana (2003). From a mineralogical perspective, the solubility and reactivity of these phases are modulated by the alkaline environment of the soil-slag matrix. Furthermore, the presence of sulfates or other activators can accelerate the dissolution of these reactive phases, leading to the formation of stable hydration products that bridge the mineral skeleton of the soil (Velten et al., 2006).

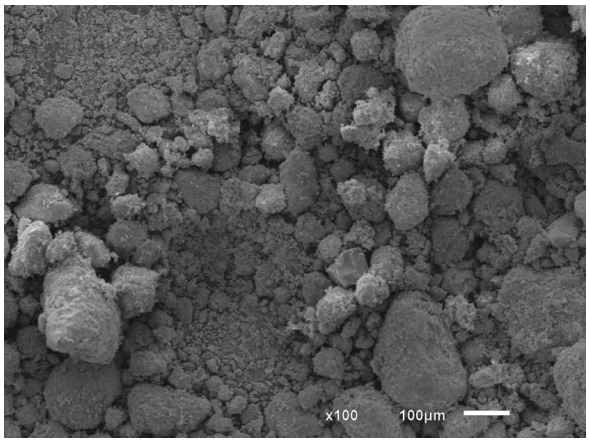


Figure 2.13: Description of sample A.

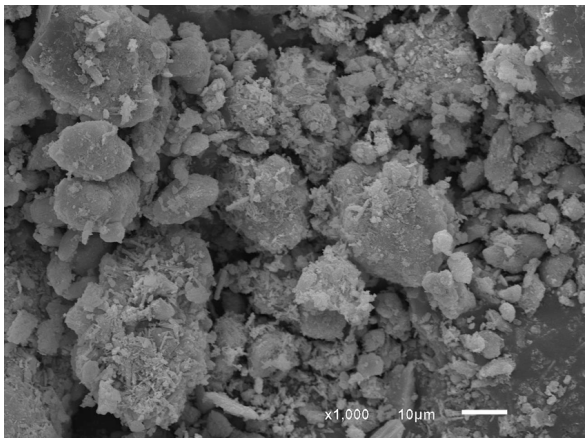


Figure 2.14: Description of sample B.

Chemically, KRS is predominantly composed of calcium oxide (CaO), silicon dioxide (SiO2), and smaller amounts of magnesium oxide (MgO), iron oxides, and other minor constituents summarized in Table 2.8. The high CaO content imparts a certain degree of alkalinity, which can be beneficial for soil stabilization, as it promotes pozzolanic reactions when mixed with clayey soils or other siliceous ones, as stated recently by Pires et al. (2019); Table 2.9 presents KRS chemical composition, studied by Dieguez (2018), also presented by Oliveira et al. (2019), and a LD-SS tested by Oliveira (2018).

Table 2.8: Main Chemical Composition of KRS (Pires et al., 2019).

Chemical Compound	**KRS Result (%)**
CaO	44.8
SiO_2	14.6
Fe_2O_3	26.0
Al_2O_3	5.1
MgO	2.7
SO_3	3.8

The pozzolanic reactions with soils contribute to the long-term strength gain and durability of the stabilized embankment material. However, the presence of free CaO and MgO in the final slag product can impart expansive properties, as these oxides may hydrate and expand upon exposure to moisture. This expansion potential is a critical consideration in geotechnical applications, as new geomaterial are formed (Santos, 2024).

The primary mineral constituents of KRS typically include dicalcium silicate (larnite, Ca_2SiO_4), calcium ferrite, free lime (CaO), periclase (MgO), portlandite ($Ca(OH)_2$),

Table 2.9: Chemical composition of KRS and LD-SS (% by mass)

Chemical Composition	**KRS (Oliveira et al., 2019)**	**KRS (Dieguez, 2018)**	**LD-SS (Oliveira, 2018)**
CaO	44.8	47.8	43.4
Fe_2O_3	26.0	16.0*	26.4
SiO_2	14.6	12.3	12.7
Al_2O_3	5.1	4.5	4.9
MgO	2.7	3.8	5.0
SO_3	3.8	1.25**	0.2
MnO	1.7	1.04	3.2
P_2O_5	0.5	0.24	1.3
TiO_2	0.3	–	0.4
Na_2O	0.1	0.12	0.2
SrO	0.1	–	0.1
K_2O	< 0.10	0.034	< 0.10

* Value corresponds to Total Fe. ** Value corresponds to Total S.

and calcite ($CaCO_3$). These minerals result from high-temperature reactions during the desulfurization process. The presence of dicalcium silicate and calcium ferrite is particularly significant, as these phases impart hydraulic and pozzolanic reactivity to the KRS (Meneguete, 2018). This reactivity is crucial for the development of the cementitious bonds that enhance the long-term strength and durability of soil-KRS mixtures.

Free lime (CaO) plays a dual role in the system of soil mixtures. While it contributes to the alkalinity necessary to promote pozzolanic reactions, its hydration leads to the formation of portlandite ($Ca(OH)_2$), which may subsequently react with atmospheric CO_2 to form calcite ($CaCO_3$). This dynamic mineralogical evolution influences both the leaching behavior and the volumetric stability of the material (Oliveira et al., 2016). Specific analysis of KRS samples has identified a mineralogical fingerprint composed of portlandite, calcite, quartz, and larnite (Ca_2SiO_4), as illustrated in the X-ray diffraction (XRD) pattern shown in (Figure 2.15)

This mineralogical diversity allows for tailored engineering solutions, as the composition is not static but evolves through ongoing hydration and carbonation processes. This transition of less stable phases, such as free lime, into stable minerals like calcite effectively mitigates potential environmental risks associated with expansion, ensuring the long-term sustainability of the KRS-based geotechnical solution (Sant'ana, 2003; Velten et al., 2006; Santos, 2013; Oliveira et al., 2016).

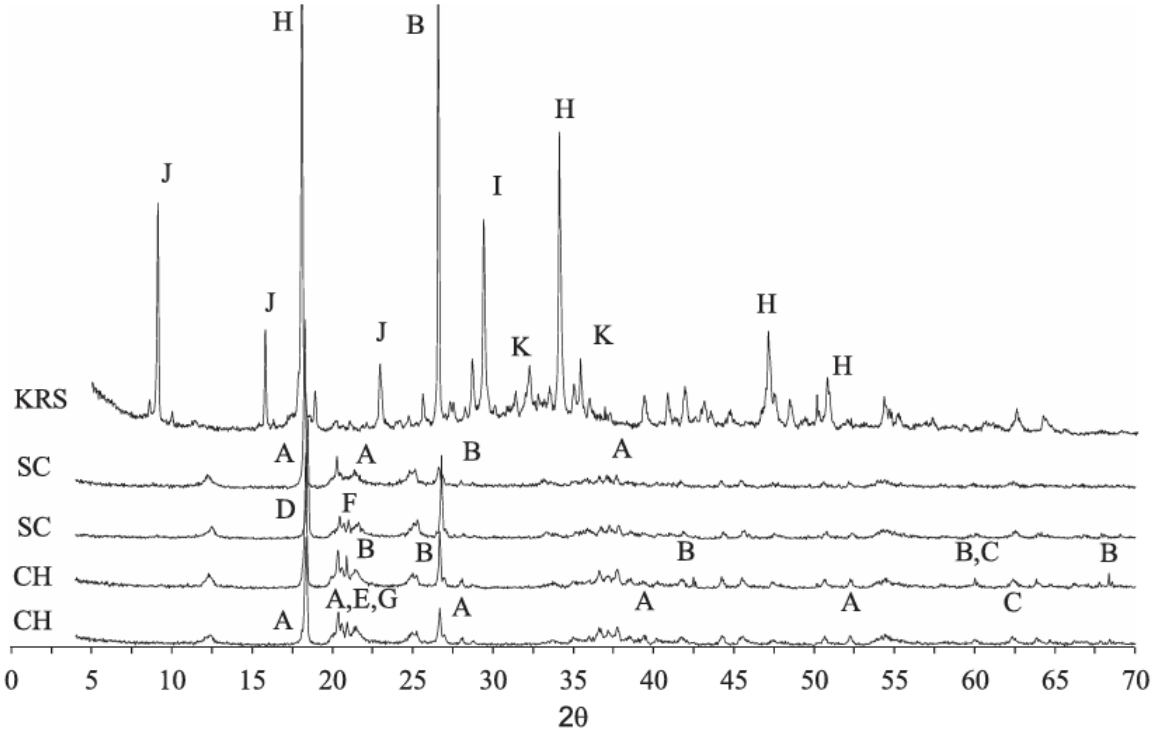


Figure 2.15: X-ray diffraction (XRD) pattern of typical soils from Espírito Santo (different CH and SC) and KRS, highlighting the following mineral phases: (H) Portlandite – $Ca(OH)_2$; (I) Calcite – $CaCO_3$; (B) Quartz – SiO_2; (A) Gibbsite – $Al(OH)_3$; (C) Kaolinite – $Al_2Si_2O_5(OH)_4$; (E) Silicon Oxide – SiO_2; (J) Ettringite – $Ca_6Al_2(SO_4)_3(OH)_{12} \cdot 26H_2O$; (D) Magnesium Aluminum Hydroxide – $Mg_6Al_2(OH)_{18} \cdot 4H_2O$; (F) Sodium Iron Oxide Silicate – $NaFeSi_2O_6$; (K) Magnesioferrite – $MgFe_2O_4$; and (G) Sodium Aluminium Silicate – $NaAlSi_3O_8$ (from Oliveira, 2018).

2.4.3 - OSR: PHYSICAL, CHEMICAL, AND MINERALOGICAL ANALYSIS (XRD/XRF)

Ornamental stone residue (OSR) is generated in abundance in the state of Espírito Santo, which establishes itself as the epicenter of the ornamental stone industry (OSI) in Brazil. In 2024, the state accounted for 82.2% of the country's total export value (ABIROCHAS, 2025), which amounted to USD 1.15 billion. The OSI, also referred to as the "dimension stone industry" in North America, generates waste throughout all processing stages required for the production of items such as countertops, tiles, and claddings.

Geotechnically, OSR is a silty material generated during the sawing and polishing of granite and marble blocks, referred to in the literature as marble/granite dust, slurry, or sludge (Prandina Farias, 2026). In Espírito Santo landfills, this residue is typically a mix of silicate and carbonate minerals (Moreira et al., 2021).

The technological landscape of the dimension stone industry has been redefined by the widespread adoption of diamond wire saw technology (Figure 2.16). This cutting process

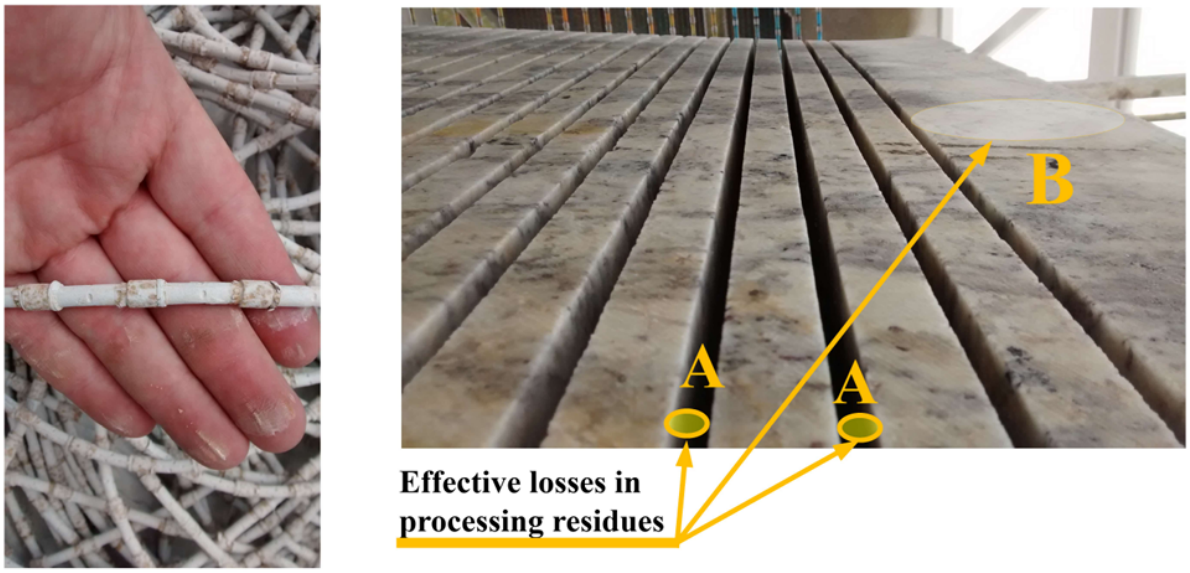


Figure 2.16: Genesis of the OSR: (A) detail of the micro-abrasion area where the cutting mechanism via diamond wire sawing acts; (B) solid part of the block left uncut due to irregularities (Photo: Prandina, 2015)

represents a significant departure from traditional gang saw methods, which relied on a complex abrasive slurry composed of steel blades, steel grit, and, most importantly, lime (CaO) to regulate viscosity and prevent oxidation.

This OSR generation occurs through a high-energy micro-abrasion process, where diamond-impregnated beads mechanically shear the rock matrix. Because water serves as the sole agent for cooling and lubrication, the cutting cycle is entirely free from chemical additives or lime (CaO). Consequently, the resulting slurry is a high-surface-area, "clean" mineral byproduct that preserves the original chemical and mineralogical signature of the parent rocks.

The chemical composition of OSR is a direct reflection of its mineralogy, forming a silt-sandy mixture that is typically low in plasticity. The residue is essentially a silicate-rich matrix derived from quartz and feldspathic minerals. The major oxides of OSR are silica (SiO_2), typically the most abundant component, often exceeding 60-70% by mass, which can contribute to the rigidity of resulting mixtures. This effect is especially pronounced in clayey soils due to particle interaction and replacement, as will be demonstrated by the studies presented in this work (Table 2.10).

Other oxides present in smaller quantities include alumina (Al_2O_3), alkali and alkaline-earth oxides (K_2O, Na_2O, CaO, MgO), iron oxides (Fe_2O_3), and titanium oxides (TiO_2). The elemental diversity varies with the parent rock's geology and industrial practices.

It's important to note the main difference between the samples presented, especially related to the CaO content, The concentration of Calcium Oxide (CaO) in Ornamental Stone

Residue (OSR) is intrinsically linked to the geological nature of the processed rock. In residues derived from calcareous rocks, such as marble, CaO levels typically range between 40% and 60%. This contrasts sharply with residues from granitic, gneissic, or gabbroic rocks ("G" rocks), which are the predominant types processed in the sawmills of Espírito Santo and exhibit substantially lower values.

Table 2.10: Chemical composition of the OSR in percentages

Elements	a	b	c	d	e	f	g	h
	Neves et al. (2018)	Oliveira et al. (2016)	Lunz (2021)	Dias (2024)	Average (a, b, c, d)	Standard Deviation (a, b, c, d)	Moreira et al. (2021)	Variation |e-g|
SiO_2	63.8	62.4	48.7	46.1	55.25	9.00	53.56	1.69
Al_2O_3	16.5	15.3	15.9	10.3	14.5	2.83	12.03	2.47
Fe_2O_3	5.3	7.6	6.4	6.8	6.53	0.99	6.41	0.12
CaO	1.3	1.6	9.8	16.5	7.3	7.14	10.61	3.31
MgO	0.8	1.1	2.4	1.1	1.35	0.69	4.5	3.15
K_2O	4.8	3.8	1.3	1.3	2.8	1.74	3.45	0.65
Na_2O	3.5	3.4	0.4	0.1	1.85	1.78	2.64	0.79
TiO_2	0.8	1.0	0.8	0.8	0.85	0.10	0.76	0.09
P_2O_5	0.2	0.2	0.2	0.2	0.2	0.00	0.32	0.12
MnO	0.1	0.1	0.2	0.1	0.13	0.05	0.08	0.05
SO_3	0.1	0.2	-	0.3	0.2	0.10	0.34	0.14
LOI	2.8	2.8	13.9	16.4	8.98	7.20	4.36	4.62

As shown in Table 2.10, the first two columns (Oliveira2016, Neves,2018) report low CaO percentages. These samples were collected directly from an industrial facility that employs diamond wire saw technology. Since this specific cutting process does not require the addition of lime (CaO) as a chemical additive, the resulting residue maintains the low calcium profile of the original silicate rocks.

In contrast, the data presented by (Lunz, 2021; Moreira, 2021; Dias, 2024) show a significant increase in CaO content. This discrepancy is explained by the sampling source: these residues were collected from exclusive OSR landfills. These sites receive waste from two distinct technologies:

- Diamond wire saws, which do not use additives;
- Traditional gang saws, which utilize metallic blades and metallic abrasives.

The traditional gang saw process necessitates the addition of lime (CaO) to the mixture to mitigate the oxidation of the metallic components, particularly iron. Because these landfills consolidate residues from both types of machinery, the subsequent processes of mixing, leaching, and dispersion cause the CaO concentration to fluctuate significantly depending on the specific coordinates of the sampling point.

The variability of OSR is illustrated in Table 3, which shows the chemical composition from four different research studies, their average, and a comparison to the median results of a larger study of 70 samples by Moreira et al. (2021). The comparison shows that the differences between the averages are small, suggesting a consistent chemical profile for OSR-G (from "G" parent rocks) in the region studied.

This differentiation is confirmed by Barrientos et al. (2010), who characterized OSR-G (granite parent rock) samples M1 through M4, as presented in Table 2.11, highlighting a fundamental technical distinction based on the industrial sawing process employed, which is critical to understanding the chemical variability of the residue and its subsequent influence on geotechnical behavior.

Samples **M1, M2, and M3** are byproducts of conventional *gang saw* technology. This process utilizes a cooling system composed of water, steel grit, and hydrated lime. The presence of these industrial additives significantly alters the chemical signature of the residue, resulting in concentrations of iron oxide (Fe_2O_3) and calcium oxide (CaO) that are substantially higher than those found in the parent rock. This chemical enrichment is of particular geotechnical interest, as the residual CaO may trigger long-term curing and cementation reactions within stabilized soil layers.

Conversely, sample **M4** is obtained through *diamond disc* or wire-cutting technology. Unlike the gang saw method, this technology does not require the addition of steel grit or lime, relying primarily on water for cooling. Consequently, the M4 residue maintains a chemical composition nearly identical to that of the parent monzogranite, exhibiting much lower levels of industrial contaminants and acting as a more chemically inert filler.

Table 2.11: Chemical composition of the samples (Oxides %).

Oxide (%)	**M1**	**M2**	**M3**	**M4**	**RP**
SiO_2	66.1	66.0	67.5	69.7	71.9
Al_2O_3	13.0	14.4	13.6	15.8	13.7
Fe_2O_3	6.60	6.00	5.30	1.59	2.55
CaO	5.40	4.20	3.60	1.80	0.94
K_2O	4.70	4.80	5.00	4.50	6.94
Na_2O	3.01	3.22	3.00	4.00	3.34
MgO	0.52	0.50	0.39	0.50	0.25
P_2O_5	0.13	0.37	0.23	0.20	0.05
MnO	0.082	0.071	0.069	0.031	0.025
SO_3	0.059	0.047	0.037	0.021	n.d.

Note: n.d. = not detected.

Determination of the chemical composition according to (Aidico et al., 2012) of the slurries coming from the processing of marble (OSR-M) in Europe, shows results of the analysis significantly distinct from the typical OSR-G of Espírito Santo.

Table 2.12: Chemical composition of the marble slurry reordered by concentration.

Chemical Group / Oxide	**Content (%)**
CaO	55.32
MgO	0.44
SiO_2	0.36
P_2O_5	0.25
SO_3	0.10
Fe_2O_3	0.04
Na_2O	0.02
TiO_2	0.02
MnO	0.01
K_2O	0.01
Al_2O_3	0.00
L.O.I (Loss on Ignition)	43.35

The mineralogical diversity of OSR is governed by its geological origin, encompassing primarily silicate and carbonate minerals. The residue's composition is, therefore, directly dependent on the type of rock processed, such as granite or marble. Granite-derived OSR (OSR-G) is predominantly composed of quartz (SiO_2), feldspars, micas, and accessory minerals. Marble-derived OSR (OSR-M) is rich in calcite. X-ray Diffraction (XRD) and Scanning Electron Microscopy (SEM) are used to identify these minerals. Investigations by Lunz (2021) using XRD on OSR mixtures showed the presence of minerals such as quartz, kaolinite, and calcite (Figure 2.17).

Galetakis & Soultana (2016), for instance, conducted an extensive review and summarized the typical chemical compositions of OSR. They noted that OSR-M is predominantly calcareous, with high concentrations of CaO, around 55%, while OSR-G is mainly siliceous, with high levels of SiO_2 reaching even 70%, converging to the same conclusions of the Brazilian references already cited.

Furthermore, SEM analysis reveals angular or sub-angular particles with irregular edges, a morphology that promotes mechanical stabilization and enhances load-bearing capacity through particle interlocking.In Figure 2.18(a), the pure soil sample exhibits a distinctly aggregated structure.

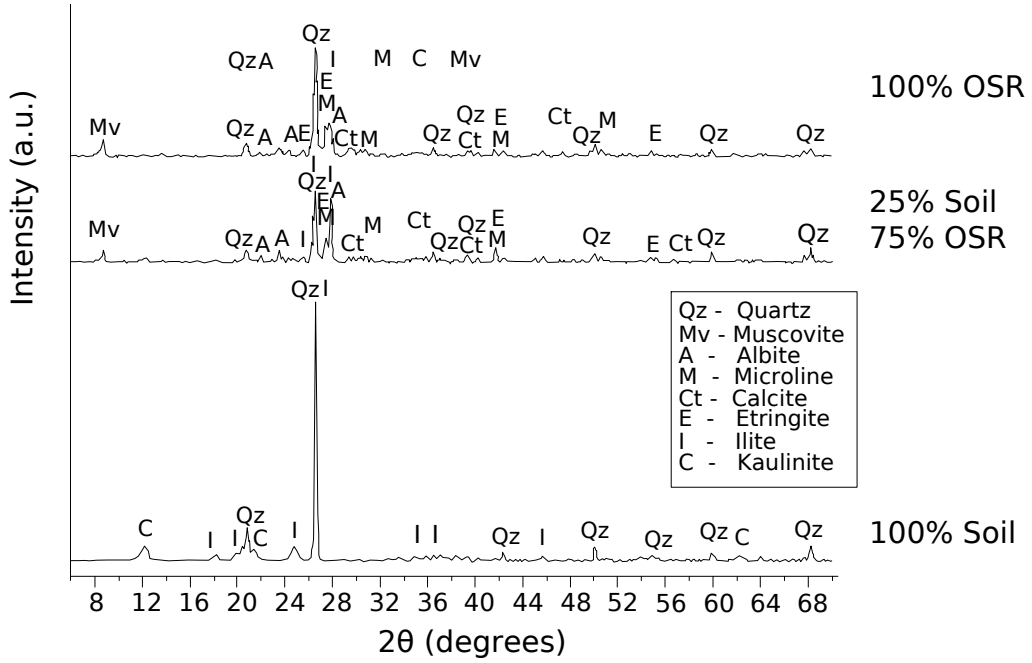


Figure 2.17: XRD pattern of OSR mixtures identifying mineral phases: quartz, kaolinite, and calcite (modified Lunz, 2021)

The soil particles are clustered into larger agglomerates, many of which appear equal to or larger than the 50 μm scale bar. This illustrates a coarser texture where individual fine particles are bound together. In contrast, Figure 2.18(b) shows the OSRs sample, which is composed of much finer, more discrete particles.

Table 2.13: Comparative of OSR-G and OSR-M Summarized Chemical Profiles Galetakis and Soultana (2016).

Elements	**OSR - Granite (OSR-G)**	**OSR - Marble (OSR-M)**
SiO_2 (%)	63.8 - 70.0	$\sim$10.0
CaO (%)	1.3 - 1.6	50.0 - 55.0
Al_2O_3 (%)	15.3 - 16.5	< 2.0
Fe_2O_3 (%)	5.3 - 7.6	< 2.0

Lohar (2023) used X-ray Diffraction (XRD) either to identify the primary minerals in OSR, finding it composed mainly of quartz, feldspar, calcite, mica, microcline, orthoclase, and kaolinite, aligned with Lunz (2021) results. The authors highlighted that the presence of these stable minerals, and the noted absence of those prone to swelling, is the primary reason for the material's non-swelling nature.

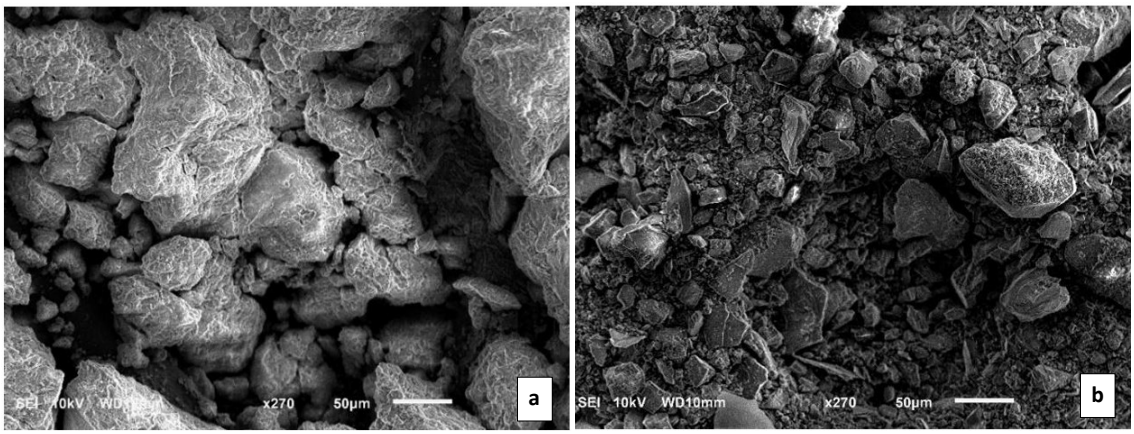


Figure 2.18: Scanning Electron Microscopy (SEM) images: (a) Pure soil sample showing aggregated structure; (b) OSRs sample showing fine discrete particles.

Despite variations, the accessory oxides and trace metals generally do not compromise the inert nature of OSR, which is environmentally compatible for use in geotechnical fills, subgrade improvement, and pavement layers (Freitas et al., 2012; Oliveira, 2015; Pequeno, 2020; Dias, 2024), results also obtained by Lohar and Shrivastava (2025), which environmental analysis indicated a low leaching risk, with heavy metal concentrations remaining within permissible limits for application in geotechnical fills, following the methodology of the U.S. Environmental Protection Agency (USEPA).

2.5 - STABILIZATION OF SOILS WITH RESIDUES

The tropical soils of Espírito Santo typically present low shear strength and high compressibility. Proper stabilization transforms these marginal materials into competent geomaterials.

2.5.1 - SOIL MIXTURES WITH SS-LD: HISTORICAL USE AND STRENGTH GAINS

For many decades, the state-of-the-practice in road engineering has utilized the California Bearing Ratio (CBR) as the standard metric for assessing the mechanical strength of paving geomaterials, especially in Brazil. This established paradigm has persisted through the advent of soil stabilization using steelmaking slags. This approach is exemplified by practical applications in the State of Espírito Santo, Brazil, where approximately 6 million metric tons of pig-iron and steelmaking slags, especially LD-SS have been utilized over the past 10 years. In these projects, the CBR test has served as the primary validation tool, measuring the substantial strength gains observed in the resulting mixtures with LD-SS.

Based on the study by Gomes et al. (2021), a characterization of LD-SS reveals a material with superior geotechnical properties for application in road base layers. The following

is a descriptive analysis of their data presented in Table 2.14. The LD-SS was classified by the AASHTO system as **A-1-a** (gravel and sand), indicating a material of excellent quality for subgrades to base layers. This a typical classification, supported by its grain size distribution, composed predominantly of gravel particles (38.50%) and sand (fine, medium, and coarse), with a low fine content (silt and clay) of only 9.30%. However, the industrial plants managed the production of the LD-SS and other slags and their GSD by the industrial process of separation and gradation, stocking them separately in typical ranges such as 0 to 12,70 mm (½"), 12,70 mm (½") to 25,4 mm (1"), 25,4 mm (1") to 38,10 mm (1 ½"), 38,10 mm (1½") to 76,2 mm (3"), and 76,2 mm up to 254 mm (10").

Table 2.14: Table 6. Geotechnical properties of the steelmaking slag (LD slag) (Adapted from Gomes et al., 2021)

Property	**LD slag**
Grain size distribution (%)	
Silt & clay	9.30
Fine sand	30.96
Medium sand	17.20
Coarse sand	4.04
Gravel	38.50
Specific gravity	3.47
Atterberg limits (%)	
Liquid limit	Non liquid
Plastic limit	Non plastic
Plasticity index	–
Soil classification	
AASHTO	A-1-a
Group index (GI)	0
Compaction characteristics	
CBR (%)	100.0
Maximum dry density (g/cm^3)	2.28
Optimal moisture content (%)	11.6
Expansion (%)	0.00

Furthermore, the material was identified as non-plastic, presenting null Atterberg limits, which minimizes risks of instability due to plasticity. Table 2.14 presents these and other basic geotechnical properties. Regarding compaction, the slag exhibits a high Maximum Dry Density (MDD) of 2.28 g/cm³, a value attributed to its coarse grain size and its high specific gravity of the grains (3.47) when driven to pavement layers. The Optimal Moisture

Content (OMC) is relatively low (11.6%) compared to natural soils, resulting in lower water consumption during construction.

In terms of bearing capacity, the **CBR test reached 100%** at the modified Proctor energy, far exceeding the minimum requirement of 80% mandated by Brazilian standards (such as DNIT ES 141/2010) for use in pavement bases. It is noteworthy that, despite the potentially expansive nature of LD-SS, the material used showed **0.00% expansion** in the CBR test, ensuring the volumetric stability required for road infrastructure. Nevertheless, this is an exception, because historically the most prevalent negative impact of LD-SS in any pavement layer is its high expansion, parameter that can reach up to 9% of volumetric expansion. This is proven by a guideline issued by Arcelor Brasil/CST (2006), which presents expansion for LD-SS mixed with other slags, including KRS, always greater than 3% in the Pennsylvania Test Method (PTM) 130/78 when applied alone (Table 2.15).

Table 2.15: Physical Characterization of the REVSOL Material (ArcelorMittal, 2016)

Property and Standard	**Value / Range**
Grain-size Distribution (DNIT – ME 080/94)	0 mm to 254 mm (0 to 10")
Plasticity (DNIT – ME 082/94 and DNIT – ME 122/94)	Non-plastic
Sand Equivalent (DNIT – ME 054/94)	> 35 %
Maximum dry apparent specific Gravity (DNIT – ME 129/94)	2.100 to 2.350 g/cm^3
Optimum Moisture Content (DNIT – ME 129/94)	12 to 16 %
California Bearing Ratio (CBR) (DNIT – ME 049/94)	< 70 %
Real specific Gravity (DNIT – ME 081/94 and DNIT – ME 084/94)	3.15 to 3.40
Unit Weight (DNIT – ME 152/95)	1.50 to 1.90 kg/dm^3
Shape Index (DNIT – ME 086/94)	0.890 to 0.930
Los Angeles Abrasion (DNIT – ME 035/94)	25 to 27 %
Expansion (METHOD PTM – 130/78)	> 3.00 %

2.5.1.1 Historical Evolution of LD-SS Availability

It is important to open a relevant explanation about LD-SS volumetric expansion, a process ignited by its age zero contact with water in its different forms in the environment: vapor and liquid. The steelmaking industry fought a battle in this matter, evolving the availability of LD-SS in its 'pure state' after generation, first to Acerita (the same strategy for Açobrita originated in the RJ state), a commercial name of LD-SS treated basically with humidification and drying cycles, once this material has been clearly identified as a soil stabilizer by different international studies.

This was a necessary evolution because the use of LD-SS alone in Brazil, outside any soil mixture, in its 'pure state', without any treatment to mitigate the 9% expansion, an excessive high level for any application, especially in pavement layers. Early attempts at pavement applications have led to excess of deformations, destroying any pavement and thus, the LD-SS reputation as a geomaterial in the 2000s. The expansion negative property spread across the technical community.

A second stage of this battle arrived with the conception of soil mixtures with more rationalized blends of the steelmaking slags available, always with the main target in mitigating expansion, once the SSI internalized the actual high potential of improvement in soil stabilization applications. This second stage led to the new form of LD-SS availability by the industry: blends with KRS and other typical steelmaking Residues, such as GBF-S.

Nevertheless, the most prevalent steelmaking slags (or residues) are LD-SS, now commercially called REVSOL. This material is the most prevalent in the blends of Table 2.15). The commercial names of the blends are now stated as "REVSOL Plus". LD-SS mixed with KRS and other steelmaking residues are novel available forms of steelmaking slags currently. Particularly, the name slag seems to be reserved for the residues with coarser GSD in the ranges of gravels and sands. REVSOL, as a commercial name, is not present yet in the national codes of DNIT or ABNT, however has been disseminated as primary coating pavement solution for rural roads in Espírito Santo.

In a commercial publication by ArcelorMittal (2016), Acerita and REVSOL appear listed, which means that they are not the same geomaterial, once Acerita has the expansion of LD-SS mitigated by industrial treatment. REVSOL is offered in two ranges of GSD: 0 to 19 mm and 19 to 32 mm.

Recent communication made available by ArcelorMittal (2025) suggests the strategic application of various steelmaking slag blends tailored to specific engineering requirements. Blends I, II and IV are still in place, as well as the two ranges of GSD for REVSOL. New commercial names arise, as Sidercal 0 a 19mm, which is the KRS itself of this study. Ecolastro,

Table 2.16: Commercial blends made available by the industry of steelmaking slags and recommended applications (ArcelorMittal, 2016)

Commercial Blend of SS	**Composition**	**Primary Applications - Suggested by the Steelmaking Industry**
Blend I	A 50/50 blend of LD-SS and KRS	Primary surfacing, yard paving, and grade elevation under clay layers.
Blend II	A blend of 1/3 LD-SS, 1/3 KRS, and 1/3 GBF-S	Base and sub-base courses for asphalt and interlocking paver pavements.
Blend III	A blend of 70% GBF-S and 30% KRS.	Base and sub-base courses for concrete and interlocking paver pavements.
Blend IV	An equal-part blend at 25% of GBF-S, KRS, LD-SS, and blast furnace sludge.	Base and sub-base courses for asphalt and interlocking paver pavements.

ranging from 32 to 75mm, and Siderita, from 0 to 200mm close to the commercial byproducts available.

2.5.1.2 Historical Impact of Expansion on LD-SS Reputation

It is important to open a relevant explanation about LD-SS volumetric expansion, a process ignited by its age zero contact with water in its different forms in the environment: vapor and liquid. The steelmaking industry fought a battle in this matter, evolving the availability of LD-SS from its "fresh" state — highly reactive and unstable — to treated forms. This transition is chemically documented by the morphological changes in the slag particles over time.

As demonstrated in Figure 2.11, the "fresh" LD-SS (at age zero) presents clean mineral surfaces where free lime (CaO) and periclase (MgO) are exposed to the environment, leading to the high expansion levels (around 9%) that historically compromised pavement integrity. In contrast, the "aged" material — equivalent to the industrially treated Acerita — exhibits a surface covered by rhombohedral calcite ($CaCO_3$) crystals. This carbonation layer acts as a chemical shield, indicating that the most critical expansion potential has been neutralized during the industrial humidification and drying cycles.

Initial attempts at pavement applications in Brazil led to excessive deformations, damaging the reputation of LD-SS as a geomaterial in the 2000s and before that. The industry's battle led to the commercial evolution of Acerita and later REVSOL, which are not merely commercial names but represent a shift in material processing to ensure volumetric stability. Still today, as a matter of fact, any civil engineer is able to mention the expansion as a major problem of LD-SS use in roads.

2.5.1.3 Geotechnical Strength Gains with LD-SS

The vast majority of practical infrastructure projects and academic research frameworks have studied the applications of steelmaking slags adopting the CBR to evaluate strength increments for embankments and pavement layers. The mechanical improvements of soil mixtures composed with LD-SS are fundamentally driven by interlocking and packing mechanisms that occur when the slag is integrated with various soil types. Furthermore, the mineralogical composition of the LD-SS—characterized by the presence of $Ca(OH)_2$, CaO, MgO, and FeO—contributes to the evolving chemical and physical stability in a soil mixture, depending on the type of the soil geology and GSD. This section provides a literature review of the evidence regarding strength gains through the use of LD-SS in soil stabilization, leveraging the extensive availability of laboratory and field data accumulated over the last decade, with some results including even the resilient modulus.

LD-SS is an abundant local byproduct, exhibit consistent quality and are readily available for large-scale infrastructure projects allowing the adoption of different strategies seeking the ORC, the MRC or the ZERO-E proportions proposed by Prandina & Farias (2025) for sub-base applications. Valuable data on LD-SS behavior, distinct from international literature, is provided by Resende (2010), who performed compaction and CLTT tests under different energies as detailed in Table 2.17.

The influence of LD-SS content on the mechanical strength of silty-clayey soils (AASHTO A-4) is detailed in the experimental data provided by Santos (2024). As illustrated in Figure 2.24, the integration of LD-SS into the soil matrix consistently yields higher bearing capacities compared to natural gravel mixtures. Specifically, at a 55% replacement ratio, the LD-SS mixture achieved a peak CBR of 65.9%, outperforming the natural gravel which reached 62.6%.

However, as the coarse aggregate percentage increases beyond this point, a slight downward trend in the CBR results is observed, with values shifting from 60.2% at 65% content to 59.5% at 75% content. Given that pure LD-SS can reach a CBR of 100%, as reported by Gomes et al. (2021), a modest result compared to the one of Resende (2010), who found 240% for CBR, it is correct to infer that the presence of the A-4 soil matrix plays an important role in the overall stability. The search for the Optimum Residue Content (ORC) becomes essential to maximize the CBR parameter in cases where it is the target parameter; the addition of specific amounts of silty soil may optimize the void-filling and packing density of the mixture. Nevertheless, once the threshold of the ORC is exceeded, the mechanical interlock between the slag particles is reduced, leading to the observed decrease in support capacity. This reinforces the strategy of balancing the soil-residue proportions to achieve the Maximum Residue Content

Table 2.17: MG-232 road CBR test on classified construction materials (from Resende, 2010)

Location	Material / Layer	TRB	CBR (%)	EXP (%)
F1 - EST.: 9+12	LD-SS Base	A-1-a	240	-0,14
F2 - EST.: 109+19	80% LD-SS Base + 20% Clayey Soil	A-1-a	180	-0,17
F3 - EST.: 209+19	Natural gravel Base	A-1-b	109	-0,02
F4 - EST.: 309+19	Natural gravel Base	A-1-a	90	0,08
F5 - EST.: 410	80% LD-SS Base + 20% Clayey Soil	A-1-a	270	-0,04
F6 - EST.: 509+10	80% LD-SS Base + 20% Clayey Soil	A-1-a	192,8	-0,08
F7 - EST.: 609+09	LD-SS Base	A-1-a	205	0
F8 - EST.: 710+05	LD-SS Base	A-1-a	265	0,08
F9 - EST.: 810+01	Natural soil Base	A-2-6	60	0,05
F10 - EST.: 907+01	Natural soil Base	A-2-5	89	0,07
F11 - EST.: 998+19	Natural gravel Base	A-1-a	179,4	0,02

(MRC) or the Zero-Expansion (ZERO-E) targets proposed by Prandina & Farias (2025a).

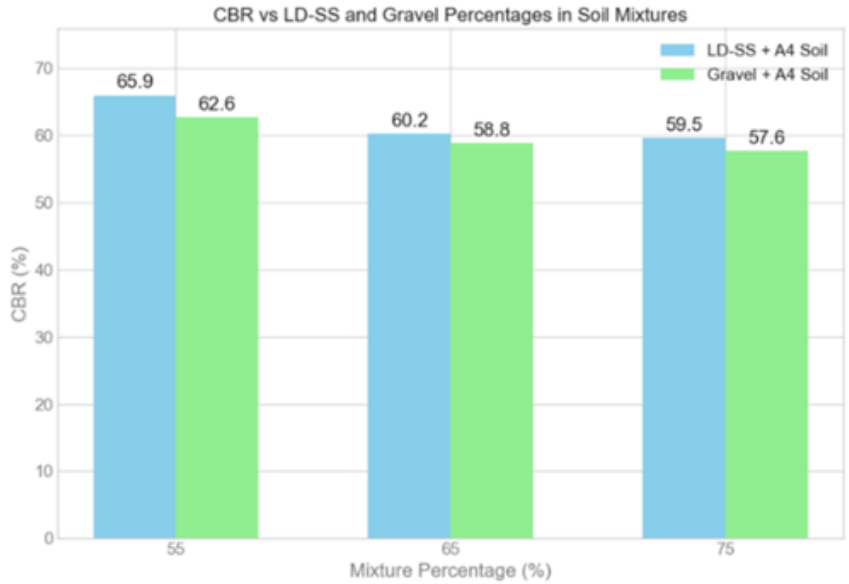


Figure 2.19: CBR vs LD-SS and gravel percentages in A-4 soil mixtures (from Santos, 2024)

In comparison to the trends observed by Santos (2024), the findings of Silva et al.

(2021) provide a more consistent perspective on the stabilization of A-4 soils. While the former identified a performance peak followed by a slight decline in bearing capacity at higher replacement ratios, the latter demonstrated a steady and linear increase in strength as the LD-SS content rose within the investigated range. Starting from a baseline CBR of 18.2% for the pure silty soil, the mixtures achieved 23.6% with 15% slag, and continued to climb to 28.3% and 39.6% for 25% and 35% slag concentrations, respectively (Figure 2.20). Although these values are more modest than those observed in clayey matrices, the behavior is remarkably consistent, indicating that the stony particles of the slag effectively reinforce the silty matrix. This linear growth suggests that for A-4 soils, the mechanical improvement is directly proportional to the amount of residue added, reinforcing the reliability of LD-SS as a stabilizing agent even in undergraduate-level experimental validations.

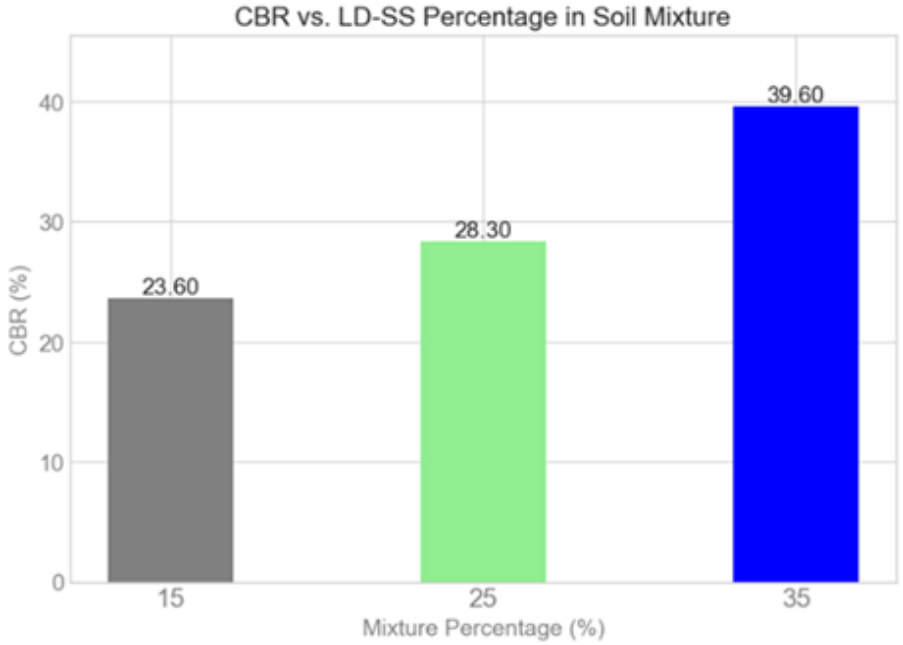


Figure 2.20: Continuous CBR growth for A-4 soil stabilized with LD-SS (modified from Silva, 2021)

The experimental study conducted by Boldrini & Pacheco (2022) provides a pragmatic analysis of the stabilization of highly plastic clayey soils from the Serra region in Espírito Santo. The base material was a fine-grained lateritic soil classified as CH (high plasticity clay) according to the USCS system. This soil is characterized by a high fine content, with approximately 70.9% of particles passing the #200 sieve (0.075 mm). Its Atterberg limits (LL = 49% and IP = 22%) and the mineralogical presence of kaolinite and hematite confirm its lateritic nature, which traditionally exhibits high support capacity when properly stabilized.

As demonstrated in Figure 2.21, the introduction of REVSOL (LD-SS) into this clayey matrix results in an significant increase in bearing capacity. While the pure soil (CH) presented a maximum CBR of 15.2%, the mixture with 50% slag content reached 234.6%. Increasing

the slag content to 70% and 80% further elevated the CBR values to 315.1% and 367.5%, respectively. These results highlight the pronounced hydraulic and mechanical interlocking effect of LD-SS when mixed with cohesive lateritic soils, far exceeding the requirements for structural pavement layers. The superior performance in comparison to the A-4 silty soils discussed previously suggests a higher chemical and physical affinity between lateritic clays and LD-SS.

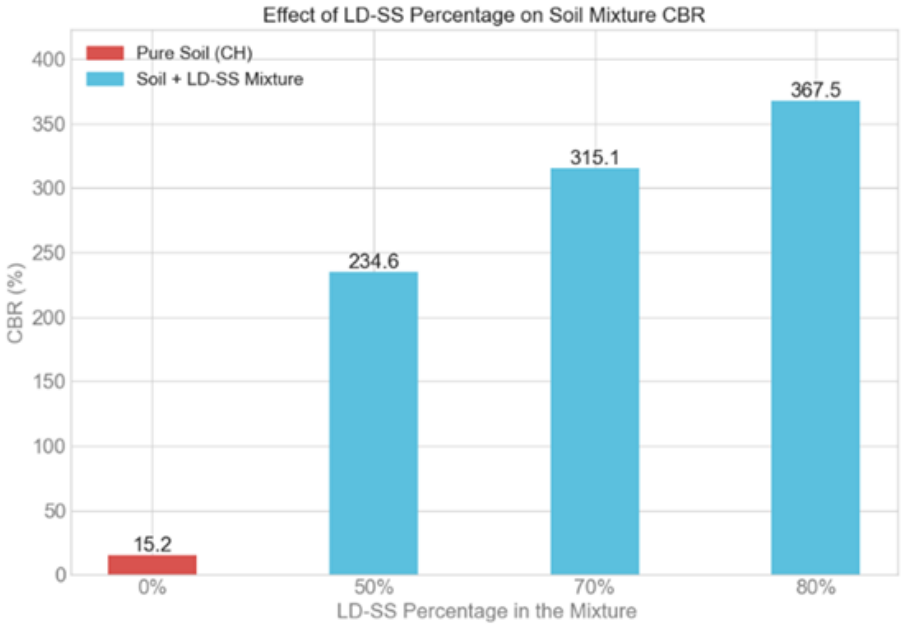


Figure 2.21: CBR vs LD-SS percentage for CH lateritic soil mixtures (modified from Boldrini & Pacheco, 2022)

Resende (2010) have also verified the impact of LD-SS on M_R which findings shown that the great positive difference of LD-SS CBR and LD-SS soil mixtures disappears when testing at CLTT to obtain MR for these 2 types of materials. The structural performance of the experimental sections on the MG-232 road was further validated through back-analysis of deflection basins obtained from Falling Weight Deflectometer (FWD) tests. As illustrated in Figure 2.23, the back-calculated resilient moduli for the different pavement layers provide a direct comparison between the pure LD-SS base and the 80/20 LD-SS/clayey soil mixture. The field results indicate that the sections stabilized with the soil-slag mixture maintained high structural stiffness, with back-calculated moduli often equivalent to those of the pure slag sections. This consistency between laboratory CLTT results and field back-analysis confirms that the addition of 20% cohesive soil does not compromise the structural integrity of the base layer. Instead, it optimizes the material's performance by providing a more stable matrix that effectively supports the traffic-induced stresses, aligning with the mechanical advantages of the soil-slag interlocking mechanisms previously discussed.

The 1089 sample was located at the EST 509+10, therefore a LD-SS mixture with

local soil by the proportion of 80/20 (LD-SS/soil), and the 1090 sample was located at the EST 70+05, a LD-SS pure initially unbound one-material layer. The CBR of the 1089 sample, a LD-SS/soil mixture, is 192,8% and for the 1090 sample, the CBR is 265%, a difference of 37%. Figure 2.23 shows the trend lines for both M_R materials. The data indicates that the initial performance gap narrows significantly under confinement; the difference accounts for less than 30% after σ_3 reaches 2 kPa (0.02 MPa), further reducing to approximately 10% at a σ_3 of 5 kPa (0.05 MPa).

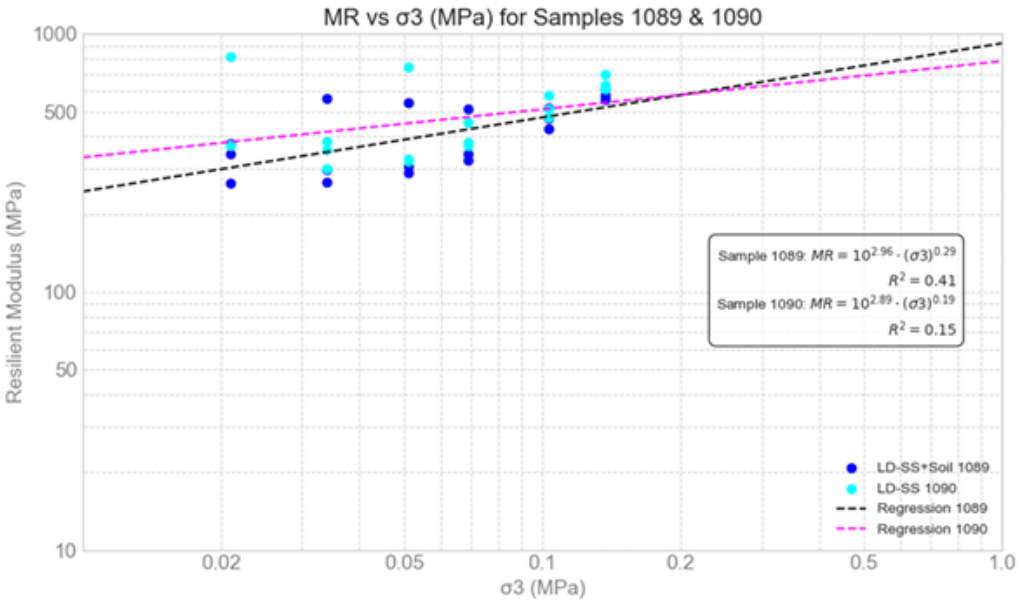


Figure 2.22: 1089 stake MR of LD-SS and 1090 stake LD-SS/soil mixture (modified from Resende, 2010)

As finally illustrated in Figure 2.23, the back-calculated resilient moduli for the different pavement layers provide a direct comparison between the sections using pure LD-SS base and the 80/20 LD-SS/clayey soil mixture. The field results indicate that the sections stabilized with the soil-slag mixture maintained high structural stiffness, with back-calculated M_R values often equivalent to those of the pure slag sections. This consistency between laboratory Cyclic Loading Triaxial Test (CLTT) results and field back-analysis confirms that the addition of 20% cohesive soil does not compromise the structural integrity of the base layer. Instead, it optimizes the material's performance by providing a more stable matrix that effectively supports traffic-induced stresses, aligning with the mechanical advantages of the soil-slag interlocking mechanisms previously discussed.

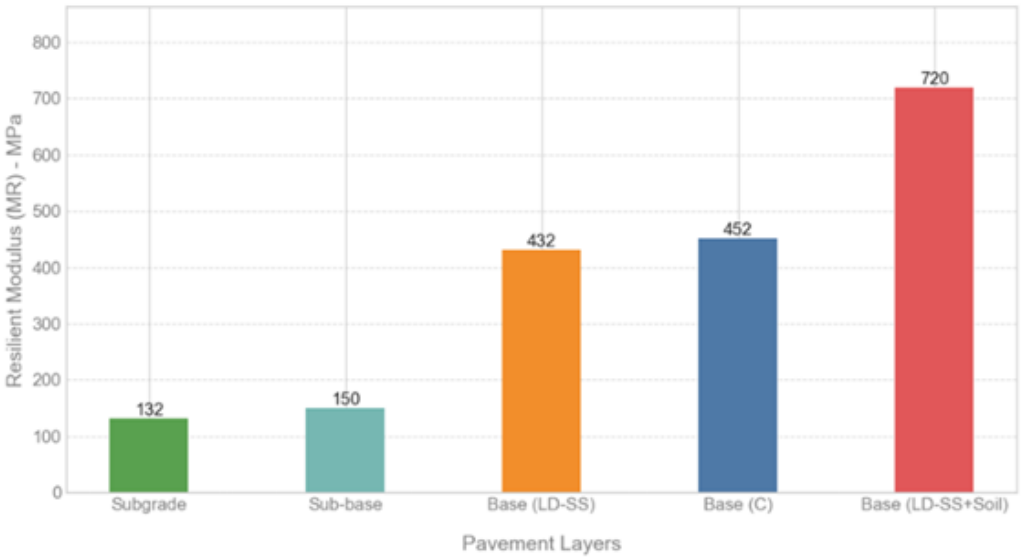


Figure 2.23: Back analysis of different pavement layers and different base layers materials including a 80% LD-SS mixed with 20% clayey soil (modified from Resende, 2010)

2.5.1.4 The Paradox of High-Performance Matrices: Analyzing the Structural Inversion in Santos (2024)

While the data from Silva et al. (2021) demonstrated a linear increase in bearing capacity for slag contents up to 35%, the broader experimental range explored by Santos (2024) revealed a counter-intuitive inversion of the common sense trend. Despite the pure LD-SS possessing a high intrinsic CBR, its integration into a high-quality lateritic-sandy matrix (LA' Type II) resulted in a performance peak followed by a distinct decline in mechanical strength.

This phenomenon can be explained by the transition from a matrix-dominated behavior to an aggregate-dominated one. In the LA' soil used by Santos (2024), which presents a naturally high CBR of 36.7%, the chemical satiety and the cationic threshold are reached much earlier than in highly plastic clays. Furthermore, the structural destruction by rigidity contrast plays a significant role; the excessive presence of rigid slag particles (above 55%) creates stress concentrations that "crush" the lateritic connections of the soil matrix, leading to the observed drop in CBR from 65.9% to 59.5% (Figure 2.24).

Despite the pure LD-SS possessing a high intrinsic CBR (frequently exceeding 100% to 200%), its integration into a high-quality lateritic-sandy matrix (LA' Type II) resulted in a performance peak followed by a distinct decline in mechanical strength.

This phenomenon, hereafter referred to as the Inversion of Common Sense in Lateritic Stabilization, can be detailed by four convergent technical factors identified in this research:

1. Reciprocal Stabilization and the "Curing" of the Residue

Contrary to the traditional view of soil as a passive substrate, the interaction between LA'

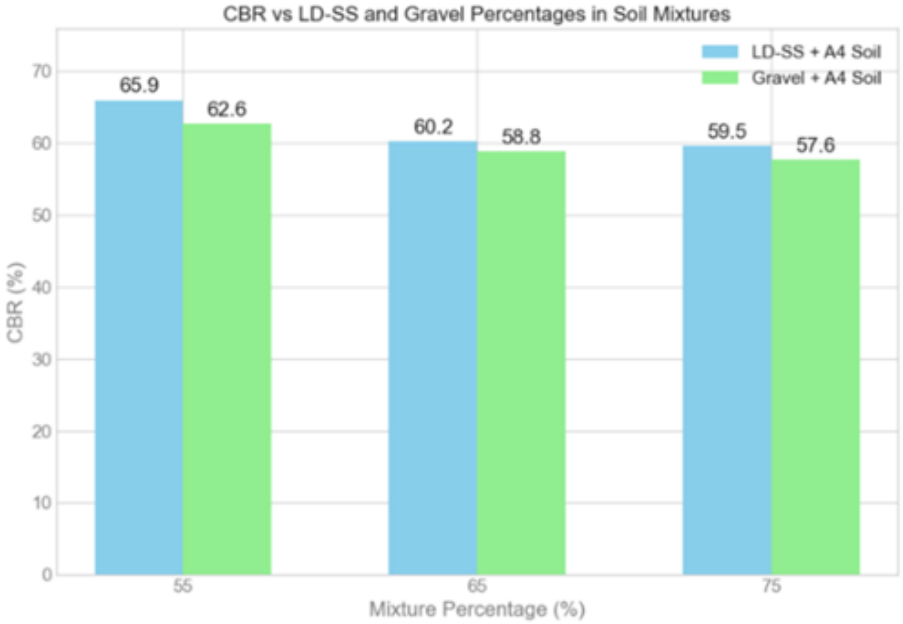


Figure 2.24: CBR inversion at high replacement ratios in A-4 lateritic soil (modified from Santos, 2024)

soils and LD-SS is a reciprocal stabilization. While the slag provides a granular skeleton and chemical cations, the lateritic matrix acts as a confining and "buffering" agent for the slag. In this synergy, the soil matrix neutralizes the expansive potential of the residue while the slag enhances the soil's friction. However, this balance is fragile; when the slag content exceeds the matrix's ability to "embrace" the aggregates, the reciprocal benefit is lost, and the mixture begins to behave as a poorly-graded granular material.

2. Chemical Satiety and the Cationic Threshold

The A-4 (LA' Type II) soil utilized by Santos (2024) is characterized by low plasticity and a naturally high CBR (36.7%). Due to the lower clay content compared to heavy plastic clays, the Cation Exchange Capacity (CEC) of the matrix is saturated much earlier. Once the "chemical shock" is achieved—where the available lime in the LD-SS has already optimized the flocculation and cementation of the fines—any additional slag acts merely as an inert aggregate. In this scenario, the "Chemical ORC" (Optimum Residue Content) is reached at lower percentages (between 30% and 55%), after which the excess chemical potential is wasted.

The A-4 (LA' Type II) soil utilized by Santos (2024) is characterized by low plasticity and a naturally high CBR (36.7%). Due to the lower clay content compared to heavy plastic clays, the Cation Exchange Capacity (CEC) of the matrix is saturated much earlier. Once the "chemical shock" is achieved—where the available lime in the LD-SS has already optimized the flocculation and cementation of the fines—any additional slag acts merely as an inert aggregate. In this scenario, the "Chemical ORC" (Optimum Residue Content) is reached at lower percentages (between 30% and 55%), after which the excess chemical potential is wasted.

3. Structural Destruction by Rigidity Contrast

The lateritic matrix possesses an inherent structural strength derived from its mineralogical arrangement. A critical factor in the observed CBR decline is the Stress Concentration at the Matrix-Aggregate Interface. Because the LD-SS particles are significantly more rigid than the lateritic matrix, an excess of these "large rigid bodies" creates points of high stress intensity under loading. As the aggregate content increases beyond 55%, these rigid particles begin to "crush" the lateritic connections of the matrix before a homogeneous distribution of stress can occur. This mechanical incompatibility leads to a localized destruction of the soil's structure, explaining why the CBR dropped from 65.9% to 59.5% as slag content increased.

The lateritic matrix possesses an inherent structural strength derived from its mineralogical arrangement. A critical factor in the observed CBR decline is the Stress Concentration at the Matrix-Aggregate Interface. Because the LD-SS particles are significantly more rigid than the lateritic matrix, an excess of these "large rigid bodies" creates points of high stress intensity under loading. As the aggregate content increases beyond 55%, these rigid particles begin to "crush" the lateritic connections of the matrix, configured as Figure 2.25c, before a homogeneous distribution of stress can occur. This mechanical incompatibility leads to a localized destruction of the soil's structure, explaining why the CBR dropped from 65.9% to 59.5% as slag content increased.

4. Dual Engineering Perspectives on the Optimum Residue Content (ORC)

The relationship between the AASHTO A-4 soil and the LD-SS can be analyzed from two distinct engineering perspectives, each defining a specific Optimum Residue Content (ORC):

Viewpoint A: Soil Matrix Stabilization. When the primary objective is the improvement of the lateritic soil, the ORC is governed by a balance of chemical and physical interactions. For the LA' Type II soil, this optimum is likely positioned below the 55% slag replacement threshold to minimize cumulative stress concentrations that would otherwise degrade the structural integrity of the lateritic matrix. The existence of chemical synergy is evidenced by the consistent widening of the gap between the CBR of LD-SS mixtures and that of natural gravel as the replacement ratio approaches the optimum. It is estimated that at the peak ORC, the difference between the CBR of the slag mixture and the gravel mixture would reach between 5 and 10 percentage points, confirming the superior performance of the residue LD-SS.

Viewpoint B: Slag-Base with Soil-Filler. Conversely, when the LD-SS is considered the primary base material, the A-4 soil functions as a mineral filler. In this scenario, the ORC for the soil-filler would logically fall between 0% and 10%, which is well described by the Figure 2.25b. This lower percentage aligns with the structural filler principle established by the physical state models of Yoder and Witczak (1975) and Yildirim and Prezzi (2015). Under this configuration, the soil provides the necessary lateral confinement to stabilize the

grain-to-grain contact of the slag skeleton. Beyond this 10% threshold, the transition towards a matrix-controlled state begins, potentially leading to the mechanical instability and loss of support capacity observed in mixtures with excessive fines.

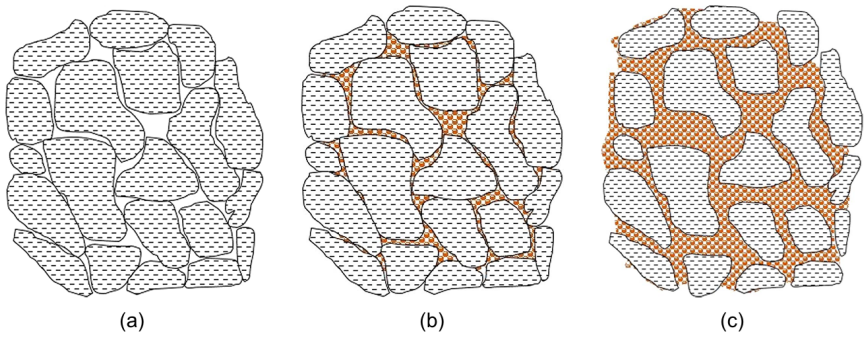


Figure 2.25: Physical states of soil-aggregate mixtures and the filler effect (modified from Yoder and Witczak, 1975; Yildirim, 2023)

These results reinforce the strategy of balancing soil-residue proportions to identify an eventual Symmetry Point where chemical cementation and mechanical interlocking are optimized, aligning with the ORC concepts proposed in this research.

In summary, the transition of LD-SS from a potentially deleterious byproduct to a high-performance geomaterial is fundamentally governed by its mineralogical maturation through hydration and carbonation. Understanding this "aging" process is essential for the technical validation of commercial treatments, such as those applied to Acerita, seeking to ensure volumetric stability in pavement layers. However, the contemporary valorization of steelmaking residues often involves the integrated use of LD-SS with other specialized byproducts, most notably Kambara Reactor Slag (KRS). While both materials share the presence of unstable mineral phases—such as free lime and periclase—their geotechnical behavior is not identical. This discrepancy is primarily rooted in their distinct metallurgical origins: whereas LD-SS is a byproduct of oxidative refining in the steel converter, KRS emerges from the hot metal desulfurization process in the Kambara Reactor. This fundamental difference in thermal cycles and chemical reagents results in distinct reactivity profiles and expansion levels, the understanding of which is crucial for the design of hybrid stabilized infrastructure, as discussed in the following section.

2.5.2 - SOIL MIXTURES WITH KRS: POTENTIAL FOR CHEMICAL STABILIZATION AND POZZOLANIC REACTIONS

The incorporation of KRS into soils generating mixtures that can be designed, a notable increase will typically happen in MDD after compaction, CBR, both of which are essential

indicators of soil improvement (Cunha, 2020; Pires et al., 2019). The improvement in MDD is attributed to the dense, angular particles of SS that fill and replace voids and soil-voids within the soil matrix, leading to a more compacted structure. This densification effect is further supported by the chemical reactivity of SS particles with the surrounding soil, which can induce secondary cementation reactions, especially in the presence of moisture and fine soil fractions (Pires et al., 2019; Oliveira, 2016). The following subsection elucidates the fundamental chemical mechanisms and physicochemical reactions governing the interaction between Kambara Reactor Slag (KRS) and the clay fractions of the evaluated soil matrices.

2.5.2.1 Chemical Mechanisms and Cation Exchange

The stabilization of high-plasticity clays using Kambara Reactor Slag (KRS) is primarily initiated by the high concentration of free calcium oxide (CaO), which typically exceeds 40% in this industrial byproduct (Fardin, 2024; Pires et al., 2019). Upon contact with the soil's moisture, KRS promotes an immediate increase in the pH of the mixture (alkaline shock), which is essential for the subsequent solubilization of silica and alumina from the clay minerals (Bridi, 2020; Fardin, 2024). This condition fulfills the classic criteria established by Eades (1966), asserting that a pH near 12.4 is mandatory for the dissolution of silicate and aluminate phases to sustain pozzolanic reactions. This initial chemical environment triggers a rapid cation exchange process where divalent calcium ions (Ca^{2+}) displace monovalent cations (such as Na^{+} and K^{+}) on the surfaces of the clay particles according to Pires et al. (2019) and Magalhães et al. (2020).

This exchange significantly reduces the thickness of the diffuse double layer surrounding the clay particles, decreasing electrostatic repulsion and the amount of absorbed water Magalhães et al. (2020); Pires-Teixeira & Pires (2021). Consequently, the soil undergoes immediate flocculation and agglomeration, transforming its texture from a plastic mass into coarser, more granular clusters as observed by Bridi (2020) and Fardin (2024). Understanding this "immediate effect"—summarized in Table 2.18—is the fundamental justification for characterizing the material at Day 0 (immediate state), as it captures the instantaneous mechanical gain derived from physical-chemical modification before the onset of pozzolanic reactions (Oliveira et al., 2019). This mechanical transformation into a resilient matrix is consistent with the seminal findings of Thompson (1966) regarding the elastic properties of calcium-stabilized soils, justifying the mechanistic evaluation adopted in this research.

Table 2.18: Chemical Mechanisms of KRS-Soil Interaction

Mechanism	Technical Description	Source(s)
High CaO Provision	High free-lime content ($> 40\%$) triggers immediate alkalinity, essential for mineral solubilization.	Eades & Grim (1966); Fardin (2024); Pires et al. (2019)
Immediate Cation Exchange	Ca^{2+} ions displace monovalent cations on clay surfaces almost instantaneously upon mixing.	Bridi (2020); Magalhães et al. (2020); Pires et al. (2019); Thompson (1966)
Double Layer Reduction	Substitution by divalent ions reduces electrostatic repulsion and adsorbed water thickness.	Magalhães et al. (2020); Pires-Teixeira & Pires (2021)
Flocculation & Agglomeration	Rapid transformation of plastic clay texture into larger, stable granular-like "flocs."	Bridi (2020); Fardin (2024)
Early-Age Stability	Presence of portlandite [$Ca(OH)_2$] and calcite ($CaCO_3$) ensures immediate mechanical stability.	Fardin (2024); Little (1995) Oliveira et al. (2019)

2.5.2.2 Formation of Cementitious Compounds

Following the initial cation exchange and flocculation, the long-term mechanical improvement of the stabilized matrix depends fundamentally on time-dependent pozzolanic reactions. In the highly alkaline environment sustained by the KRS, solubilized silica and alumina from the clay react with the available calcium to precipitate cementitious products, primarily Calcium Silicate Hydrate (C-S-H) and Calcium Aluminate Hydrate (C-A-H) Fardin (2024); Pires et al. (2019). The formation of these specific hydrates was first mineralogically established in the United States by Eades & Grim (1960), who identified these compounds as the primary binders in calcium-stabilized clay systems.

These cementitious gels crystallize over time, binding the flocculated soil particles into a rigid macroscopic skeleton. This mechanism aligns with the fundamental structural model proposed by Herzog & Mitchell (1963), where the development of a cemented matrix leads

to the significant gains in the Resilient Modulus (M_R) observed in this study. Furthermore, secondary mineralogical transformations, including the formation and consumption of ettringite within the matrix, play a crucial role in microstructural densification. As consolidated by the investigations of Hunter (1988) on mineral growth in stabilized clays, this process effectively occupies interstitial voids, reducing the porosity of the compacted layer and further amplifying its overall structural resistance (Oliveira et al., 2019). A summary of these long-term microstructural and cementitious mechanisms is presented in Table 2.19.

Table 2.19: Microstructural and Long-Term Cementitious Mechanisms of KRS-Soil Stabilization

Mechanism	**Technical Description**	**Source(s)**
Pozzolanic Precipitation (C-S-H & C-A-H)	Solubilized silica and alumina react with available calcium in a highly alkaline environment to precipitate cementitious hydrates.	Eades & Grim (1960); Fardin (2024); Pires et al. (2019)
Rigid Skeleton Development	Crystallization of cementitious gels binds flocculated soil particles into a rigid macroscopic matrix, driving the long-term gain in Resilient Modulus (M_R).	Herzog & Mitchell (1963)
Microstructural Densification	Secondary mineralogical transformations, including the dynamics of ettringite, occupy interstitial voids and drastically reduce layer porosity.	Hunter (1988) Oliveira et al. (2019)

To understand the stabilization potential of KRS, it is essential to analyze its behavior in challenging geological environments, such as the saprolitic soils of the Brazilian coast. Magalhães et al. (2022) conducted a significant investigation using a Non-Lateritic Silt (NS'), classified as a gneissic saprolitc AASHTO A-4, clayey yellow silt soil. Unlike the "noble" lateritic soils, this material is characterized by higher moisture sensitivity and a precarious natural bearing capacity (CBR $\approx 12\%$).

The results of the 70% slag mixtures (LD-SS and KRS) with 30% of this non-lateritic soil reveal a counter-intuitive phenomenon. While the incorporation of the byproducts significantly improved the bearing capacity compared to the natural soil, the increase in compaction energy did not yield linear gains. As shown in Table 2.20, the highest mechanical performance was achieved at Intermediate energy, while the Modified energy actually led to a reduction in CBR values.

Table 2.20: Comparison of CBR, MDD, and OMC for 70% Slag and 30% Non-Lateritic Soil (S2) mixtures under different compaction energies (Adapted from A. J. Magalhães et al., 2022)

Proctor	**70% LD-SS**			**70% KRS**		
Energy	**CBR (%)**	**MDD (g/cm^3)**	**OMC (%)**	**CBR (%)**	**MDD (g/cm^3)**	**OMC (%)**
Standard	84.0	2.17	10.8	79.0	2.07	14.2
Intermediate	**120.0**	**2.20**	**10.6**	**109.0**	**2.11**	**13.6**
Modified	96.0	2.12	9.7	98.0	2.14	12.9

This behavior, where the Modified energy "destroys" the gain in bearing capacity, suggests a structural degradation threshold. In non-lateritic matrices, the excessive shear stress and impact of Modified compaction may cause particle crushing at the aggregate-soil interface or the breakdown of the fragile saprolitic connections. This phenomenon provides a robust scientific justification for the methodology adopted in the forthcoming stages of this doctoral research, which will focus exclusively on **Intermediate energy**, once the majority of soils tested were colected in Espírito Santo sites. This choice ensures the optimization of the mechanical interlock between the KRS and the soil matrix without inducing the deleterious effects of over-compaction, thereby identifying the true operational ceiling of the stabilized layer.

The incorporation of LD-SS and KRS into fine-grained soils generally enhances their engineering performance by simultaneously altering plasticity and increasing mechanical strength. The primary stabilization mechanism involves cation exchange, where calcium ions (Ca2+) released by the slag replace monovalent ions on clay surfaces, promoting flocculation-agglomeration and compressing the diffuse double layer (Andrade, 2018; Fardin, 2024; Meneguete, 2018). This physicochemical alteration typically reduces the Liquid Limit and increases the Plastic Limit, leading to a marked decrease in the Plasticity Index and swell potential. Consequently, the soil becomes more workable and easier to compact, facilitating the achievement of target densities (Sant'ana, 2003; Rohde et al., 2003; Zumrawi & Eltayeb, 2016)

These microstructural changes directly translate into macrostructural improvements in Shear Strength (S_u) and Unconfined Compressive Strength (UCS). The gain in strength is attributed to the combined effects of increased internal friction, provided by the rough texture of slag particles, and the development of cohesion through the formation of cementitious gels (C-S-H and C-A-H) from pozzolanic reactions (Ramos, 2018; Fardin, 2024; Nunes, 2024; Oliveira et al., 2019; Shen et al., 2009; Yi et al., 2015).

Gomes et al. (2021) is another study which have compared the performance of KRS and LD-SS. Testing the materials in broader range for subgrade improvement, they indirectly identified the Optimal (ORC) and Maximum (MRC) Residue Contents that maximize CBR, thereby enhancing structural integrity, as illustrated in Figure 2.26. In the context of primary

surfacing (unpaved roads), where another gnaissic saprolitic A-4, clyey yellow silt soil (NS' – Non-Lateritic) acts as the matrix, the addition of slag promotes an inversion in the plasticity curve and a significant leap in structural support.

Figure 2.26 details the performance indicators for the optimum design: the CBR variation (a) shows exponential growth in bearing capacity as slag content increases; the Plasticity Index (b) undergoes a drastic reduction due to cationic shock; the CBR sensitivity to moisture (c) decreases, ensuring structural resilience during rainy periods; and the Optimum Moisture Content (d) adjusts as the granular skeleton becomes predominant. These data corroborate the strategy proposed by Prandina & Farias (2026), suggesting that the Optimum Residue Content (ORC) must be calibrated to ensure the mixture not only achieves peak support but also maintains the chemical and physical stability required for each specific pavement layer.

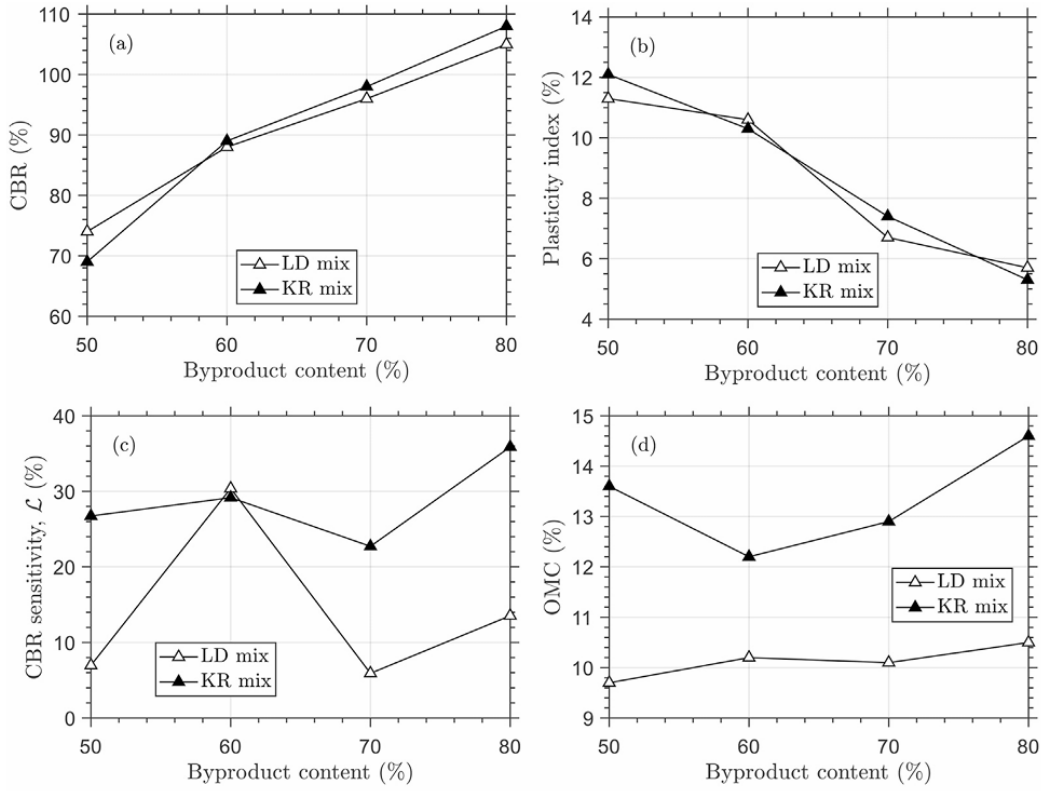


Figure 2.26: Performance indicators for ORC of soil/LD-SS and soil/KRS: variation of CBR (a), Plasticity index (b), CBR sensitivity to moisture (c), and OMC (d), at different LD slag (LD-SS, open symbols) and KR slag (KRS, solid symbols) contents (Modified from Gomes et al., 2021)

To complete the overview on soil-KRS mechnical gains, Bastos (2022) presents the evolution of the CBR values presented in Table 2.21, which reveals a dual-stage strengthening mechanism. The initial leap in performance, where the poor-quality Soil AE shifts from 25.3% to over 80% (Intermediate energy), is primarily driven by **cationic shock**. The immediate release of Ca^{2+} from the KRS induces flocculation of the clay minerals, reducing plasticity and

establishing a rigid initial framework through improved particle interlocking.

The secondary performance leap is evidenced by the results after 28 days of curing, where the CBR reaches 110.0%. This significant increment is attributed to **pozzolanic reactions**, where the high-pH environment promotes the formation of cementitious hydrates (CSH and CAH) that weld the slag aggregates to the soil matrix. This chemical reinforcement not only explains the high CBR values but also provides the scientific basis for the superior Resilient Modulus (MR) results discussed in the following section, as the stabilized matrix transitions from a purely frictional material to a semi-rigid, high-performance geomaterial.

Table 2.21: CBR results for natural soils and stabilized mixtures based on laboratory characterization (Adapted from Bridi, 2020; Furieri, 2019; Nepomuceno, 2019)

Soil / Mixture Type	**CBR (%) Intermediate**	**CBR (%) Modified**	**CBR (%) 28-Day Cure**
Solo AE (A-7-6)	22.7	25.3	–
Solo JP6 (A-2-6)	49.9	89.1	–
AE + 20% KRS	81.2	103.2*	110.0**
JP6 + 3% Cement (SMC)	–	128.5	–

*Value obtained from the consolidated laboratory records of Nepomuceno (2019).

**Result for AE + 20% KRS mixture cited from Bridi (2020).

In detail, the chemical stabilization mechanisms take place, the first phenomenon is the cationic shock, the latter complemented by pozzolanic activity. Beyond the physical densification described by the MDD-CBR correlation, the structural evolution of the soil-slag mixture is further enhanced by these sequences of complex chemical interactions. This stabilization initiates with the *cationic shock*, where the release of calcium ions (Ca^{2+}) triggers immediate ion exchange and flocculation-agglomeration of the clay minerals. This immediate phase reduces plasticity and establishes a stable initial framework.

Subsequently, the mixture undergoes long-term *pozzolanic reactions*. In the high-alkalinity environment maintained by the slag, dissolved silica and alumina react with calcium to form cementitious products (CSH and CAH). These hydration products fill capillary voids and weld the particles into a permanent, cemented matrix. This chemical synergy not only explains the superior performance observed after the 96-hour immersion but also guarantees the structural durability and increased stiffness required for high-performance pavement layers.

While the empirical gains in CBR provide a clear indication of the immediate and long-term bearing capacity increments, they represent a static perspective of the material's strength. The true engineering value of the chemical synergy—derived from the initial flocculation and the subsequent development of cementitious hydrates—lies in its ability

to enhance the dynamic stiffness and durability of the pavement structure. Therefore, to move beyond traditional empirical design abundantly evidenced and understand how these stabilized matrices respond to repeated traffic loads, it is essential to evaluate their mechanistic performance. This transition from static support to dynamic stiffness, quantified by the Resilient Modulus (M_R), reveals a fundamental rewrite of the soil's mechanical behavior, shifting from a moisture-sensitive substrate to a high-performance, stress-dependent geomaterial, under the still state-of-the-art MeDiNa methodology, which is figthing its on batle to take the state-of-the-practice place where it belongs.

2.5.2.3 Resilient Modulus (MR) of KRS-Soil Mixtures

This section consolidates the technical transition from empirical support (CBR) to mechanistic performance (Resilient Modulus), where the impact of KRS on lateritic matrices becomes truly evident. The studies by Bastos (2022) and Pires et al. (2019) provide a compelling demonstration of how industrial residues can fundamentally rewrite the mechanical behavior of local soils through chemical and physical synergy.

To evaluate the stiffness of stabilized layers under repeated traffic loading, Bastos (2022) selected two lateritic matrices from the Espírito Santo coastal region: *Soil AE* (A-7-6; LG'), a yellowish clay with low natural support, and *Soil JP6* (A-2-6; LA'), a high-quality reddish-brown clayey sand.

The transformation observed through the addition of 20% KRS is remarkable. In its natural state, the A-7-6 clay exhibits a "decreasing stiffness" behavior typical of cohesive materials, where the stiffness decreases as the deviator stress (σ_d) increases. However, the incorporation of KRS induces a "stiffness-increasing" effect, characteristic of high-quality granular materials.

The M_R versus the deviator stress graph of the soils and a KRS-soil mixture is presented in Figure 2.27 and shows the excellent results of the addition of 20% KRS, transforming positively the performance of the soil in respect to the MR. The use of KRS has the potential to stabilize a locally available, poor-quality cohesive soil (A-7-6), creating a material that outperforms even a standard, untreated granular fill (A-2-6).

This has significant economic and logistical advantages, as it can reduce the need to haul in more expensive quarry materials. The stabilization has not only made the soil mixture greater in strength; it fundamentally transformed its mechanical behavior from that of a low-quality clay into a high-performance, increasing stiffness material suitable for robust pavement structures.

In summary, the integration of LD-SS and KRS into soil matrices leads to significant

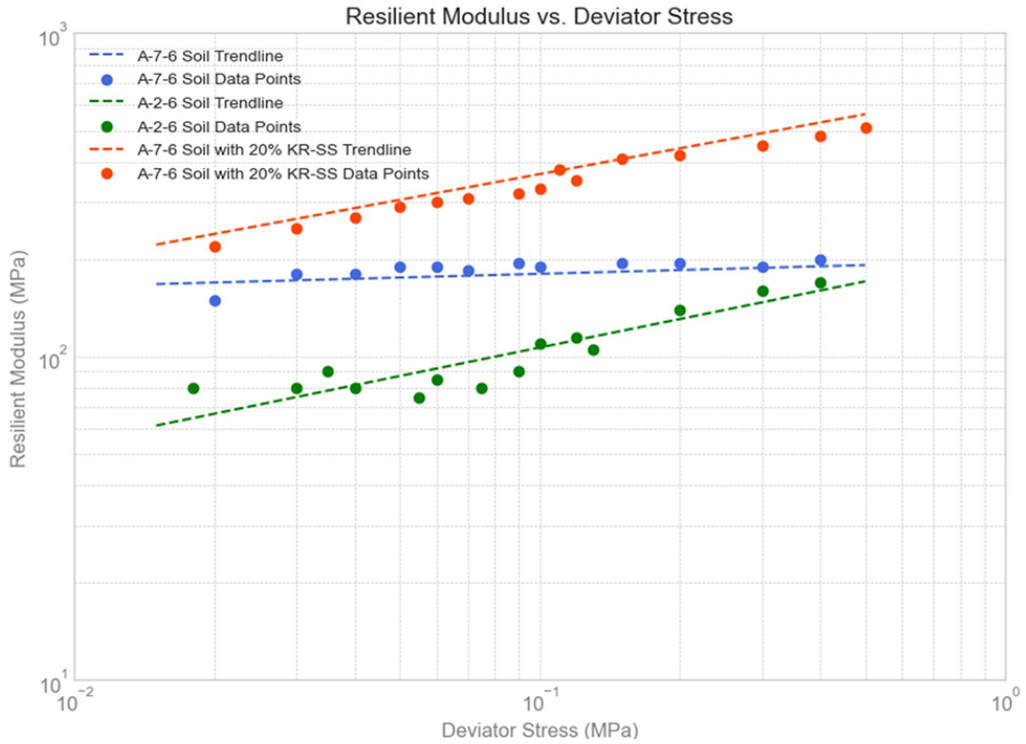


Figure 2.27: Resilient Modulus (M_R) vs. deviator stress (σ_d) for natural soils and the AE + 20% KRS mixture, highlighting the shift to stiffness-increasing behavior (Modified from Bastos, 2022)

gains in strength and rigidity, represented in the modulus of resilience (M_R), primarily through mechanical stabilization mechanisms. The resulting mixtures exhibit improved elastic response under repeated loading, making them suitable for demanding geotechnical applications such as pavement layers.

KRS and LD-SS present aggressive chemical stabilization potential. When mixed with clayey soils, both can trigger a three-phase process (Pires et al., 2019):

- **Cation Exchange (Immediate):** Calcium ions (Ca^{2+}) from the **KRS** displace monovalent ions on clay surfaces, reducing the **Plasticity Index (PI)** (Fardin, 2024).
- **Nucleation and Skeleton Formation (Short-term):** Granular slag particles form an interlocked skeleton, increasing stiffness (Oliveira et al., 2019).
- **Pozzolanic Reactions (Long-term):** Calcium reacts with soil silica and alumina to form **C-S-H** and **C-A-H** gels (Ramos, 2018).

Pires et al. (2019) demonstrated that adding 20% **KRS** to clayey soil increased the **CBR** to 132% and the **Resilient Modulus** (M_R) to over 1,100 MPa—double the stiffness of sandy soil stabilized with 3% Portland cement. This reinforces the status of these mixtures as high-performance, stress-dependent geomaterials.

The incorporation of Ornamental Stone Residue KRS significantly enhances the M_R of problematic high-plasticity soils, such as those classified as A-7-5 and A-7-6. This improvement is primarily driven by a reduction in the plasticity index, which shifts the cohesive matrix toward a more granular behavior, thereby mitigating plastic flow and permanent deformation Braz (2024); Lunz (2021); Mello (2019); Nascimento (2019).

Recent investigations by Mendoza2023 and Fardin2024 provide crucial data on the Resilient Modulus (M_R) of these binary systems, highlighting the profound impact of the stabilizer's grain size distribution (GSD). The majority of KRS generated is typically a coarse material, with only 5% to 10% of its particles passing the #200 sieve.

Dynamic triaxial testing of a local red sandy clay—classified as SC (USCS) and A-7-6 (AASHTO) with a Group Index (GI) of 5—reveals a low-resilience matrix. This soil is highly susceptible to variations in confining stress (σ_3) and deviatoric stress (σ_d), as demonstrated by the log-log regression models in Figure 2.28. The incorporation of 20% KRS (full natural GSD) significantly elevates the M_R behavior, confirming the structural benefits of the chemical mechanisms and the mechanical advantage of introducing coarser particles into the soil matrix.

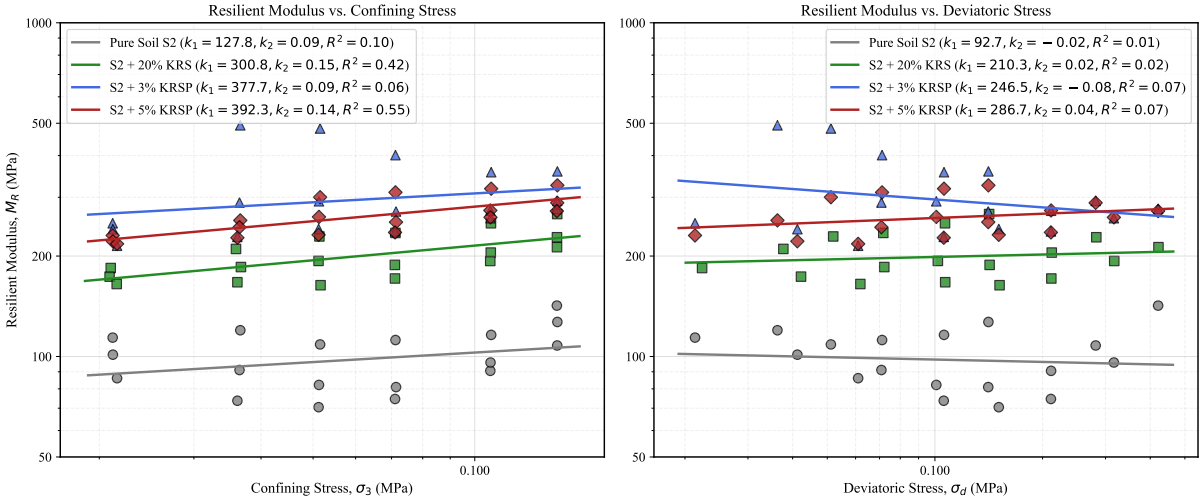


Figure 2.28: Log-log regression analysis of Resilient Modulus (M_R) versus confining and deviatoric stresses for pure and KRS-stabilized soil specimens (Adapted Mendoza, 2023; Fardim, 2024).

However, the most remarkable finding from these recent studies is the granulometric sensitivity of the stabilization process, captured by the 3D composite model surfaces in Figure 2.29. When KRS is introduced exclusively as a fine powder (KRSP), addition rates as low as 3% and 5% generate M_R surfaces that drastically outperform the 20% full-GSD mixture across various stress states.

Specifically, the mechanical performance of the 5% KRSP mixture significantly exceeded initial expectations, providing a highly stiff and stable matrix that mitigates typical

decreasing stiffness behavior. This phenomenon indicates that a higher specific surface area exponentially increases the availability and reactivity of free lime, intensifying the alkaline shock and cation exchange. Furthermore, the finer particles act as an effective mineral filler, optimizing the physical framework and particle packing of the matrix. This binary baseline demonstrates that while the chemical nature of KRS is fundamental, optimizing the physical skeleton is a frontier for maximizing the mechanistic performance of pavement layers.

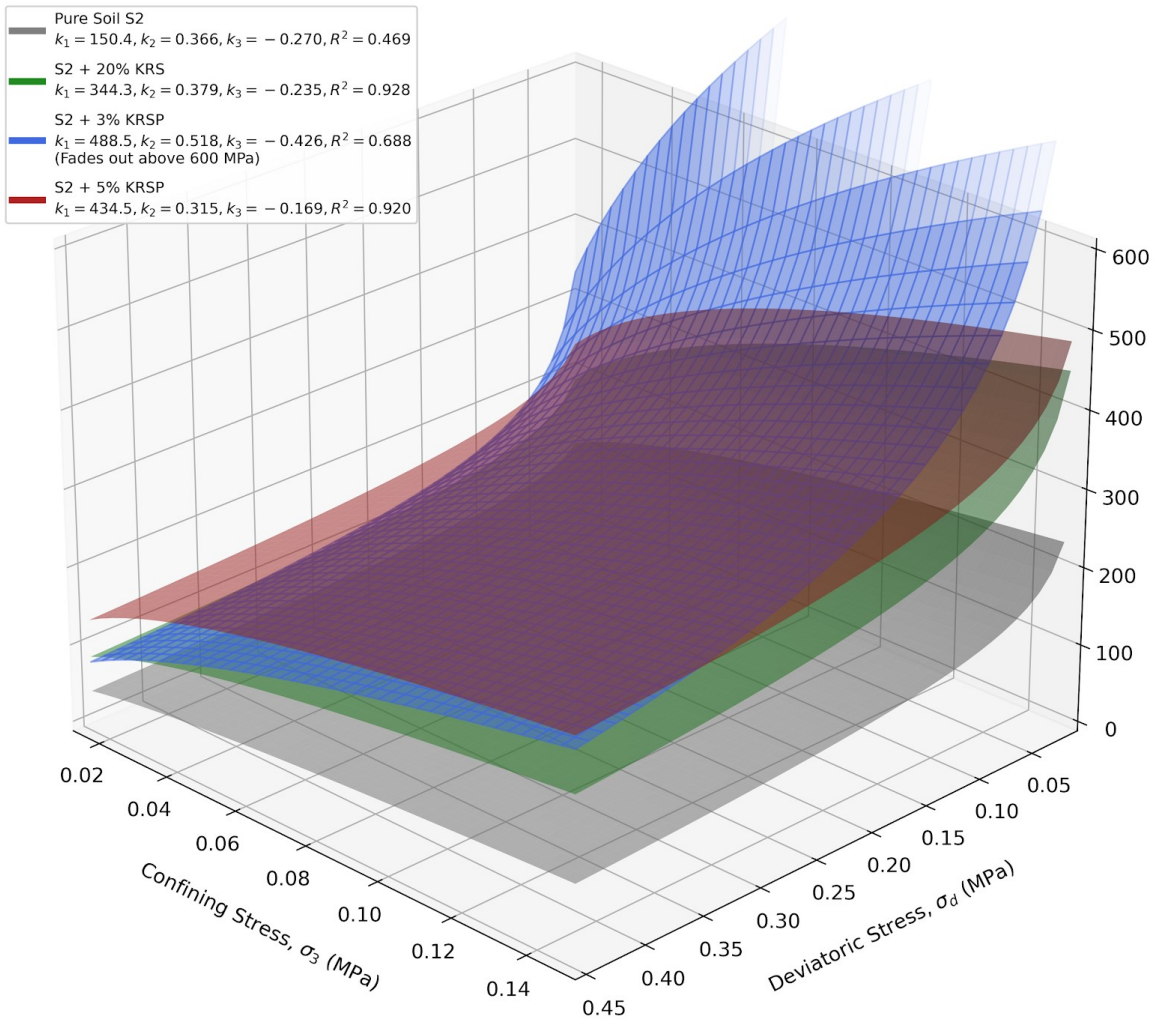


Figure 2.29: Consolidated 3D Resilient Modulus surfaces representing the composite MeDiNa model ($M_R = k_1 \cdot \sigma_3^{k_2} \cdot \sigma_d^{k_3}$). The 3% KRSP surface fades out above 600 MPa to enhance the visualization of the lower-stress boundaries.

2.5.2.4 Permanent Deformation of KRS-Soil Mixtures

Based on the research conducted by Mendoza (2023) regarding permanent deformation (PD), the following section provides a technical analysis of the experimental findings for mixtures adopting 3 and 5% KRS content in KRS-soil mixtures. The evaluation of permanent

deformation conducted by Mendoza (2023) was limited to a single-stage test featuring one stress pair for each investigated mixture. These specimens were tested after a curing period of 4 days. Despite the limited stress states, the experimental data allowed for the determination of the Monismith model parameters for both mixtures.

The accumulated plastic strain (ϵ_p) as a function of the number of load cycles (N) in a single stage permanent deformation test was characterized using the power-law formulation proposed by Monismith et al. (1975):

$$\epsilon_p = A \cdot N^B \tag{2.15}$$

Where:

- ϵ_p represents the accumulated plastic strain;
- A and B are specific experimental coefficients;
- N is the number of applied load cycles.

The regression analysis yielded a high degree of fit (R^2) for both cases, as summarized in Table 2.22:

Table 2.22: Monismith model parameters for SKRSP mixtures (adapted from Mendoza, 2023).

Mixture	**Model**	**Coefficient A (k_1)**	**Coefficient B (k_2)**	R^2
SKRSP3	$\epsilon_p = A \cdot N^B$	0.0200	0.1246	0.9794
SKRSP5	$\epsilon_p = A \cdot N^B$	0.0254	0.1324	0.9660

As presented by Mendoza (2023), upon reaching 150,000 load cycles, the recorded permanent deformation values were 0.0883% for mixture KRSP3 and 0.123% for mixture KRSP5. As illustrated in Figure 2.31, the increase in the percentage of the byproduct correlated with higher deformation values, suggesting that byproduct content influences the material's overall deformability.

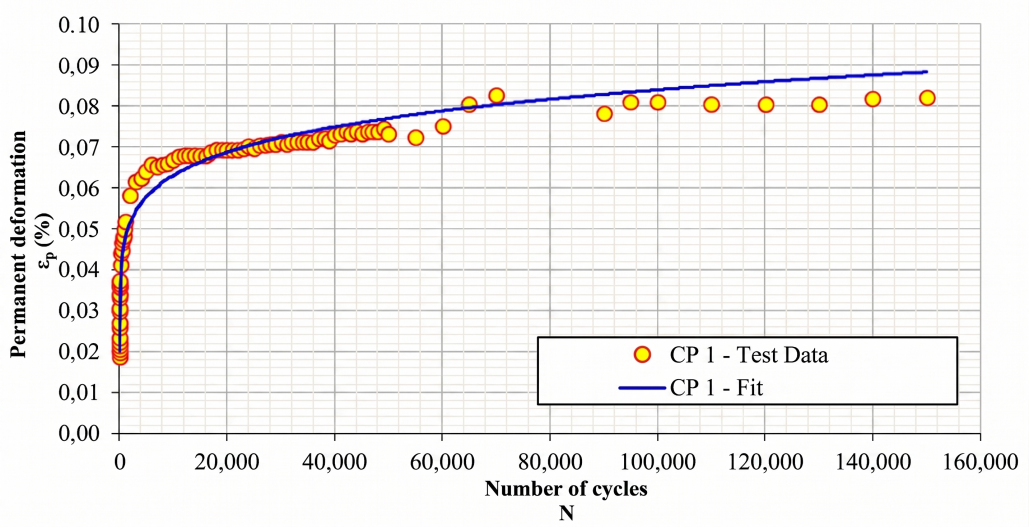


Figure 2.30: Accumulated permanent strain (ϵ_p) for KRSP3 mixture (adapted from Mendoza, 2023).

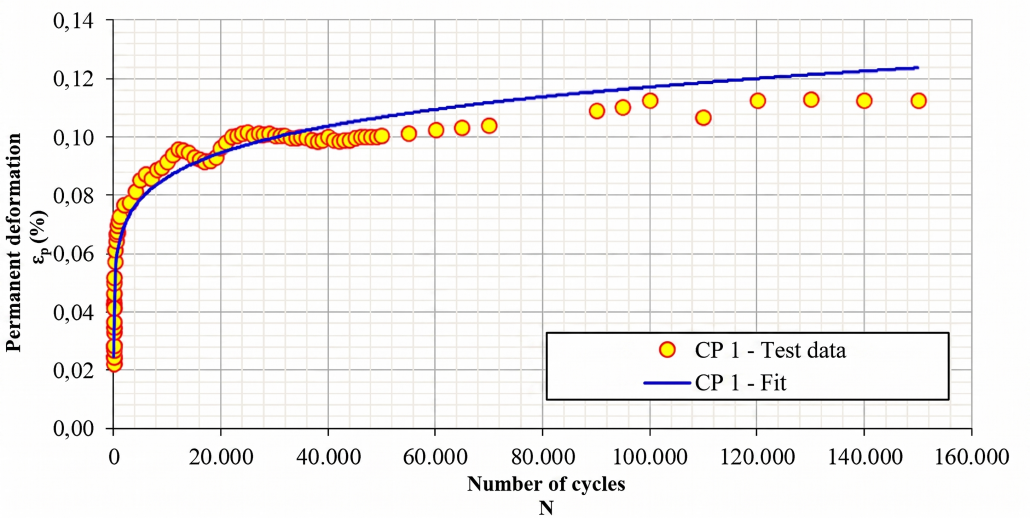


Figure 2.31: Accumulated permanent strain (ϵ_p) for KRSP5 mixture (adapted from Mendoza, 2023).

According to Mendoza (2023), the analysis of the experimental curves revealed a clear tendency toward the stabilization of permanent deformations as the number of loading cycles increased. To classify this behavior, the results were evaluated against the criteria specified in the DNIT 179/2018-ME standard and the behavioral models shown in Figure 2.32 and Figure 2.33:

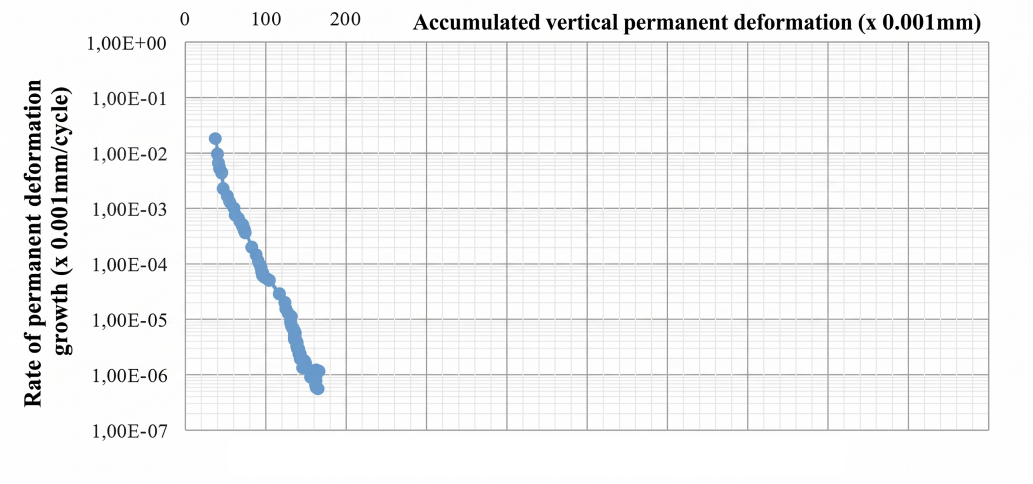


Figure 2.32: Behavioral analysis of the material based on permanent deformation — KRSP3 (from Mendoza, 2023).

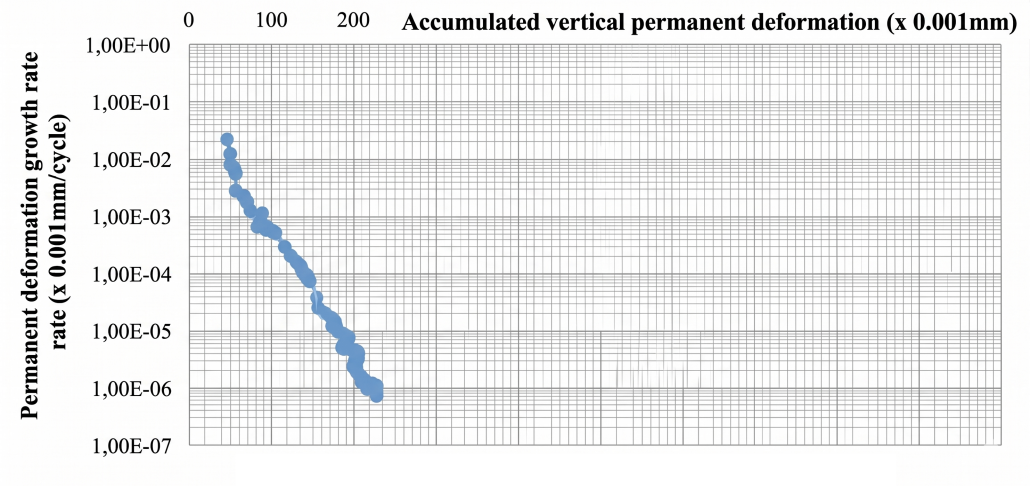


Figure 2.33: Behavioral analysis of the material based on permanent deformation — KRSP5 (from Mendoza, 2023).

- **Behavior Classification:** Both KRSP3 and KRSP5 mixtures exhibited Type A behavior, also known as Plastic Shakedown (or plastic accommodation).
- **Graphical Interpretation:** This state is identified mathematically when the rate of permanent strain increase ($d\epsilon_p/dN$) becomes parallel to the Y-axis (accumulated strain) after a specific number of cycles, as demonstrated in Figure 2.32 and Figure 2.33.
- **Pavement Viability:** The attainment of plastic shakedown indicates that these materials will not contribute significantly to rutting distress over time. Consequently, they are considered ideal candidates for application in pavement layers.

This enhanced physical and chemical stability is critical for the mechanistic-empirical assessment of pavement layers required by the Brazilian MeDiNa method, which has been

gaining traction with different studies in other countries. Reflecting the increased Resilient Modulus (MR) observed in laboratory testing L. B. d. S. Ramos (2018), the evaluation of long-term structural performance has evolved beyond empirical indices like CBR to explicitly include the prediction of Permanent Deformation (PD) P. M. d. Souza, Oliveira, Lima, & Fernandes Júnior (2022).

The mechanistic approach allows for the identification of "Shakedown" behavior (Type A), validating the use of alternative materials like KRS-soil mixtures. These materials often demonstrate superior resistance to rutting and stable plastic accommodation in field applications, even when their conventional index properties might suggest otherwise (Cabral, 2021; Bona & Guimarães, 2021). Table 2.23 summarizes the permanent deformation parameters and performance results for the studied mixtures.

Table 2.23: Summary of Mechanical Characterization and Mechanistic Performance Parameters for Granular and Stabilized Materials

Soil Type / Material	Classification / Origin	Conventional Properties	Resilient Modulus (MR)	Permanent Deformation (PD)	Relevant Observations	Source
Stabilized Soils of Espírito Santo State						
Clayey Soil + 20% KR Slag (S1KR20%)	Original Soil: A-7-6 (Low-quality clay). Origin: BR-101/ES.	CBR (Mod.): 103.2% | Expansion: 0.03%	Avg MR: 1107.9 MPa	Excellent field performance (HVS), with low final deformation.	Transformed a poor soil into a high-performance material, superior to cement solutions in terms of stiffness (MR).	Pires et al. (2019)
Sandy Soil + 3% Cement (S2PC3%)	Original Soil: A-2-6 (Good quality sand). Origin: BR-101/ES.	CBR (Mod.): 128.1% | Expansion: N/A	Avg MR: 587 MPa	Control parameter in the field (HVS): excellent performance and low deformation.	Conventional high-performance solution used as a reference for the slag mixture.	
Tropical Soils - Case Studies						
Laterita from BR-163/PA	A-7-6 (Clayey gravel).	CBR: 62.8% | Expansion: 0.24%	Avg MR: 522 MPa. Model (Pezo): k1=6.79, k2=0.48, k3=-0.31.	Max PD: 1.7 mm (in 200 mm specimen). Shakedown behavior (Type A) in all tests.	Excellent mechanical behavior, despite CBR being lower than the normative minimum (80%), validating the mechanistic	Bona & Guimarães (2021)
Sandy Soil (Soil 02 - Pernambuco)	MCT: LA' | AASHTO: A-4 | USCS: SM.	CBR: 30.0% | Expansion: 0.00%	Avg MR: 488 MPa. Model (Compound): k1=601.39, k2=0.36, k3=-0.36.	Total DP: 0,7 mm (σ3=120 kPa / σd=360 kPa). (Guimarães Model): Ψ_1=0.076, Ψ_2=0.043, Ψ_3=0.912, Ψ_4=0.047.	Model (Guimarães, 2009):Meets sub-base criteria by CBR and presents excellent resistance to PD.	Sousa et al. (2024)
Clayey Soil (Soil 01 - Pernambuco)	MCT: LG' | AASHTO: A-6 | USCS: ML.	CBR: 12.8% | Expansion: 30.0%	Avg MR: 438 MPa. Model (Compound): k1=354.12, k2=0.33, k3=-0.52.	DP Total: 6,5 mm (sob σ3=120 kPa / σd=360 kPa). Modelo (Guimarães): Ψ_1=0.209, Ψ_2=-0.45, Ψ_3=1.73, Ψ_4=0.056.	Despite low CBR and very high expansion, the MCT classification indicates potential for use. Presents high plastic deformability.	
Granular Soils (Mossoró, state capital of Rio Grande do Norte, Brazil)						
Soil AB	A-2-4.	CBR: 41.9% | Expansion: 0.00%	Model (Pezo): k1=590.8, k2=0.22, k3=0.14.	Guimarães Model: Ψ_1=0.72, Ψ_2=0.18, Ψ_3=-0.21, Ψ_4=0.09.	Good performance, with low PD accumulation and good shakedown behavior. Indicated for sub-base.	Cabral (2021)
Mixture (Soil AB + Crushed Stone)	Mixture 50% soil AB + 50% granitic crushed stone.	CBR: 69.3% | Expansion: 0.00%	Model (Pezo): k1=935.8, k2=0.33, k3=-0.02.	Guimarães Model: Ψ_1=1.15, Ψ_2=0.25, Ψ_3=-0.15, Ψ_4=0.02.	High resistance to PD with rapid accommodation. Indicated for base layer.	
Soil SM	A-3 (fine sand).	CBR: 9.8% | Expansion: 0.10%	Model (GuimarÃ£es): k1=260.2, k2=1.09, k3=-0.98, k4=0.01.	Guimarães Model: Ψ_1=0.17, Ψ_2=-0.25, Ψ_3=0.72, Ψ_4=0.23.	Excessive rutting in tests, indicating low stiffness and tendency to rupture under higher stresses.	

2.5.2.5 Novel Stress-Dependent Anthropogenic Geomaterial

The evolution described above reveals a **fundamental rewrite of the soil's mechanical behavior**, shifting from a moisture-sensitive substrate to a high-performance, **stress-dependent anthropogenic geomaterial**. This transformation is analyzed under the state-of-the-art *MeDiNa* methodology, which is currently leading the challenge to replace (in the market) outdated state-of-the-practice empirical methods (CBR, for example) with a robust mechanistic-empirical approach.

Under this new paradigm, the material is no longer treated as a passive natural soil vulnerable to saturation, but as a custom-engineered substance. By calibrating the **Optimum Residue Content (ORC)**, defining the **Maximum Residue Content (MRC)**, and identifying an eventual **Symmetry Point**, the resulting mixture achieves a stable mechanical skeleton. Unlike natural soils that rely on transient matric suction for strength, this anthropogenic geomaterial derives its stiffness from optimized grain-to-grain contact and long-term pozzolanic "welding."

Consequently, the Resilient Modulus (M_R) of these mixtures becomes primarily a function of confining and deviator stresses rather than environmental moisture fluctuations. This shift confirms that the integration of KRS and LD-SS provides a structural "shield" for the pavement, ensuring that the layer's integrity is maintained by its internal constitutive law, effectively positioning these byproducts as high-value structural assets in modern pavement engineering.

The novel paradigms established by the described scenario of KRS and LD-SS geotechnical applications in embankments and pavements can be listed:

1. The End of Moisture Dependency

In traditional pavement design, the subgrade is often the "weak link" because its strength is a prisoner of its moisture content. When natural soils saturate, they lose the matric suction that provides their stability. By engineering an anthropogenic geomaterial using slag, the stabilization process (cationic shock followed by pozzolanic "welding") creates a rigid, insoluble skeleton. This shifts the material's behavior from being moisture-sensitive to being stress-dependent.

2. Mechanistic Superiority (The MeDiNa Era)

As the industry moves toward mechanistic-empirical methodologies like MeDiNa, the focus shifts to the Resilient Modulus (M_R). Slag-soil mixtures don't just "improve" the soil; they often outperform traditional granular bases and even cement-treated layers in terms of stiffness and fatigue resistance. Finding the "Symmetry Point"—the perfect balance where the soil matrix provides lateral confinement to the rigid slag aggregates—allows for a level of

structural predictability that natural soils simply cannot offer.

3. The Circular Economy and Ethics of Engineering

Beyond the mechanical gains, there is a powerful logistical and environmental argument. Using local, abundant residues to replace expensive, quarried natural aggregates solves two problems at once: it reduces the carbon footprint of hauling materials and prevents the accumulation of industrial byproducts. When a stabilized mixture can achieve a Resilient Modulus that, for some especial soils, exceeds 1,000 MPa using what has been called as "poor" local soils/clays, and it challenges the very necessity of traditional quarrying for many road layers. This alignment of technical performance, economic efficiency, and environmental sustainability is what makes the argument for slag residues nearly undeniable in modern, robust pavement design.

The optimization of particle size distribution and the selection of appropriate SS types further enhance these benefits, positioning slags as high-value and sustainable materials for soil improvement n geotechnical engineering (Bastos, 2022; K. P. M. Medeiros, 2019; C. F. Oliveira, 2018; L. B. d. S. Ramos, 2018; A. D. d. Resende, 2010; Sant'Ana, 2003).

This mechanistic evolution, backed by the transition to the **MeDiNa** methodology, reveals a fundamental rewrite of the soil's mechanical behavior, shifting from a moisture-sensitive substrate to a robust structural asset where the state-of-the-art methodology finally finds the experimental ground it deserves: become the regular and routinely state-of-the-practice.

The next section:

Considering the clear benefits evidenced throughout this systematic review, a fundamental research question emerges: is there room for another residue in the field of soil stabilization? Could the staggering 3 million metric tons of OSR generated in Brazil (Prandina, 2013) finally find its place in the geotechnical universe of geomaterials for embankments and pavements?"

2.6 - POTENTIAL: SOIL STABILIZATION WITH OSR

This section is an adaptation of the articles "Ornamental stone industry waste in soil mixtures for geotechnical applications: a literature review," published by Prandina and Farias (2026) in the journal *Transportes*, and "Road infrastructure adopting siderurgical and ornamental stone industrial residues," published by Prandina & Farias (2025a) in the journal *Foco*. It is important to highlight that the publication in *Transportes* represents a comprehensive evolution and expansion of the research initially presented in the *Foco* article, respectively qualified as A3

and B2 in Quali Capes ranking system of journal when the papers were published.

To address the synthesis of geotechnical applications for OSR, this section employs a narrative review methodology. The selection of this approach is primarily driven by the limited availability of peer-reviewed national literature specifically targeting OSR in geotechnical contexts. Consequently, the review prioritizes influential works that characterize the domestic state-of-the-art, bypassing the requirement for an exhaustive or strictly systematic search protocol. The scientific robustness of including local academic outputs—such as theses and dissertations that have not yet reached international journals—is validated by their rigorous alignment with the established international peer-reviewed body of work, as mapped in Table 2.24.

Table 2.24: Connection between Brazilian research and international peer-reviewed literature (from Prandina & Farias, 2026)

Brazilian Reference cited	**Referenced journal paper**	**Country**	**Publisher**
Dias (2024) and Lunz (2021)	Eltwati et al. (2020). Potential of granite dust to improve the engineering properties of soft soils for road construction.	Libya	Science Proceedings Series.
Dias (2024) and Mello (2019)	Galetakis & Soultana (2016). A review on the utilisation of quarry and ornamental stone industry fine by-products in the construction sector.	Greece	Construction and Building Materials.
Dias (2024)	Lohar & Shrivastava (2025). Feasibility of granite processing waste as a fill material in geotechnical applications.	India	Materials Today: Proceedings.
Dias (2024)	Moraes, Oliveira & Pires (2018). Characterization of Stone Slurry Waste for Reutilization Purposes as Building Construction Material.	Brazil	Journal of Geological Resource and Engineering.
Dias (2024) and Prandina & Farias (2025); Prandina, Fall & Sedano (2017)	Sivrikaya, Kıyıldı & Karaca (2014). Recycling waste from natural stone processing plants to stabilise clayey soil.	Turkey	Environmental Earth Sciences.
Dias (2024) and Prandina & Farias (2025); Prandina, Fall & Sedano (2017)	Lohar & Shrivastava (2025). Beneficial use of dimensional stone industry wastes in geotechnical fills: Geotechnical, environmental and economic perspectives.	India	Resources Policy

To capture the most contemporary scientific developments and expand upon the conceptual foundations established by Prandina and Farias (2025), the literature review prioritizes works published from 2015 onward. This timeframe is methodologically significant

as it coincides with a period of intensified research on waste valorization in Brazil. More importantly, this period marks a pivotal maturation in Brazilian pavement engineering: the cultural and technical transition from traditional empirical methods (CBR) toward advanced mechanistic methodologies based on the Resilient Modulus (M_R). Prior to 2015, geotechnical research involving residues was often incipient and focused on natural materials; even when materials like steel slag were utilized in the field, their application was driven by immediate necessity and validated through empirical means. Consequently, focusing on the post-2015 era ensures that the state-of-the-art in OSR research is aligned with modern mechanistic design, providing the necessary data for integration into contemporary state-of-the-practice frameworks.

Prior to this period, mechanistic research was incipient using residues and focused on natural materials, even as residues like steel slag (SS) were already being applied in the field out of practical necessity, validated by empirical methods . Therefore, focusing the review on this period makes it possible to capture the state-of-the-art in geotechnical research on residues (such as OSR) that is aligned with modern mechanistic practice.

2.6.1 - THE IMPLEMENTATION GAP: OSR VS. STEEL SLAG

A defining paradox in the Brazilian geotechnical landscape is the "Implementation Gap" observed between academic research and field application. While steelmaking slags have successfully transitioned from empirical field use to standardized mechanistic validation, Ornamental Stone Residue (OSR) remains largely confined to the "state-of-the-art" in laboratory settings.

In the industrial cluster of Espírito Santo—the heart of national OSR generation—there is a conspicuous absence of documented practical geotechnical applications in major or any scale infrastructure projects, whether as a standalone material or in soil mixtures. This lack of "practical proof" presents a methodological challenge: since the absence of implementation is rarely the subject of peer-reviewed journals, the evidence of this gap relies on professional expertise and anecdotal field observation. This void underscores the pioneering nature of the current research, which seeks to provide the technical validation necessary to bridge the distance between academic/scientifc proven potential and effective state-of-the-practice.

The fragmentation of the ornamental stone sector further exacerbates this implementation gap. Given that the technology for cutting, polishing, and processing stone is relatively accessible, it has given rise to an industry characterized by high capillarity but small individual scale. Historically, as these companies transition from extraction (Primary Sector) to transformation (Secondary Sector) to provide value-added products, they have operated

without significant regulatory oversight or collective organization regarding their environmental liabilities. As a result, the prevailing practice has been to simply pay for the disposal of residues rather than investing in valorization strategies. This decentralized industrial context justifies the need for an unprecedented and comprehensive geotechnical review, which is essential to establish the technical baselines that the industry has yet to organize, whether for OSR as a standalone material or in soil mixtures.

2.6.2 - TYPICAL GRAIN SIZE DISTRIBUTION (GSD) OF OSR

The physical and morphological characterization of OSR is the fundamental descriptor for its application as an anthropogenic geomaterial in embankments and pavement structures. As a solid byproduct of industrial stone processing—specifically the cutting, sawing, and polishing of different geologic rock types, such as marble and granite blocks—OSR can represent up to 40% of the original quarried volume, with fine particles from cutting slurries accounting for approximately 26% of the total material (Mello, 2019; Dias, 2024), aligned with the Montani (2021) numbers.

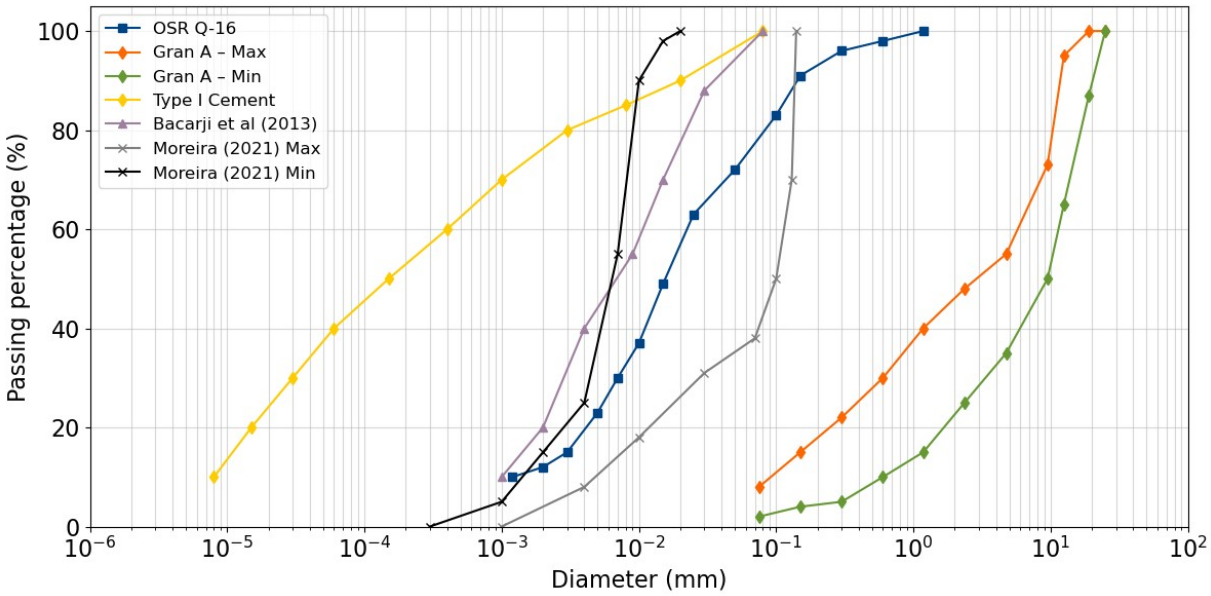


Figure 2.34: Grain Size Distribution (GSD) of OSR samples compared to Type I Portland cement and Canadian Granular A (Gran A) limits (Modified from Prandina et al., 2017).

Extensive characterization studies, such as the analysis of 70 samples from Espírito Santo landfills by Moreira (2021), define OSR as a fine, well-graded material predominantly composed of silt and fine sand. The particle size distribution typically ranges from medium sand (0.250 mm) to the very fine clay fraction (0.00024 mm), with approximately 80% of the particles passing the 0.053 mm sieve. As illustrated in Figure 2.34, the GSD of OSR samples often spans the boundary between the physical limits of Type I Portland cement and Canadian

"Granular A" (Gran A) specifications, highlighting its dual potential as both a high-quality mineral filler and a stable structural skeleton (Prandina et al., 2017).

The lithological origin of the residue serves as a primary determinant of its geotechnical performance. A notable example is the sample designated as OSR Q-16, collected in 2016, which is derived specifically from a quartzite (Q) parent block. Unlike marble-based OSR, quartzite residues typically exhibit a higher silica content—comparable to granitic OSR—along with distinct abrasive properties that can significantly influence the internal friction angle of soil-residue mixtures. This specific sample highlights the inherent challenges in evaluating the diverse metamorphic rock byproducts within the OSR spectrum. Consequently, meticulous lithological tracking remains the ideal scientific approach to ensure structural integrity, whether the material is destined for mass embankments or high-performance pavement structures.

Table 4 synthesizes the geotechnical characterization of OSR from national and international literature, revealing a consistent predominance of the silt fraction, which typically ranges from 61% to 75%.

Table 2.25: Geotechnical characterization and classification of OSR: Summary of national and international findings (from Prandina & Farias, 2026).

Study / Source	Material and Origin	Particle Size (%)			Classification / Key Findings
		Silt	Clay	Sand / Gravel	
Barrientos (2010)	OSR-G: granite sawdust from Spain	70–75	10–15	10–20	Classified as a sandy clayey silt, corresponding to a low-plasticity silt (ML) under the USCS.
Oliveira (2015)	OSR from a processing plant in São Paulo (mixture of syenite, granite, and gneiss)	62	18	20	ML (low-plasticity silt). Contains 80% fines with a Plasticity Index of 5%. Environment: Class II B (Inert).
Mello (2019)	Typical OSR from Espírito Santo, Brazil	63	27	10	Characterized by a high percentage of fines.
Dias (2024)	OSR from ADAMAG landfill (ES), from diamond wire saw process	61	35	4	A-6 (TRB) and ML (SUCS) with an Index Group (IG) of 16. The material is non-plastic (NP). A 50/50 mixture with soil was classified as Class II B (Inert).

This high concentration of fines dictates the material's classification as low-plasticity silt (ML) under the USCS or as A-4 and A-6 according to the TRB system. Data from Brazilian research (Oliveira, 2015; Mello, 2019) show strong alignment with international studies Barrientos et al. (2010), confirming a uniform global geotechnical profile for these residues. While Brazilian practice follows NBR 7181 (ABNT, 2016) for GSD, the current absence of a specific technical code for OSR is mitigated by existing DNIT and ABNT guidelines that already permit the inclusion of industrial residues in earthworks and pavements. Furthermore, OSR exhibits a specific gravity and grain density comparable to those of natural aggregates. However, the inherent variability in its properties necessitates systematic screening and separation by lithological source to ensure maximum performance, whether the residue is utilized as a standalone material or integrated into soil mixtures (Chicon, 2019).

2.6.3 - IMPLICATIONS FOR GEOTECHNICAL STABILIZATION

The synergistic interaction of mineralogical, chemical, and physical attributes—notably the fine particle size and angular grain morphology—positions OSR as a high-potential candidate for soil stabilization in road infrastructure. Recent geotechnical investigations by Lohar and Shrivastava (2025) confirm that OSR is fundamentally non-plastic and non-swelling, exhibiting hydraulic conductivity comparable to silty sands. Their findings highlight the robust stability of these residues, with internal friction angles ranging from 36.5° for marble-based OSR (OSR-M) to 44.8° for granitic OSR (OSR-G). These improvement mechanisms can be broadly categorized into two primary fronts:

I) **Chemical Stabilization:** Chemical stabilization: while traditionally achieved with cement or lime, the integration of OSR can contribute to the stabilization process due to its mineralogical affinity with soil particles. Although OSR is primarily a non-reactive material, its fine siliceous and calcareous fractions can enhance the matrix through the filler effect and, in specific alkaline environments, provide a substrate for secondary pozzolanic interactions, reinforcing the long-term mechanical strength.

II) **Mechanical and Granulometric Stabilization:** This process involves optimizing the soil's granular skeleton by blending it with OSR, a strategy particularly vital in regions where high-quality natural aggregates are scarce. The incorporation of fine-grained OSR into natural soils optimizes the overall particle size distribution (PSD), leading to a denser arrangement and a reduced void ratio. This stabilization of the granular skeleton is essential for increasing load-carrying capacity and ensuring that the mixture meets the Resilient Modulus (M_R) thresholds required for modern pavement structures.

The concentration of Ornamental Stone Residue (OSR) in Brazilian industrial hubs, particularly in Espírito Santo, enhances the logistical and economic viability of its geotechnical application. Utilizing OSR as either a mineral filler or a grading corrector provides a sustainable mechanism for upgrading marginal local soils into high-performance engineering materials.

Given that subgrade stability is a primary determinant of pavement longevity, OSR serves as an effective stabilizing agent for problematic soils—such as expansive clays—which typically suffer from high compressibility and low shear strength (Rao & Chittaranjan, 2010). The integration of fine OSR particles into the soil matrix optimizes essential engineering properties, including density and plasticity, particularly in high-moisture environments (Gautam et al., 2018; Mishra et al., 2015). Beyond technical improvements, OSR usage expedites construction through faster subgrade drying and provides significant cost savings by minimizing

the reliance on conventional borrow pits. The consolidated research findings for granite and marble residues are detailed in Tables 2.26 and 2.27.

Table 2.26: Properties of Soils Stabilized with OSR from granite Summary of Research Findings (from Prandina & Farias, 2025a)

Soil Type	Granite Dust (%)	Key Par.	Initial Value	Final Value	Change Improvement	Reference(s)
Soft Soils (general)	8%	CBR	N/A	Best results at 8%	Sig. incr.	Eltwati et al. (2020)
Red Earth, Kaolinite,	20-80%	LL, PL, PI	Var.	Reduced	Sig. red.	Amulya et al. (2021)
Marine Clay	Imp. s. add	MDD	N/A	Increased by ~88%	+88%	
Black Cotton Soil	Up to 50%	CBR	N/A	Increased	Cont. inc.	
High Plastic Silt	Up to 60%	Shear Strength	N/A	Sig. imp.	N/A	
Expansive Soil (Egypt)	20% (opt.)	UCS, CBR	N/A	Max at 20% GD	Sig. increase	Abdelkader et al. (2022)
Lateritic Soil (Nigeria)	24%	UCS, PI	N/A	Met specs	Sig. imp.	Emmanuel et al. (2021)
Clay Soil (India)	30% (GS) + 0.5%	CBR (28d)	Low	>20%	Subs. increase	Amulya et al. (2023)

Notes: Imp – Improvement; Var – Variable; Sig. Incr. – Significantly increase; Sig. Incr. – Significantly improvement; Imp. s. add. - (Not specified, but implies significant addition); Opt. - optimum

Enhancements in the California Bearing Ratio (CBR) of stabilized subgrades directly correlate with a reduction in required pavement thickness, yielding substantial material and economic savings (Mishra, 2015). The performance of fine industrial residues like OSR in improving soil workability and durability—comparable to the behavior of fly ash—underscores their technical viability for subgrade reinforcement (Gautam et al., 2018).

Beyond its application in soil-residue blends, OSR exhibits high potential as a non-conventional standalone structural fill. This approach facilitates large-scale waste management while preserving natural soil resources. According to Lohar & Shrivastava (2025), OSR is characterized as a non-plastic and non-swelling material with favorable stability under varying moisture conditions. Mechanical evaluations reveal high internal friction angles—ranging from 36.5° for marble to 44.8° for granite residues—and Maximum Dry Densities (MDD) between 1.58 g/cm^3 and 1.84 g/cm^3.

Table 2.27: Properties of Soils Stabilized with OSR from marble Summary of Key Research Findings (from Prandina & Farias, 2025a)

Soil Type	Marble Dust/Slurry (%)	Key Parameter	Initial Value	F.V. or B.R.	Change/Imp. (%)	Reference(s)
Expansive Clay	GD	Att. Limits, Swell	N/A	Reduced	Decrease	Abdelkader et al. (2022)
Soil (CRRI, India)	20% (MSD)	CBR	12.5%	17.7%	+41.6%	Misra et al. (2010)
Expansive Soil (Ethiopia)	16% (WMD) + 16% (CG)	CBR	1.00%	22.69%	+2169%	Belihu et al. (2025)
	16% (WMD) + 16% (CG)	UCS	112.9 kPa	311.7 kPa	+176%	
Expansive Soil (Rwanda)	25% (WMD)	CBR	1.1%	4.82%	+338%	Irakoze et al. (2025)
	25% (WMD)	UCS (28d)	93.2 kPa	219.5 kPa	+135%	
Silty Soil (CRRI)	10% MSD	UCS	N/A	Inc. 12%	+12%	Rajgor, & Pitroda (2013)
	30% MSD	UCS	N/A	Inc. 20%	+20%	

Notes: GD – granite dust; MSD – marble stone dust; WMD: waste marble dust; CG cinder gravel;

The validation of OSR for such applications adheres to comprehensive assessment frameworks, such as the United States Environmental Protection Agency (USEPA) beneficial use guidelines. These frameworks ensure that geotechnical performance is balanced with environmental safety—specifically regarding leachate and heavy metal content—and economic viability compared to traditional natural fills. Consequently, whether utilized as a stabilizing agent or as a standalone structural mass, OSR provides a robust technical solution for modern infrastructure challenges.

The technical feasibility of OSR as a primary construction material is further supported by international case studies. In Northwest Spain, Navarro et al. (2008) investigated the potential of granite OSR—with an annual production volume exceeding 350,000 m^3—as a standalone material for embankment fills. Their findings indicated that while the residue's mineralogy closely mirrors the parent granite rock, it contains minor fractions of calcite (3%) and steel grit derived from the industrial sawing process. Geotechnical performance evaluations, specifically settlement analyses of compacted earthfills, yielded "quite encouraging" results, suggesting high structural stability.

Lohar and Shrivastava (2025) presented a methodology for evaluating the beneficial use of residues as standalone geotechnical fills, adhering to the United States Environmental Protection Agency (USEPA) framework (Figure 2.35). Within this context, the systematic

characterization of OSR serves as a critical technical complement to the regulatory requirements of the USEPA roadmap.

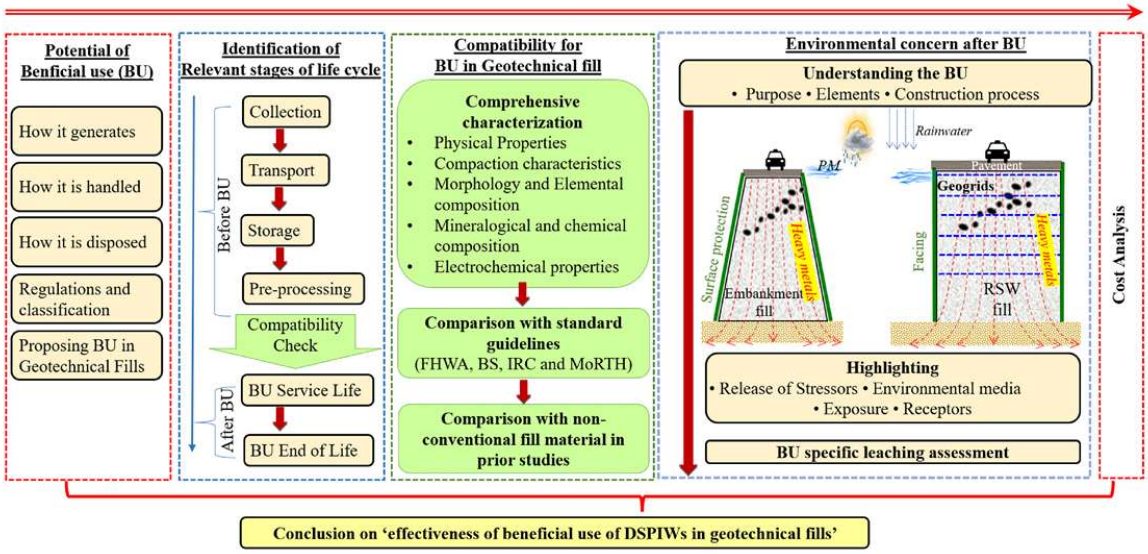


Figure 2.35: Methodology for evaluation of OSR beneficial use in geotechnical fills, following the USEPA framework (Adapted from Lohar & Shrivastava, 2025).

While the assessment by Lohar and Shrivastava (2025) provides a robust roadmap for the standalone utilization of residues, the systematic characterization of OSR serves as a critical technical complement to this framework, particularly when dealing with soil-waste mixtures. The integration of mineralogical and physical properties into the beneficial use evaluation allows for a deeper understanding of the stabilization mechanisms—such as the filler effect and the enhancement of the granular skeleton. Consequently, this research extends the scope of the traditional USEPA framework, bridging the gap between macro-level regulatory compliance and micro-level mechanical interaction in pavement infrastructure.

However, a critical consensus emerges between the findings of Navarro et al. (2008) and Lohar & Shrivastava (2025): both emphasize the urgent requirement for more robust characterization to facilitate effective practical application. Despite promising outcomes from numerical modeling and laboratory testing, the transition to standardized field implementation remains an ongoing challenge. This observation directly aligns with the identified "Implementation Gap," reinforcing the necessity of the present research to bridge the divide between theoretical potential and field-proven engineering, whether for bulk embankment masses or high-performance pavement structures.

2.6.4 - OSR MAXIMUM DRY DENSITY (MDD) AND OMC

The compaction behavior of soil-OSR mixtures is governed by the Specific Gravity (G_s) of the constituents, the geologic characteristics, and the resulting grain size distribution. Research indicates that the G_s of OSR typically ranges from 2.587 to 2.770 (Santos et al., 2017; Mello et al., 2019; Braz et al., 2024). However, this value is highly sensitive to the industrial processing technology employed. Moraes et al. (2018) demonstrated that residue from conventional metallic blade looms exhibits a significantly higher G_s (2.84) compared to diamond wire looms (2.56). This discrepancy arises from the presence of steel grit and high iron content—up to 24.1%—resulting from the abrasive wear of the metallic blades, a characteristic absent in diamond wire processing.

Proctor compaction tests across standard (S), intermediate (I), and modified (M) energies reveal that OSR incorporation shifts the peak MDD and OMC according to the proportion and nature of the blend. For compacted OSR alone, MDD values range from 15.71 kN/m^3 to 19.50 kN/m^3, with corresponding OMC values between 9.2% and 24.5% (Oliveira, 2015; Chicon, 2019; Dias, 2024). This impact is observed across the soil spectrum, from silt-rich to coarser materials like sand and gravel. Initially, OSR performs a filler function, occupying the intergranular voids to increase the MDD and typically decrease the OMC. However, excessive OSR content disrupts the grain-to-grain contact of the original soil skeleton—transitioning the mixture toward a matrix-supported structure. This shift often results in a gap-graded distribution, which increases the overall void ratio and leads to a subsequent reduction in MDD (Mello et al., 2019; Silva & Isewaki, 2018).

The synthesis of these geotechnical interactions is presented in Table 2.2. Analysis of the literature shows that 57% of documented cases (8 out of 14 references) report positive gains in MDD through careful adjustment of the OSR-to-soil ratio and compaction energy. This underscores that maximizing mechanical performance requires precise moisture control and a granular association that prevents the formation of a silty, gap-graded matrix. Typical compaction curves illustrating these shifts are shown in Figure 2.36, originated from the study conducted by Lunz (2021) highlights the contrasting effects of OSR integration on two distinct soil matrices: a highly plastic clay and a clayey sand. The first soil, designated as BR-120, is classified as a high-plasticity clay (A-7-5) with a Plasticity Index (PI) of 30, exhibiting a minimum Maximum Dry Density (MDD) of 14.72 kN/m^3 in its pure state. The second soil, designated as VILA, is a clayey sand (A-2-4) with a PI of 10, characterized by a robust granular skeleton and a significantly higher initial MDD of 17.17 kN/m^3.The compaction results demonstrate the mechanical duality of OSR as a grading modifier.

In the clayey matrix (BR-120), the OSR acts as a structuring agent; the introduction

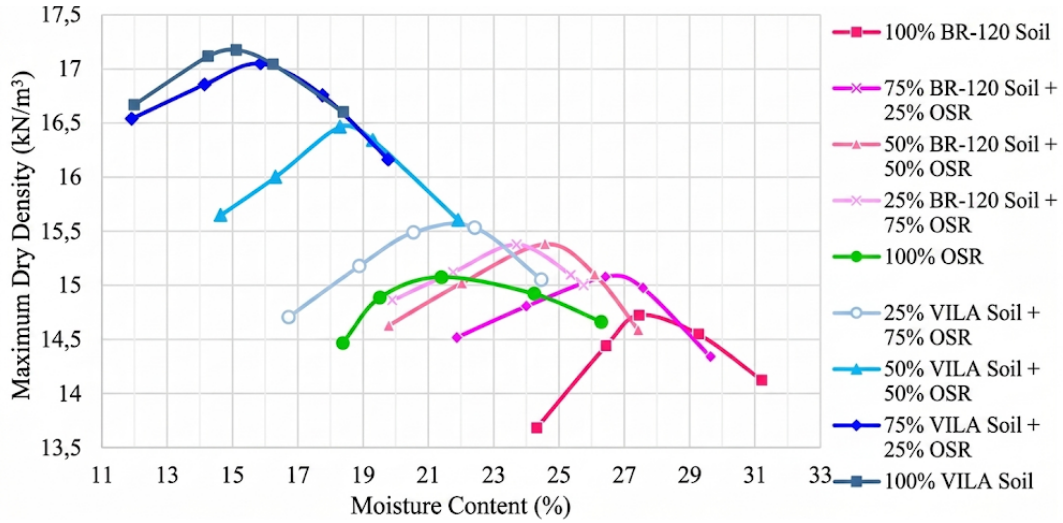


Figure 2.36: Standard Proctor compaction curves for soil-OSR mixtures: contrasting gradation optimization in clayey soil (BR-120) and the excess filler effect in sandy soil (VILA) (Adapted from Lunz, 2021).

of silt-sized particles optimizes the grain size distribution, reducing the void ratio and progressively increasing the MDD. Conversely, the sandy soil (VILA) illustrates the "excess filler" phenomenon. Because the sandy skeleton is already densely packed, the inclusion of OSR beyond a 25% threshold disrupts the grain-to-grain contact of the sand particles. This displacement forces a transition from a grain-supported to a matrix-supported structure, resulting in a subsequent decrease in MDD as the finer OSR particles increase the overall void ratio. In the case of the VILA soil, the ORC for MDD improvement would be positioned between 0 and 25% and for the BR-120 soil, the ORC is positioned between 50 and 75%.

2.6.5 - ATTERBERG LIMITS AND OSR-SOIL CLASSIFICATION

Atterberg limits—specifically the Liquid Limit (LL) and Plastic Limit (PL)—are fundamental indicators of soil consistency and potential geotechnical performance. The Plasticity Index (PI), defined as the difference between LL and PL, quantifies the range of moisture over which a soil behaves plastically. Incorporating OSR into natural soils typically induces significant shifts in these limits, which is a critical factor for meeting subgrade and subbase acceptance criteria that often mandate maximum LL and PI values to minimize moisture sensitivity (Dias, 2024).

The primary mechanism for this alteration is the disruption of the clay matrix by the non-plastic, silt-sized OSR particles. This introduction of coarser, non-reactive material reduces the soil's overall water retention capacity, leading to a concurrent drop in both LL and PL (Cardoso, 2019). Laboratory evidence shows that expansive soils are particularly sensitive to OSR admixtures; for instance, a 30% OSR content can reduce the LL from 65% to 31%, while

a 40% addition can lower it further to 25% (Braz, 2024), as evidenced by the sharp trends illustrated in Figure 2.37.

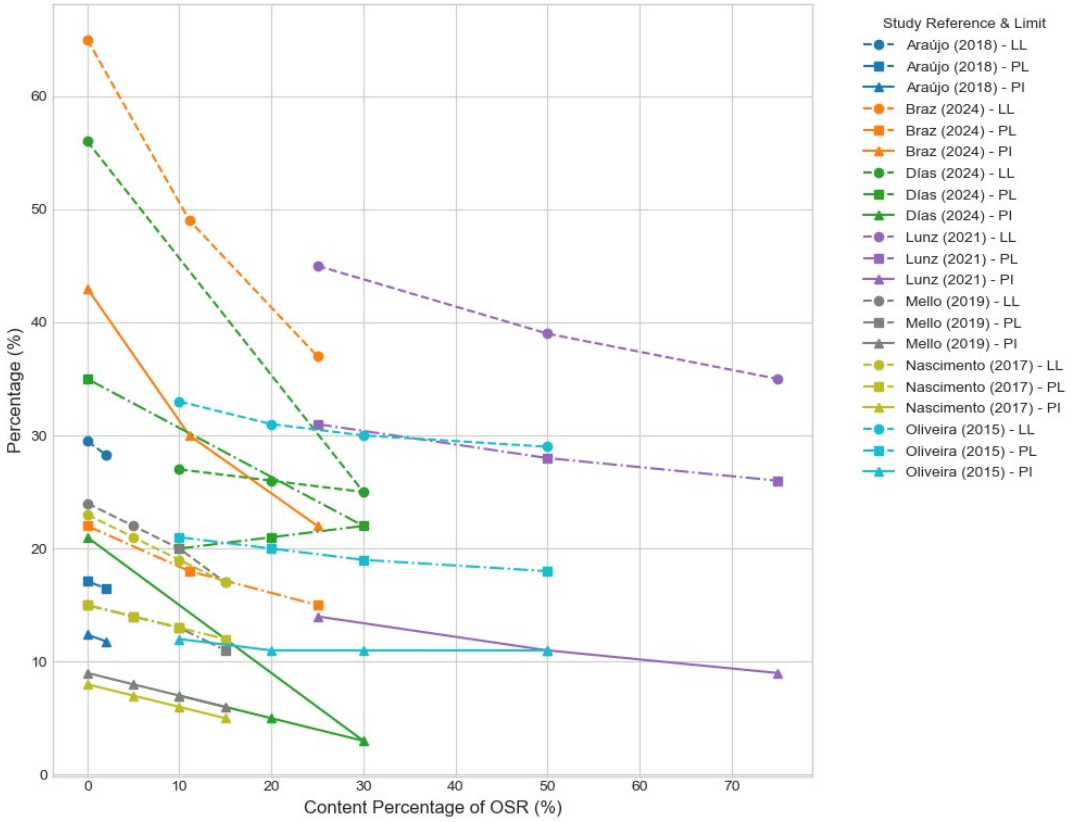


Figure 2.37: Variation of Liquid Limit (LL), Plastic Limit (PL), and Plasticity Index (PI) across different soil-OSR mixtures as reported in literature (Prandina & Farias, 2026).

Such reductions in LL and PL directly correlate to a diminished PI, reflecting a stiffer and less compressible material (Mello, 2019; Braz, 2024). These findings are corroborated by Sivrikaya et al. (2014), who evaluated various stone waste types and observed a consistent classification shift: high-plasticity clays (CH) were effectively transformed into low-plasticity silts (ML). This transition signifies a fundamental improvement in soil behavior, moving from highly moisture-sensitive states to more stable, workable geotechnical materials. The trends observed across different studies regarding these limit alterations are shown in Figure 2.37.

2.6.6 - UNCONFINED COMPRESSIVE STRENGTH (UCS)

Unconfined Compressive Strength (UCS) serves as an essential indirect parameter for assessing the mechanical improvement of soils treated with OSR. As a rapid and cost-effective laboratory test, it allows for the comparative analysis of various stabilization strategies and their suitability for pavement layers. The mechanical behavior, compactability, and resulting strength of these composites are heavily influenced by the OSR's non-plastic nature and its mineralogical

composition—primarily quartz and calcite—particularly when integrated into clayey matrices dominated by kaolinite or illite (Lunz, 2021).

The gain in UCS is intrinsically linked to shear strength, which is governed by particle arrangement and the specific interactions between the soil matrix and stabilizing agents. OSR modifications to particle size distribution and porosity directly influence these resistance mechanisms (Cardoso, 2019). Studies by Cardoso (2019), shown in Figure 2.38 displays the unconfined compressive strength (UCS) test results for various OSR-soil mixtures, while Figure 2.39 presents the corresponding indirect tensile strength results from diametral compression tests.

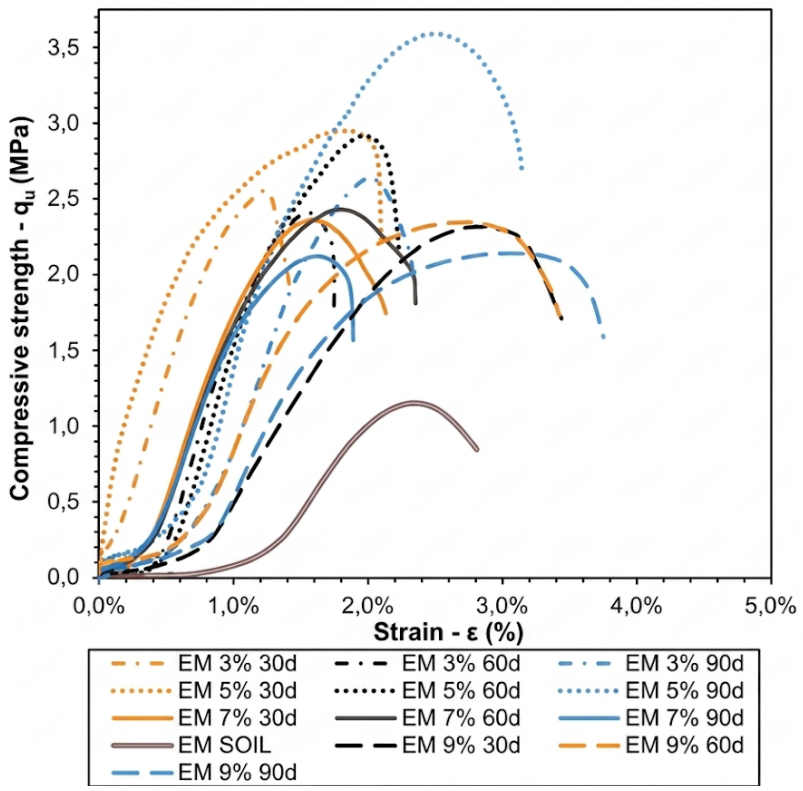


Figure 2.38: Unconfined Compressive Strength (UCS) test on A2-5 soil and soil-OSR specimens compacted on Modified energy (Adapted from Cardoso, 2019).

Cardoso (2019) evaluated the Unconfined Compressive Strength (UCS) of pure soils and soil-OSR mixtures (at contents of 3%, 5%, 7%, and 9%) using three Proctor compaction energies (Standard, Intermediate, and Modified) and curing periods of 30, 60, and 90 days. The results demonstrated that increasing compaction energy and curing time significantly enhances strength, with the best performance achieved at 90 days of curing. Mixtures with 3% and 5% residue stood out as the most effective, reaching maximum values of 3.02 MPa at intermediate energy (3% OSR) and 3.59 MPa at modified energy (5% OSR), considerably exceeding the values of the pure soil, which ranged between 417.10 kPa and 1,148.38 kPa depending on the applied energy. Statistically, the 3% content was identified as having the best overall

performance, which the author attributes to the optimal amount of fines and improved particle packing, reflecting the peaks of dry specific weight obtained in compaction tests.

The parent soil utilized by Cardoso (2019) is characterized as a granular material with a predominant sandy fraction. Grain size distribution (GSD) analysis indicates that 100% of the particles pass through the #10 sieve (2.0 mm), while 18% pass through the #200 sieve (0.075 mm), identifying it as a coarse-grained soil with a notable silt content. Regarding consistency, the soil presents a Liquid Limit (LL) of 47.8, a Plastic Limit (PL) of 42.0, and a resulting Plasticity Index (PI) of 5.8. According to the Unified Soil Classification System (USCS), the material is classified as a Silty Sand (SM), whereas under the AASHTO (TRB) system, it is categorized as an A-2-5 soil. This classification reflects a material with low compressibility and moderate drainage capacity, typical of the sandy matrices found in the studied region.

Regarding the Indirect Tensile Strength test (Brazilian Test), Cardoso (2019) observed that the addition of OSR directly influences tensile strength, showing improvements over pure soil, which recorded values between 67.34 kPa (standard energy) and 141.92 kPa (modified energy).

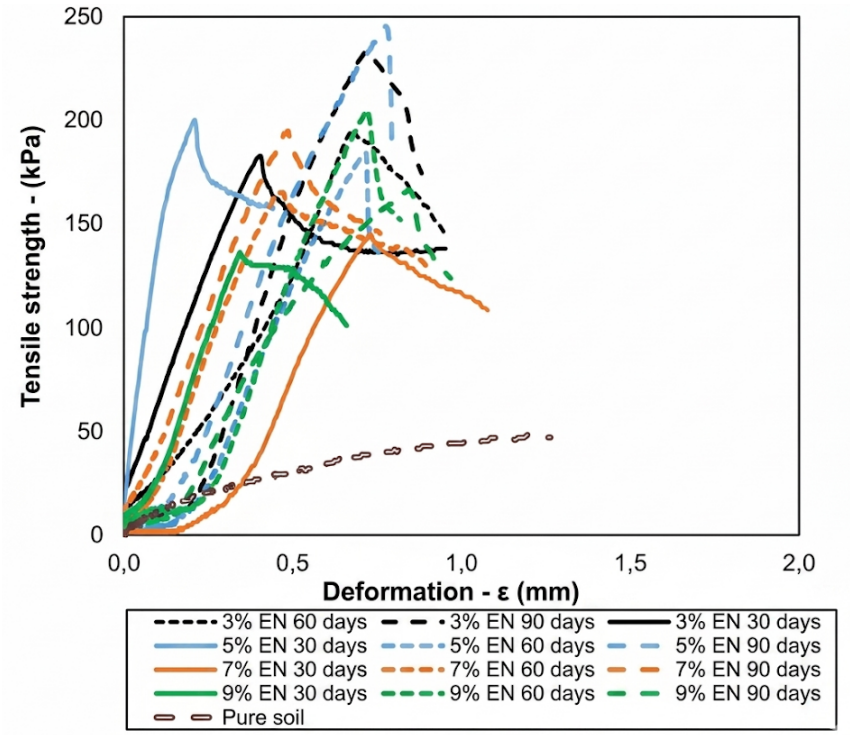


Figure 2.39: Tensile strength by diametral compression – Standard Proctor energy (Brazilian Test) A2-5 soil and soil-OSR specimens (Adapted Cardoso, 2019).

The study indicated that the specimens exhibited brittle failure, with low deformations in the range of 0.50% to 0.90%. Statistical analysis confirmed the superiority of the 3% and 5% contents, while higher dosages (7% and 9%) resulted in less significant performances, with the 9% mixture at standard energy showing strength values close to those of the natural soil.

Scherer et al. (2023) assessed the stabilization of a clayey soil for pavement applications using higher OSR replacement rates of 15%, 25%, and 35%. Their results demonstrated a 29% increase in UCS for the 15% OSR blend compared to the untreated soil, whereas the 35% mixture maximized the CBR with a 23% improvement. Ultimately, the 15% OSR proportion was recommended as the optimal residue content (ORC) for subgrade reinforcement, primarily driven by its superior compressive strength performance. which indicate significant strength gains with moderate residue additions.

The mechanical behavior of the BR-120 clayey soil from the study of Lunz (2021), classified as LG's, L (Ignatius, 1991) > 0,3, under unconfined compression reveals that OSR incorporation promotes significant strength increments, except for the 25% residue mixture. In Figure 2.40, while the pure soil presented an average UCS of approximately 160 kPa, the 25% OSR addition resulted in an 11% reduction in strength (142.38 kPa), likely due to an unfavorable pH far from 12, insufficient CaO to perform effective cation exchange. Conversely, maximum performance was achieved at a 75% OSR content, reaching 293.94 kPa—an 83% increase compared to the original soil. This substantial gain is attributed to cation exchange, flocculation, and soil particle aggregation, alongside improved particle interlocking as the clay fraction is replaced by silt fractions from the residue.

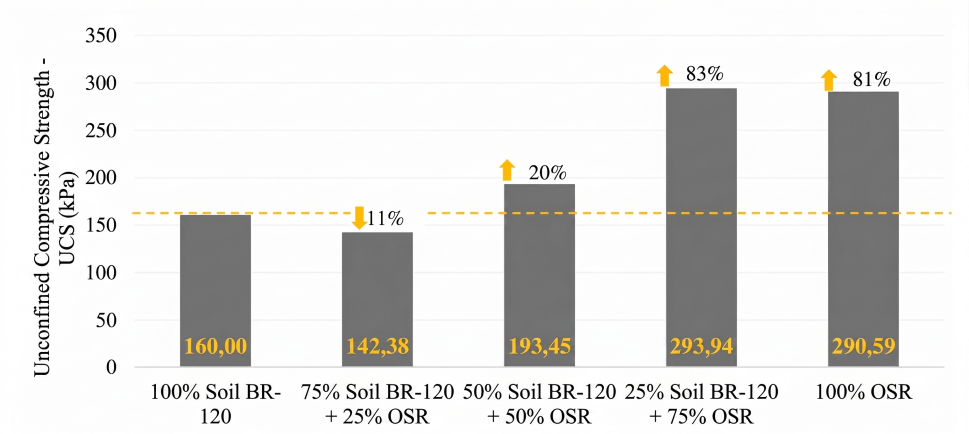


Figure 2.40: UCS function of OSR content (Modified Lunz, 2021)

When OSR is utilized in conjunction with traditional binders, the synergy can further enhance structural capacity. Aguiar (2019) demonstrated that in soil-cement mixtures (with a fixed 6% cement content), the progressive addition of OSR consistently increased the UCS, with a 30% OSR dosage reaching a strength of approximately 380 kPa. However, despite these positive contributions, the strength gains from OSR alone are generally inferior to those of traditional binders, suggesting that high-demand infrastructure projects may require mixed stabilization strategies (Nascimento et al., 2019; Dias, 2024).

A critical observation in UCS research is the existence of an optimal residue content,

which may vary between immediate and long-term performance. Vikas and Ramana (2023) identified that for uncured expansive soil samples, the UCS peaked at a 30% OSR content (339 kPa) before decreasing at higher dosages. Interestingly, for samples subjected to curing (7 to 28 days), the strength continued to increase up to a 40% residue content. This divergence suggests that while immediate strength is primarily a function of compaction and granular packing, long-term performance may be enhanced by latent pozzolanic potential, allowing for higher utilization rates of the residue in stabilized layers.

It is imperative to recognize that Ornamental Stone Residue (OSR) is not merely a mineral byproduct but a complex industrial composite containing chemical additives from processing stages. In facilities utilizing metallic blade cutting systems, the addition of calcium oxide (CaO) is common, while the polishing stages often introduce epoxy resins into the waste stream. Consequently, OSR functions as a reactive geomaterial rather than a purely inert filler. This chemical signature explains the significant strength gains observed over extended curing periods in studies such as Cardoso (2019). The presence of CaO can trigger slow-acting pozzolanic reactions or self-cementing behavior when interacting with soil minerals or the residue's own silica content. Furthermore, the residual resins may act as secondary binders with distinct polymerization scales. This dual nature—combining physical particle packing with time-dependent chemical stabilization—justifies why UCS and tensile strength continue to evolve up to 90 days, transitioning the material from a simple waste product to a performance-enhanced stabilizer.

The technical benefits of OSR integration in soil stabilization are likely a synergy between physical skeleton optimization and a latent chemical binding effect. Therefore, future studies should focus on the quantitative determination of these chemical agents—specifically the residual CaO and epoxy resin concentrations—to accurately assess the actual binder potential of the residue. Such characterization will be fundamental to decoupling the purely mechanical gains from the time-dependent chemical stabilization, allowing for the development of more precise predictive models for long-term pavement performance.

2.6.7 - CALIFORNIA BEARING RATIO (CBR) OF/WITH OSR

The California Bearing Ratio (CBR) remains a cornerstone in pavement engineering for assessing the suitability of soils and geomaterials for subgrades and structural layers. Despite the evolution toward more representative mechanistic parameters, such as the Resilient Modulus (MR), the CBR continues to be the primary classificatory metric in both national and international standards. In Brazil, for instance, the DNIT 108/2009-ES standard establishes strict minimum CBR thresholds for embankment layers and subgrades (DNIT, 2025). Its persistence in road engineering is justified by its cost-effectiveness, procedural simplicity, and

the extensive historical database available to practitioners and researchers.

Barrientos et al. (2010) studied pure granite residues (OSR-G) and showed a clear correlation established between compaction energy, Maximum Dry Density (MDD), and the resulting CBR values. When OSR is integrated into natural soils, the impact on bearing capacity is highly dependent on the residue content and the mineralogical characteristics of the host soil. For example, clayey soils (e.g., A-7-6) with moderate natural bearing capacity can exhibit significant enhancement when treated with OSR under optimized designs (Nascimento, 2019).

Table 2.28: CBR values for Sample M1 under different compaction and saturation conditions (Adapted from Barrientos et al., 2010).

Test Condition	**Blows**	ω (%)	ρ_d (Mg/m^3)	**CBR**$_{2.5}$ **(%)**	**CBR**$_{5.0}$ **(%)**
Non-saturated	15	19.2 ± 2.4	1.49 ± 0.10	18 ± 8	19 ± 10
	30	17.9 ± 1.3	1.63 ± 0.04	37 ± 8	43 ± 12
	60	15.4 ± 3.5	1.79 ± 0.15	61 ± 10	73 ± 14
Soaked	15	36.5	1.21	4	4
	30	29.3	1.62	18	31
	60	35.1	1.56	28	34

Under the level of modified compaction energy (60 blows), the unsaturated residue achieved CBR values of up to 73%, classifying it as a material with very low deformability and high bearing capacity for structural fills. Even after saturation, well-compacted samples maintained a CBR of 34%, confirming the durability and mechanical stability of OSR as a borrow material for road infrastructure.

However, the gain in bearing capacity is not linear, necessitating the identification of an Optimum Residue Content (ORC). Lunz (2021) demonstrated a clear trajectory of CBR improvement after 25% of OSR content, with 75% OSR mixture achieving a CBR significantly higher than that of the pure soil (Figure 2.41). This underscores that the systematic determination of the ORC through laboratory testing is essential to harness the full potential of OSR, ensuring that the residue acts as a reinforcing agent rather than a disruptive filler within the soil matrix.

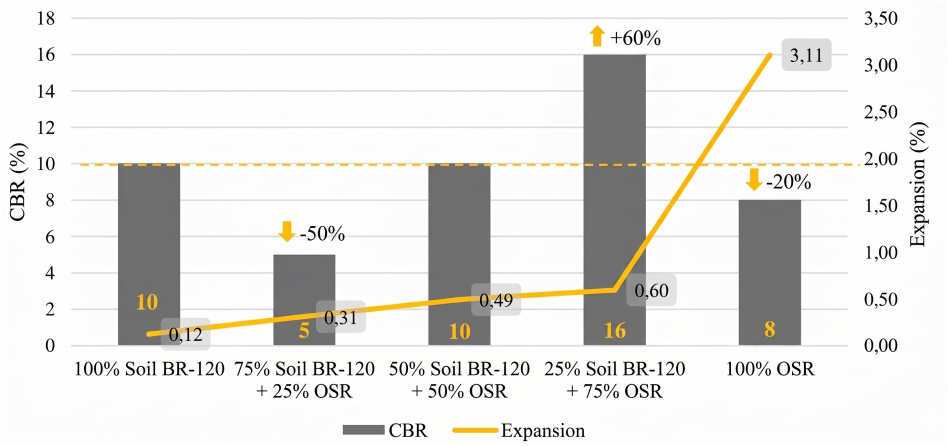


Figure 2.41: CBR and expansion function of OSR content (Modified Lunz, 2021)

The geotechnical behavior of the BR-120 clayey soil (classified as LG's) mixed with OSR shows that expansion values increased proportionally with OSR content, with pure 25% lateritic soil and 75% OSR reaching 0.6%. Consequently, these mixture are suitable for subgrade reinforcement layers, as CBR values remain far above the minimum treshold of 6%, however not reaching the 20% threshold required for sub-bases.

The experimental data reveals that the addition of OSR triggered a sharp increase in the CBR, elevating the material from a low-strength state (9.13%) to values exceeding 42% at higher residue concentrations. This enhancement allowed all tested mixtures to meet the regulatory requirements for road sub-base layers, which typically demand a minimum CBR of 20%. Furthermore, while the expansion percentage showed an upward trend as more fines were introduced, all values remained safely below the 1% limit established by DNIT standards, peaking at 0.69% for the 50% OSR content. These findings underscore the role of OSR as a high-performance mechanical stabilizer, capable of optimizing lateritic soil matrices for heavy traffic applications.

Table 2.29: CBR and Expansion results for soil-OSR mixtures (Adapted from Farias et al., 2018a).

OSR Content (%)	**CBR (%)**	**Expansion (%)**
0% (Natural Soil)	9.13	0.10
20%	28.61	0.52
30%	29.50	0.61
40%	40.21	0.68
50%	42.55	0.69

The clayey soil analyzed by Farias et al. (2018) exhibits a typical lateritic behavior, a characteristic identified by the steep slope of its compaction curve. While Farias et al. (2018) cite Pinto (2006) regarding this behavior, it is historically attributed to the pioneering work of

Ignatius (1991). This distinction is vital: although traditional granulometric analysis (sieving) classifies the soil as A-4 (silts), its mineralogical reality is that of an acidic lateritic clay rich in iron and aluminum oxides.The massive strength gain observed when mixing this "A-4" soil with OSR—materials with ostensibly similar grain sizes—cannot be explained by physical packing alone. Instead, it is highly probable driven by a cationic shock and subsequent chemical stabilization. As demonstrated by Barrientos et al. (2010), OSR (particularly from gang saws) possesses a highly basic pH (between 10 and 12) due to residual CaO.

The classification of the host soil as A-4 under the AASHTO system obscures its lateritic nature. The steep compaction curve (Ignatius, 1991) and the high pH of the OSR (Barrientos et al., 2010) suggest that the strength gain is a result of cationic shock rather than simple physical grain-size adjustment.

2.6.7.1 The Paradox of Performance Degradation: The Case of Dias (2024)

The study by Dias (2024) stands as a cautionary tale in geotechnical stabilization, where a flawed initial strategy effectively "engineered" the degradation of a high-quality soil. By attempting to stabilize a naturally robust sandy soil with excessive amounts of Ornamental Stone Residue (OSR), the research documented a systematic decline in all key performance indicators.

The parent soil utilized by Dias (2024) was a high-grade sandy material Figure 2.42 , called in Brasil "saibro", with one of the highest CBR on record in the country, of approximately 40%, far exceeding the intrinsic bearing capacity of the residue itself. For comparison, pure OSR from similar industrial processes (diamond wire) typically yields a soaked CBR in the 30-34% range (Barrientos et al., 2010). Consequently, the volumetric replacement of a superior granular matrix with a silt-clay filler (A-6) was inherently counterproductive.

- **Stiffness Decay**: The 30% OSR mixture suffered a 21% reduction in Resilient Modulus (M_R) compared to the reference soil, transitioning a stiff foundation into a more deformable layer.
- **Structural Dilution**: As OSR content increased, the mixture's CBR plummeted to 20.2% (Figure 2.43), effectively halving the original soil's strength just to meet the minimum regulatory threshold for sub-bases.
- **Density Loss**: The inclusion of the lighter residue particles disrupted the sandy skeleton, leading to a progressive decrease in Maximum Dry Density (MDD).



Figure 2.42: General view of the soil deposit utilized for the study (Source: Author, 2026).

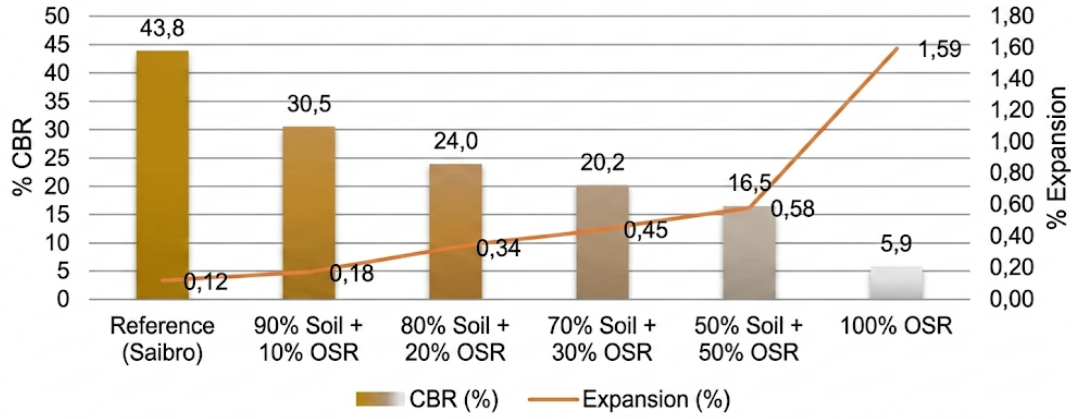


Figure 2.43: CBR losses and expansion in different contents of soil-OSR mixtures, (Adapted from Dias, 2024).

This work confirms our central thesis: coarse soils require minimal filler (0–10%, or even 0–5%) only to seal residual voids. Conversely, the massive gains seen in fine-grained or lateritic soils (A-4) are driven by the cationic shock and chemical synergy of high-pH OSR (pH 12). In those cases, where the OSR's CBR is significantly higher than the parent soil's, gains continue to grow even at high replacement rates (>50%). Dias (2024), however, represents the inverse—an unintended demonstration of how the wrong dosage can turn a high-performance soil into a mediocre mixture.

2.6.7.2 High Potential for Lateritic A-4 Soil Stabilization

The results presented in Figure 2.44 are a remarkable geotechnical transformation, presenting visual proof of optimized lateritic soil. The chart illustrates the profound effect of OSR integration on both California Bearing Ratio (CBR) and expansion for a seemingly moderate acidic lateritic soil (A-4).

With an initial CBR of only 9.13%, the addition of OSR triggered a massive and immediate leap in bearing capacity, tripling the original value at just 20% OSR content (28.61%). This upward trajectory continued to increase significantly, with the 50% OSR mixture achieving a pronounced 42.55% CBR. As detailed in Section 2.5.1.4, this extraordinary strength gain isn't simply a matter of grain-size adjustment. Instead, it is probably driven by cationic shock. The acidic lateritic matrix, characterized by a steep compaction curve (Ignatius, 1991), is 'cured' by the high concentration of Ca^{2+} ions from the basic OSR (Barrientos et al., 2010). This chemical synergy triggers flocculation and initializes pozzolanic reactions, converting a low-modulus silt into a coherent, high-performance base material.

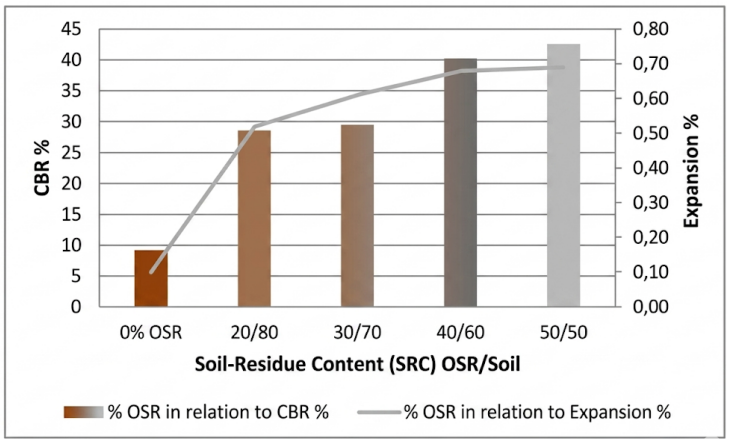


Figure 2.44: Professional dual-panel synchronized bar chart visualizing the pronounced CBR increase and low expansion in soil-OSR mixtures, with annotation explaining the cationic shock mechanism in lateritic A-4 soil (Adapted from Farias et al., 2018).

Crucially, while CBR soared, expansion remained exceptionally relatively low, peaking at 0.69%. All soil-residue mixtures stayed safely below the 1% limit established by DNIT standards for sub-bases, confirming that the high-strength gains do not compromise material stability. This chart is visual evidence that transforms lateritic silts from challenging engineering soil into structurally robust geomaterials through tailored chemical-physical synergy with an abundant residue such as OSR.

2.6.8 - RESILIENT MODULUS OF OSR-SOIL MIXTURES

The Resilient Modulus (M_R) is a critical parameter for assessing soil deformation under cyclic loading in pavement applications. The incorporation of OSR significantly enhances the M_R of problematic high-plasticity soils (e.g., A-7-5 and A-7-6 classes). This improvement is driven by a reduction in the plasticity index, which shifts the cohesive matrix toward a more granular behavior, thereby mitigating plastic flow and permanent deformation (Mello, 2019; Nascimento, 2019; Lunz, 2021; Braz, 2024).

As detailed in Table 2.30, this stabilization occurs through synergistic physical restructuring and chemical interactions. Consequently, optimizing the OSR dosage—defined as the Optimum Residue Content (ORC)—through Cyclic Load Triaxial Tests (CLTT) is essential. A properly calibrated mixture balances strength gains with adequate ductility, ultimately extending the service life and structural integrity of the pavement layers (Cardoso, 2019; Prandina, 2025).

Table 2.30: Mechanisms and geotechnical effects of OSR addition to cohesive soils

Mechanism / Concept	**Description**	**Resulting Geotechnical Effect**
Physical Modification & Granulometric Improvement	Fine, non-plastic OSR particles act as a filler, occupying voids within the aggregated structure of a cohesive soil: • Reduction of the plastic clay fraction overall influence; • Creates a denser particle skeleton with a probably better grain-to-grain contact.	• Reduced plasticity index (PI) • Reduced potential for swelling and deformation • Increased stiffness and a higher MR
Optimal Residue Content (ORC)	The improvement in stiffness is non-linear and depends on the OSR percentage: • Below ORC: OSR particles effectively fill voids and reinforce the soil's structure. • Above ORC: Excess fine OSR particles begin to dominate and push the soil's structural skeleton apart, reducing intergranular friction.	• Below ORC: Steady increase in MR. • At ORC: Peak (maximum) MR is achieved. • Above ORC: Decrease in MR.

Dias (2024) investigated the stabilization of an A-2-4 soil using 10% to 30% OSR for pavement layers. While the 30% OSR mixture satisfied the regulatory California Bearing Ratio (CBR) and swelling thresholds for subbase applications according to the Brazilian DNIT standards, it demonstrated a 21% reduction in Resilient Modulus (M_R) at higher stress states relative to the untreated reference soil (Figure 2.45). This outcome indicates that for non-plastic granular materials, excessive OSR contents can compromise stiffness. Consequently, restricting the residue to lower replacement rates (3–10%) is recommended, as minimal filler addition is more likely to enhance M_R through optimized particle packing.

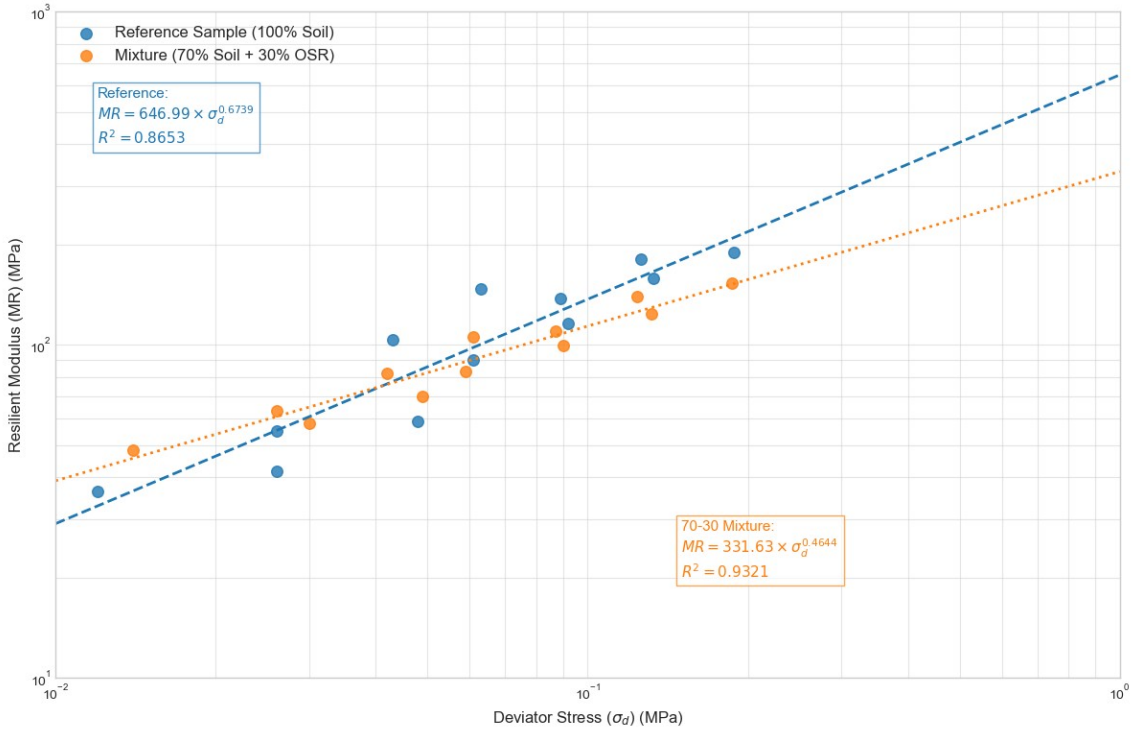


Figure 2.45: Resilient Modulus (M_R) of an A-2-4 soil mixed with OSR (modified from Dias, 2024).

In Brazilian pavement engineering, subgrade evaluation has transitioned from traditional empirical indices, such as the California Bearing Ratio (CBR), to a modern mechanistic-empirical framework embodied in the National Pavement Design Method (MeDiNa). While the CBR remains applicable in specific legacy contexts (e.g., DNIT 108/2009-ES), MeDiNa models pavement performance based on fundamental mechanical properties. Consequently, the Resilient Modulus (M_R) has replaced the CBR as the primary input for characterizing the structural response of unbound layers to traffic loading. This shift toward a performance-based parameter is essential for rigorously assessing alternative geomaterials, such as the OSR-soil mixtures investigated in this study.

Demonstrating this mechanistic approach, Jaffar et al. (2022) evaluated the M_R of an A-6 clay stabilized with marble waste (OSR-M) at dosages ranging from 3% to 13% by dry weight. Through Cyclic Load Triaxial Tests (CLTT), the authors observed a progressive stiffness increase, peaking at an impressive 546 MPa with a 9% OSR-M addition. However, exceeding this Optimum Residue Content (ORC) led to a structural decline, with the modulus dropping to 384 MPa at a 13% replacement rate (Figure 2.46). As elucidated by the researchers, this pronounced stiffening effect is fundamentally chemical: the calcium-rich OSR-M induces the flocculation and aggregation of clay particles, while simultaneously

fostering the development of cementitious bonds that rigidly bind the newly granularized matrix.

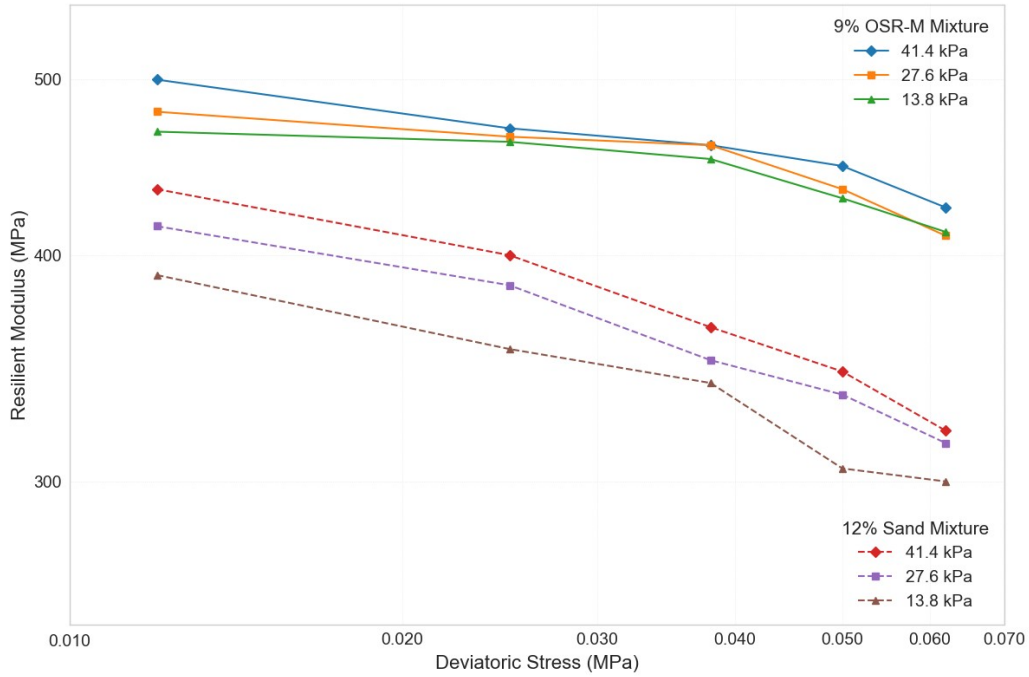


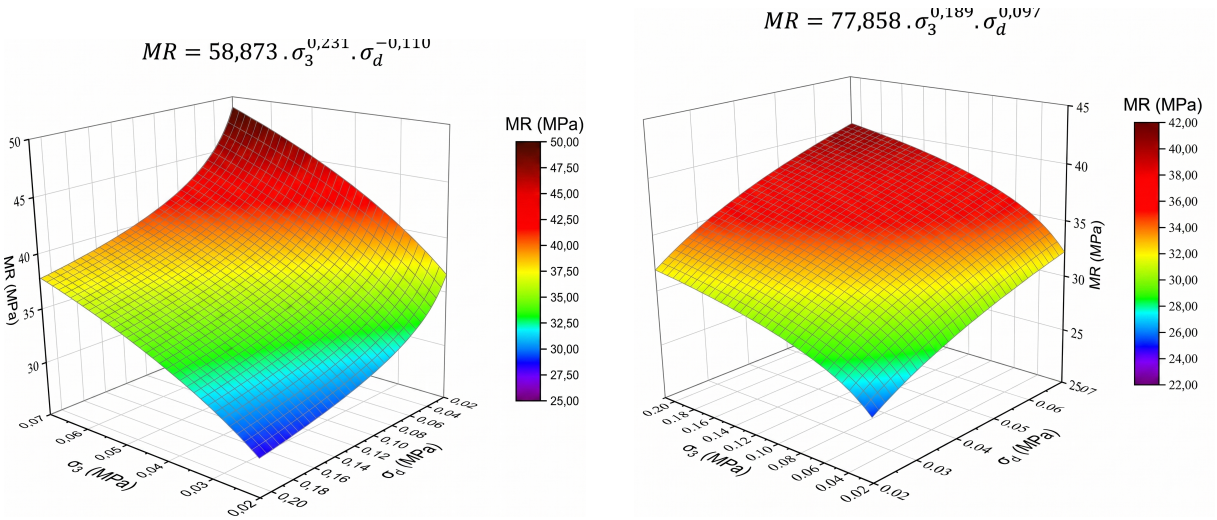
Figure 2.46: MR results of: i) ORC of OSR-M added to A-6 soil; ii) Optimum proportion of sand added to the same A-6 soil (modified from Jaffar et al., 2022).

The investigation conducted by Lunz (2021) on the clayey soil from BR-120 provides a compelling case for the use of high-volume Ornamental Stone Sludge (SOSP/LBRO) in pavement layers. The mechanistic behavior is best captured through the 3D response surfaces of the composite model ($M_R = k_1 \cdot \sigma_3^{k_2} \cdot \sigma_d^{k_3}$), which allow for a simultaneous visualization of how confinement (σ_3) and deviatoric stress (σ_d) influence stiffness.

Figure 2.47 presents the surfaces for the pure BR-120 soil and the mixture with 75% residue. To an inattentive reader, the two surfaces might appear almost identical in curvature and orientation, potentially leading to the premature conclusion that the OSR addition results in negligible mechanical changes or merely maintains the original soil's properties. However, a rigorous inspection of the geometric projection reveals a critical technical detail: the deviatoric stress (σ_d) axis in the 75% OSR plot is inverted relative to the pure soil reference.

This axis inversion is significant because it masks the true shift in the material's stress-dependency. Although the absolute M_R values for the 75% mixture are slightly lower than those of the pure soil, they remain within a comparable range. Lunz (2021) concludes that this similarity, when paired with the substantial environmental benefit of replacing three-quarters of the natural soil with industrial waste, renders the mixture technically and sustainably viable for subgrade reinforcement layers. The subtle change in the surface's "anchor

points" and its response to cyclic shear (governed by k_3) underscores a structural reorganization of the matrix that would be overlooked without a detailed analysis of the graphical scales.



(a) 100% BR-120 Pure Soil.

(b) 25% Soil + 75% OSR Mixture.

Figure 2.47: Comparison of 3D Resilient Modulus response surfaces for BR-120 soil and OSR mixture. Note the inversion of the σ_d axis in the mixture plot (b) (modified from Lunz, 2021).

Figure 2.48 shows Santos and Leandro (2017) study of ternary mixtures with OSR suggested by this author in 2017.

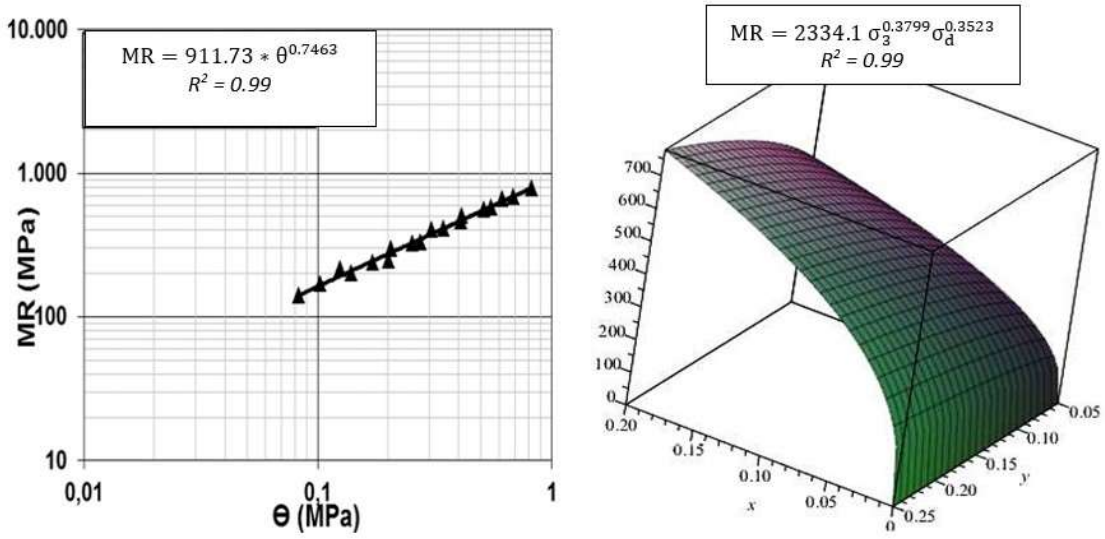


Figure 2.48: M_R graphs obtained from the models for the first mix (5% OSR, 40% RAP, 55% gravel): (i) Simplified Model θ (Bulk stress); (ii) Composite Model (modified from A. S. Santos & Leandro, 2017).

Teixeira et al. (2017a, 2017b) also investigated the same ternary mixtures comprising lateritic gravel, Reclaimed Asphalt Pavement (RAP), and granite residue (OSR-G) for base and

subbase applications. Noting that traditional base materials typically exhibit Resilient Modulus (M_R) values between 300 and 500 MPa, Santos and Leandro (2017) demonstrated the structural viability of these alternative blends. Specifically, a mixture containing 5% OSR-G, 40% RAP, and 55% gravel achieved an M_R of 332 MPa at simulated base depths . Adjusting the RAP content to 60% (with 35% gravel) resulted in a comparable modulus of 316 MPa.

Corroborating these findings, Teixeira et al. (2017a) recorded even higher stiffness in similar formulations through Cyclic Load Triaxial Tests (CLTT). Their mixture of 5% OSR-G, 50% RAP, and 45% gravel reached an impressive M_R of 466 MPa, while a blend with 30% RAP and 65% gravel yielded 411 MPa. Consequently, Teixeira et al. (2017b) concluded that limiting the OSR addition to 5% by mass successfully preserves the matrix's structural integrity while meeting all technical criteria for pavement bases. This consistent performance highlights a highly advantageous engineering trade-off: OSR can effectively substitute a portion of conventional aggregates without sacrificing pavement stiffness. Such an approach offers a sustainable pathway for urban infrastructure, simultaneously repurposing industrial byproducts and mitigating the depletion of virgin natural resources.

3 - MATERIALS AND METHODS

The experimental program of this doctoral research was designed to evaluate the interaction between industrial residues and distinct soil matrices following a multi-stage experimental and analytical approach designed to evaluate the physical and mechanical properties of Brazilian tropical soils, especially ones from Espírito Santo, stabilized with local industrial byproducts: OSR and KRS.

This research adopted three tropical soils investigated in this research. The first two—a clayey soil from **Espírito Santo (ES)** and a typical porous clay from the **Federal District (Brasília)**—were selected to evaluate regional variability in binary stabilization. The third soil, sourced from **Cariacica (ES)**, was strategically sampled from an active borrow pit at a shallow depth, immediately beneath the organic A horizon. This specific soil represents a **marginal material** at the technical threshold for embankment construction, exhibiting a low California Bearing Ratio (CBR) between 4% and 6%. The geological context of each site is mapped to correlate pedological formation with the observed mechanical responses.

To provide a comprehensive roadmap of the experimental program, the select tropical soil matrices are systematically categorized based on their pedological origin, degree of laterization, and corresponding stabilizing agents. Table 3.1 outlines the strategic distribution of these three baseline soils across the different research stages, mapping each geotechnical environment to its respective binary or ternary waste-incorporation framework.

Table 3.1: Summary of the investigated tropical soils, geological origins, and associated waste stabilization systems.

Soil Designation & Origin	**Thesis Section**	**Laterization & Tropical Behavior**	**Stabilization System & Target Residues**
Caramuru Soil (Santa Leopoldina, ES)	Section 3.1	Lateritic (High Laterization Degree)	Binary System (Soil + OSR)
SG-12 Soil (UnB, Brasília, DF)	Section 3.1	Transitional Lateritic (Porous Cerrado Clay)	Binary System (Soil + OSR)
Espírito Santo Clay (Regional Interior / Cariacica)	Sections 3.2 & 3.3	Non-Lateritic (Marginal / Highly Plastic Clay)	Binary (Soil + KRS) & Ternary (Soil + KRS + OSR)

The research is structured into three primary experimental blocks, as described below, alongside a comprehensive characterization of the residues and mixtures which combined form the novel geomaterials and their respective collection sites.

The first stage (Section 3.1) focuses on binary mixtures for subbase applications, incorporating two distinct tropical soils—one from the state of Espírito Santo (ES) and another from the Federal District (Brasília)—blended with Ornamental Stone Residue (OSR). This campaign involves extensive Resilient Modulus (RM) testing to assess how regional soil variability influences the stabilization effectiveness of OSR.

The second stage (Section 3.2) explores the mechanical and microstructural synergy within binary and ternary systems. This block utilizes a representative clayey soil from Espírito Santo and introduces a pioneering investigation into ternary mixtures, combining soil with both OSR and Kambara Reactor Slag (KRS). This approach represents a contribution to the field, as the simultaneous use of these two distinct industrial byproducts in soil stabilization remains unexplored in the literature. Furthermore, this phase incorporates a critical evaluation of chemical kinetics through controlled **curing periods of 0, 4, and 28 days**, allowing for the assessment of time-dependent strength gain and microstructural evolution. The methodology for this stage integrates and expands upon findings from the author's previous research submitted to ASCE, providing a robust framework for understanding the "Double Action Mechanism" in soil-waste stabilization.

Finally, the third stage (Section 3.3) addresses long-term structural performance through an advanced series of cyclic loading tests. This phase employs a specific soil from Cariacica (ES) mixed with OSR, targeting the characterization of both Resilient Modulus and Permanent Deformation (PD) parameters. This soil was strategically selected to represent materials at the technical threshold for embankment applications. Collected from an active borrow pit, the samples were extracted from a shallow depth, specifically just beneath the organic A horizon, to capture the properties of a low-bearing capacity material. With a California Bearing Ratio (CBR) ranging between 4% and 6%, this soil characterizes a lower-bound capacity scenario for road construction, typical of marginal materials used in embankments and final embankment layers. These results are critical for the mechanistic-empirical modeling of pavement service life using the Brazilian MeDiNa method, testing the efficiency of OSR in upgrading poor-quality soils into viable structural components.

The following sections detail the origin and collection of the residues, the physical-chemical characterization protocols, and the specific testing matrices employed in each of the three experimental groups.

3.1 - BINARY OSR-SOIL MIXTURES FOR SUBBASE APPLICATIONS

The first stage of this research evaluates the interaction between Ornamental Stone Residue (OSR) and two pedologically distinct soil matrices, representing a strategic cross-section of

Brazilian tropical geotechnics. By selecting soils from the mountainous region of Espírito Santo (Caramuru) and the Central Plateau (SG-12), the study aims to determine if the stabilizing effects of OSR—driven by suction enhancement and the filler effect—are universal across different mineralogical environments or site-specific.

Both materials represent high-quality natural geomaterials, characterized by a predominantly lateritic behavior and significant bearing capacity, with California Bearing Ratio (CBR) values reaching 20% under intermediate Proctor compaction energy. Classified as A-4 according to the TRB system and identified as low-plasticity silty clays (CL/ML) under the USCS, these soils serve as the baseline for evaluating OSR effectiveness in subbase applications. The selection aimed to provide a comprehensive analysis across the following distinct environments:

- **Caramuru Soil (Espírito Santo):** Sourced from the Caramuru quarry in the municipality of Santa Leopoldina, ES. This soil is a regional available source as a natural geomaterial used in some local infrastructure projects within the Espírito Santo industrial cluster, directly reflecting the reality of the state's roadwork challenges, including academic research during the years of 2017 and 2018.
- **SG-12 Soil (Brasília):** Collected from the experimental geotechnical site of the University of Brasília. This soil represents a typical tropical sediment from the Central Plateau, highly studied and well-characterized in Brazilian literature. Its inclusion is strategic: being distant from coastal laterization processes and possessing a distinct chemical signature, it serves as a baseline to verify if the OSR "filler" and suction effects are universal or site-specific.

Both soils are classified as A-4 according to the TRB system and are identified as low-plasticity silty clays (CL/ML) under the USCS, with CBR reaching 20% of both soils for the intermediate Proctor energy. The physical and mechanical properties of the natural soils are tested and summarized in Table 3.4.

3.1.1 - MIXTURE PROPORTIONS AND DOSAGE RATIONALE

The experimental matrix for the binary mixtures was designed to evaluate the sensitivity of high-quality soil matrices to the inclusion of OSR. For both the Caramuru (ES) and SG-12 (Brasília) soils, which exhibit lateritic behavior and adequate natural mechanical properties, an incremental dosage strategy was adopted: 0%, 5%, 10%, 15%, and 30% of OSR by total dry mass.

The rationale for this range is twofold:

- **Control and Initial Improvement (0–15%):** The lower percentages aim to identify the efficiency of the OSR as a mineral filler and its role in enhancing matrix suction, targeting a performance boost without significantly altering the soil's primary cohesive structure.
- **Threshold Analysis (30%):** The inclusion of a 30% dosage serves to investigate the potential "saturation point" of the filler effect in lateritic soils. This allows for the observation of the transition from a soil-dominant behavior to a more complex interaction where the residue significantly contributes to the granular skeleton of the mixture.

This systematic variation is essential to determine the optimal OSR content that maximizes the Resilient Modulus (RM) for subbase applications, providing a baseline for comparison with the more challenging soils addressed in subsequent sections. The experimental matrix for this stage is summarized in Table 3.2.

Table 3.2: Experimental matrix for the Brasília soil (SG-12) stabilized with OSR.

Sample ID	SG-12 Soil (%)	OSR (%)	Technical Objective
SG-0 (Natural)	100	0	Control reference (Porous lateritic clay)
SG-5	95	5	Initial filler effect and suction study
SG-10	90	10	Intermediate physical stabilization
SG-15	85	15	Standard dosage for subbase comparison
SG-30	70	30	Investigation of the matrix saturation point

Despite the identical percentage increments, the application of OSR to the Caramuru soil follows a distinct geomorphological rationale. While the SG-12 represents the porous, highly-weathered sediments of the Central Plateau, the Caramuru soil serves as a proxy for the residual materials of the crystalline basement in the mountainous region of Espírito Santo. The maintenance of the same dosage levels (5%, 10%, 15%, and 30%) is intentional, as it allows for a direct bilateral comparison of how the residue's mineralogy interacts with different clay-mineral assemblages and particle arrangements, as detailed in Table 3.3.

Table 3.3: Experimental matrix for the Santa Leopoldina soil (Caramuru) stabilized with OSR.

Sample ID	Caramuru Soil (%)	OSR (%)	Technical Objective
CR-0 (Natural)	100	0	Control reference (Residual gneissic soil)
CR-5	95	5	Particle size distribution optimization
CR-10	90	10	Resilient performance enhancement
CR-15	85	15	Regional practice benchmarking (ES)
CR-30	70	30	Evaluation of granular-dominant behavior

3.1.2 - CARAMURU REGION SOIL (SANTA LEOPOLDINA, ES)

The material was extracted from the quarry located in Santa Leopoldina (refer to Figure 3.1 and Figure 3.2). Geologically, the region is part of the Ribeira Fold Belt, characterized by a

crystalline basement of gneissic and granitic rocks. The resulting soil (ranging from saprolite to mature residual soil) is strongly influenced by the rugged terrain and high rainfall indices of the Espírito Santo mountain range, which define its mechanical and mineralogical behavior.



Figure 3.1: Location of the Caramuru borrow pit and delimitation of sampling areas (GEOBASES, 2026).

3.1.3 - SG-12 SOIL FROM UNB EXPERIMENTAL SITE (BRASÍLIA, DF)

Sampling was conducted at the UnB geotechnical experimental site (Figure 3.3). The geological setting of Brasília's Plano Piloto, where the tests were conducted, is primarily composed of rocks belonging to the Paranoá Group, characterized by low-grade metamorphism. This lithostratigraphic succession displays an interbedding of various strata, including fine-to-medium-grained quartzites (Q3 unit), clayey metasiltstones (S unit), sandy (R3 unit)

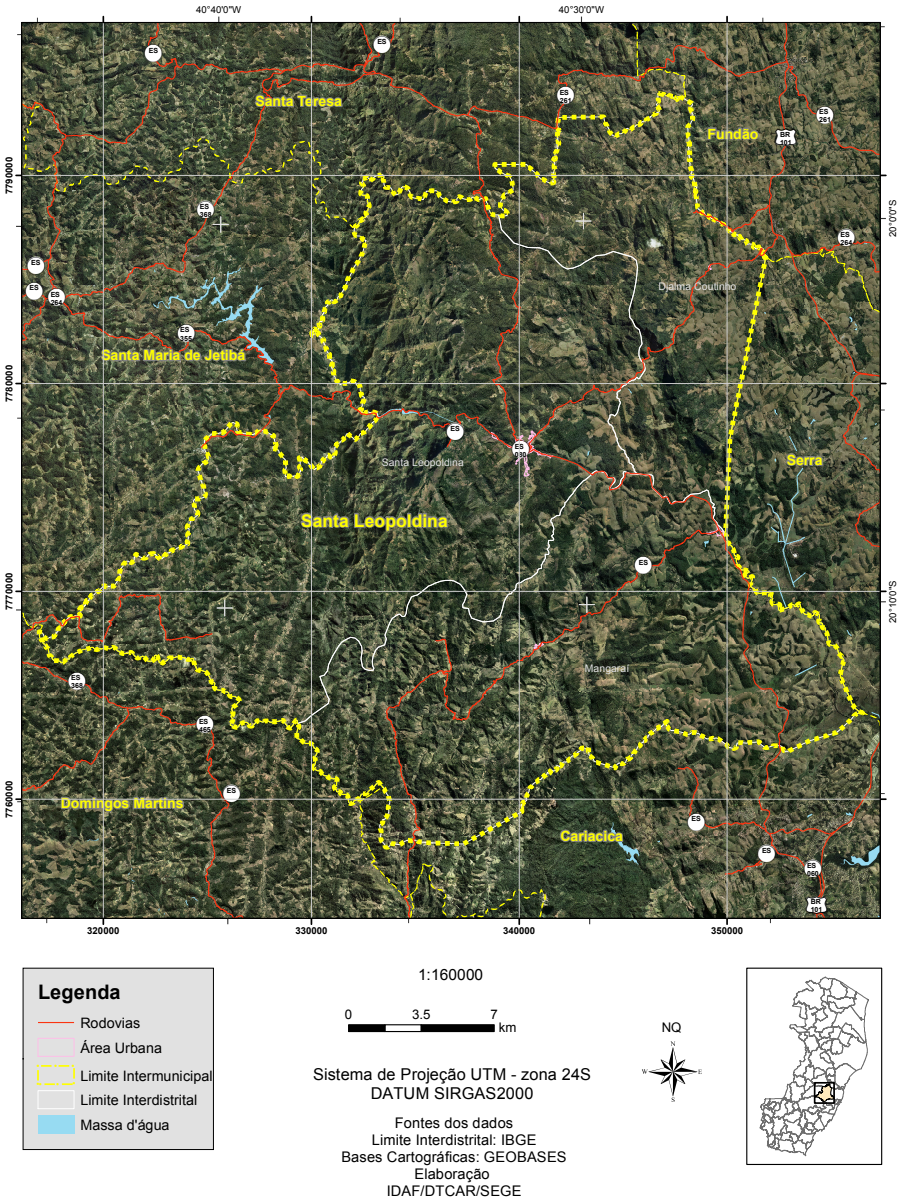


Figure 3.2: Regional map of the Santa Leopoldina region (IDAF, 2026).

and clayey (R4 unit) metarhythmites, as well as slates (A unit), following the classification proposed by Silva & Campos (1998).

The pedological profile of the Brazilian Federal District (DF) is highly representative of the Cerrado region. In its natural state, these soils exhibit high drainage capacity, even when clay fractions reach up to 90%. This high permeability is primarily attributed to the aggregation of clay particles into sand-sized clusters within these acidic environments.

As highlighted by Camapum (1994), shallow underground excavations in this region frequently encounter collapsible, reddish to reddish-yellow clayey horizons. These materials are locally classified by geotechnical engineers as "porous clay". This specific soil type comprises varying proportions of clay, silt, and sand, with its mineralogical and granulometric distribution



Figure 3.3: General view of the Geotechnical Experimental Site at the University of Brasília (UnB), near the SG-12 sampling area (Geotecnia UnB, 2026).

governed by the local geological domain.

3.1.4 - THE OSR APPLIED AND ITS SOURCE

The OSR utilized in the study of this section originates from a major stone-processing hub in the Greater Vitória, Espírito Santo. The collection points were standardized to ensure consistency, focusing on sampling the OSR directly from the fresh deposit under its filter press (Figure 3.4).



(a) (b)

Figure 3.4: OSR recovery system at the Vitória Stone facility: (a) overview of the automated filter press; (b) extraction of the solid residue after the pressing cycle.

To visualize in advance the structural relationships and particle size characteristics of these baseline components, their consolidated particle size distribution (GSD) curves are comparatively illustrated in Figure 3.5. This comparison highlights the structural contrast between the well-graded residual matrix of the Caramuru soil, the naturally aggregated

cluster behavior of the porous SG-12 Cerrado clay, and the highly uniform, fine-grained distribution of the pure OSR Q-16 acting as a mineral filler. Quantifying these granulometric boundaries in their natural, non-deflocculated states is fundamental to understanding the physical mechanisms—namely the structural packing optimization, filler efficiency, and matrix suction enhancement—that govern the resilient modulus (M_R) response of the resulting binary subbase mixtures.

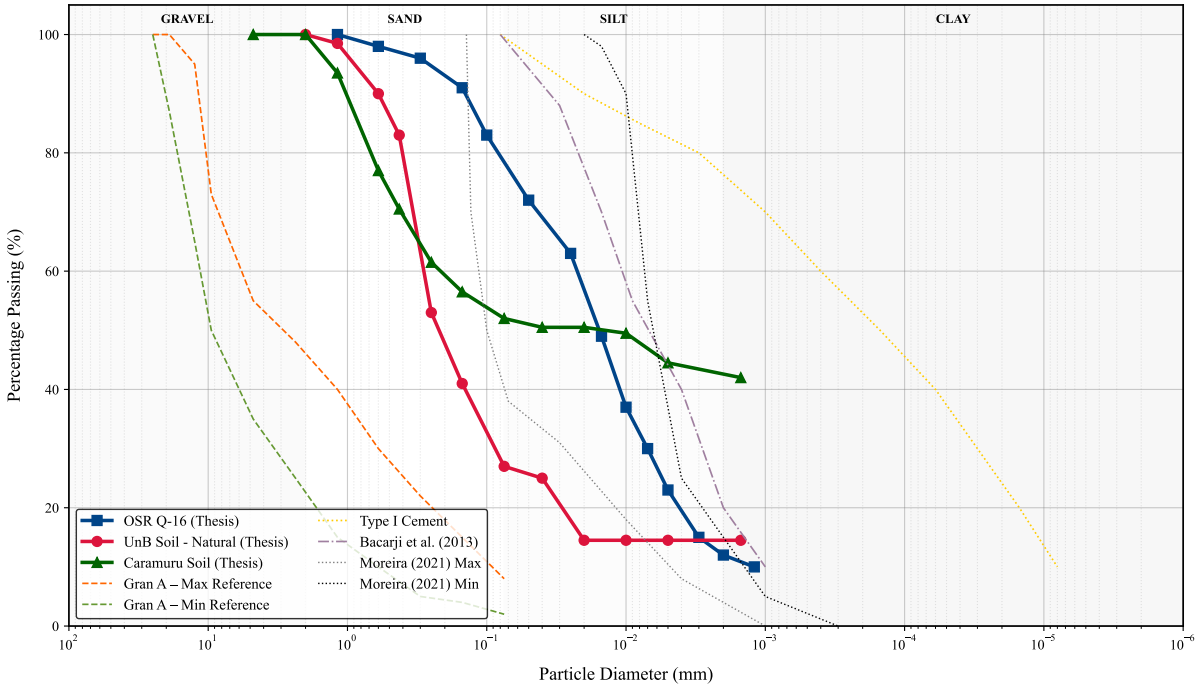


Figure 3.5: Consolidated particle size distribution (GSD) curves for the baseline materials evaluated in Section 3.1: Caramuru soil, natural SG-12 soil, and pure OSR Q-16 mineral filler.

The production of this residue is intrinsically linked to modern stone-cutting technologies. The facility utilizes **diamond wire saw technology**, a process that has largely replaced traditional gang saws in the last decade. Unlike older methods that required a complex abrasive slurry containing steel grit and **lime (CaO)** to facilitate cutting and prevent oxidation, the diamond wire process uses only water for cooling and lubrication.

Consequently, the OSR generated is a chemically uniform mineral byproduct, reflecting the exact mineralogy of the parent silicate rocks (predominantly granites and quartzites) without exogenous calcium contamination. This is a critical factor for this research, as it ensures that the stabilization effects observed in the soil-OSR mixtures are not influenced by cementitious reactions derived from industrial additives, but rather by the residue's intrinsic physical and mineralogical properties.

Table 3.4: Geotechnical properties of the natural soils from Brasília (SG-12 EGS) and from Caramuru Borrow Pit, later tested in Vitória, state capital of Espírito Santo (from Prandina, 2019).

Property	**SG-12 Soil (UnB)**	**Caramuru Soil (ES)**
Specific Gravity (G_s)	2.67	2.67
Liquid Limit (WL, %)	34	30
Plasticity Limit (WP, %)	25	22
Plasticity Index (PI, %)	9	8
Optimum Moisture (%, Interm.)	22.0	16.0
Max. Dry Density (kN/m^3, Interm.)	15.65	17.93
Effective Cohesion (c', kPa)	21.4	17.6
TRB Classification	A-4	A-4
USCS Classification	CL	CL

To ensure the repeatability of the experimental results, the OSR was subjected to a standardization protocol upon arrival at the laboratory. The dehydrated OSR "cakes" collected from the filter press was initially crumbled and spread in thin layers to be air-dried.

Following drying, the material was manually pulverized and sieved through a **#40 mesh (0.425 mm)** to remove any occasional coarse fragments or industrial contaminants. The resulting fine powder was then homogenized and stored in airtight containers to maintain a constant hygroscopic moisture content throughout the mixing and compaction stages of the research.

3.2 - OSR ON BINARY KRS-SOIL MIXTURES

This stage investigates the chemo-mechanical interactions in binary (Soil-KRS) and ternary (Soil-OSR-KRS) systems. Unlike the lateritic materials typically favored in Brazilian road engineering due to their satisfactory performance, the soil selected for this phase was intentionally chosen for its **non-lateritic behavior**.

The underlying scientific strategy is to evaluate the “upgrading” potential of Kambara Reactor Slag (KRS). Given that literature consistently reports significant relative strength gains with KRS, this research employs a more challenging, marginal soil matrix. The goal is to verify if the KRS-driven stabilization can elevate poor-quality, non-lateritic soils to performance levels comparable to those of stabilized lateritic materials.

3.2.1 - SOIL SELECTION: NON-LATERITIC BEHAVIOR

The soil was sampled from an inland region of Espírito Santo, still close to the coastal zones where laterization processes has been reported more prevalent, from a borrow pit of a state road in construction arond 50 km from Vitória, the state capital. This material is a A-7-6, CH clayey soil, exhibits a typical non-lateritic behavior, characterized by higher sensitivity to moisture and lower natural bearing capacity (CBR=7.9%). By selecting a material at a "technical disadvantage," the research provides a robust stress-test for the proposed chemical activators.

3.2.2 - KAMBARA REACTOR SLAG (KRS)

The Kambara Reactor Slag (KRS) was provided by **ArcelorMittal Tubarão**. As a byproduct of the hot metal desulfurization process in the Kambara Reactor, this slag is rich in free lime (CaO) and other alkaline components, making it a potent chemical activator for soil stabilization. In this research, KRS acts as the primary agent for the "Double Action Mechanism," providing the necessary alkalinity to trigger cationic exchange and provide the CaO for long-term pozzolanic reactions within the soil-waste matrix. The KRS was collected in its typical coarse GSD, result of industrial processing at an aggregate treatment facility.

3.2.3 - OSR FOR TERNARY SYSTEMS

The OSR used specifically in this stage was supplied by **Levantina Natural Stone**. Consistent with the material described in previous sections, this residue is generated through diamond wire sawing, ensuring a calcium-free mineral filler. In the ternary mixtures, the OSR is expected to complement the chemical action of the KRS by providing physical filling (filler effect) and potential nucleation sites for the formation of cementitious products.

To map and contrast the physical dimensions of these constituent phases, their cumulative particle size distribution (GSD) curves are comparatively illustrated in Figure 3.6. This granular analysis highlights the structural disparity and complementary nature of the materials: the KRS provides a coarse skeleton with a substantial gravel fraction, the raw soil yields a clay-dominant matrix, and the OSR functions strictly as a high-surface-area, silty mineral filler in its aggregated state. The integration of these distinct granulometric boundaries forms the physical baseline for the packing optimization and subsequent chemo-mechanical stabilization investigated in the binary and ternary mixtures.

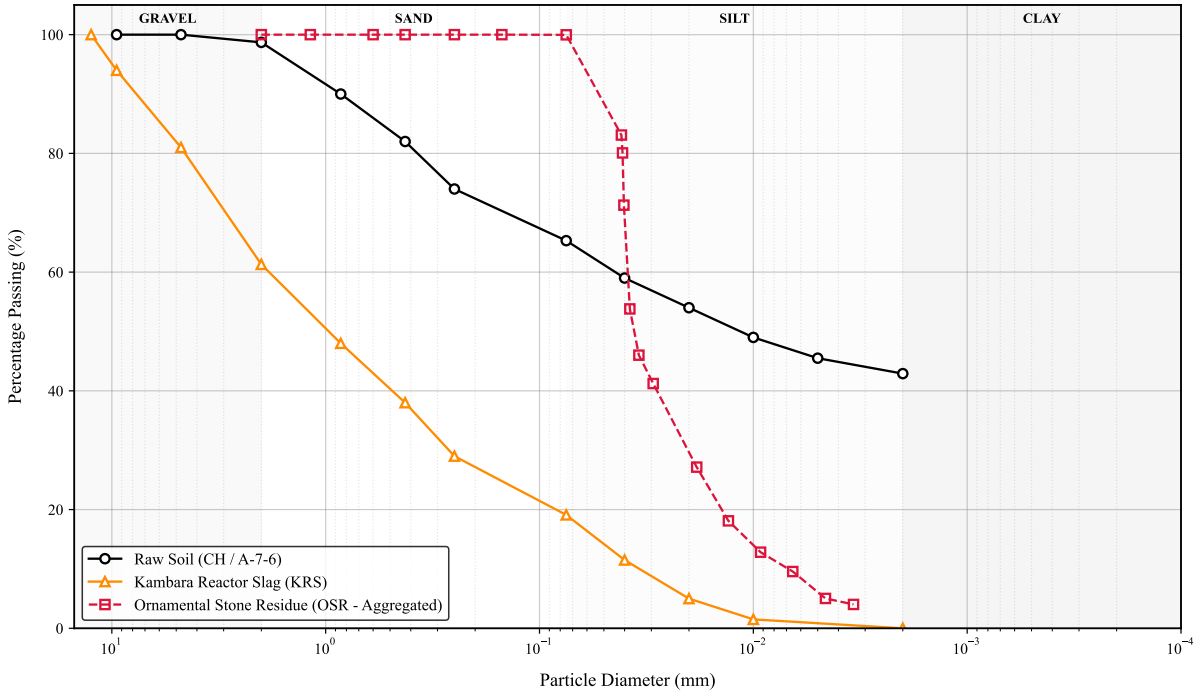


Figure 3.6: Comparative particle size distribution (GSD) curves for the raw materials utilized in Section 3.2 (Soil, KRS, and aggregated OSR) classified under standard geotechnical fractions.

3.2.4 - DOSAGE DESIGN AND MIXTURE PROPORTIONS

The experimental matrix was designed based on the most prevalent stabilization practices within the Espírito Santo industrial cluster. The proportions were defined in two distinct stages to evaluate both binary and ternary interactions:

- **Binary Systems (Soil-OSR):** Two primary ratios were established based on dry mass proportions of $85/15$ and $80/20$ (Soil:OSR). These ratios reflect the standardized dosages used in regional infrastructure projects for soil improvement with stone residues in the state of Espírito Santo.
- **Ternary Systems (Soil-OSR-KRS):** Building upon the binary baselines, the **Kambara Reactor Slag (KRS)** was incorporated as a chemical activator. The KRS content was calculated as an **additive percentage** (5% and 10%) over the total dry mass of the pre-established binary mixtures.

This additive approach ensures that the Soil:OSR ratio remains constant while the influence of the slag's chemical activation is isolated and evaluated as an incremental factor in the system's mechanical performance. The resulting nomenclature for the samples follows the pattern [Soil:OSR Ratio] + [%KRS], as detailed in Table 4.9.

Table 3.5: Revised experimental matrix: Soil-KRS binary bases and OSR additive variations.

Mixture Type	Soil:KRS Ratio	OSR Content (%)	Sample ID
Binary (Base 1)	85:15	0%	85/15
Ternary 1a	85:15	5%	85/15 + 5%OSR
Ternary 1b	85:15	10%	85/15 + 10%OSR
Binary (Base 2)	80:20	0%	80/20
Ternary 2a	80:20	5%	80/20 + 5%OSR
Ternary 2b	80:20	10%	80/20 + 10%OSR

3.2.5 - CURING PROTOCOL AND TESTING MATRIX FOR BINARY SOIL-KRS MIXTURES

The evaluation of time-dependent strength gain in the non-lateritic plastic clay (CH) is structured around the interaction between the Soil:KRS ratios and the curing intervals. Table 4.6 details the experimental design, highlighting the integration between immediate CBR characterization and subsequent Resilient Modulus (RM) testing.

Table 3.6: Experimental matrix for binary Soil-KRS mixtures: Curing periods and testing protocols.

Mixture ID	Soil:KRS Ratio	Curing (Days)	Test Performed
85/15-0d	85:15	0	CBR (Immediate) and RM
85/15-4d	85:15	4	Resilient Modulus (RM)
85/15-28d	85:15	28	Resilient Modulus (RM)
80/20-0d	80:20	0	CBR (Immediate) and RM
80/20-4d	80:20	4	Resilient Modulus (RM)
80/20-28d	80:20	28	Resilient Modulus (RM)

3.3 - OSR FOR UPGRADING REJECTED MARGINAL SOILS FOR FINAL EMBANKMENT LAYERS

This stage focuses on the potential of **Ornamental Stone Residue (OSR)** to upgrade the geotechnical performance of marginal soils that fail to meet the minimum regulatory requirements for critical pavement layers. The material selected for this phase is a clayey soil from **Cariacica (ES)**, which serves as a representative "worst-case scenario" for regional road construction.

3.3.1 - GEOTECHNICAL THRESHOLD AND SOIL REJECTION

The investigated soil exhibits a California Bearing Ratio (**CBR**) of approximately 4.5%. Under Brazilian infrastructure standards, this value categorizes the material as suitable only for the

embankment body, where the minimum requirement is typically $CBR > 2\%$.

However, the soil is strictly **rejected** for use in **final embankment layers** or subgrade reinforcement, which generally require a minimum CBR of 6% to 8% depending on the design criteria. By utilizing a soil that is "on the edge" of technical acceptability, this research tests if the mechanical stabilization provided by OSR is sufficient to bridge this gap, transforming a rejected material into a viable structural component for the upper 60 cm of the embankment.

3.3.2 - ADVANCED CHARACTERIZATION FOR MEDINA MODELING

To validate this "upgrading" process beyond the empirical CBR, the soil-OSR mixtures are subjected to an advanced testing protocol:

- **Resilient Modulus (RM):** To determine the elastic stiffness and the stress-dependency of the stabilized matrix.

For the experimental campaign detailed in Section 3.1, the resilient modulus tests were conducted using a Universal Testing Machine (UTM) manufactured by IPC Global. The testing protocol, cyclic load application, and data acquisition were controlled via the manufacturer's dedicated resilient modulus testing software (module UTM_41, version 2.04).

Table 3.7: Technical specifications of the data acquisition system transducers.

Channel / Parameter	Transducer Model / Description	Span	Linearised
A: Axial Force	STC-2000 Load Cell	12 kN	No
B: Actuator Displacement	Internal LVDT AC15 (ILC)	30 mm	No
C: Axial Strain #1	LVDT D6/05000AG (± 2.5 mm)	5 mm	Yes
D: Axial Strain #2	LVDT D6/05000AG (± 2.5 mm)	5 mm	Yes
E: Confining Pressure	Pressure Transducer 3435	2,000 kPa	No

Subsequently, the experimental program detailed in Section 3.2 utilized an Owntec Triaxial Dinâmico Pro (Code MS161). The apparatus is capable of applying dynamic loads of up to 40 kN, ensuring the application of appropriate stress paths to model the mechanical behavior of the stabilized soil-residue matrices.

These results are tailored for integration into the **MeDiNa** (the Brazilian Mechanistic-Empirical Design method), allowing for a direct assessment of how the inclusion of OSR extends the pavement's service life when utilizing otherwise marginal local materials.

3.4 - BEHAVIOR OF SOILS FROM ESPÍRITO SANTO - BARREIRAS FORMATION

The Barreiras Group represents one of the most significant and geographically extensive geological units along the Brazilian coast, stretching approximately 4,000 kilometers (F. Nunes et al., 2011). The geotechnical behavior of these soils is deeply influenced by their sedimentary origin, consisting of unconsolidated Tertiary sediments ranging from fine silts to immature coarse sandstones (Vieira & Menezes, 2015), including the presence of "cohesive horizons" that exhibit high resistance when dry but lose strength upon saturation (Sartório, 2014). Therefore, these soils are notoriously heterogeneous and moisture-sensitive.

A critical feature is the occurrence of cohesive horizons, which are controlled generating excess fines and destroying the structural skeleton of the soil (Bona, Silveira, Guimarães, & Azevedo Junior, 2022). Understanding this nature is vital for compaction, as the energy applied must create a stable matrix against environmental fluctuations (Sartório, 2014).

Determining the optimal compaction energy—Normal (N.E.), Intermediate (I.E.), or Modified Proctor (M.E)—is a fundamental engineering challenge. This decision involves balancing mechanical strength, economic efficiency, and the preservation of the soil's structure, such as avoiding grain breakage in lateritic materials (Sartório, 2007; Souza Júnior, 2005). In Espírito Santo, researchers and practitioners have developed standards, such as the "Intermodified" energy (42 blows), to meet the high-demand requirements (Sartório, 2007).

I.E. is widely adopted in researches with soils of Espírito Santo and by the State Department of Roadways (DER-ES) for subbase layers and earthworks (Sartório, 2014). It offers higher support capacity (CBR) than Normal energy without the excessive pressure of Modified energy, which can be detrimental to certain tropical soil structures (Sartório, 2007).

According to the MCT classification, lateritic Barreiras soils (LG', LA') maintain a high support capacity even when saturated (F. Nunes et al., 2011; Sartório, 2007). For these, Intermediate or Intermodified energy is often optimal to avoid crushing aggregates. Conversely, non-lateritic soils (NS', NA') are highly sensitive to moisture and may require Modified energy to achieve a stable structure (DNIT, 2016; Souza Júnior, 2005).

Research into these soils, particularly for the **BR-262** and road expansions, has determined that **Intermediate Energy** is the optimal compaction effort for the following reasons:

- **Particle Crushing Prevention:** Many Barreiras sediments contain immature quartz and weathering feldspars. **M.E.** ($E_{mod} \approx 2,700\ kJ/m^3$) provides high impact that often crushes these grains, generating excess fines and destroying the structural skeleton of the soil (Bona et al., 2022).

- **Stiffness Optimization: Intermediate energy (I.E., $E_{int} \approx 1,300\ kJ/m^3$)** achieves a density that maximizes the M_R without the structural degradation associated with over-compaction (Schiavo et al., 2019).
- **Permeability and Suction:** I.E. preserves a pore structure that maintains better drainage and **matrix suction** in unsaturated states, which is critical for the stability of lateritic "Purple Clays" found in the formation (Schiavo et al., 2019). Over-compaction can lead to a brittle state that cracks during dry seasons or becomes unstable under high pore pressures during heavy rain.

3.4.1 - CLASSIFICATION USING THE LATERIZATION INDEX (L)

According to the methodology proposed by Ignatius (1991), the tropical behavior of soils and their respective mixtures can be quantified by the **Laterization Index (L)**. This index represents the slope of the dry branch of the compaction curve and serves as a proxy for the stability of micro-aggregates and the soil's sensitivity to moisture variation. The mathematical definition of the index is given by the slope of the linear regression or the rate of change between the dry unit weight (γ_d) and the moisture content (w) before reaching the optimum moisture content:

$$L = \frac{\Delta\gamma_d}{\Delta w} \tag{3.1}$$

The calculation for the evaluated sample, based on the experimental data points from the red compaction curve of Figure 2.36 (red ■ marker), it can be extracted from the graph:

- **Data Point 1:** $w_1 = 24.3\%$; $\gamma_{d1} = 13.7\,\text{kN/m}^3$
- **Data Point 2:** $w_2 = 26.4\%$; $\gamma_{d2} = 14.45\,\text{kN/m}^3$

$$\Delta\gamma_d = 14.45 - 13.7 = 0.75\,\text{kN/m}^3 \tag{3.2}$$

$$\Delta w = 26.4 - 24.3 = 2.1\% \tag{3.3}$$

$$L = \frac{0.75}{2.1} \approx \mathbf{0.357}\,\frac{\text{kN/m}^\mathbf{3}}{\%} \tag{3.4}$$

Following the criteria established by Ignatius (1991), the material is classified based on the magnitude of L as shown in Table 3.8:

The calculated value of $L \approx 0.357$ places the sample of the soil firmly within the **lateritic behavior** category. This high slope indicates that the soil particles (or the soil-waste

Table 3.8: Classification of tropical behavior based on the Laterization Index.

Value of L	**Geotechnical Behavior**
$L \geq 0.30$	Lateritic
$0.15 \leq L < 0.30$	Transitional
$L < 0.15$	Non-Lateritic / Saprolitic

matrix) are highly susceptible to the lubricating effect of water during the initial compaction phases, leading to a rapid increase in dry density. This characteristic is typical of well-structured tropical soils with stable micro-aggregation, providing adequate performance for pavement base and subbase applications.

3.5 - TESTING PROTOCOL

The selection of the resilient modulus (M_R) testing protocols across the different stages of this research followed an operational evolution coupled with an intentional alignment with design frameworks. In the initial experimental phase (Section 3.1), during the commissioning and calibration of the dynamic triaxial equipment, testing was conducted using the factory-integrated software environment. Due to the initial operational learning curve and system constraints regarding custom stress-path definitions, the pre-programmed, automated routine of AASHTO T 307 was selected, which automatically enforced pre-defined stress sequences without user-defined parameterization.

Subsequently, for the experimental block detailed in Section 3.2, the protocol was updated to the Brazilian standard DNIT 134/2018-ME to ensure strict compliance with the structural input requirements of the national mechanistic-empirical design software, MeDiNa. Crucially, the adoption of both distinct normative frameworks served as a robust comparative validation; the experimental results demonstrated that both the international (AASHTO) and national (DNIT) testing routines are fully capable of providing consistent, stable, and highly reliable stress paths for characterizing the non-linear resilient response of these alternative soil-waste geomaterials.

Table 3.9 systematically summarizes the comprehensive geotechnical and pavement testing standards adopted throughout this doctoral investigation.

Geotechnical applications for OSR and KRS mixed with soils targeting stabilization in fills, final layers of embankments, subgrade reinforcement, subbase and bases are overseen in this research through pavement engineering tests such as compaction, CBR, MR, and PD after their classical geotechnical characterization. Soils properties improved by different residues are studied in different percentages in the mixtures, or as soils are added to the OSR to improve its properties, a strategy suggested by Sivrikaya, Kıyıldı, & Karaca (2014).

Any soil-residue mixture to form a new local geomaterial should attend the same studies of pavement engineering regular materials. This rule, includes MR and other studies, which allows the simulation of mechanical loads on a pavement layer and partially the environmental interaction through the pavement moisture change/measurements. As the Brazilian engineering culture has not yet been using extensively the MR as the major parameter, CBR tests were also part of the research.

Table 3.9: Geotechnical and pavement testing program summary.

Application / Section	**Test Name**	**ABNT NBR Standard Adopted**	**ASTM / AASHTO Equivalent Code**
All Sections	Grain Size Distribution	7181 (2016)	D422
Basic Characterization	Specific Gravity of Solids	6508 (1984)	D854
	Consistency Limits (LL/PL)	6459 / 7180 (2016)	D4318
	Proctor Compaction[1]	7182 (2016)	D698 / D1557
	California Bearing Ratio	9895 (2016)	D1883
Section 3.1	Resilient Modulus (MR)	AASHTO T 307	D8237
	Unconf. Comp. Strength (UCS)	12770 (1992)	D2166
Section 3.2	Resilient Modulus (MR)	DNIT 134/2018-ME	AASHTO T 307

[1] *Note: OSR alone tested at three energies; Soils and mixtures tested at Intermediary energy.*

All soils and OSR went through classical geotechnical testing program consisting of the following: grain size distribution, sieve and hydrometer analyses (ABNT NBR 7181, 2016a/ ASTM D 422), Specific gravity (ABNT NBR 6508, 1984 / ASTM: D 854–02), Consistency limits (ABNT NBR 7180, 2016b; ABNT NBR 6459, 2016c / ASTM D4318). Proctor Compaction at the 3 different energies: standard, intermediary and modified for the OSR alone and intermediate energy for soils and soil mixtures (ABNT NBR 7182, 2016d / ASTM D698, ASTM D1557).

KRS is a residue which is not being applied alone, only as a soil stabilizer, therefore, it went though only basic characterization, but not compaction, CBR, MR, and PD tests.

4 - RESULTS AND MECHANISTIC-EMPIRICAL DISCUSSION

This chapter provides a comprehensive analysis of the experimental results, serving as the analytical core where the interaction between industrial byproducts and distinct tropical soil matrices is evaluated through a multi-stage approach. The initial focus is directed toward the physical characterization of the geomaterials, establishing the geotechnical baseline for the soils chosen to be part of this research, a tropical one from Espírito Santo (ES) and other from Brasília, alongside the Ornamental Stone Residue (OSR). By investigating the regional variability and the genesis of these tropical soils, the following sections aim to delineate how the specific characteristics of each collection site influence the stabilization effectiveness of binary mixtures, providing the necessary context for the mechanical behavior discussed in the subsequent experimental blocks.

Building upon this characterization, the discussion advances to Stage I, which addresses the mechanical performance of binary systems specifically designed for sub-base applications. Through extensive Resilient Modulus (RM) testing, the research evaluates the mechanistic response of soil-OSR blends under cyclic loading, transitioning from traditional empirical parameters to the mechanistic requirements of the Brazilian MeDiNa method. A central objective of this stage is the identification of the Optimum Residue Content (ORC) for each soil, determining the stabilization peak where the integration of OSR improves the mechanical behavior with greater gain for sub-base layers. This analysis will lead to understanding the thresholds of geotechnical improvement and the limits of residue incorporation, especially in cases where high waste contents may lead to structural instability or resilient modulus degradation.

4.1 - OSR MIXED WITH A LATERITIC SOIL OF ESPÍRITO SANTO

The materials utilized in this experimental stage—specifically the lateritic soil and the Ornamental Stone Residue (OSR)—were previously detailed in Chapter 3 (Section 3.1). The soil was collected from the Caramuru borrow pit, located in the municipality of Santa Leopoldina (ES), representing a typical regional lateritic clay. The OSR was obtained from Vitória Stone, a major processing plant in the region. This section expands upon those descriptions by analyzing the mechanical synergy and physical compatibility of these materials when blended for pavement sub-base applications.

4.1.1 - BASIC CLASSIFICATION OF GEOMATERIALS

The grain size distribution (GSD) is a fundamental parameter for understanding the packing potential and the hydraulic behavior of the soil-residue mixtures. Figure 4.1 presents the grading curves for four distinct materials analyzed in this research: the OSR-Q, the two primary soils (UnB/Brasília and Caramuru/ES), and the OSR grading reported by Bacarji, Toledo Filho, Koenders, Figueiredo, & Lopes (2013) as a reference for consistency.

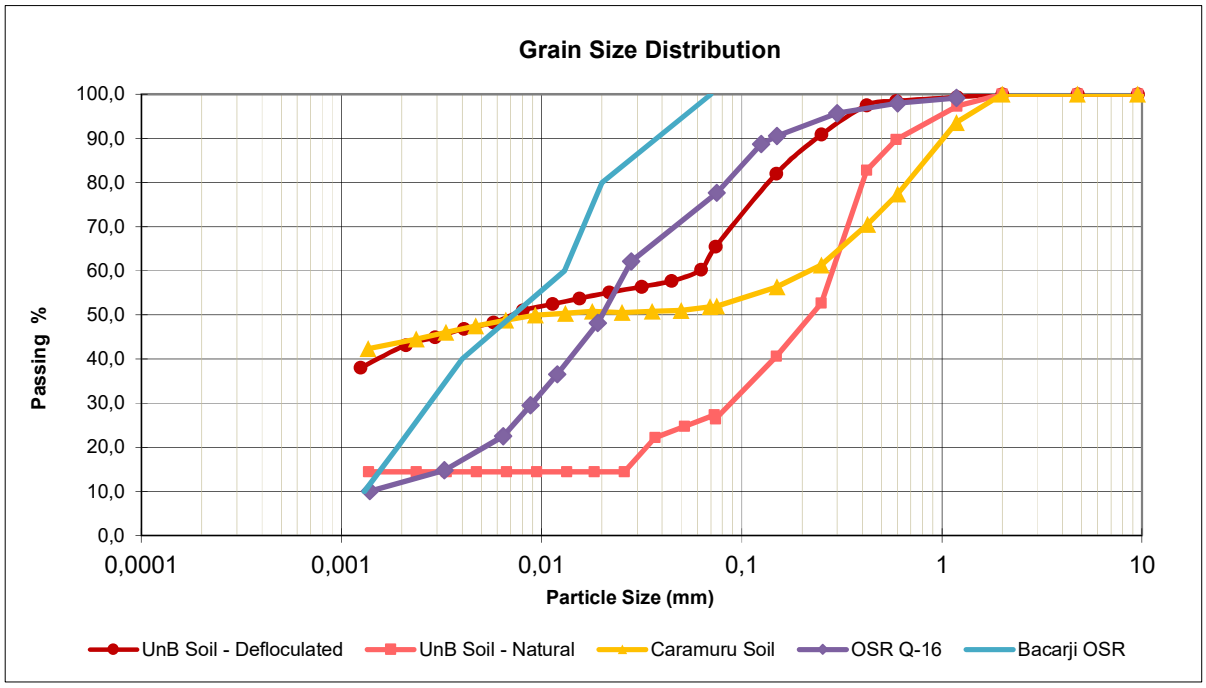


Figure 4.1: Grain size distribution of OSR-Q (2016), Caramuru soil (also called Vitória soil), SG-12 UnB site soil (Brasília) with and without deflocculant, and reference OSR from Bacarji et al. (2013).



Figure 4.2: Collection of the Brasília (SG-12 UnB site) soil; (center) Soil and OSR transport for drying; (right) Hydrometeer test for grain size analysis.

The distribution curves reveal that both the Caramuru and the UnB soils exhibit characteristics typical of sub-base materials, with particle size fractions aligned with Brazilian

infrastructure standards. Both soils are classified as A-4 according to the TRB classification system, indicating a predominant silty-clayey matrix with moderate plasticity.

The influence of the deflocculant on the UnB soil's hydrometer test reveals the high degree of flocculation inherent in its lateritic structure. OSR is significantly finer than both natural soils, that will act as a non-plastic silty filler within the future mixtures.

Figure 4.3 also presents another sample of OSR-Q GSD obtained with and without defloculant use. The classification shows that both soils are low plasticity silts, nevertheless the GSD of the soils with defloculants show greater percentage of clay particle size. In the case of the OSR, only 1.3% of the particles are clay size, smaller than 0.02 mm without defloculant and 5.8% when defloculants are applied.

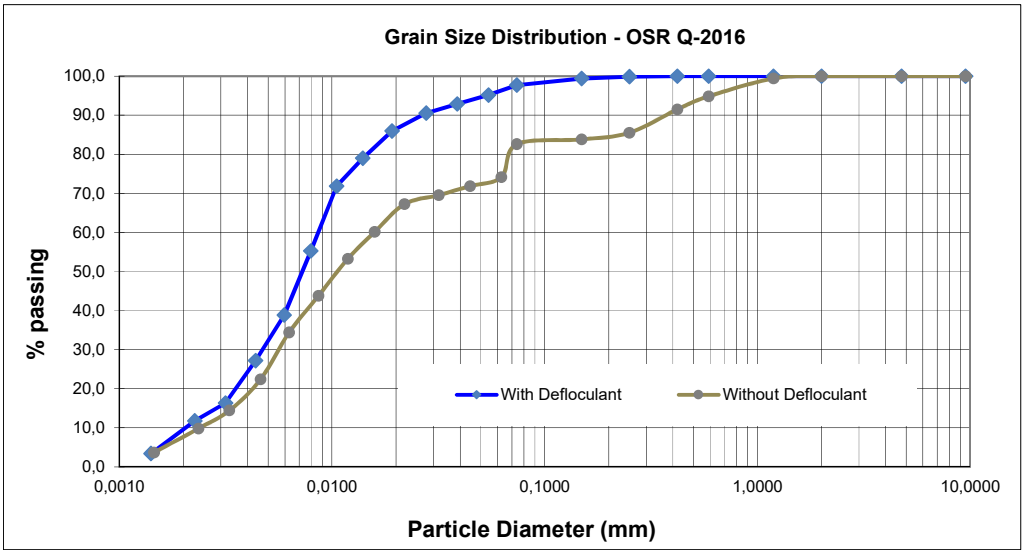


Figure 4.3: Grain size distribution of OSR-Q (2016) with and without deflocculant.

The Atterberg Limits limits WL and WP were obtained for the samples individually and later for each soil-OSR mixture and Figure 4.4 shows the chart of WL of the formed geomaterials with different percentages of OSR. It is observed in Figure 4.4 a trend of small reduction on the WL when percentage of OSR increases in the mixture. Both soils of ES and SG12 were similarly affected by the presence of OSR. Comparing the SG12 and ES soils, the reduction in WL is proportionally and the total amount greater in the ES soil, with WL falling from 34 to 31% after the addition of 30% of OSR. Figure 10 shows the behavior of WP when OSR is mixed to the Brasilia and Espírito Santo Soil. The reduction in WP is proportionally and the total amount greater in the ES soil, with WP falling from 25 to 23% after the addition of 30% of OSR.

The plasticity index (PI) fell 1% for both the ES and SG12 soils. It is observed in Figures 4.4 and 4.5 trends of small reduction on the WP when OSR increases in the mixtures.

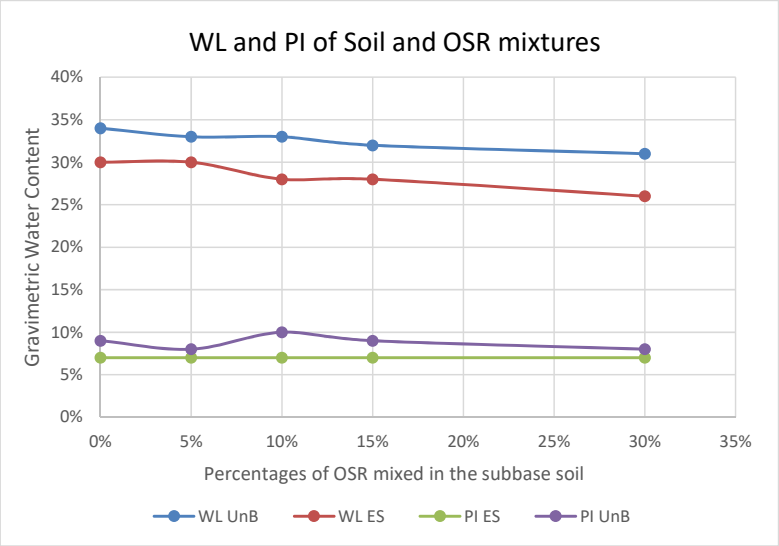


Figure 4.4: WL and PI of Brasília (SG-12 UnB site) and Espírito Santo (ES) soils mixed with different percentages of OSR-Q

Both soils of SG12 and ES were similarly affected by the presence of OSR, which can be explained by the similarity of their particle size range, leading to same scale interaction, even though the OSR has clearly less cohesion indicated in its very small value of PI.

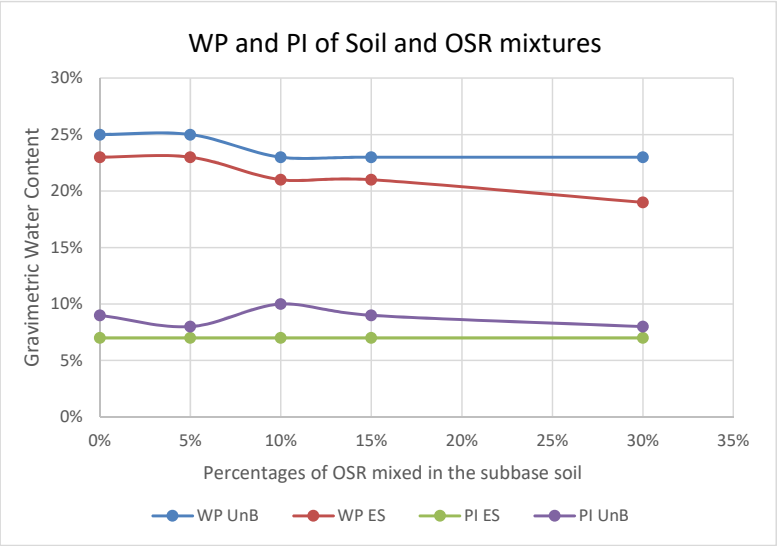


Figure 4.5: WP and PI of Brasília (SG-12 UnB site) and Espírito Santo (ES) soils mixed with different percentages of OSR-Q.

The compaction curves of the ES (Vitória) soil is presented in the Figure 11 with the 3 different energies applied on the same soil deposit: normal, intermediary and modified energies. The compaction curves of the OSR-Q is presented in the Figure 12 with the 2 different energies applied on 3 samples: normal, intermediary test at UFES laboratory and at UnB, the test applied the intermediary energy.

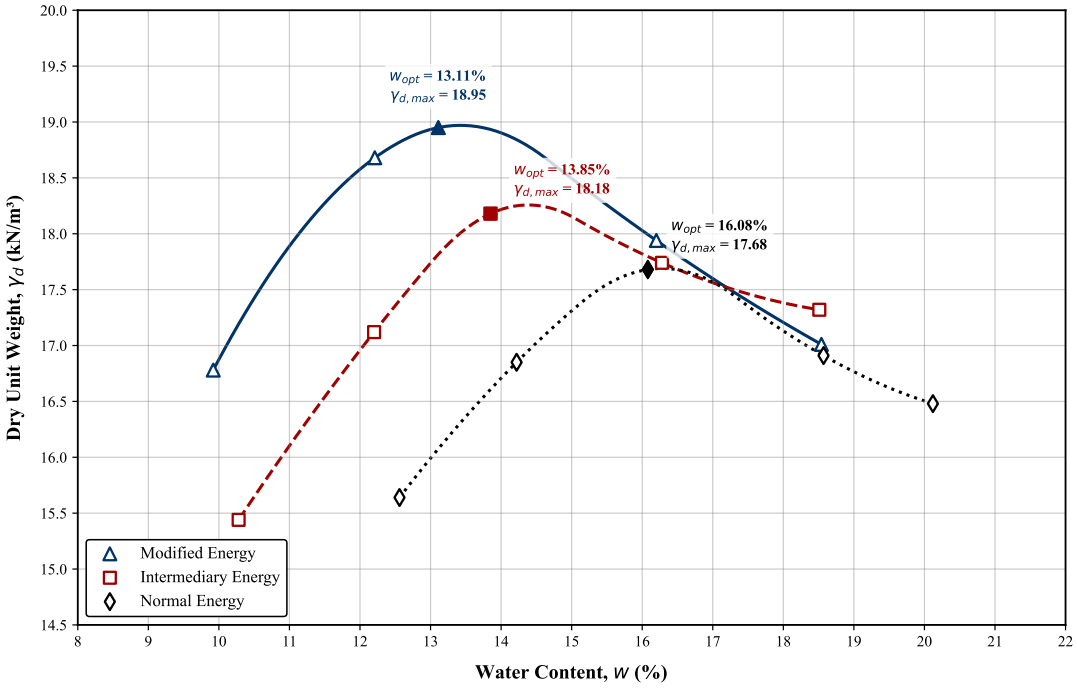


Figure 4.6: Compaction curves of Espírito Santo (Vitória-ES) soil with the 3 different energies

To evaluate the influence of compaction effort on the structural packing and volumetric state of the Caramuru soil, the experimental compaction curves obtained under Normal, Intermediary, and Modified Proctor energies are comparatively analyzed alongside their theoretical saturation lines ($S = 80\%$ and $S = 100\%$), as illustrated in Figure 4.7 (a), (b), and (c), respectively.

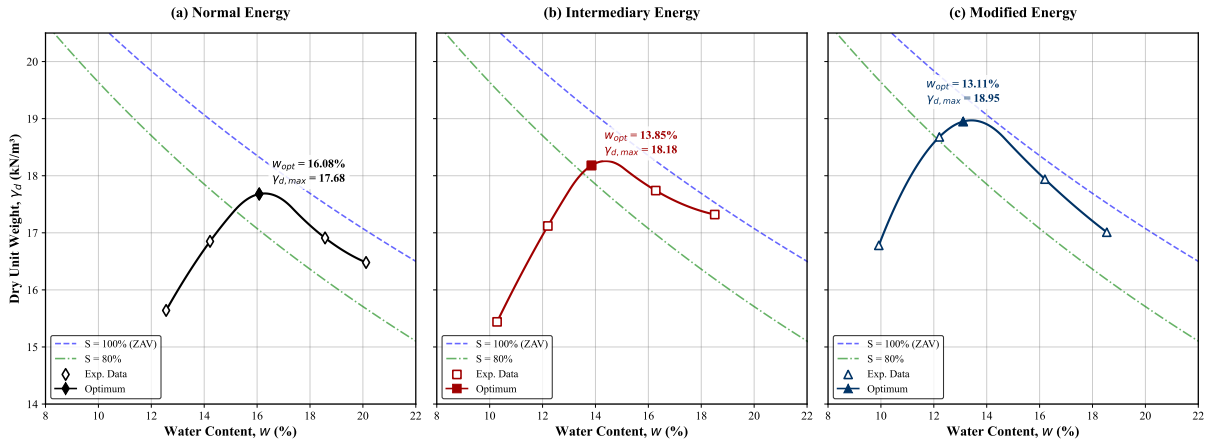


Figure 4.7: Compaction curves of Espírito Santo (Vitória-ES) soil with the 3 different energies

This multi-energy framework highlights a classical tropical geomechanical behavior: as the compaction effort increases, the compaction path undergoes a distinct shift upward and to the left, yielding systematically higher maximum dry unit weights ($\gamma_{d,max}$) at lower optimum water contents (w_{opt}). More importantly, the systematic positioning of the curves relative to the Zero Air Voids (ZAV) line ($S = 100\%$) visualizes the progressive reduction of the internal

air-void matrix, demonstrating how higher dynamic energies optimize particle interlocking and tightly constrain the material's subsequent susceptibility to moisture-induced degradation.

After literature review and some compaction tests conducted, it has been understood that the behavior of mixed subbase-type soil with OSR, the focus of the research, could be properly reached using the intermediary energy, once typically the Brazilian soils need more than the normal energy to achieve their best performance.

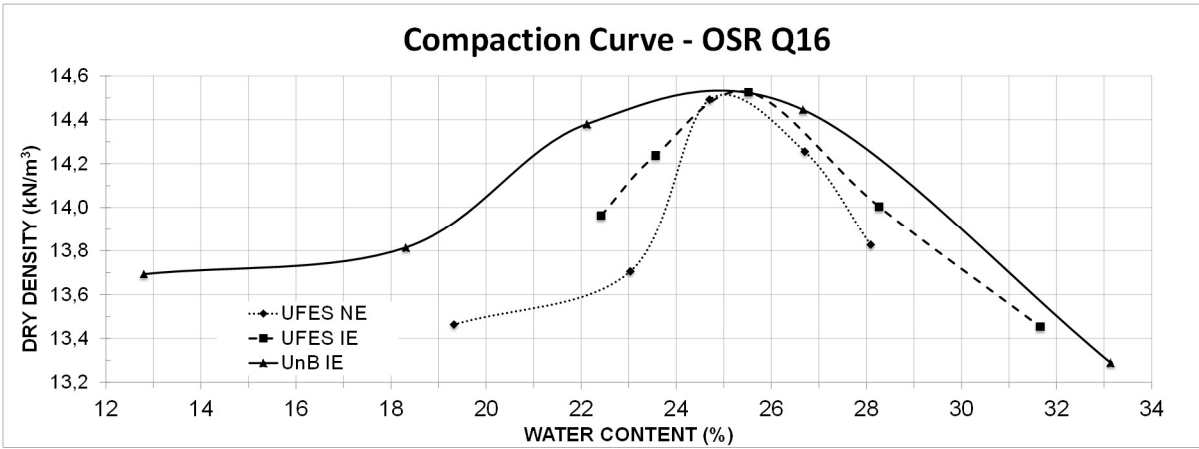


Figure 4.8: Compaction curves of OSR with different energies

Both Espírito Santo (Vitória) and Brasília (SG-12 UnB site) soils were mixed with OSR at rate of OSR/soil of 5%, 10%, 15%, and 30% as mass percentage. Results of basic classification are presented in Table 4.1.

Table 4.1: Compaction parameters of soil-OSR mixtures with different percentage rates

Sample	Specific gravity	Liquid limit (%)	Plasticity Limit (%)	Plasticity Index (%)	Optimum Moisture (%)	Maximum Dry Density * (kN/m^3)	USCS	TRB
OSR	2,64	29	26	3	25	14,5	ML	A-4
Soil SG12	2,67	34	25	9	22,0	15,65	CL	A-4
SG12+5%	2,67	33	25	8	20,0	16,30	CL	A-4
SG12+10%	2,67	33	23	10	19,8	15,82	CL	A-4
SG12+15%	2,67	32	23	9	19,0	16,30	CL	A-4
SG12+30%	2,66	31	23	8	19,8	15,65	CL	A-4
Soil Espírito Santo	2,67	30	22	8	16.0	17,93	CL	A-4
ES+5%	2,67	30	23	6	15.5	17,91	ML	A-4
ES+10%	2,67	28	21	7	15.1	17,88	ML	A-4
ES+15%	2,67	28	21	7	15.6	17,68	ML	A-4
ES+30%	2,66	26	19	7	16,5	17,41	ML	A-4

* Intermediary Energy

The OSR is mixed to the soil in dry conditions, however even in dry conditions somes clusters of OSR spreaded has been observed. The Figure 4.9 shows the mixed ES soil and OSR in dry conditions with the OSR cluster formation. After the addition of water, a bag was used

to homogenize the sample moisture and the OSR cluster could still be observed. These OSR clusters might have initially got smaller amount of moisture leading to a dryer zones inside a wetter soil matrix.



Figure 4.9: Close view of the mixed OSR (white particles) in the soil matrix (yellow partciles)

Figure 4.10(a) presents the superimposed compaction curves for the SG-12 soil mixtures across a range of 0% to 30% soil residue content (SRC) by dry weight. This layout synthesizes three independent sets of compaction tests executed across distinct institutional laboratories (UnB and UFES) by different operators (Mr. Ricardo and Mr. Davidson), ensuring a comprehensive verification of the material's compaction parameters under intermediate Proctor energy. The collective compaction paths demonstrate a unified boundary response where the curves maintain physical consistency, highlighting that the internal arrangement of the soil-waste matrix varies systematically rather than erratically with progressive soil replacement by OSR.

The corresponding evolution of the Optimum Moisture Content (OMC) as a function of the residue addition rate is detailed in Figure 4.10(b). As the non-plastic Ornamental Stone Residue (OSR) is incrementally incorporated into both the Brasília (SG-12) and the Espírito Santo (Caramuru) soil matrices, a distinct behavioral trend is observed. Because the pure rock byproduct exhibits a significantly higher natural optimum moisture requirement ($w_{opt} = 25.0\%$) than the natural tropical soils evaluated in this research, its progressive introduction alters the internal pore structure and surface area of the blend. Consequently, an increase in the global matrix moisture level is required to lubricate the particle contacts effectively and achieve the maximum packing state under intermediate dynamic compaction effort.

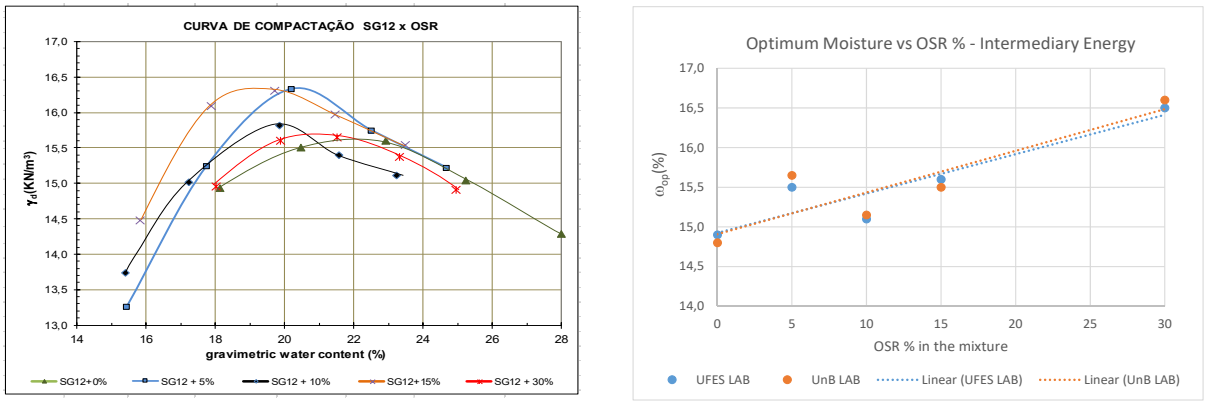


Figure 4.10: Compaction and moisture parameters for the soil-OSR blends: (a) superimposed compaction curves, and (b) Optimum Moisture Content (OMC) evaluation as a function of the OSR content.

To provide a comprehensive volumetric breakdown of each individual matrix, the experimental compaction curves for the natural Brasília soil, its binary mixtures, and the pure mineral byproduct are plotted sequentially with their respective theoretical saturation bounds ($S = 80\%$ and $S = 100\%$) in Figure 4.11.

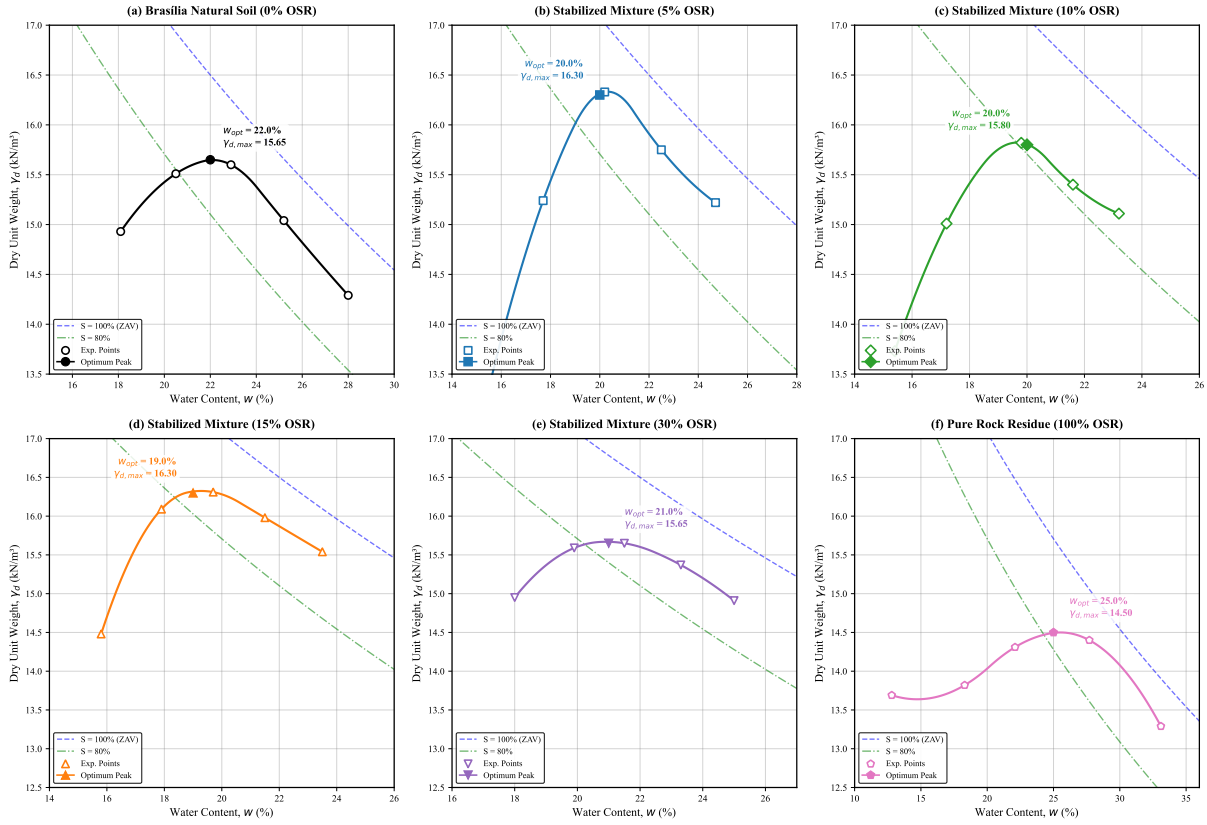


Figure 4.11: Compaction and saturation matrix for the Brasília (SG-12) soil-OSR systems: (a) natural soil (0% OSR), (b) 5% OSR, (c) 10% OSR, (d) 15% OSR, (e) 30% OSR mixtures, and (f) pure rock residue (100% OSR) mapped against their respective 80% and 100% (ZAV) saturation lines.

This itemized multi-panel visualization provides a highly useful and detailed diagnostic of each specific composition, explicitly charting the progression of the material's structural packing and its proximity to the Zero Air Voids (ZAV) limit. By decomposing the matrix into separate plots, the physical impact of the rock residue on the compaction path can be analyzed with high precision, confirming that the granular arrangement remains stable and safely bounded by fundamental soil mechanics laws across all studied dosage thresholds.

To contrast these volumetric shifts with the ultimate bearing capacity of the alternative geomaterials, Figure 4.12 couples the density thresholds with the resulting mechanical performance. Figure 4.12(a) documents the Maximum Dry Density (MDD) path, exposing a localized discrepancy between the host matrices; while the OSR addition in the gneissic residual soil from Espírito Santo triggers a slight, continuous reduction in the MDD baseline at intermediate energy, the Central Plateau sediments display a more stable density plateau.

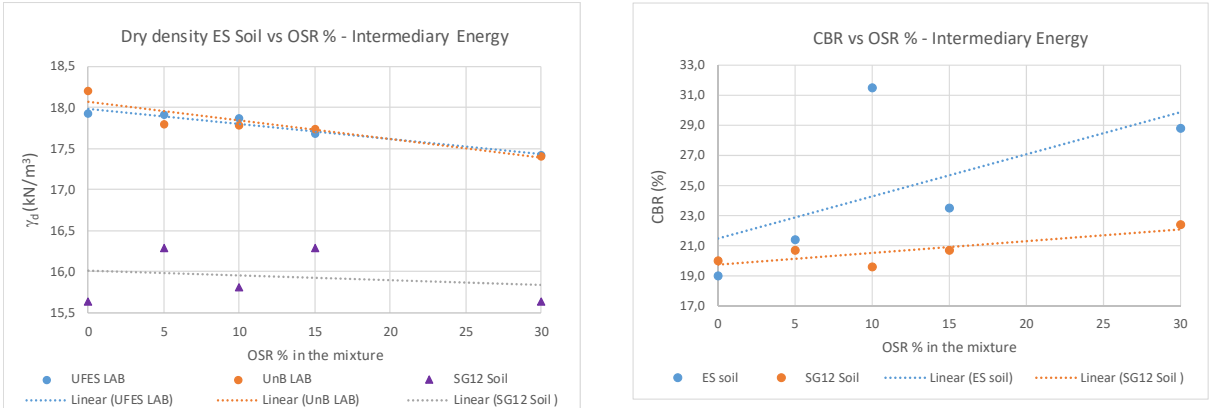


Figure 4.12: Advanced mechanical and density characterization for the soil-waste geomaterials: (a) Maximum Dry Density (MDD) trends under intermediate compaction, and (b) California Bearing Ratio (CBR) performance mapping across distinct residue substitution rates.

Conversely, the California Bearing Ratio (CBR) results mapped in Figure 4.12(b) underscore a direct, highly favorable correlation for both tropical soils, where progressive residue incorporation yields systematically higher bearing capacities up to the 30% substitution limit. Although both alternative mixtures achieve substantial structural optimization, the slightly lateritic clusters of the SG-12 soil demonstrate greater responsive gains relative to its natural state, confirming the mechanical efficacy of utilizing inert stone fines to reinforce the static and dynamic stability of unbound pavement layers.

4.1.2 - STRATEGIES FOR DISCURSSIONS OF CLTT ON VITÓRIA SOIL AND OSR MIXTURES

The following sections discuss the results of the Cyclic Load Triaxial Tests (CLTT) performed on the mixtures of Espírito Santo (Vitória) soil and OSR. The analysis transitions from the

empirical characterization previously discussed to a mechanistic evaluation of the Resilient Modulus (M_R), following the requirements for pavement design using the MeDiNa software.

The CLTT tests were conducted in strict accordance with AASHTO T307, focused on the natural lateritic soil initially collected in Vitória (VIX) and its respective interactions with the Ornamental Stone Residue. The subsequent sections explore the empirical characterization and the non-linear resilient parameters of the VIX-OSR matrices to provide understanding of the material's structural response, the results for each OSR content are presented through a standardized sequence of seven analytical plots, organized into four main figures per mixture:

1. **Individual Specimen 3D Modeling:** Two separate 3D surface plots showing the experimental M_R data for each specimen (CP), including the calculated Composite (DNIT) Universal models parameters (k_1, k_2, k_3) and the respective coefficients of determination (R^2).

2. **Representative Average Behavior:** A combined 3D surface representing the average resilient behavior of the two tested specimens. This visualization is critical for identifying the global stiffness trend of the mixture under different stress states (σ_3 and σ_d).

3. **Slice Analysis of the 3D Composite Model Regression Surface:** Two 2D "slice" plots derived from the 3D surfaces resulting from the model's regression. These allow for a detailed evaluation of the material's stiffness sensitivity to stress changes. The first slice analyzes M_R as a function of deviatoric stress (σ_d) to identify whether the modulus increases or decreases when subjected to increments in stress at a constant confining pressure (σ_3) of 20 kPa (0.02 MPa), while the second focuses on M_R versus σ_d at a higher confinement level of 70 kPa (0.07 MPa).

4. **Bivariate Sensitivity Models:** A final figure presenting two distinct bivariate models: M_R versus σ_3 and M_R versus σ_d. These plots decouple the stress components to clarify which stress state—confinement or shear—is more dominant in the stabilization of the soil-OSR matrix.

The subsequent subsections detail these results for the natural soil (0% OSR) and the stabilized mixtures (5%, 10%, 15%, and 30% OSR). A data quality control and filtering criteria have been supervising the raw results from the Cyclic Load Triaxial Tests (CLTT) to ensure the reliability of the Resilient Modulus (M_R) models.

In accordance with established geotechnical engineering practices, specific data points were filtered or excluded based on the following criteria:

Transducer Sensitivity and Resolution: At low stress levels, particularly when the confining pressure (σ_3) was significantly higher than the deviatoric stress (σ_d), the resulting resilient vertical displacements occasionally might have approached the lower resolution limits of the displacement transducers (LVDTs). In these instances, the signal-to-noise ratio may be increased, leading to high discrepancies in M_R values between redundant specimens. Points which could show such instability were sometimes removed to allow complementary observations on typical instrument-induced bias in the mechanistic models for the tests which adopted standard AASHTO T 307 sequences (specifically sequences 1, 4, 7, 10, and 13), which confining stress often equaled or exceeded the deviatoric stress.

Stress State Inconsistency ($\sigma_3 > \sigma_d$): For certain soil-OSR mixtures, stress states where the confinement stress exceeded the shear component resulted in erratic resilient behavior that did not reflect the material's actual structural performance in a pavement layer. These points often generated "mathematical noise" that compromised the physical meaning of the k_2 and k_3 parameters in the Universal Model.

Statistical Convergence and Outlier Removal: Data points that deviated significantly from the observed physical trend (outliers) and caused a substantial decrease in the coefficient of determination (R^2) were analyzed for experimental error. If no physical justification for the deviation was found (such as premature sample degradation), these points were discarded to ensure a representative regression of the material's stiffness over the analyzed stress spectrum.

Specimen Redundancy Check: A comparative analysis was performed between the two specimens of each mixture. When a single load cycle showed a discrepancy greater than 15% between the two samples without a corresponding geotechnical explanation, that specific stress state was re-evaluated or excluded to maintain the integrity of the average representative model.

To achieve a highly realistic and physically consistent representation of the resilient modulus function, which is inherently stress-dependent, this research distinguishes between the full experimental dataset and the geomechanically optimized subsets, herein designated as **"filtered data"**. In standard triaxial routines such as AASHTO T 307, several sequences subject the specimen to stress pairs where the confining pressure equals or exceeds the dynamic deviatoric stress ($\sigma_3 \geq \sigma_d$). While useful for establishing laboratory baseline boundaries, these configurations represent transient unloading phases that do not occur within an actual pavement structure subjected to moving traffic, where vertical shear stress strongly dominates the field.

Including these unrepresentative stress points in the constitutive modeling introduces severe mathematical noise, forces the geomaterial to behave artificially as a confined fluid, and severely corrupts the physical interpretation of the k_2 and k_3 parameters in the Universal Model. Consequently, to isolate these instrumental effects and safeguard the predictive integrity of the pavement structural design, the subsequent analysis systematically contrasts the three-dimensional response surfaces under two rigorous criteria: the complete, unfiltered AASHTO series versus the optimized **filtered data** surfaces, where unrepresentative stress pairs have been geomechanicamente suppressed.

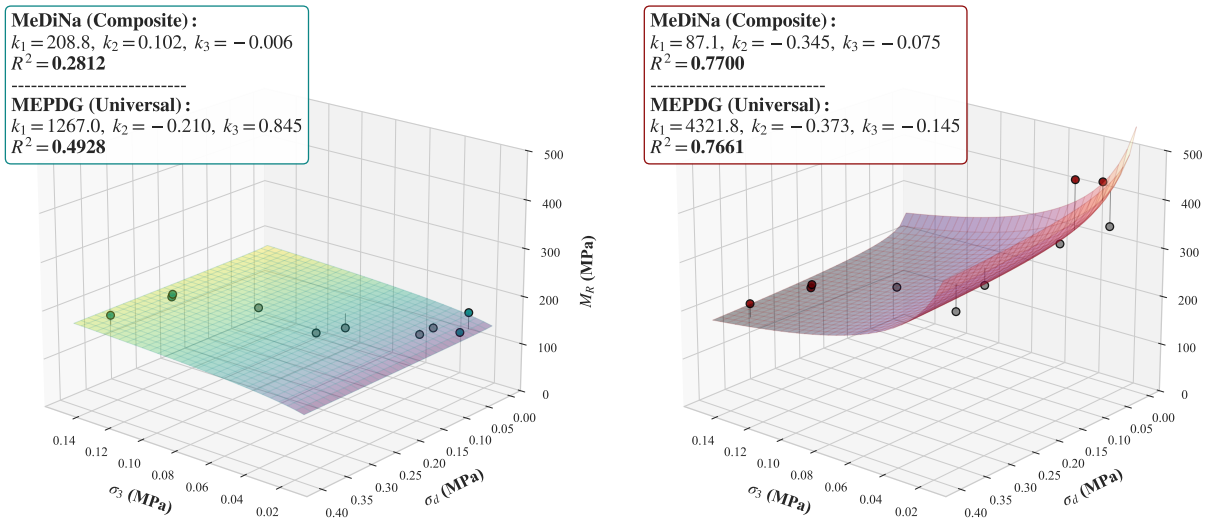
The raw data are publicly available through the Graduate Program in Geotechnics (PPGG/ENC/FT/UnB). The datasets utilized in the plots are tabulated in the appendix, along with the quality control source codes developed for this research. The first set of tests, conducted in accordance with AASHTO T307, focused on soils from the state of Espírito Santo, initially tested in Vitória, follows in the next section.

4.1.3 - EVALUATION OF REFERENCE RESILIENT BEHAVIOR VITÓRIA SOIL - 0% OSR CONTENT

The natural soil sample from the Caramuru borrow pit (0% OSR) establishes the constitutive baseline for mechanical comparison. As a typical regional lateritic clay with a silty-granular matrix, its resilient response serves as the "zero point" to quantify the structural gains provided by the subsequent incorporation of Ornamental Stone Residue (OSR). The comparison of 3D regression surfaces for the two redundant specimens (Figure 4.13) reveals the inherent variability of natural tropical soils and the challenges of instrumental resolution in low-stiffness materials.

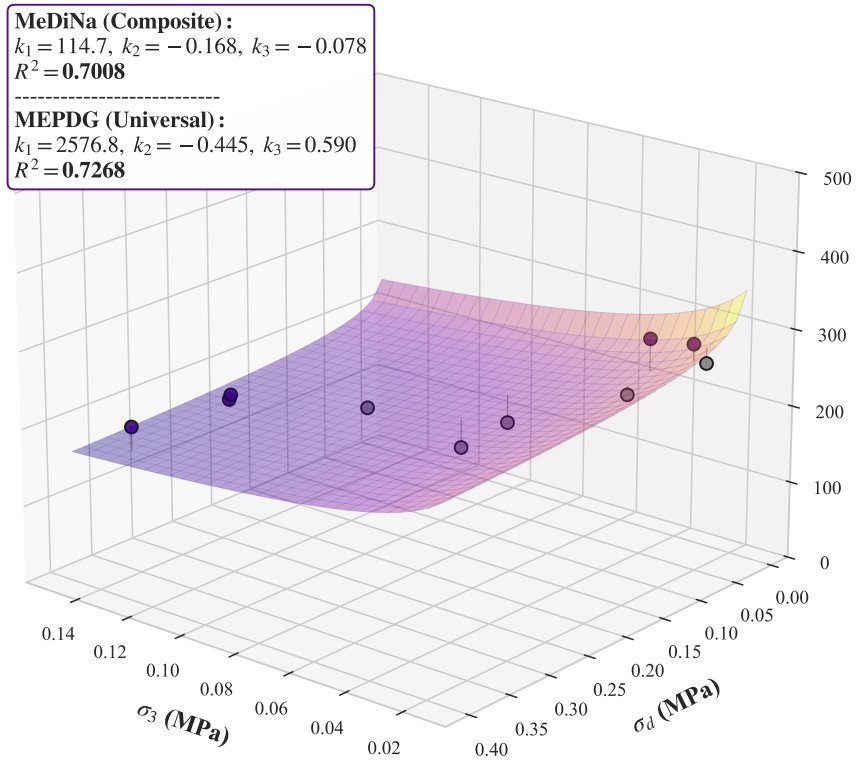
Specimen CP1 presented a notably low coefficient of determination ($R^2 = 0.2812$) for the MeDiNa model, reflecting the high data dispersion discussed in the quality control criteria—likely due to the lower limit of LVDT sensitivity under high σ_3/σ_d ratios. Conversely, specimen CP2 exhibited a more stable regression ($R^2 = 0.7700$), though it revealed an atypical rheological signature with a negative k_2 parameter (-0.345). While CP1 follows the traditional theory of stiffness gain through confinement ($k_2 = 0.102$), CP2 suggests that without a stabilization filler, the natural soil matrix may undergo structural rearrangement or local instability under increasing confining pressures.

Figure 4.14 consolidates the representative mechanical behavior of the Vitória soil. The average model dampens the individual discrepancies of the specimens, reaching a statistically acceptable convergence for design purposes ($R^2 \approx 0.70$).



(a) AASHTO - VIX CP1 (0% OSR) **(b) AASHTO - VIX CP2 (0% OSR)**

Figure 4.13: 3D Resilient Modulus models comparison for Vitória soil (0% OSR): (a) specimen CP1; (b) specimen CP2.



Average Resilient Modulus: VIX (0% OSR)

Figure 4.14: Average Resilient Modulus 3D surface for Vitória soil (0% OSR) including MeDiNa and MEPDG model parameters.

The orientation of the 3D surface indicates that the stiffness of the untreated soil is confined to a lower range, rarely exceeding 250 MPa across the analyzed stress spectrum. The global parameters obtained ($k_1 = 114.7$, $k_2 = -0.168$, and $k_3 = -0.078$) define this material as a purely resilient-degradant matrix, providing the fundamental input data for subsequent MeDiNa simulations of the reference structure.

The diagnostic slices presented in log-log scale (Figure 4.15) clarify the material's sensitivity to shear. Under constant confining pressures of 0.02 MPa (low) and 0.07 MPa (structural), the descending slopes of both specimen models are different. The CP2 descending slope confirms the *reduction in stiffness* phenomenon. The CP1 shows a transition to a stable MR with respect to deviator stress. In this natural soil, increasing the deviatoric stress (σ_d), it does not generate stiffness increasing. It triggers micro-slippage between particles and a relaxation of the granular skeleton, leading to a progressive drop in the Resilient Modulus, with different intensity.

The log-log representation reveals that this degradation follows a linear exponential rate, proving that the absence of OSR filler or aglutinating fines prevents any *stiffness increasing* effect at this stage.

The decomposition of stress sensitivity in Figure 4.16 isolates the Dunlap (confinement) and Hicks (shear) effects. The $M_R \times \sigma_3$ plot highlights a dichotomy: while CP1 follows the traditional theory of interparticular friction gain, CP2 demonstrates a loss of stiffness with confinement, mathematically signaling an unstable internal structure in the pure soil.

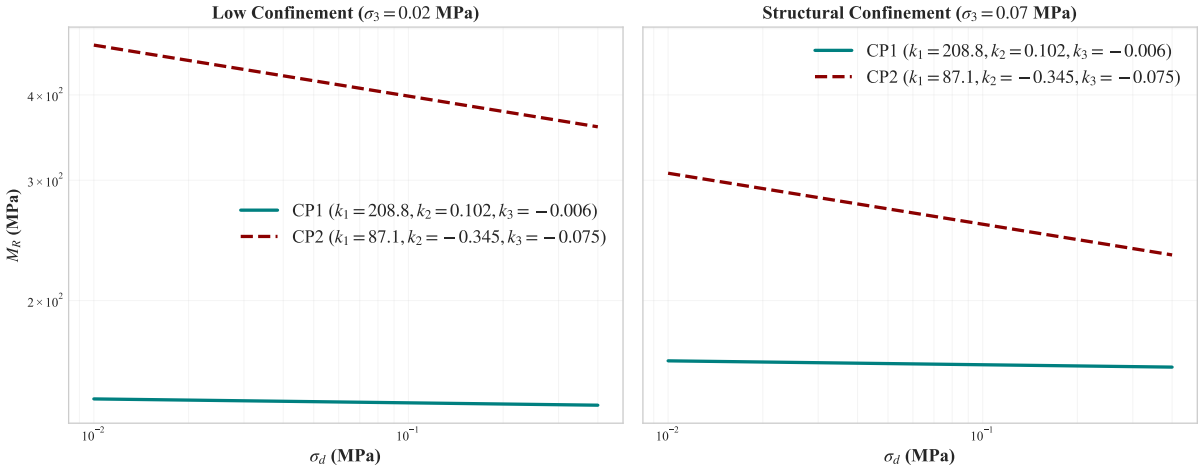


Figure 4.15: Evaluation of the Vitória soil (0% OSR) stiffness sensitivity to stress changes at low ($\sigma_3 = 0.02$ MPa) and structural ($\sigma_3 = 0.07$ MPa) confinement levels.

- **Specimen CP1:** Demonstrates a notably stable and resilient behavior. In the $M_R \times \sigma_3$ relationship, the positive slope confirms the traditional granular theory where increased

confining pressure enhances interparticular friction and stiffness. More significantly, the $M_R \times \sigma_d$ plot also exhibits a positive inclination, suggesting that this specific specimen does not suffer from shear degradation within the tested range. This absence of MR decreasing indicates a well-locked structural arrangement that maintains its integrity even under increasing deviatoric loads.

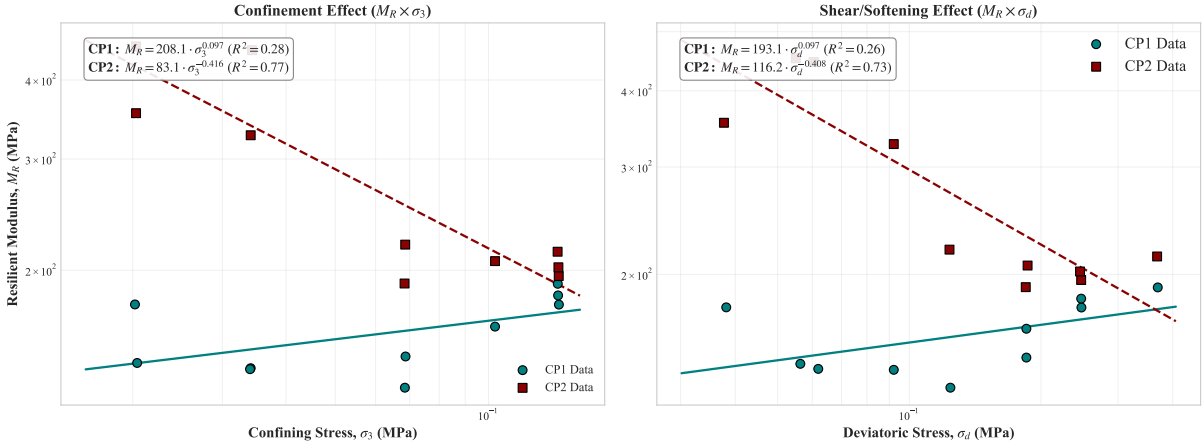


Figure 4.16: 1D Bivariate sensitivity models for Vitória soil (0% OSR): (left) confinement effect ($M_R \times \sigma_3$); (right) shear effect ($M_R \times \sigma_d$).

- **Specimen CP2:** Presents a contrasting, unstable mechanical signature. The negative slope in the $M_R \times \sigma_3$ plot ($k_2 = -0.416$) signals an anomalous response where the natural soil fails to stabilize under confinement. Furthermore, the $M_R \times \sigma_d$ relationship reveals a sharp negative inclination ($k_3 = -0.408$), characterizing a severe MR decreasing phenomenon. In this case, the increment of deviatoric stress would suggest a collapse of the resilient modulus, highlighting a possible structural vulnerability of the untreated soil matrix to shear-induced deformation.

However, the natural soil sample from the Caramuru borrow pit (0% OSR) establishes the constitutive baseline for this research. Its CBR at the level of 20%, the classification as a competent subgrade or even as a sub-base geomaterial is accepted, and its resilient response must be interpreted considering the inherent variability of laboratory compaction processes.

The comparison between specimens in Figure 4.13 highlights that CP1 represents a typical mechanical behavior expected for this soil. Its Resilient Modulus (MR) values stabilize around 150 MPa, showing a balanced response to stress increments. Conversely, CP2 exhibits an initial over-stiffness, likely an artifact of the compaction process (over-compaction), which shifts its regression surface to higher plateaus but introduces internal instabilities.

The average surface in Figure 4.14 reflects a transition between these two states. While the MeDiNa model parameters ($k_1 = 114.7$) represent a conservative project baseline, the data

set confirms that even in its natural state, the soil can reach stiffness levels near 250 MPa at higher deviatoric stress levels, provided the granular arrangement is sufficiently dense.

The diagnostic slices in Figure 4.15 also allows for a specimen quality inspection. CP1 shows a stable trend, with its Resilient Modulus maintaining a consistent level around 150 MPa as the deviatoric stress (σ_d) increases. In contrast, CP2 starts at a higher stiffness plateau (approaching 400 MPa at low σ_d) but experiences a sharp "negative ramp." This behavior is not indicative of an incompetent soil, but rather of a specimen with excessive initial rigidity that relaxes as the structure adjusts to the loading cycles. Even with this MR decreasing effect, CP2 sustains MR values near 250 MPa at the highest levels of σ_d, confirming the material's load-bearing capacity.

The bivariate analysis in Figure 4.16 confirms this diagnosis. The positive slopes in both σ_3 and σ_d for CP1 validate its consistency as a reference material. The unstable slopes of CP2, while showing higher absolute MR values, underscore the sensitivity of the natural soil's granular skeleton to initial molding conditions. This dichotomy will be explored when OSR is used as a stabilizing agent to reduce such sensitivity and provide a more uniform structural response across the pavement layer.

4.1.4 - EVALUATION OF RAW DATA AND QUALITY CONTROL IMPACT VITÓRIA SOIL - 0% OSR CONTENT

The documentation of unfiltered data is essential to validate the statistical treatment process and ensure the reliability of pavement design models. This analysis exposes the rheological inconsistencies and instrumental noise present across the 18 sequences of the Resilient Modulus test for the natural Vitória soil, serving as a technical justification for the rigorous Quality Control (QC) adopted in this research.

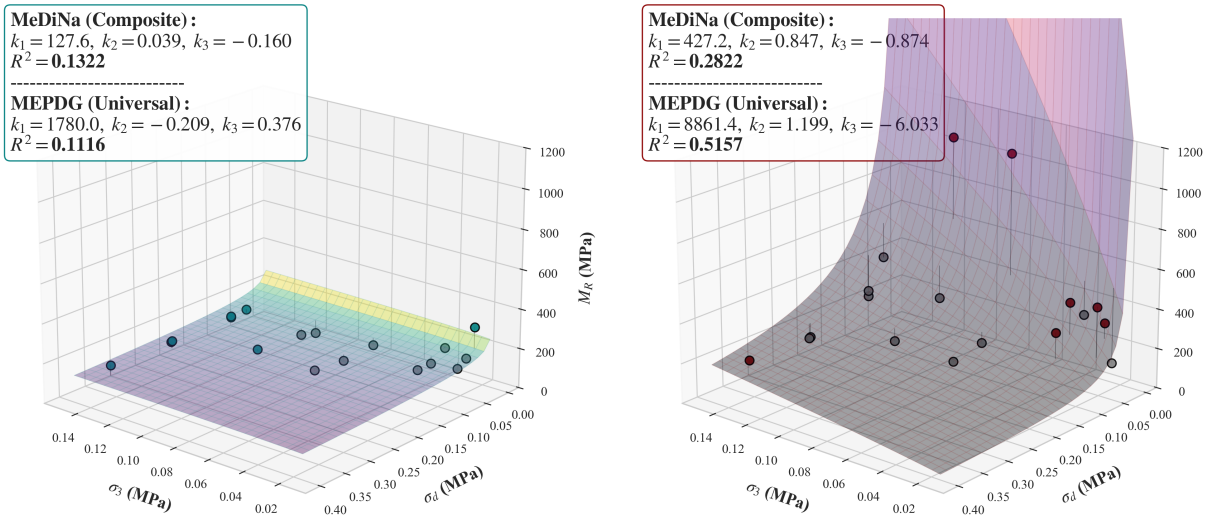
4.1.4.1 Unfiltered 3D Individual Modeling

The three-dimensional visualization of the integral data (Figure 4.17) reveals the deleterious impact of anomalous sequences on model calibration.

In specimen CP1, dispersion is evident under low stress levels, resulting in an extremely low coefficient of determination ($R^2 = 0.1322$). Specimen CP2 presents extreme outliers exceeding 1000 MPa (notably Sequence 10), floating drastically above the regression surface.

These outliers severely distort the MeDiNa model parameters. In CP2, the inclusion of noise artificially inflates the k_1 parameter to 427.2 and k_2 to 0.847, masking the structural

instability previously discussed and suggesting a confinement-induced stiffening that is statistically unsustainable ($R^2 = 0.2822$).



(a) AASHTO - VIX CP1 [UNFILTERED] **(b) AASHTO - VIX CP2 [UNFILTERED]**

Figure 4.17: 3D Models Impact Without QC for Vitória soil (0% OSR): (a) unfiltered specimen CP1; (b) unfiltered specimen CP2.

4.1.4.2 Average Unfiltered Surface and Stress Sensitivities

The log-log diagnostic slices (Figure 4.18) and bivariate models (Figure 4.19) demonstrate that, without filtering, the constitutive trends of Dunlap and Hicks are obscured. Specimen CP2 exhibits an unrealistic "negative ramp" at low deviatoric stresses (σ_d), starting from levels near 1000 MPa—a behavior incompatible with the silty-granular clay matrix.

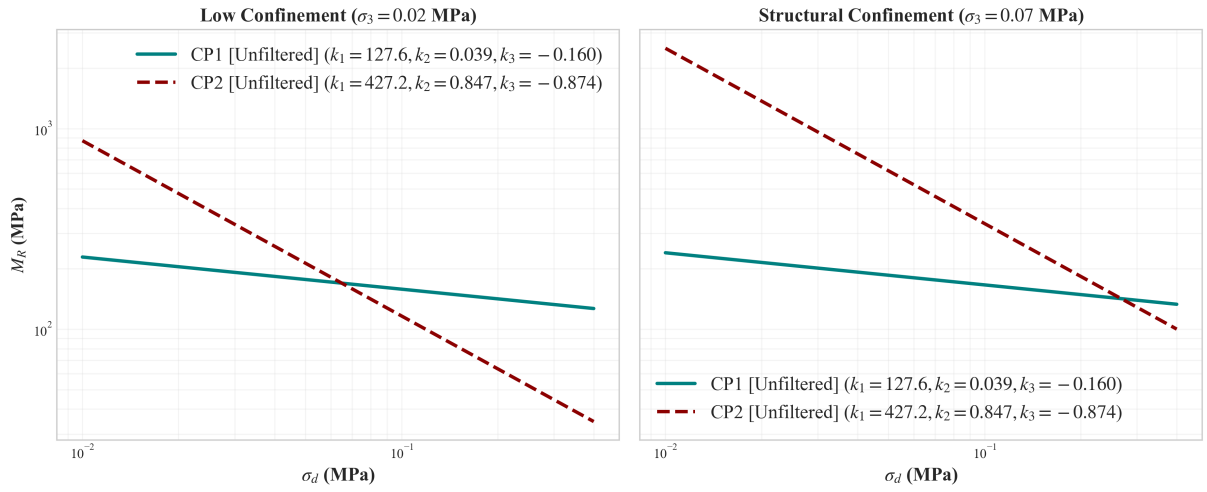


Figure 4.18: Evaluation of impact without QC on the Vitória soil (0% OSR) stiffness sensitivity to stress changes at low and structural confinement levels.

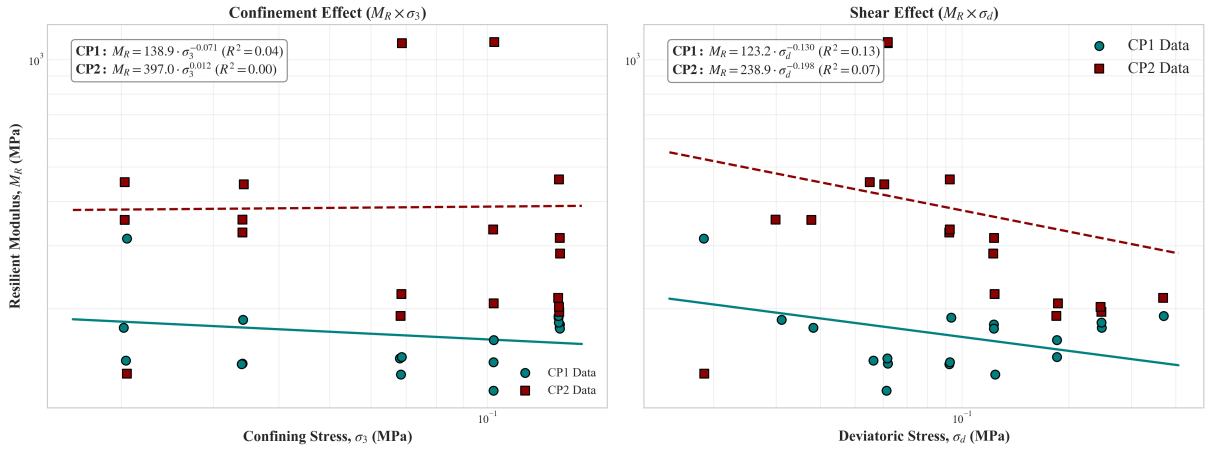


Figure 4.19: 1D Bivariate Models [UNFILTERED]: (left) confinement effect; (right) shear effect.

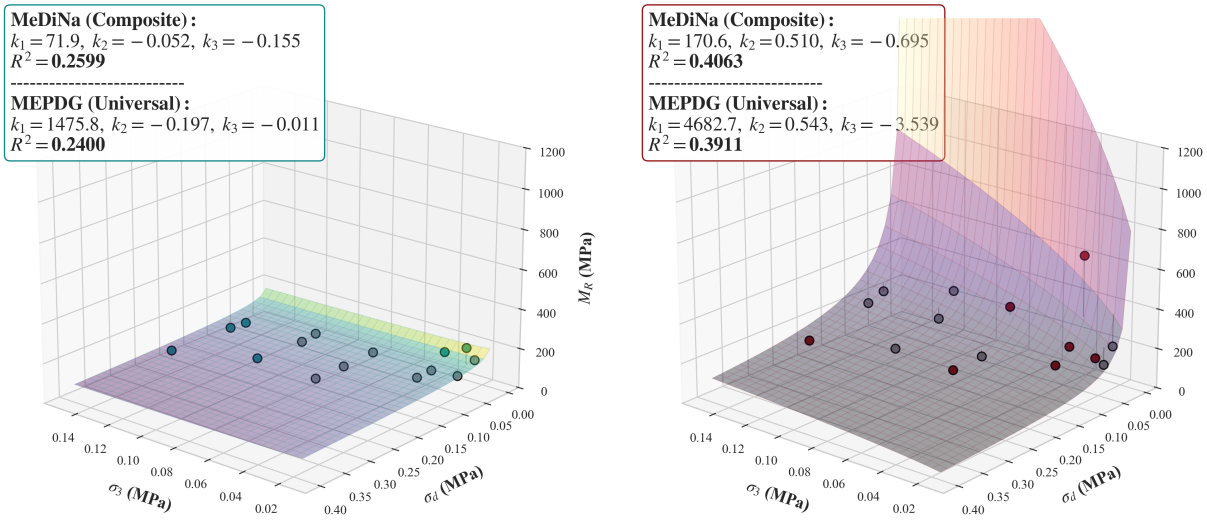
In Figure 4.19, the regression lines for confinement and shear effects show negligible or irrelevant coefficients of determination ($R^2 \approx 0.04$ to 0.13). This scenario confirms that laboratory instrumental variability dominates the mechanical response when quality control is absent, reinforcing the necessity of the filters applied in previous sections, which allowed for R^2 values near 0.70 by isolating the actual resilient behavior of the material.

4.1.5 - EVALUATION OF RESILIENT BEHAVIOR: VITÓRIA SOIL - 5% OSR CONTENT

The incorporation of 5% Ornamental Stone Residue (OSR) into the Vitória soil marks the transition from a natural state to a granulometrically stabilized matrix. This analysis demonstrates how the initial addition of residue modifies the soil structure through the filler effect and reveals the material's sensitivity to compaction energy.

The 3D regression surfaces (Figure 4.20) show a significant magnitude divergence between the redundant specimens. While CP1 maintains a lower stiffness profile ($k_1 = 71.9$, $k_2 = -0.052$, and $k_3 = -0.155$), CP2 reaches substantially higher M_R values ($k_1 = 170.6$), including a notable peak of 653.02 MPa at Sequence 4.

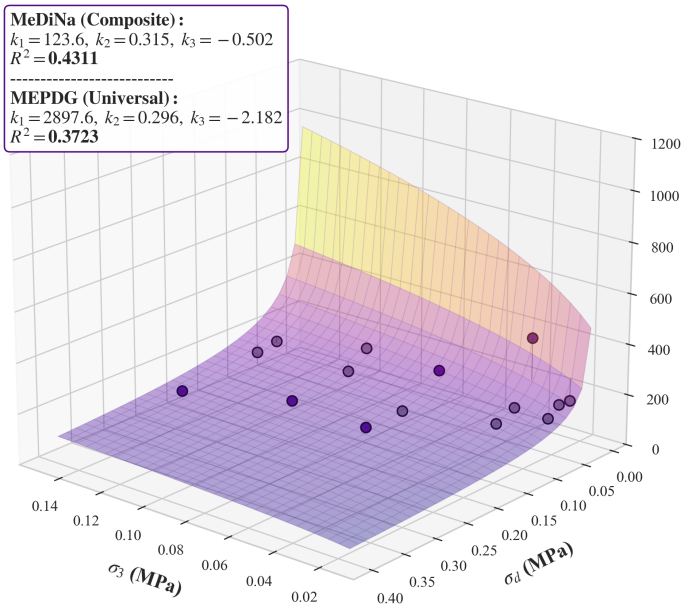
Rather than an instrumental error, this behavior is interpreted as an authentic response to laboratory compaction variability. In CP2, a likely involuntary increase in compaction energy resulted in a lower void ratio and higher initial interlocking. In materials with low plasticity and a high granular fraction reinforced by fines (OSR), this denser state triggers the phenomenon of **impeded dilatancy**: as confining pressure increases, the granular skeleton "locks" (*stiffness increasing*), generating stiffness peaks before deviatoric deformation initiates structural relaxation.



(a) AASHTO - VIX CP1 (5% OSR) **(b) AASHTO - VIX CP2 (5% OSR)**

Figure 4.20: 3D Resilient Modulus models comparison for Vitória soil (5% OSR): (a) specimen CP1; (b) specimen CP2.

Figure 4.21 presents the average resilient behavior, where the MeDiNa model yields $k_1 = 123.6$ and, importantly, a positive $k_2 = 0.315$. The natural Vitória borrow material has a reduced fines fraction (passing #200 sieve). The 5% OSR would act primarily as a **filler**, optimizing the packing of larger soil particles.



Average Resilient Modulus: VIX (5% OSR)

Figure 4.21: Average Resilient Modulus 3D surface for Vitória soil (5% OSR) including MeDiNa and MEPDG model parameters.

This rearrangement would have increased the effective contact area between grains and raises the apparent cohesion of the matrix. Mechanically, this would lead to densification, to mitigate the unstable behavior seen in the pure soil (0% OSR), shifting the average surface to a more predictable and competent stiffness plateau.

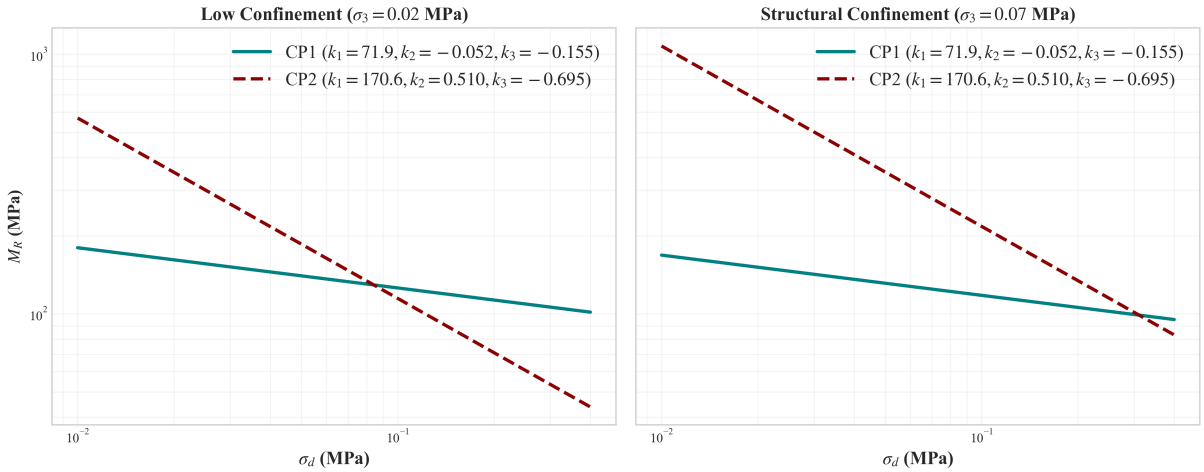


Figure 4.22: Evaluation of the Vitória soil (5% OSR) stiffness sensitivity to stress changes at low ($\sigma_3 = 0.02$ MPa) and structural ($\sigma_3 = 0.07$ MPa) confinement levels.

The log-log diagnostic slices (Figure 4.22) and bivariate regressions (Figure 4.23) clarify the rheological status. Although both specimens still exhibit *MR decreasing* (k_3 negative), the OSR presence could offer some level of structural stabilization when comparing the slices of MR of 0 and 5% OSR content, once in this SRC, a higher level of moduli can be observed. In the $M_R \times \sigma_3$ relationship, CP2 shows a positive slope ($k_2 = 0.05$ in 2D log-log).

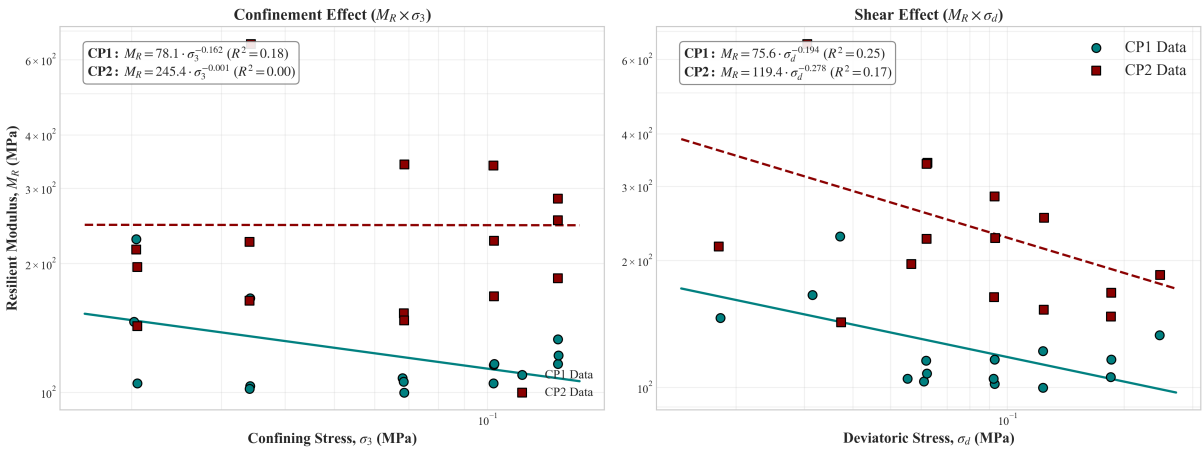


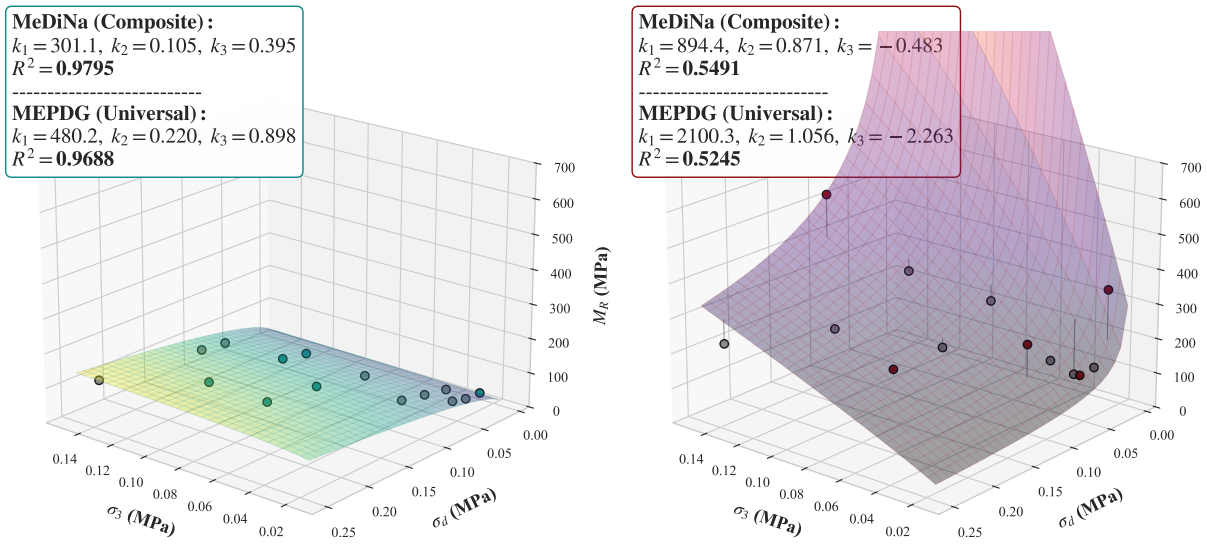
Figure 4.23: 1D Bivariate sensitivity models for Vitória soil (5% OSR): (left) confinement effect ($M_R \times \sigma_3$); (right) shear effect ($M_R \times \sigma_d$).

The $M_R \times \sigma_d$ plot confirms that while the matrix remains sensitive to shear ($k_2 =$

-0.15 for CP1 and -0.24 for CP2), the "design lines" in log-log scale are now positioned at a lower stiffness magnitude. This proves that the expected initial filler effect did not provide any increment gain against traffic-induced stresses, and the level of MR has been reduced.

4.1.6 - EVALUATION OF RESILIENT BEHAVIOR: VITÓRIA SOIL - 10% OSR CONTENT

The incorporation of 10% Ornamental Stone Residue (OSR) marks a critical threshold in the mechanical stabilization of the Vitória soil. At this level of substitution, the OSR residue reaches a point where the fines fraction begins to govern the apparent cohesion and the capillary locking of the matrix.



(a) AASHTO - VIX CP1 (10% OSR) **(b) AASHTO - VIX CP2 (10% OSR)**

Figure 4.24: 3D Resilient Modulus models comparison for Vitória soil (10% OSR): (a) specimen CP1; (b) specimen CP2.

The comparison of 3D surfaces reveals a high-quality regression for specimen CP1 ($R^2 = 0.9795$), with parameters $k_1 = 301.1$, $k_2 = 0.105$, and a notably positive $k_3 = 0.395$. Specimen CP2, while showing higher data dispersion ($R^2 = 0.5491$), maintains significantly higher stiffness levels ($k_1 = 894.4$), with its modulus consistently exceeding 700 MPa under higher confinement levels. This disparity is interpreted as an authentic response to laboratory compaction variability. In CP2, small variations in molding density trigger a severe structural locking (*stiffness increasing* governed by confinement), driving the stiffness to monumental peaks.

Figure 4.25 presents the average resilient behavior ($R^2 = 0.6120$), yielding a composite $k_1 = 577.6$ and a moderately negative $k_3 = -0.255$. This global stabilization

indicates that while the mixture remains predominantly resilient-degradant on average, the magnitude of the modulus has more than doubled compared to the pure soil, establishing a highly competent structural plateau for pavement layers.

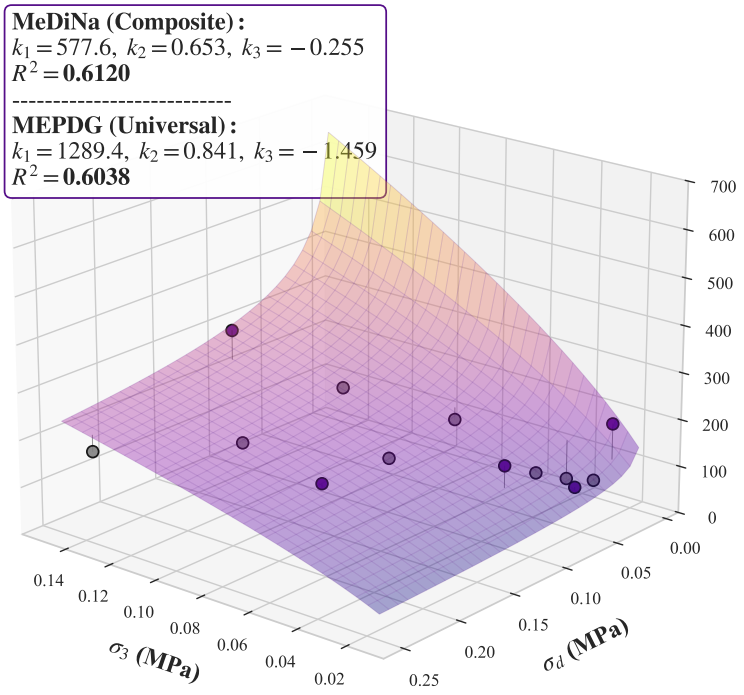


Figure 4.25: Average Resilient Modulus 3D surface for Vitória soil (10% OSR) including MeDiNa and MEPDG model parameters.

The diagnostic slices reveal a significant rheological shift. At 10% OSR, CP1 displays an atypical *stiffness increasing* behavior, where the Resilient Modulus increases as the deviatoric stress (σ_d) rises, evidenced by the positive slope in both low and structural confinement scenarios.

In contrast, CP2 preserves the basal *reduction in stiffeness* ($k_3 = -0.483$), yet starting from an extremely high magnitude. This confirms that at this concentration, the residue acts as a rigid filler that can lock the granular skeleton under shear.

The bivariate analysis in log-log scale underscores the robustness of the OSR-induced rheological signature. Both specimens show a consistent and clear gain in stiffness with confining pressure ($k_2 = 0.38$ for both). In the $M_R \times \sigma_d$ plot, the apparent stability or slight MR increasing (stiffness increasing) must be interpreted with caution due to the AASHTO T 307 protocol, where σ_d increments occur simultaneously with σ_3 increases. Nevertheless, the high R^2 for CP1 (0.93) in the deviatoric sensitivity plot proves the stability of the structured matrix, independent of localized compaction anomalies.

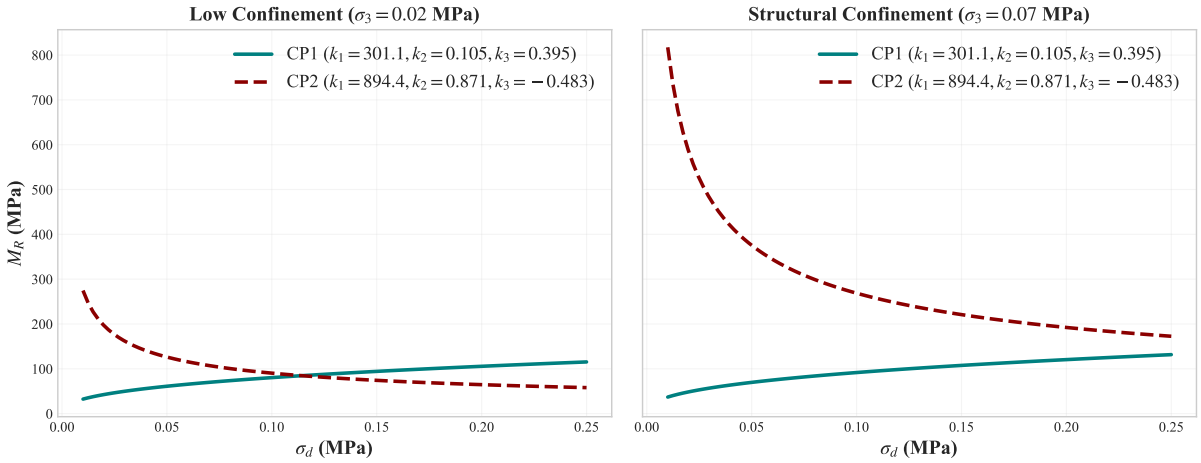


Figure 4.26: Evaluation of the Vitória soil (10% OSR) stiffness sensitivity to stress changes at low ($\sigma_3 = 0.02$ MPa) and structural ($\sigma_3 = 0.07$ MPa) confinement levels.

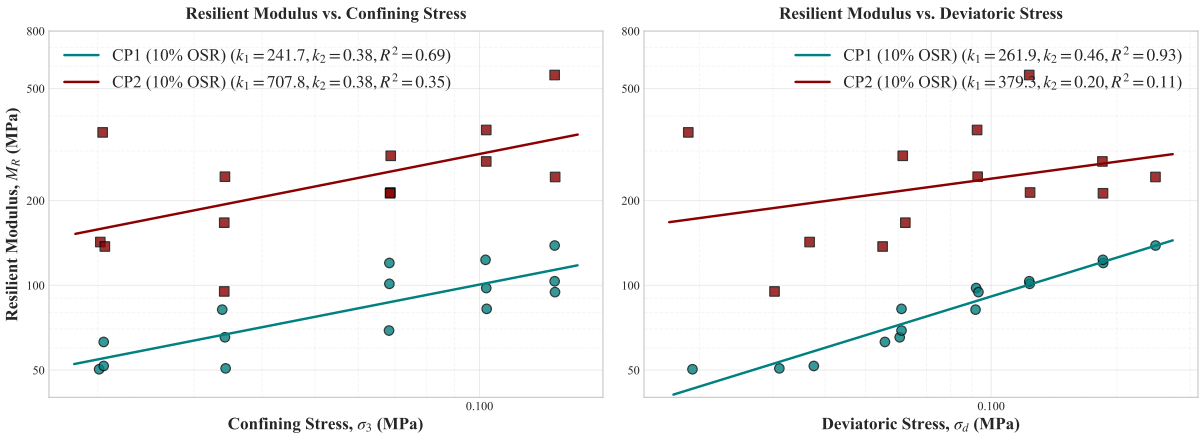


Figure 4.27: 1D Bivariate sensitivity models for Vitória soil (10% OSR): (left) confinement effect ($M_R \times \sigma_3$); (right) shear effect ($M_R \times \sigma_d$).

The analysis of the mechanical slices at constant confining pressures ($\sigma_3 = 20$ and 70 kPa) reveals a phenomenon of "structural engagement" unique to the 10% OSR content. While this mixture reached the highest static resistance (CBR $\approx 31\%$), its resilient performance at low stress levels presents a lower baseline compared to previous concentrations.

In the natural soil (0% OSR) and the 5% OSR mixture, the specimen CP1 maintained a relatively high and stable resilient baseline, fluctuating between 150 and 180 MPa at low confining pressures. However, at 10% OSR, the CP1 specimen exhibits a "stiffness floor" significantly lower, starting near the 50-80 MPa range. This reduction to a level below 100 MPa, as noted, is statistically robust ($R^2 = 0.9795$) and indicates that the 10% substitution level triggers a structural shift in the matrix.

The discrepancy between the record-high CBR (31%) and the lower initial MR (100

MPa) can be explained by the difference in strain levels and loading mechanisms:

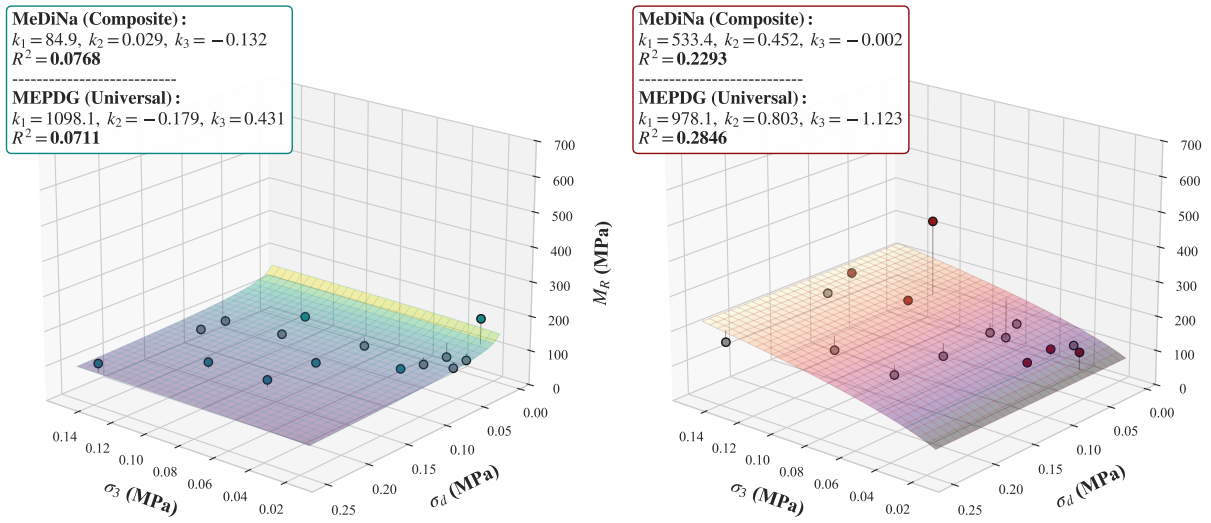
- **CBR (Static/High Strain):** The OSR fines at 10% concentration optimize the particle packing, creating a dense matrix with high apparent cohesion and internal friction. In a static punch test like the CBR, where this mixture reached a level of approximately 31%, this dense packing prevents shear failure, resulting in high bearing capacity.
- **MR (Dynamic/Low Strain):** At low confining pressures ($\sigma_3 = 20$ kPa), the excess of OSR fines may initially act as a "cushion" or separator between the larger soil grains. Without sufficient confinement to "lock" the skeleton, the matrix exhibits higher elastic deformability, resulting in a Resilient Modulus (MR) baseline below 100 MPa. This level is notably lower than the thresholds observed in the 0% and 5% OSR extracts.

The transition to the 70 kPa slice clarifies the material's potential. As the confinement increases, the 10% OSR matrix undergoes a **stiffness increasing** effect, as evidenced by the positive k_3 parameter ($k_3 = 0.395$) for specimen CP1. Unlike the 0% and 5% mixtures, which suffer from *MR decreasing* and lose stiffness as traffic load increases, the 10% CP1 specimen gains stiffness. Its MR rises from the low 100 MPa range toward approximately 130 MPa as the deviatoric stress (σ_d) increases (Figure 4.26 .

This behavior suggest that the 10% OSR mixture is a "stress-activated" material. The lower 100 MPa threshold is not an indication of failure, but rather could indicate a starting point of stiffness increasing-governed resilient response that surpasses the pure soil's capacity as the structural demand grows.

4.1.7 - EVALUATION OF RESILIENT BEHAVIOR: VITÓRIA SOIL - 15% OSR CONTENT

The evaluation of the mixture containing 15% Ornamental Stone Residue (OSR) reveals a sharp inflection in the stiffness gain trend observed in previous dosages. While the 5% and 10% additions promoted some level of structural strengthening and *stiffness increasing* peaks, the 15% content presents a significant drop in the Resilient Modulus (M_R), returning to lower stiffness thresholds. This phenomenon is governed by a critical transition in the micromechanics of the granular skeleton.



(a) AASHTO - VIX CP1 (15% OSR) **(b) AASHTO - VIX CP2 (15% OSR)**

Figure 4.28: 3D Resilient Modulus models comparison for Vitória soil (15% OSR): (a) specimen CP1; (b) specimen CP2.

The 3D regression surfaces (Figure 4.28) exhibit a severe degradation in modular magnitude and statistical reliability. Specimen CP1 presents a k_1 of only 84.9 and a near-zero correlation ($R^2 = 0.0768$), while CP2, although reaching higher absolute values ($k_1 = 533.4$), fails to maintain the structural stability seen in the 10% OSR dosage ($R^2 = 0.2293$).

- **Void Saturation and Loss of Grain-to-Grain Contact:** Up to the 10% addition level, the OSR acted as a beneficial filler, optimizing particle packing. At 15%, the volume of fines exceeds the available void volume of the original soil skeleton. Mechanically, the excess residue begins to push the larger soil grains apart, breaking the rigid grain-to-grain contact. The structure effectively "floats" within a fine, non-plastic matrix generated by the residue.

- **Lubrication Effect and Rheological Reversal:** Without the interlocking of the coarse skeleton, the resilient behavior is no longer governed by the soil grains but is dominated by the OSR fine paste. Under cyclic loading, this matrix acts as a "cushion" or lubricant, facilitating internal micro-sliding under shear stresses. This explains why the *stiffness increasing* phenomenology (which generated peaks above 1,000 MPa at 10% OSR) disappeared completely; specimen CP1 returned to a basal *reduction in stiffness* state ($k_3 = -0.132$), and CP2 exhibited an almost flat, unstable response ($k_3 = -0.002$).

Figure 4.29 demonstrates the impact on the average composite model, where the average k_1 dropped to 288.6, a reduction of approximately 50% compared to the 10% OSR content ($k_1 = 577.6$).

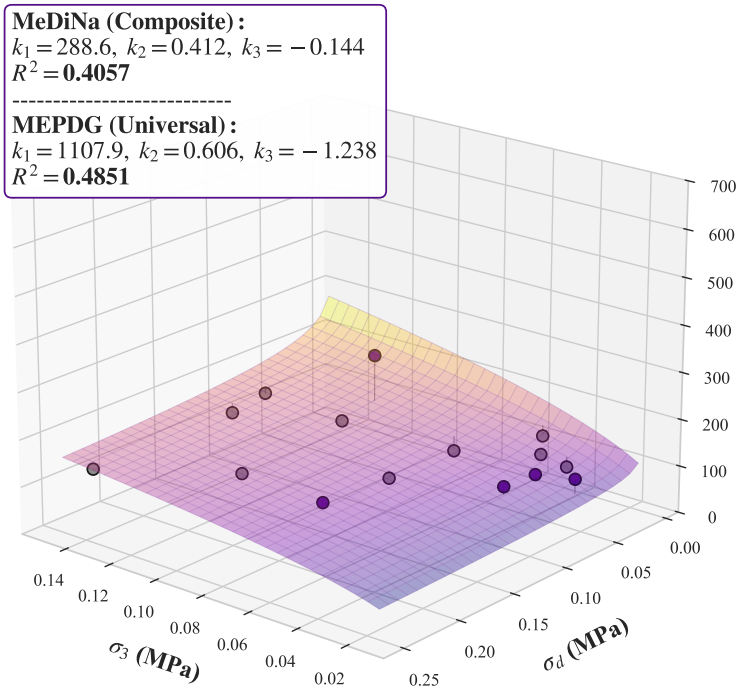


Figure 4.29: Average Resilient Modulus 3D surface for Vitória soil (15% OSR) including MeDiNa and MEPDG model parameters.

The diagnostic slices (Figure 4.30) clarify the rheological reversal observed at this dosage. With the incorporation of 15% OSR, the volume of fines exceeds the available void volume of the original soil skeleton, causing the particles to "float" within a non-plastic matrix. Consequently, the *stiffness increasing* phenomenon previously seen at 10% OSR disappears.

Specimen CP1 returns to a basal *MR decreasing* state ($k_3 = -0.132$), whereas CP2 exhibits a Resilient Modulus response that remains practically constant despite the increment in deviatoric stress ($k_3 = -0.002$). This behavior in CP2 does not strictly characterize MR increasing or decreasing but rather a state of rheological transition.

The significant lack of repeatability observed between the pair of specimens—evidenced by the sharp decline in the coefficients of determination ($R^2 = 0.07$ for CP1 and $R^2 = 0.22$ for CP2)—highlights the mixture's sensitivity to excess residue. This variability justifies the methodological practice adopted for other materials in this research (such as the SG-12 soil), where a third specimen is tested to resolve uncertainties and achieve a more rigorous evaluation. Ultimately, the excess residue acts as a lubricant that facilitates micro-sliding between grains, compromising the structural stability of the matrix.

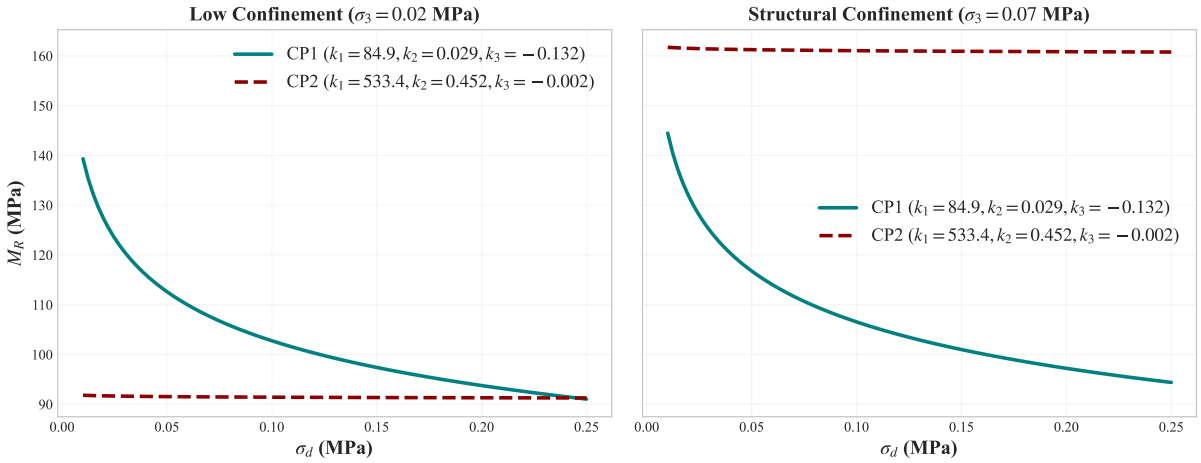


Figure 4.30: Evaluation of the Vitória soil (15% OSR) stiffness sensitivity to stress changes at low ($\sigma_3 = 0.02$ MPa) and structural ($\sigma_3 = 0.07$ MPa) confinement levels.

The bivariate analysis (Figure 4.31) confirms the structural collapse. The $M_R \times \sigma_3$ relationship for CP1 shows a null slope ($k_2 = -0.02, R^2 = 0.00$), indicating that the material has lost its ability to gain stiffness through confinement—a typical characteristic of saturated or over-filled matrices.

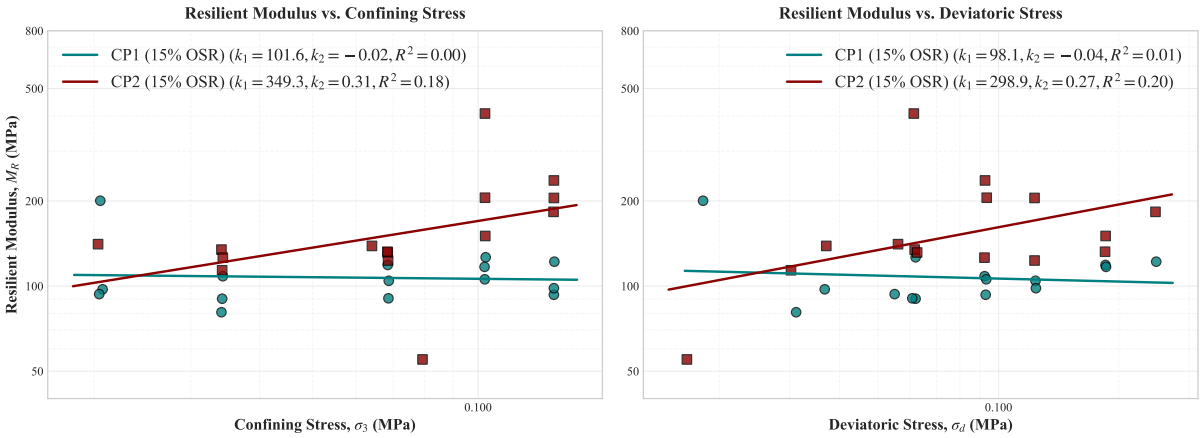


Figure 4.31: 1D Bivariate sensitivity models for Vitória soil (15% OSR): (left) confinement effect ($M_R \times \sigma_3$); (right) shear effect ($M_R \times \sigma_d$).

It is concluded that the optimum dosage for the mechanistic utilization of OSR in this soil type lies within the 5% to 10% range, beyond which the excess fines compromise the bearing capacity of the pavement layer.

4.1.8 - STRATEGIC REEVALUATION OF 30% OSR: FROM STRUCTURAL FAILURE TO INFRASTRUCTURE VIABILITY

Although the 30% Ornamental Stone Residue (OSR) content presents a sharp reduction in stiffness when compared to the optimized levels (5% and 10%) for base and subbase layers, a contextualized geomechanical analysis reveals significant technical and environmental potential for applications in lower pavement layers and embankment cores.

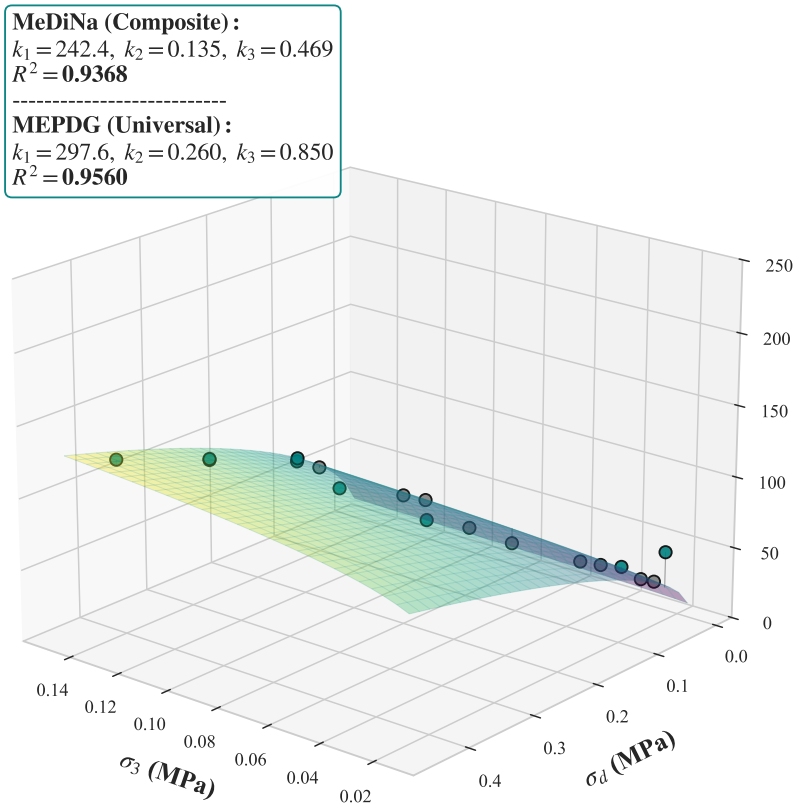


Figure 4.32: 3D Resilient Modulus model for Vitória soil (30% OSR) demonstrating highly predictable structural behavior.

The Resilient Modulus (M_R) results for the 30% OSR mixture fluctuate between 30 and 120 MPa. For base courses subjected to high deviatoric stress bulbs, such values are insufficient. However, for subgrade or embankment layers, this stiffness threshold represents above-average performance. Natural foundation soils often operate with M_R values in the 30 to 60 MPa range.

The 3D surface model (Figure 4.32) reveals an exceptional coefficient of determination ($R^2 = 0.9368$ for the MeDiNa model). This represents a drastic structural reorganization compared to the chaos observed at 15% OSR. At 30% addition, the residue ceases to be a mere additive and effectively becomes the dominant skeleton of the matrix. This highly predictable,

stable behavior guarantees a robust lower boundary of resilient stiffness, outperforming the *in natura* soil, especially in critical saturation scenarios.

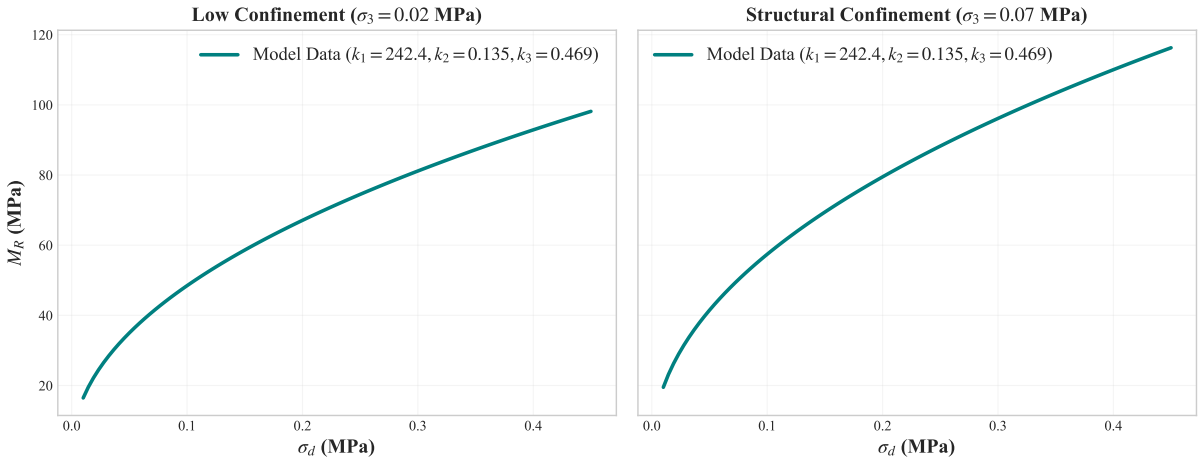


Figure 4.33: Evaluation of the Vitória soil (30% OSR) stiffness sensitivity to stress changes showcasing pronounced MR increasing under structural confinement.

The technical viability of the 30% content is grounded in the geostatic stress field. Considering a compacted mass with a coefficient of earth pressure at rest (K_0) of approximately 0.6, a confining stress (σ_3) of 30 kPa corresponds to a vertical stress of 50 kPa, typical of a depth of about 2.7 meters within the road prism.

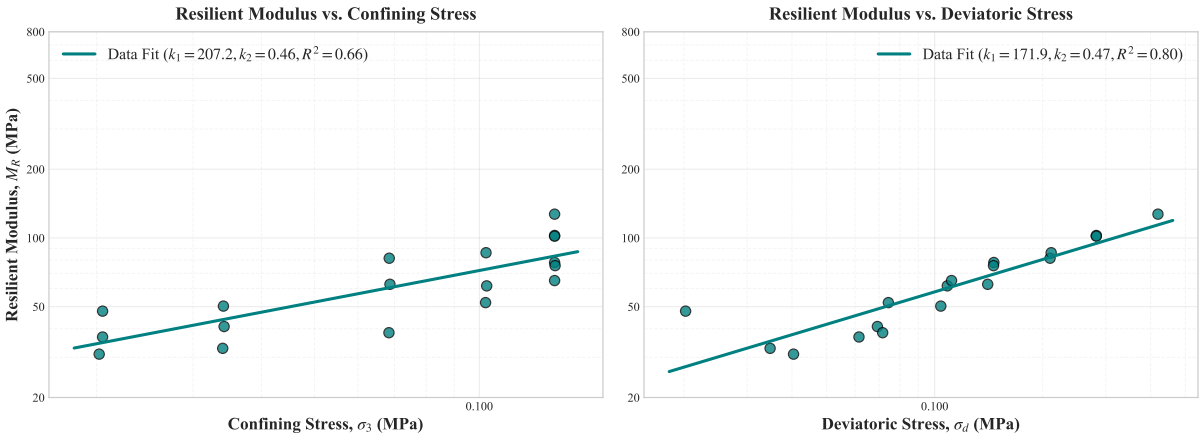


Figure 4.34: 1D Bivariate sensitivity models for Vitória soil (30% OSR) confirming positive correlation with both confining and deviatoric stresses.

In this confined state, the *stiffness increasing* behavior observed in the tests becomes a major structural advantage. As evidenced by the diagnostic slices (Figure 4.33) and the bivariate models (Figure 4.34), the material exhibits a strong positive sensitivity to shear ($k_3 = 0.469$ and a 2D deviatoric $R^2 = 0.80$). The material gains stiffness under the weight

of the overlying layers, providing a stable support platform. Furthermore, transforming the original clayey matrix into a predominantly inert silty-sandy matrix eliminates pathologies of excessive plasticity and volumetric expansion typical of tropical subgrades.

The distinction between noble layers and infrastructure layers might dictate the scale of residue consumption in infrastructure design. While bases and subbases are thin (15 to 20 cm), limiting waste sequestration even over kilometric extensions, embankments and subgrades involve meters of thickness.

The adoption of the 30% content shifts the OSR from a stabilizing additive to a volumetric borrow pit substitute. In embankments 3 to 4 meters high, using this proportion enables the massive sequestration of thousands of tons of industrial waste per kilometer of road, alleviating the pressure on natural borrow pits. By integrating the 30% content into earthworks, the road infrastructure assumes a dual function:

- **Geotechnical Function:** To provide a platform with a California Bearing Ratio (CBR) consistently above 6%, surpassing the acceptance threshold for poor-quality materials and approaching the behavior of granular materials.
- **Socio-Environmental Function:** To mitigate the environmental liability of the ornamental stone sector in the State of Espírito Santo, drastically reducing disposal in industrial landfills or irregular dumps through circular economy applied at an infrastructure scale.

Therefore, while the 30% OSR content marks the efficiency limit for pavement layers subjected to high deviatoric stresses, it proves to be the point of maximum socio-environmental viability for earthworks. The observed stability of the resilient moduli, the pronounced *MR increasing* effect, and the capacity to consume large volumes of waste allow this mixture to be classified as a High-Performance Infrastructure Geomaterial. It is capable of transforming the road prism into an active agent of the circular economy without compromising the mechanistic integrity of the structure.

4.2 - OSR MIXED WITH A LATERITIC SOIL OF BRASILIA

This section discusses the results of the Cyclic Load Triaxial Tests (CLTT) either, performed on the mixtures of Brasília (SG-12 at UnB site) soil and OSR. The analysis transitions from the empirical characterization previously discussed to a mechanistic evaluation of the Resilient Modulus (M_R), following the requirements for pavement design using the MeDiNa software.

To provide a granular understanding of the material's structural response, the results for each OSR content are presented through a standardized sequence of seven analytical plots, organized into four main figures per mixture, as described in the last session.

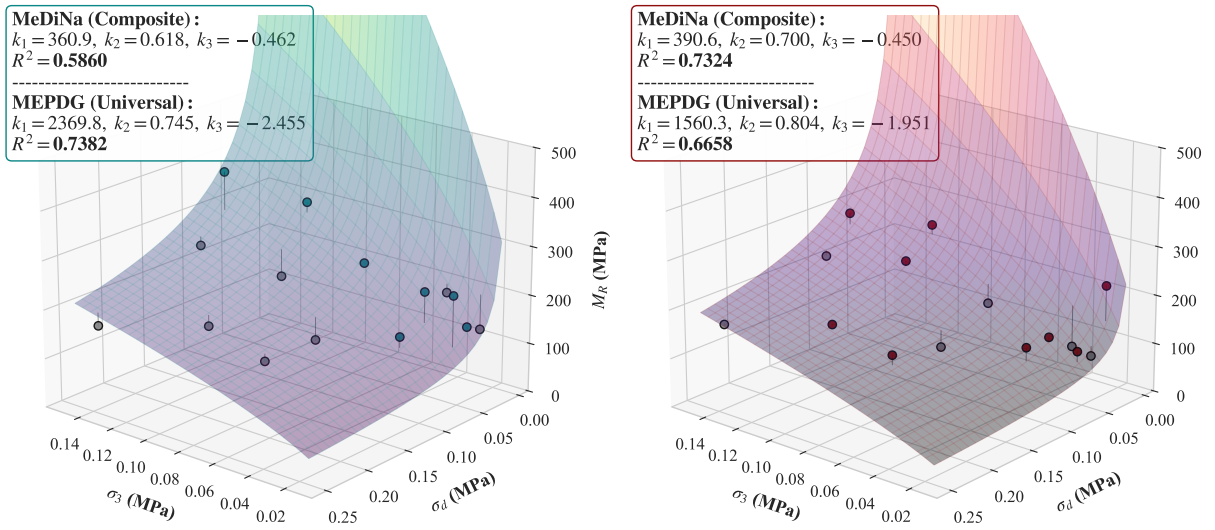
4.2.1 - EVALUATION OF REFERENCE RESILIENT BEHAVIOR BRASÍLIA SOIL - 0% OSR CONTENT

The natural soil sample from the SG-12 UnB site (0% OSR) establishes the constitutive baseline for mechanical comparison. As a typical regional lateritic clay with a silty-granular matrix, its resilient response serves as the "zero point" to quantify the structural gains provided by the subsequent incorporation of Ornamental Stone Residue (OSR).

The evaluation of the natural Brasília soil (0% OSR), utilized as the control group, reveals a remarkably stable mechanical signature characteristic of tropical soils with transitional behavior. The analysis of the response surfaces, particularly the diagnostic slices at constant confining stresses, allows for the isolation of the mineralogical structure's effect on the material's stiffness.

The 3D regression models (Figure 4.35) demonstrate high repeatability between the redundant specimens. Specimen CP1 yielded a k_1 parameter of 360.9 ($R^2 = 0.5860$), while CP2 presented a highly consistent k_1 of 390.6 ($R^2 = 0.7324$).

The physical transition of the SG-12 specimens from the cyclic triaxial environment to the compression testing machine is a critical procedural step for correlating resilient and static mechanical properties. Following the completion of the Resilient Modulus (M_R) protocol, the specimens of the natural soil (0% OSR) were carefully removed from the triaxial cell for subsequent unconfined compressive strength testing. As illustrated in Figure 4.36, the specimens maintained significant structural integrity after being subjected to thousands of load cycles. This macroscopic persistence is a direct reflection of the slightly lateritic behavior previously discussed, where the 'pseudo-cohesion' provided by iron and aluminum oxides prevents premature collapse and stabilizes the granular skeleton even under dynamic deviatoric stress. The absence of visible cracks or excessive bulging at this stage confirms that the resilient baseline of the natural soil is supported by a robust mineralogical matrix.



(a) AASHTO - BSB CP1 (0% OSR) **(b) AASHTO - BSB CP2 (0% OSR)**

Figure 4.35: 3D Resilient Modulus models comparison for natural Brasília soil (0% OSR): (a) specimen CP1; (b) specimen CP2.



Figure 4.36: Visual inspection of natural SG-12 soil specimens (0% OSR) after cyclic loading triaxial testing, prior to the unconfined compression test.

Both specimens exhibit strong dependency on confining stress (positive k_2) and a clear susceptibility to shear degradation (negative k_3).

The average composite surface (Figure 4.37) synthesizes this stable behavior, achieving a robust coefficient of determination ($R^2 = 0.7724$) with parameters $k_1 = 369.9$, $k_2 = 0.659$, and $k_3 = -0.463$.

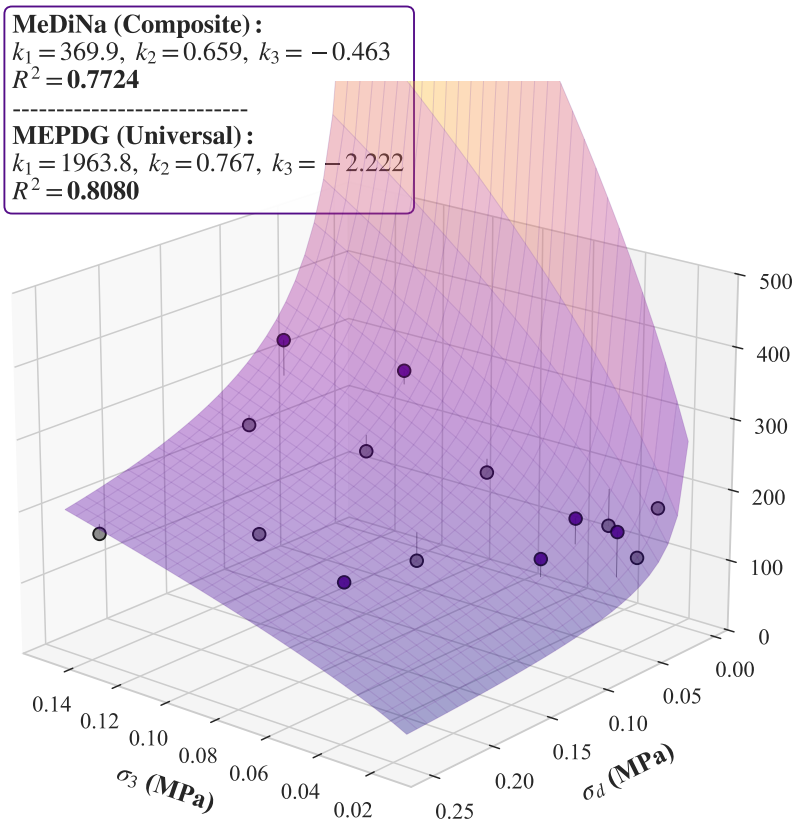


Figure 4.37: Average Resilient Modulus 3D surface for natural Brasília soil (0% OSR) including MeDiNa and MEPDG model parameters.

This stability acts as a perfect baseline to evaluate the structural changes induced by OSR addition in subsequent mixtures.

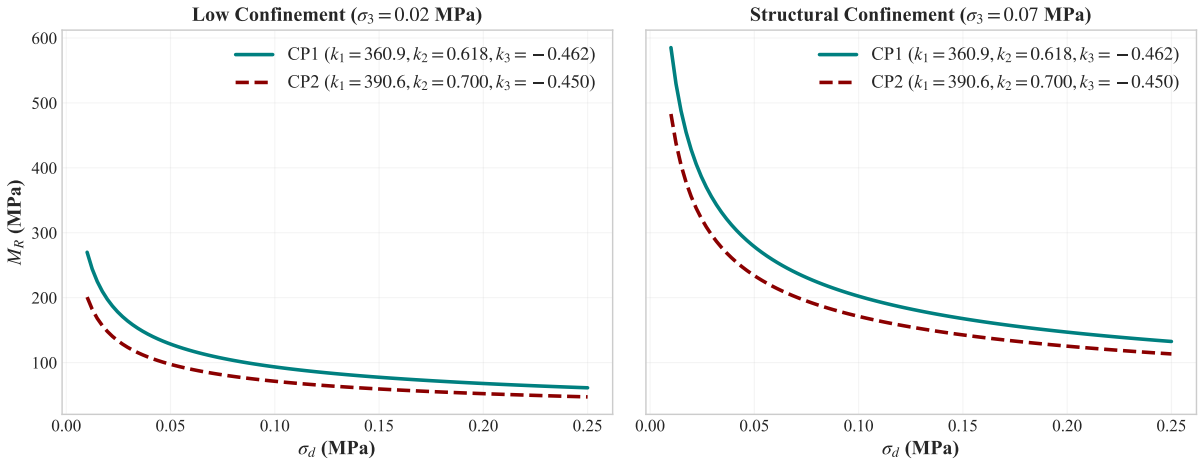


Figure 4.38: Evaluation of the natural Brasília soil (0% OSR) stiffness sensitivity to stress changes at low ($\sigma_3 = 0.02$ MPa) and structural ($\sigma_3 = 0.07$ MPa) confinement levels.

Parallel Consistency and Stress Thresholds

Observing the *MR decreasing* curves in the diagnostic slices for low ($\sigma_3 = 0.02$ MPa) and structural ($\sigma_3 = 0.07$ MPa) confinement levels (Figure 4.38), a highly consistent geometry is evident. The stiffness degradation curves driven by the increasing deviatoric stress (σ_d) are practically parallel to each other, separated by a distinct vertical "step". This distance highlights the material's high dependency on the confining stress (an expressive and positive k_2 parameter). The consistency of these slopes proves that the shear degradation mechanism ($k_3 < 0$) occurs at a uniform rate, regardless of the lateral pressure imposed.

To provide a comprehensive understanding of the resilient behavior of the natural Brasília soil (0% OSR), the *decreasing stiffness* phenomenon is presented in both scalar (Figure 4.38) and log-log (Figure 4.39) dimensions. This dual perspective can offer a good perspective of the non-linear constitutive model.

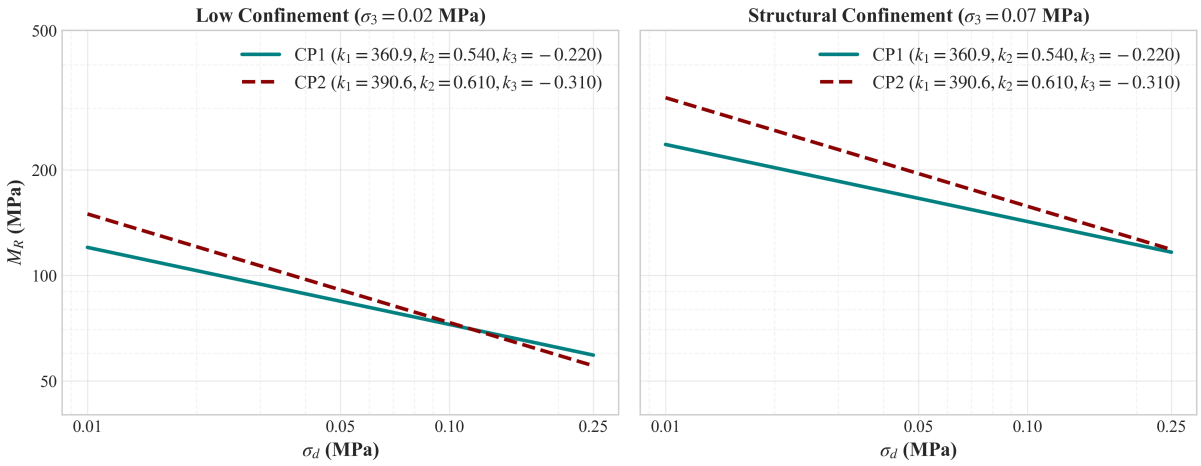


Figure 4.39: Log-Log evaluation of the natural Brasília soil (0% OSR) stiffness sensitivity to stress changes at 0.02 MPa and 0.07 MPa confining pressures.

The comparison between the two representations reveals fundamental geomechanical insights:

- **Geometric Parallelism and k_3 Stability:** In the scalar plots, the specimens exhibit a pronounced decay in Resilient Modulus (M_R) as the deviatoric stress (σ_d) increases, yet the curves for both confining levels remain remarkably parallel. When transitioned to a log-log scale (Figure 4.39), this parallelism is linearized into two straight lines with identical negative slopes ($k_3 \approx -0.46$). This confirms that the rate of shear-induced "relaxation" or decreasing MR (decreasing stiffness) is an intrinsic property of the lateritic matrix, independent of the applied confinement.

- **Confining Step (k_2 Influence):** The vertical distance (the "step") between the 0.02 MPa and 0.07 MPa slices remains constant in the logarithmic domain. This demonstrates that the confining stress effectively shifts the stiffness magnitude (governed by $k_2 \approx 0.66$) without interfering with the shear degradation mechanism.

- **Specimen Redundancy:** The near-perfect overlap of CP1 and CP2 in both scales underscores the high reliability of the SG12 natural soil sampling. While the material exhibits significant MR decreasing (dropping from nearly 300 MPa to below 150 MPa at low confinement), this behavior is mathematically stable and predictable, providing a secure baseline for infrastructure design.

In summary, the linearization of the MR decreasing curves in Figure 4.39 proves that the resilient decay is governed by a consistent power-law relationship. This "relaxed" yet stable response is the hallmark of the slightly lateritic Brasília soil, where the possible explanation is the oxide-coated matrix which might provide a stress-sensitive structural framework.

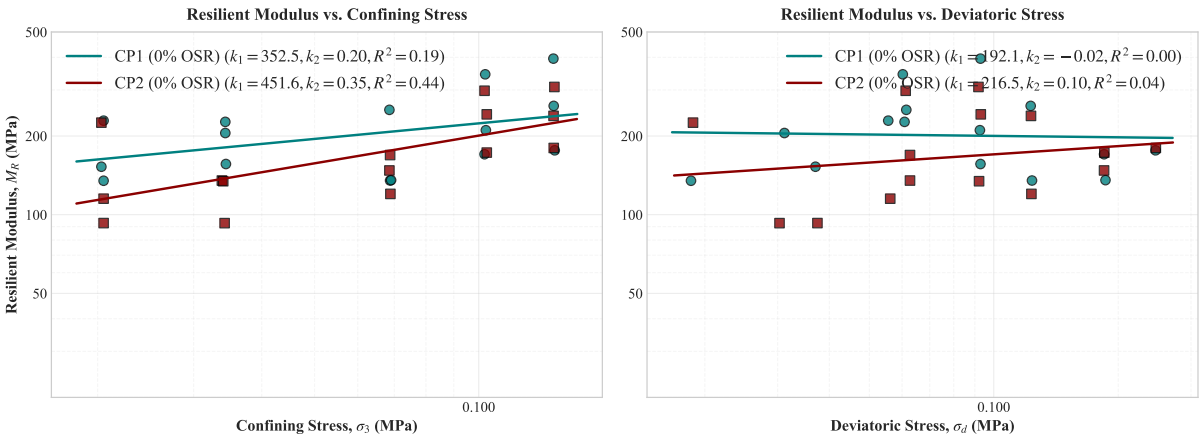


Figure 4.40: 1D Bivariate sensitivity models for natural Brasília soil (0% OSR): (left) confinement effect ($M_R \times \sigma_3$); (right) shear effect ($M_R \times \sigma_d$).

Micromechanics of the Slightly Lateritic Soil ($0.15 < L < 0.30$)

The stabilized behavior of the granular skeleton is directly supported by the pedogenesis of the SG12 soil. With a laterization index (L) between 0.15 and 0.30, the material is classified as exhibiting slightly lateritic behavior. In this transitional range, the silty-clayey fines begin to be coated by iron and aluminum oxides and hydroxides, typical of tropical weathering.

This oxide film acts as a weak cementing agent, conferring a "pseudo-cohesion" to the granular matrix. This incipient cementation can be suggested as a structural consistency seen in the bivariate models (Figure 4.40): the matrix possesses sufficient inherent stiffness to

prevent abrupt collapses under shear, while retaining a frictional nature that reacts promptly to confinement.

Constitutive Model Synthesis

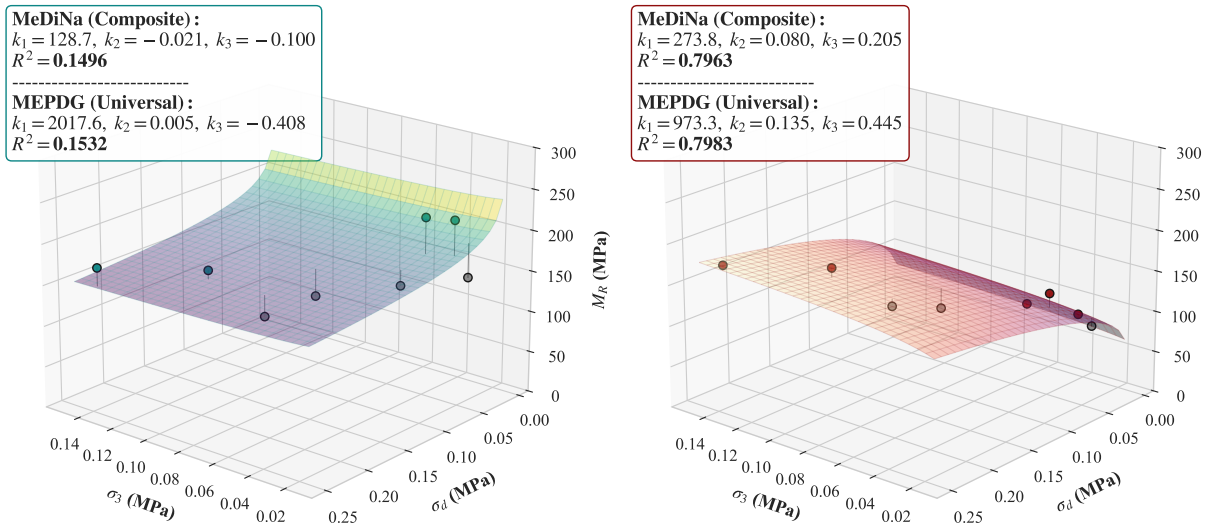
Mechanically, this mild laterization explains the equilibrium of the non-linear model. The natural material does not reach the sharp stiffness peaks of (*increasing MR*) seen in mixtures with heavy OSR addition because the natural pseudo-cohesion of the oxides is progressively broken by the continuous increase in σ_d (justifying the mild *decreasing stiffness* profile). However, unlike pure saprolitic soils, the laterized matrix does not collapse, keeping the slice curves parallel and predictable. This predictability makes the SG12 an excellent foundation material and a perfect control group to demonstrate the stiffness leap caused by the artificial introduction of OSR fines.

Geomechanical Filtering: The Influence of Realistic Stress States

The proper evaluation of a geomaterial for pavement applications requires that the laboratory stress states closely mimic the physical conditions experienced in the field. During standard AASHTO T 307 sequences, specifically sequences 1, 4, 7, 10, and 13, the applied confining pressure exceeds the deviatoric stress ($\sigma_3 > \sigma_d$). Under these essentially isotropic or high-confinement/low-shear conditions, the natural Brasília soil exhibited anomalous stiffness jumps, with the Resilient Modulus (M_R) approaching 400 MPa.

In the operational reality of upper pavement layers and shallow subgrades, traffic induces a stress tensor where the vertical deviatoric load vastly exceeds lateral confinement. Including points where $\sigma_3 > \sigma_d$ introduces an artificial stiffening effect into the regression models. The soil behaves as a confined fluid, gaining resistance purely from the triaxial chamber's pressure rather than from its internal structural interlocking. To capture the true working behavior of the material, a geomechanical filter was applied, removing all stress pairs where the deviatoric stress did not surpass the confinement.

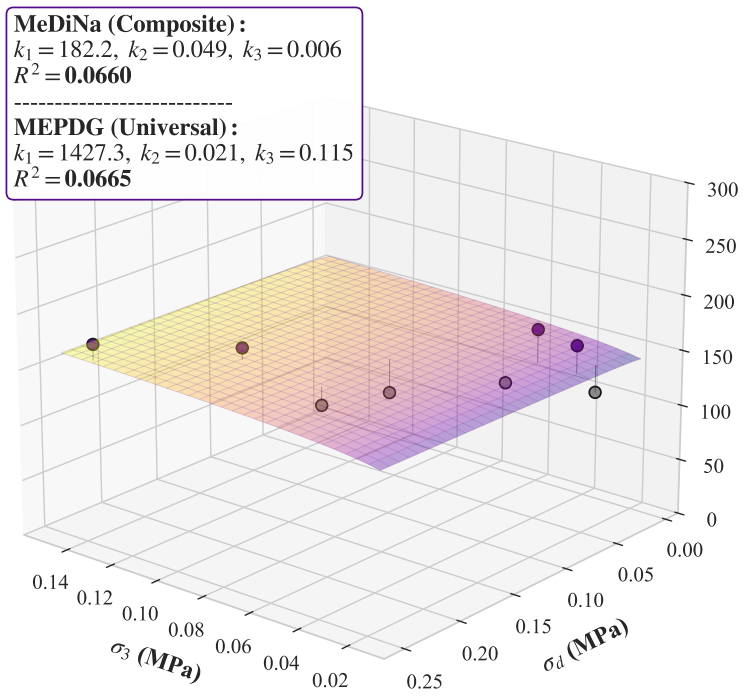
The application of this filter reveals the stark reality of the *in natura* soil's mechanical vulnerability. Without the artificial crutch of excessive confinement, the statistical and structural coherence of the material degrades significantly. As observed in the filtered 3D models (Figure 4.41), CP1 loses its responsiveness to stress variations, yielding a flat response with near-zero k_2 and k_3 parameters and a severe drop in correlation ($R^2 = 0.1496$). While CP2 retains some structural integrity ($R^2 = 0.7963$), the composite average suffers a massive reduction in baseline stiffness.



(a) AASHTO - BSB CP1 (0% OSR) **(b) AASHTO - BSB CP2 (0% OSR)**

Figure 4.41: Filtered 3D Resilient Modulus models ($\sigma_d \geq \sigma_3$) for natural Brasília soil (0% OSR): (a) specimen CP1; (b) specimen CP2.

Composite average 3D resilient modulus model for the filtered Brasília soil (0% OSR). The surface in Figure 4.42 illustrates the baseline stiffness derived from the combined behavior of specimens CP1 and CP2.



Average Resilient Modulus: BSB (0% OSR)

Figure 4.42: Filtered Average Resilient Modulus 3D surface for natural Brasília soil (0% OSR).

Rheological Divergence: The Unpredictability of the Natural Matrix

A critical micromechanical phenomenon is exposed by the filtered diagnostic slices in the logarithmic domain (Figure 4.43). When the artificial stability of high confining pressures ($\sigma_3 > \sigma_d$) is removed, the redundant specimens exhibited a profound rheological divergence.

While the specimens had previously shown parallel and predictable behavior under unfiltered conditions, the realistic stress states expose the material's structural bipolarity. Specimen CP1 exhibits a mild *decreasing stiffness* response ($k_3 = -0.100$), characterized by a negative slope where shear stresses progressively break down the lateritic pseudo-cohesion. Conversely, specimen CP2 displays a *increasing MR* behavior ($k_3 = 0.205$), with a positive slope indicating that the deviatoric stress mobilized granular friction and internal interlocking.

This stark duality reveals the extreme sensitivity of the *in natura* SG-12 soil to microscopic variations in compaction density and moisture content. Without a dominant and uniform rigid skeleton, the natural matrix cannot guarantee a consistent load-transfer mechanism under active traffic. Depending on localized micro-structural arrangements, the soil unpredictably alternates between cohesion-dominated failure (decreasing stiffness) and friction-dominated resistance (increasing stiffness).

From a pavement engineering perspective, this lack of repeatability represents a severe structural flaw. A mechanistic-empirical design cannot rely on a subgrade or subbase layer that exhibits such erratic rheological shifts under identical stress paths. This erratic baseline fundamentally validates the core hypothesis of this research: the incorporation of Ornamental Stone Residue (OSR) is not merely an alternative to increase absolute stiffness, but an engineering necessity to homogenize the matrix, suppress this rheological unpredictability, and enforce a stable, dominant granular skeleton capable of reliably supporting dynamic traffic loads.

The filtered average model (Figure 4.42) drops the k_1 parameter from the previous unfiltered level of 369.9 down to 182.2, with a negligible coefficient of determination ($R^2 = 0.0660$). This near-zero R^2 is not a testing error, but a geomechanical statement: when subjected exclusively to realistic shear-dominant stress states, the natural lateritic matrix lacks a coherent interlocking mechanism. The pseudo-cohesion of the iron oxides is insufficient to maintain a stable power-law relationship under active traffic loads.

The bivariate logarithmic regression (Figure 4.43) visualizes this phenomenon. The pronounced data scatter, particularly in CP1, proves that the previously observed mathematical stability was heavily dependent on states of high lateral pressure.

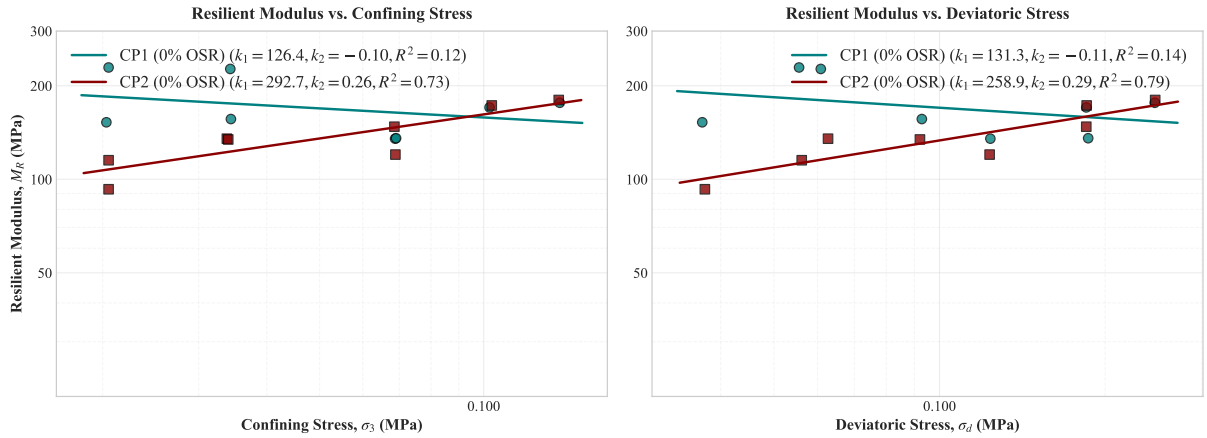


Figure 4.43: Filtered 1D Bivariate sensitivity models for natural Brasília soil (0% OSR) demonstrating data scatter under realistic shear conditions.

Ultimately, this filtered analysis confirms that the *in natura* SG-12 soil, while macroscopically stable, is highly susceptible to shear and heavily reliant on deep confinement to maintain rigidity. It is inherently unsuitable for the dynamic, unconfined demands of upper pavement layers. This vulnerability establishes the fundamental engineering justification for incorporating Ornamental Stone Residue (OSR): to introduce the necessary frictional interlocking and structural stability that the natural tropical soil inherently lacks when sheared.

4.2.2 - EVALUATION OF RESILIENT BEHAVIOR: BRASÍLIA SOIL (SG12) - 5% OSR CONTENT

The incorporation of 5% Ornamental Stone Residue (OSR) into the Brasília lateritic soil triggers a fundamental shift in the material's mechanical response. While the natural soil exhibited rheological instability under realistic stress states, the stabilized mixture demonstrates a highly predictable and statistically robust behavior, providing the necessary consistency for mechanistic-empirical pavement design.

The individual 3D surfaces (Figure 4.44) reveal a remarkable synchronization of the resilient response. Unlike the divergent behavior seen in the natural soil, all three specimens now follow a consistent *decreasing stiffness* trend, with k_3 parameters ranging from -0.278 to -0.846. This convergence indicates that the OSR fines have successfully homogenized the matrix, establishing a dominant granular skeleton that suppresses the unpredictable "bipolarity" of the original lateritic structure.

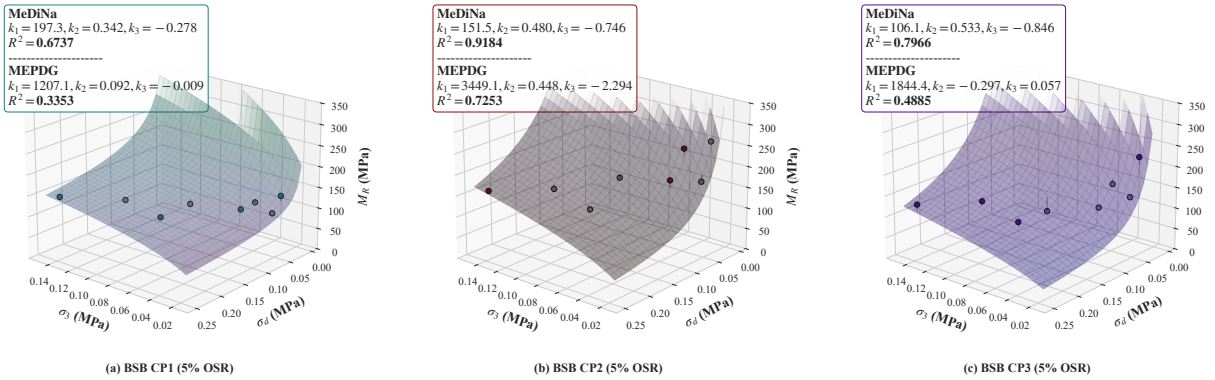


Figure 4.44: Filtered 3D Resilient Modulus models ($\sigma_d \geq \sigma_3$) for Brasília soil with 5% OSR: (a) specimen CP1; (b) specimen CP2; (c) specimen CP3 (6-month storage).

The filtered average model (Figure 4.45) synthesizes this structural improvement, achieving a robust coefficient of determination ($R^2 = 0.8710$). This represents a massive statistical upgrade from the natural soil's baseline ($R^2 \approx 0.06$). The stabilization of the k_1 parameter at 144.9, combined with a significant confining sensitivity ($k_2 = 0.469$), confirms that the mixture is now a reliable engineering material with predictable stiffness thresholds.

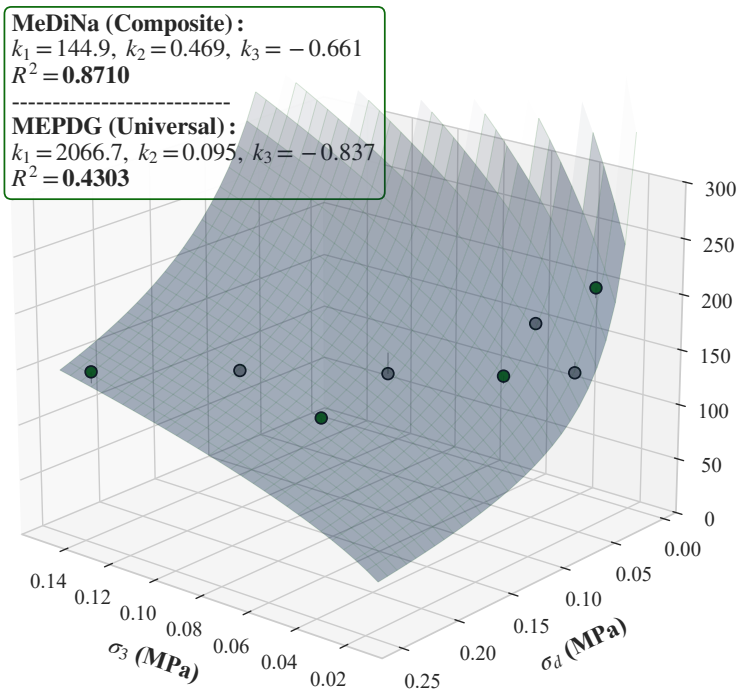


Figure 4.45: Average Resilient Modulus 3D surface for Brasília soil (5% OSR) demonstrating a high coefficient of determination ($R^2 = 0.8710$).

Rheological Transition and the "Filler Effect"

The diagnostic slices (Figure 4.46) highlight the global gain in stiffness. Under structural confinement ($\sigma_3 = 0.07$ MPa), the mixture maintains a Resilient Modulus between 140 and 160 MPa even at the highest deviatoric stresses. This performance confirms the success of the residue as a "filler" agent, densifying the matrix and optimizing inter-particle contacts.

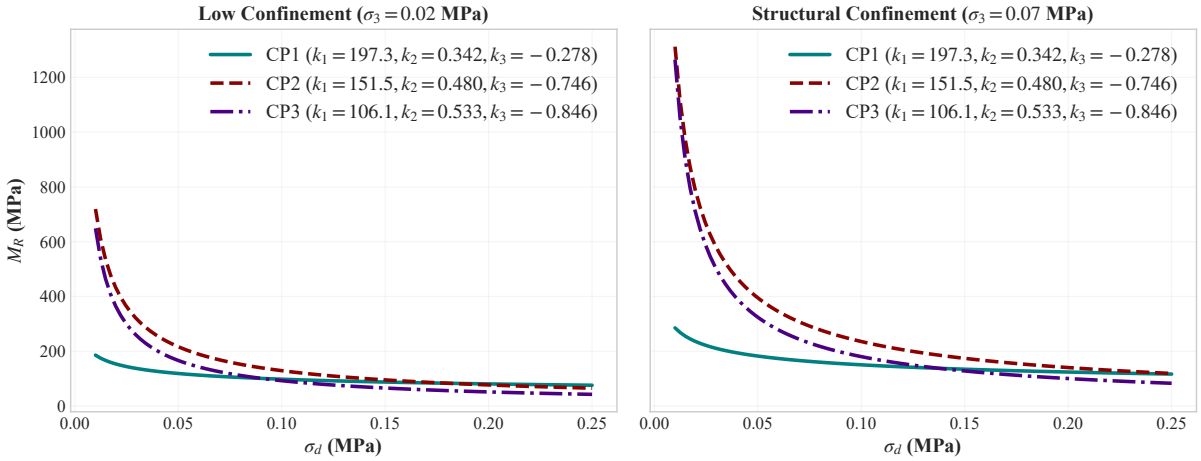


Figure 4.46: Linear evaluation of the Brasília soil-OSR mixture (5% OSR) stiffness sensitivity to stress changes at low (0.02 MPa) and structural (0.07 MPa) confinement levels.

The transition from the natural soil's erratic response to the stabilized mixture's parallel (MR) decreasing stiffness curves suggests that the OSR matrix mitigates shear degradation. Although the material still exhibits *decreasing stiffness*, the decay rate is uniform and controlled, suggesting that the rigid skeleton resists deformation up to a well-defined yield point.

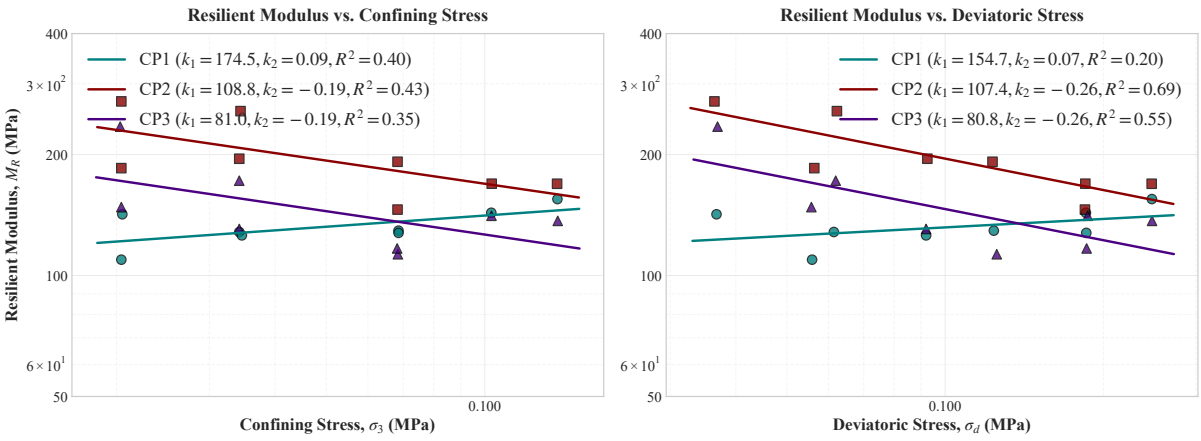


Figure 4.47: 1D Bivariate sensitivity models for Brasília soil (5% OSR) confirming strong correlation with shear and confinement in the logarithmic domain.

Temporal Stability and Infrastructure Application

The evaluation of specimen CP3, tested after 6 months of material storage, provides critical insights into temporal stability. Despite the storage period, the OSR's stabilization potential remained latent. CP3 achieved a consistent R^2 of 0.796, with stiffness levels equivalent to those of fresh specimens. This implies that OSR-soil mixtures are less sensitive to laboratory handling delays than initially assumed, maintaining their void-filling and granular-locking capacity.

Mechanistically, while the mixture's modulus drops at high deviatoric stresses, it excels in deeper structural layers. As a sub-base or subgrade reinforcement, where traffic stresses are dissipated and geostatic confinement prevails, the 5% OSR mixture operates at its peak efficiency. It delivers high support capacity without the risk of abrupt shear failure, making it an ideal candidate for sustainable infrastructure under DNIT standards.

4.2.3 - EVALUATION OF RESILIENT BEHAVIOR: BRASÍLIA SOIL (SG12) - 10% OSR CONTENT

The analysis of the 10% Ornamental Stone Residue (OSR) mixture introduces a critical validation of the geomechanical filtering approach ($\sigma_d \geq \sigma_3$). Preliminary evaluations using standard, unfiltered AASHTO sequences erroneously suggested a structural catastrophe, where the stiffness gains achieved at 5% OSR appeared to be completely lost. However, isolating the realistic shear-dominant stress states reveals that the 10% mixture maintains a reasonably stable mechanical performance, free from the artificial stiffening caused by excessive hydrostatic confinement.

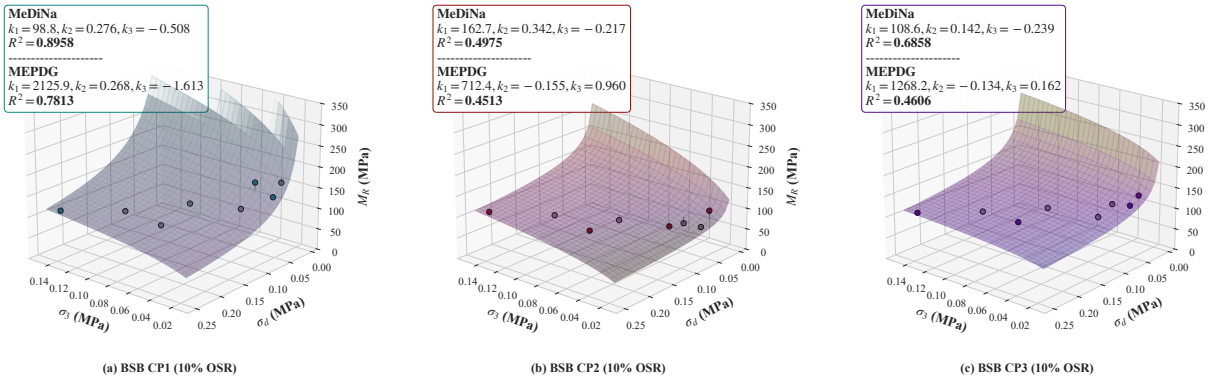
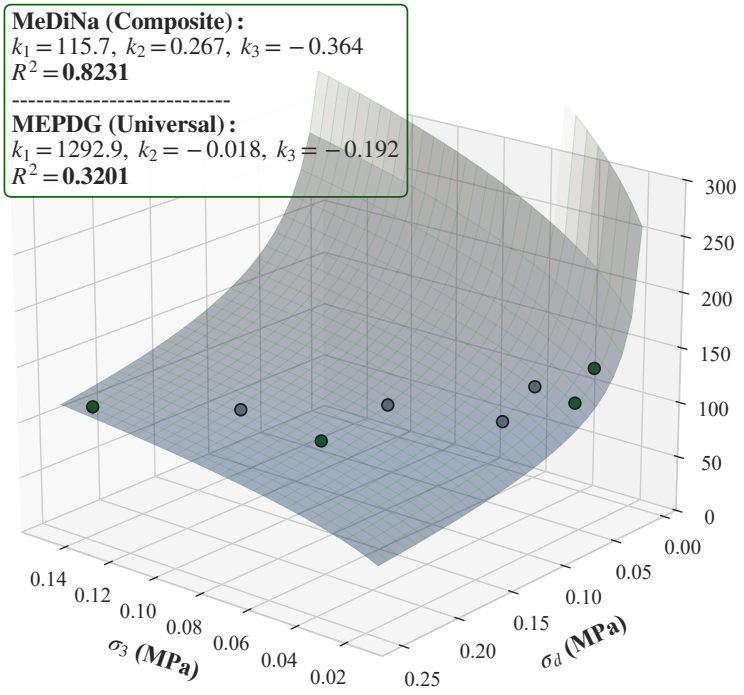


Figure 4.48: Filtered 3D Resilient Modulus models ($\sigma_d \geq \sigma_3$) for Brasília soil with 10% OSR: (a) specimen CP1; (b) specimen CP2; (c) specimen CP3.

The individual 3D surfaces (Figure 4.48) demonstrate that the material's structural integrity is preserved. The filtered average model (Figure 4.49) establishes a robust composite coefficient of determination ($R^2 = 0.8231$). It yields a k_1 parameter of 115.7, a confining

sensitivity (k_2) of 0.267, and a shear degradation parameter (k_3) of -0.364. These parameters confirm that the matrix does not collapse under traffic loads but instead undergoes a predictable *decreasing stiffness* process, highly suitable for mechanistic-empirical design using MeDiNa.



Average Resilient Modulus: BSB (10% OSR) [Filtered]

Figure 4.49: Average Resilient Modulus 3D surface for Brasília soil (10% OSR) demonstrating sustained statistical reliability ($R^2 = 0.8231$).

Stiffness Magnitudes and Rheological Consistency

A key finding lies in the absolute magnitude of the Resilient Modulus (M_R). As observed in the diagnostic slices (Figure 4.50), at intermediate deviatoric stresses (around 100 kPa), the material sustains an M_R between 120 and 150 MPa. This behavior practically mirrors the high-performance threshold established by the 5% OSR mixture.

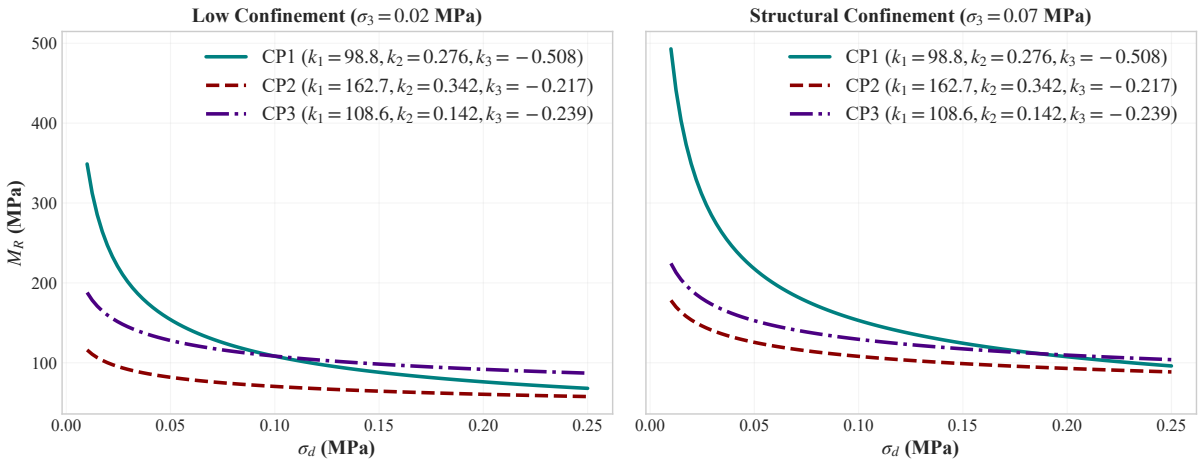


Figure 4.50: Linear evaluation of the Brasília soil-OSR mixture (10% OSR) stiffness sensitivity to stress changes at low (0.02 MPa) and structural (0.07 MPa) confinement levels.

When subjected to maximum deviatoric stresses (σ_d approaching 250 kPa), the modulus exhibits a controlled decline, settling into a lower plateau between 70 and 100 MPa. This gradual yielding—rather than an abrupt structural failure—reinforces the efficacy of the OSR as a stabilizing filler. The matrix accommodates the high shear stresses by allowing internal micro-sliding while preventing a total loss of bearing capacity.

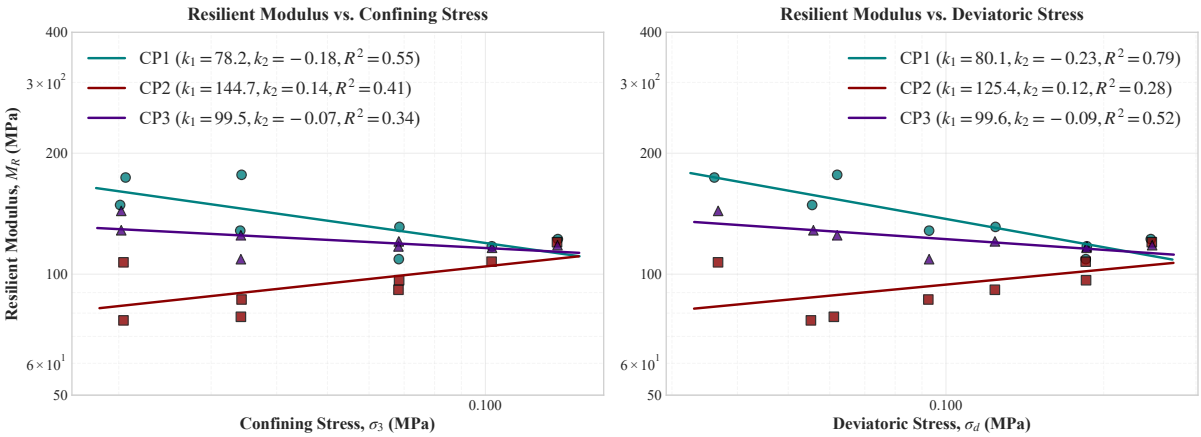


Figure 4.51: 1D Bivariate sensitivity models for Brasília soil (10% OSR) under realistic shear conditions.

Bivariate Analysis and Matrix Transition

The 2D Log-Log Bivariate Regression (Figure 4.51) provides further micromechanical insight. In the $M_R \times \sigma_d$ relationships, the well-defined negative slopes (with R^2 reaching up to 0.79 for CP1) mathematically visualize the consistent *decreasing stiffness* signature.

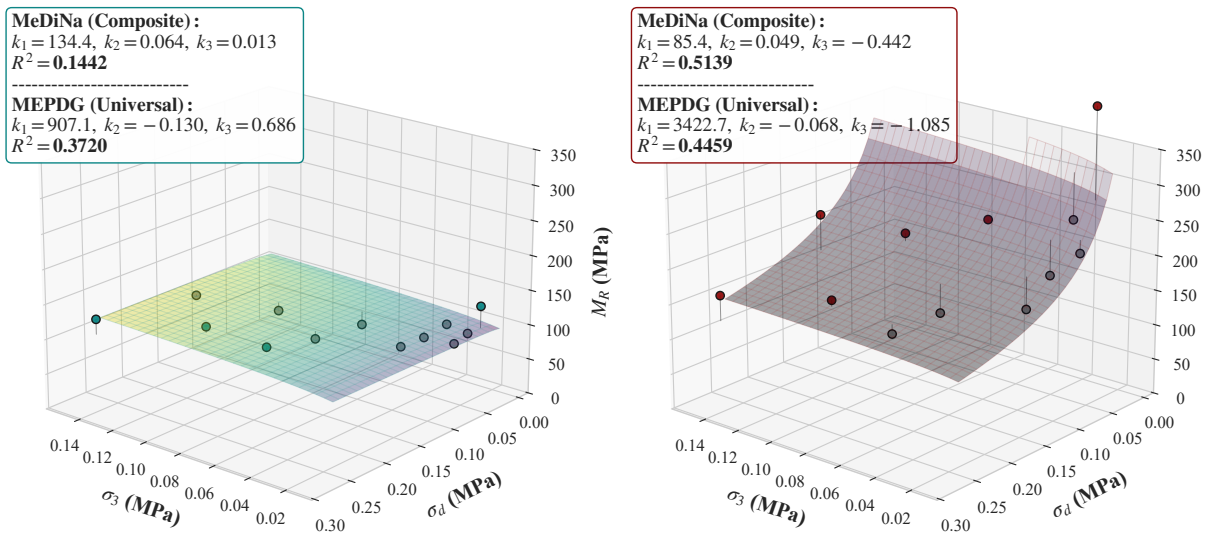
Interestingly, the scatter observed in the confining stress plots ($M_R \times \sigma_3$) suggests that

at 10% OSR, the micromechanical arrangement of the material begins to transition. The volume of non-plastic fines (OSR) starts to compete with the natural lateritic matrix, slightly reducing the material's ability to gain stiffness purely from lateral pressure compared to the 5% dosage (evidenced by the drop in the average k_2 from 0.469 to 0.267).

Nevertheless, the 10% OSR mixture remains a highly viable infrastructure geomaterial. Its behavior confirms that, provided it is shielded from the highest surface stresses (i.e., allocated to sub-base or subgrade reinforcement layers), it delivers a stable, predictable, and resilient foundation. The geomechanical filter successfully proved that the assumed "catastrophe" was an artifact of unrealistic testing conditions, unveiling a robust and functional 10% OSR matrix.

4.2.4 - EVALUATION OF RESILIENT BEHAVIOR: BRASÍLIA SOIL (SG12) - 15% OSR CONTENT

The geomechanical evaluation of the 15% Ornamental Stone Residue (OSR) mixture provides a critical milestone in understanding the saturation threshold of the "filler effect". With the application of the realistic stress filter ($\sigma_d \geq \sigma_3$), the potential structural catastrophe induced by unrepresentative high-confinement laboratory conditions was completely bypassed. However, the data reveals that at 15% substitution, the material enters a new micromechanical state, characterized by a complex interaction between the natural lateritic matrix and the high volume of non-plastic rock fines.



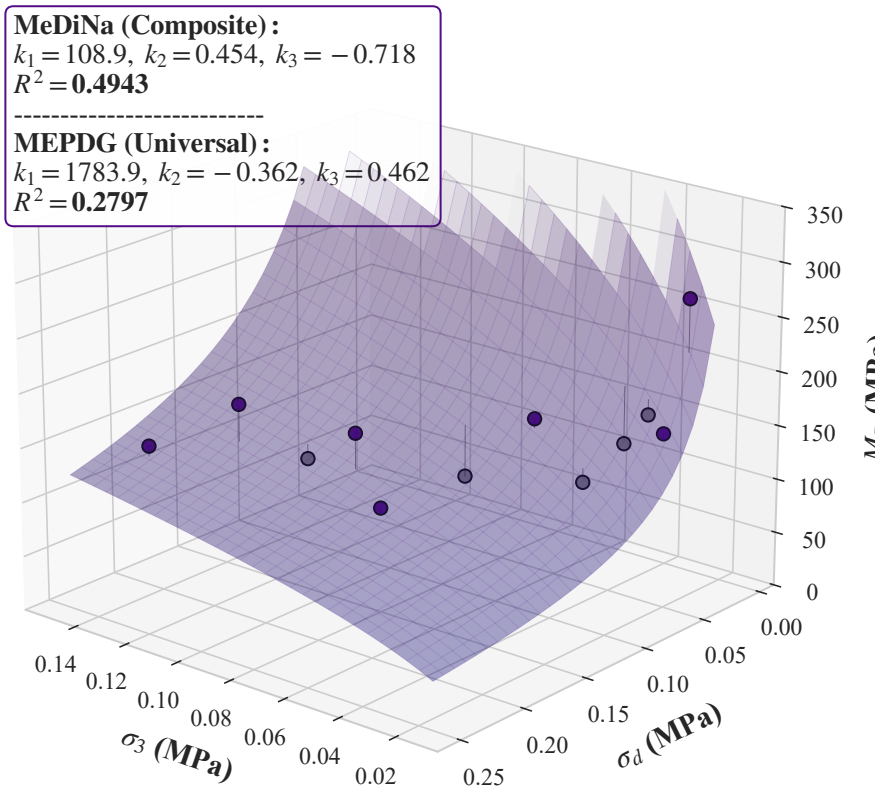
(a) AASHTO - BSB CP1 (15% OSR)

(b) AASHTO - BSB CP2 (15% OSR)

Figure 4.52: Filtered 3D Resilient Modulus models ($\sigma_d > \sigma_3$) for Brasília soil with 15% OSR: (a) specimen CP1; (b) specimen CP2.

The individual 3D surface models (Figure 4.52) immediately highlight a profound

rheological divergence between the specimens, reminiscent of the "bipolarity" observed in the natural soil (0% OSR). Specimen CP1 exhibits an almost entirely flat response, with a highly rigid base but minimal sensitivity to both confinement ($k_2 = 0.064$) and shear ($k_3 = 0.013$), resulting in a low coefficient of determination ($R^2 = 0.1442$). Conversely, specimen CP2 re-establishes a strong *decreasing stiffness* curve ($k_3 = -0.442$, $R^2 = 0.5139$), heavily influenced by the applied deviatoric load.



Average Resilient Modulus: Soil BSB & 15% OSR Content [Filtered]

Figure 4.53: Average Resilient Modulus 3D surface for Brasília soil (15% OSR) demonstrating the structural compromise of the mixture.

The average regression model (Figure 4.53) synthesizes this transitional state. The composite MeDiNa model yields a moderate fit ($R^2 = 0.4943$) with $k_1 = 108.9$, $k_2 = 0.454$, and a pronounced $k_3 = -0.718$. The recovery of the confining sensitivity (k_2) in the average model suggests that the mixture still relies on lateral pressure to lock the grains. However, the severe negative k_3 indicates that the lateritic pseudo-cohesion is no longer the primary support mechanism; the excess OSR fines act as a lubricant under high shear, causing the modulus to drop.

Rheological Transition: The Limits of the Filler Effect

The diagnostic *decreasing stiffness* slices (Figure 4.54) clearly depict the consequences of exceeding the optimal OSR content. At intermediate deviatoric stresses ($\approx$ 100 kPa), the Resilient Modulus sustains values around 100 to 120 MPa. While this still represents a functional material for sub-base layers, it is a definitive step down from the 140-160 MPa peaks observed at the 5% and 10% OSR dosages.

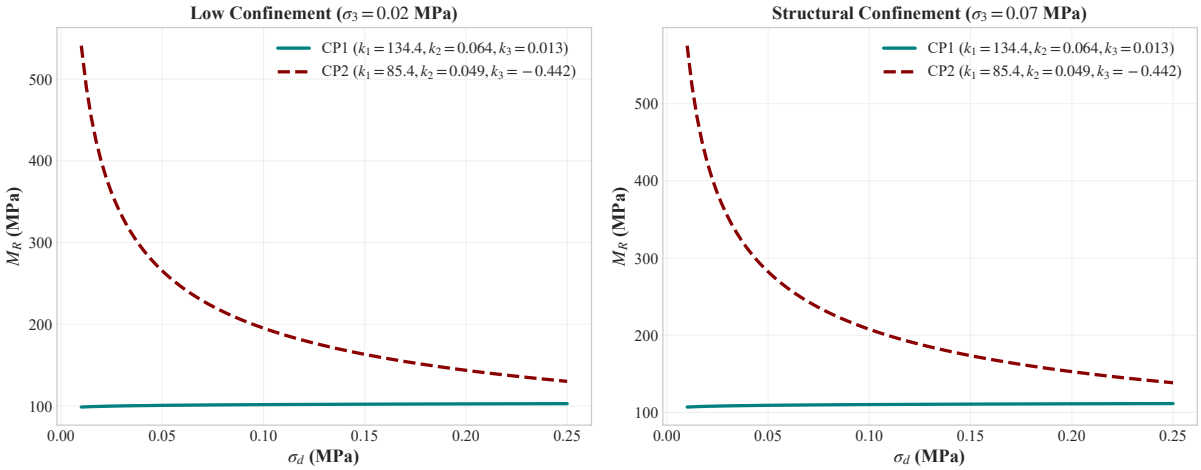


Figure 4.54: Revised linear decreasing (MR) stiffness analysis for Brasília soil (15% OSR) demonstrating the divergent behavior of the specimens.

The most critical insight is derived from the average composite model ($k_3 = -0.718$). Under maximum shear conditions (σ_d approaching 250 kPa), the average modulus declines sharply, reaching levels between 70 and 100 MPa. This behavior suggests that at a 15% substitution rate, the matrix reaches a "saturation point." At this stage, the OSR fines are no longer merely densifying the natural soil voids; instead, the excessive volume of non-plastic rock dust begins to physically separate the coarser soil aggregates. This phenomenon, known as matrix separation, causes the material to lose its effective structural interlocking, forcing it to rely almost exclusively on friction—a mechanism that is easily compromised under high dynamic loads.

Bivariate Diagnostics

The 2D Log-Log Bivariate Regression (Figure 4.55) provides mathematical confirmation of this structural instability. Unlike the 5% and 10% OSR mixtures, which maintained high statistical coherence, the 15% mixture displays significant data scatter.

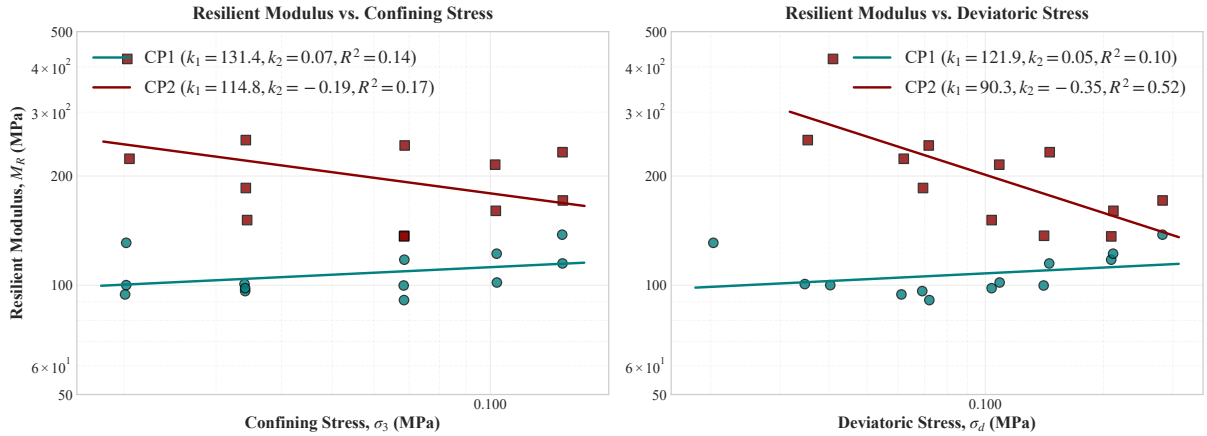


Figure 4.55: 1D Bivariate sensitivity models for Brasília soil (15% OSR) illustrating the breakdown of structural correlation.

In the $M_R \times \sigma_d$ relationship, the R^2 values drop notably (CP1 yielding only 0.14 and CP2 reaching 0.51), indicating that the power-law model struggles to capture a consistent rheological signature. Furthermore, the $M_R \times \sigma_3$ plots reveal that the material's sensitivity to confinement is erratic (k_2 values fluctuating between 0.06 and 0.45). This lack of correlation is the mechanical fingerprint of a saturated matrix: the material's response is no longer governed by a predictable granular skeleton, but rather by localized and unstable contact points within the excess fine-grained residue.

In conclusion, while the 15% OSR mixture is not a complete geomechanical failure—and could theoretically serve as a subgrade capping layer—it represents a point of diminishing returns. The optimal "filler effect" has been surpassed, replacing a reasonably stable, interlocked matrix of the 5% and 10% dosages with a friction-dependent system that is highly vulnerable to shear-induced decreasing stiffness.

4.2.5 - SATURATION THRESHOLD AND INFRASTRUCTURE PERFORMANCE: 30% OSR CONTENT

The analysis of the 30% Ornamental Stone Residue (OSR) mixture identifies the geomechanical saturation point for the Brasília (BSB) soil matrix. At this dosage, the mechanical identity of the host lateritic soil is effectively obliterated by the excessive volume of residue, leading to a response driven exclusively by the physical properties of the rock fines. As illustrated in the 3D surface (Figure 4.56), the original cohesive structure of the Brasília soil is disintegrated at 30% substitution.

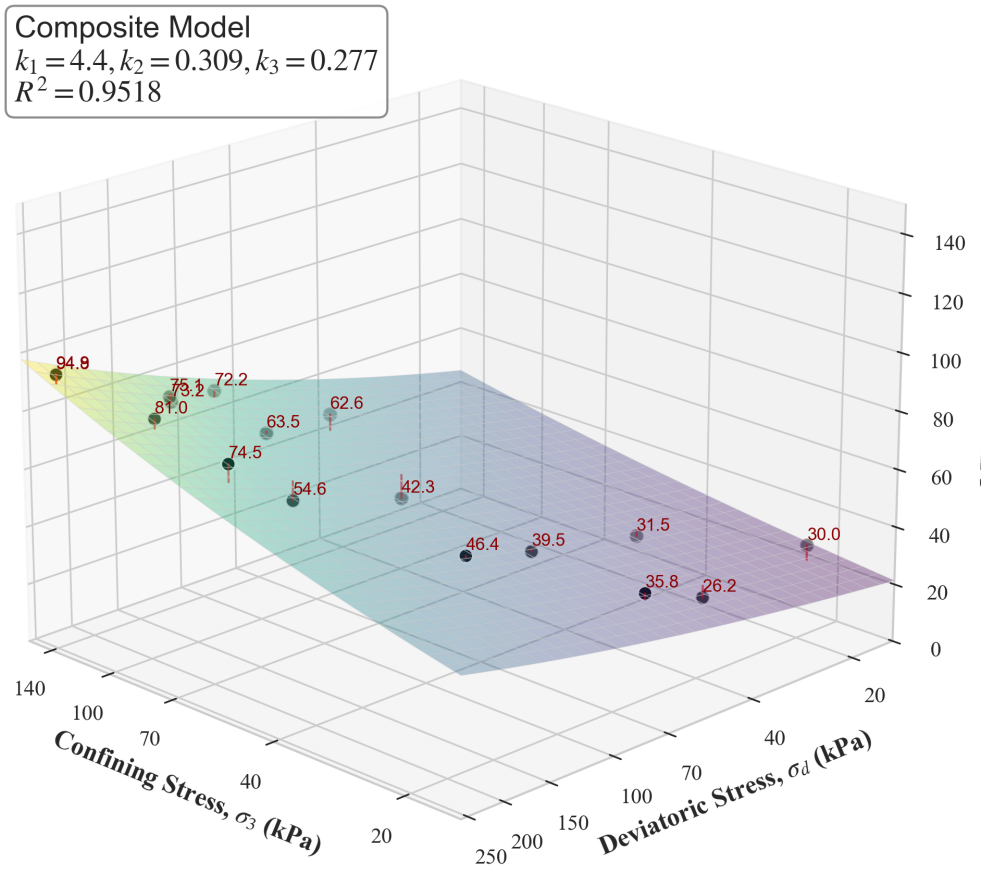


Figure 4.56: 3D Resilient Modulus surface for BSB soil at 30% OSR: The disintegration of the cohesive matrix leads to the "Floating Soil" phenomenon, with stiffness values stabilized at a lower baseline.

The "Floating Soil" Phenomenon and Structural Transition

The Resilient Modulus (M_R) values, which orbit between 30 and 120 MPa, confirm that the soil particles have transitioned to "float" within an inert mass of OSR silt. The drastic drop in stiffness compared to the 5% and 10% dosages renders the material insufficient for environments ubjected to high deviatoric stress bulbs.

Rheological Inversion: Transition to Increasing Stiffness ($k_3 > 0$)

A fundamental rheological shift occurs at this threshold. Unlike the natural soil and low-OSR mixtures, the stress slices and bivariate models (Figure 4.57) reveal an inversion in the shear sensitivity parameter. The material begins to exhibit *increasing stiffness* behavior ($k_3 > 0$), although this phenomenon develops at a much lower M_R level. This is the characteristic signature of non-cohesive granular materials, where stiffness gains depend strictly on the

increase of confining pressure and the micro-rearrangement of particles under cyclic loading.

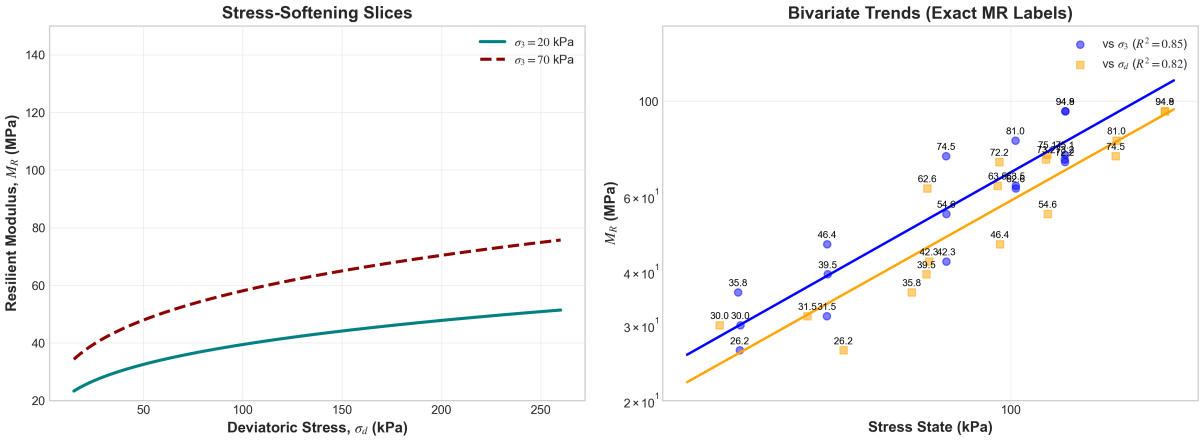


Figure 4.57: Mechanistic diagnostic of the 30% OSR BSB matrix: (left) Transition to increasing (MR) stiffness in 2D slices; (right) Bivariate Log-Log trends showing the dominant influence of stress states on the frictional matrix.

Strategic Re-evaluation: Infrastructure Viability and Environmental Impact

Despite the stiffness reduction for upper pavement layers, a contextualized geomechanical analysis reveals that the 30% OSR mixture reaches its peak technical and environmental viability when applied to deeper structural layers and embankment bodies:

1. **Geotechnical Benchmarking:** While 30–120 MPa is low for base courses, it represents superior performance for subgrades and reinforcement layers. Natural foundation soils in the region often operate in the 30–60 MPa range. Thus, 30% OSR provides a predictable, resonably more robust stiffness that exceeds *in natura* soil performance, especially under critical saturation conditions.

2. **Synergy with Geostatic Stress Fields:** At depths associated with embankment bodies, the observed *increasing stiffness* becomes a structural asset. The material gains stiffness under the weight of overlying layers, offering a stable, non-plastic platform that eliminates typical tropical subgrade pathologies such as excessive plasticity and volumetric expansion.

3. **The Road Prism as a Circular Economy Unit:** The 30% dosage allows OSR to transition from a stabilizing additive to a volumetric borrow-pit substitute. This proportion enables the massive sequestration of industrial waste, mitigating the environmental liability of the ornamental stone sector while reducing the pressure on natural borrow pits.

In conclusion, the 30% OSR content defines the *Point of Maximum Socio-Environmental Efficiency*. Although it marks the limit of efficiency for layers subjected to high deviatoric stresses, it qualifies the mixture as a **High-Performance Infrastructure Geomaterial**, reconciling mechanistic integrity with large-scale industrial waste recovery.

4.2.6 - SUMMARY OF CONSTITUTIVE PARAMETERS

Table 5.31 and Table 4.3 present the compiled non-linear regression parameters for the Composite Model (MeDiNa/DNIT) and the Universal Model (MEPDG), respectively, across all tested soils and OSR dosages.

Table 4.2: Summary of Non-Linear Parameters - Composite Model (MeDiNa/DNIT)

Soil	**% OSR**	**Specimen**	k_1	k_2	k_3	R^2	M_R **(MPa)***
BSB	0%	CP1	128.7	-0.021	-0.100	0.1496	185.1
BSB	0%	CP2	273.8	0.080	0.205	0.7963	112.5
BSB	**0%**	**Average**	**182.2**	**0.049**	**0.006**	**0.0660**	**147.9**
BSB	5%	CP1	197.3	0.342	-0.278	0.6737	113.2
BSB	5%	CP2	151.5	0.480	-0.746	0.9184	189.0
BSB	5%	CP3 (6 mo.)	106.1	0.533	-0.846	0.7966	142.5
BSB	**5%**	**Average**	**144.9**	**0.469**	**-0.661**	**0.8710**	**148.6**
BSB	10%	CP1	98.8	0.276	-0.508	0.8958	140.1
BSB	10%	CP2	162.7	0.342	-0.217	0.4975	78.6
BSB	10%	CP3	108.6	0.142	-0.239	0.6858	122.1
BSB	**10%**	**Average**	**115.7**	**0.267**	**-0.364**	**0.8231**	**113.4**
BSB	15%	CP1	134.4	0.064	0.013	0.1442	100.8
BSB	15%	CP2	85.4	0.049	-0.442	0.5139	239.3
BSB	**15%**	**Average**	**108.9**	**0.454**	**-0.718**	**0.4943**	**141.3**
VIX	0%	CP1	208.8	0.102	-0.006	0.2812	142.5
VIX	0%	CP2	87.1	0.345	-0.075	0.7700	27.9
VIX	**0%**	**Average**	**114.7**	**0.168**	**-0.078**	**0.7008**	**74.0**
VIX	10%	CP1	301.1	0.105	0.395	0.9795	65.7
VIX	10%	CP2	894.4	0.871	0.483	0.5491	7.6
VIX	**10%**	**Average**	**577.6**	**0.653**	**0.255**	**0.6120**	**21.9**
VIX	15%	CP1	84.9	0.029	-0.132	0.0768	109.9
VIX	15%	CP2	533.4	0.452	-0.002	0.2293	91.5
VIX	**15%**	**Average**	**288.6**	**0.412**	**-0.144**	**0.4057**	**86.4**
VIX	**30%**	**Single**	**242.4**	**0.135**	**0.469**	**0.9368**	**38.2**

* Reference M_R calculated for typical sub-base stress states: $\sigma_3 = 0.02$ MPa and $\sigma_d = 0.06$ MPa.

Table 4.3: Summary of Non-Linear Parameters - Universal Model (MEPDG)

Soil	**% OSR**	**Specimen**	k_1	k_2	k_3	R^2	M_R **(MPa)***
BSB	0%	CP1	2017.6	0.005	-0.408	0.1532	185.1
BSB	0%	CP2	973.3	0.135	0.445	0.7983	112.6
BSB	**0%**	**Average**	**1427.3**	**0.021**	**0.115**	**0.0665**	**149.3**
BSB	5%	CP1	1207.1	0.092	-0.009	0.3353	124.0
BSB	5%	CP2	3449.1	0.448	-2.294	0.7253	214.3
BSB	**5%**	**Average**	**2066.7**	**0.095**	**-0.837**	**0.4303**	**173.2**
BSB	10%	CP1	2125.9	0.268	-1.613	0.7812	151.5
BSB	10%	CP2	712.4	-0.155	0.960	0.4513	89.1
BSB	**10%**	**Average**	**1292.9**	**-0.018**	**-0.192**	**0.3201**	**124.6**
VIX	0%	CP1	1267.0	0.210	-0.845	0.4928	108.0
VIX	0%	CP2	4321.8	0.373	-0.145	0.7661	450.1
VIX	**0%**	**Average**	**2576.8**	**0.445**	**-0.590**	**0.7268**	**243.4**
VIX	10%	CP1	480.2	0.220	0.898	0.9688	63.0
VIX	10%	CP2	2100.3	1.056	2.263	0.5245	444.2
VIX	**10%**	**Average**	**1289.4**	**0.841**	**1.459**	**0.6038**	**215.7**
VIX	15%	CP1	1098.1	-0.179	0.431	0.0711	120.0
VIX	15%	CP2	978.1	0.803	-1.123	0.2846	86.1
VIX	**15%**	**Average**	**1107.9**	**0.606**	**-1.238**	**0.4851**	**91.7**
VIX	**30%**	**Single**	**297.6**	**0.260**	**0.850**	**0.9560**	**38.8**

4.2.7 - UCS TESTS: RESULTS ON SPECIMENS AFTER CLTT

This section investigates the effects of unconfined Compressive Strength (UCS) on soil properties by performing it on soil samples after the application of cyclic loading.

Certainly, after the MR results, the specimens will undergo materialized changes in soil structure (densification, particle rearrangement, degradation of cementation if applicable), changes in density and void ratio, generation or dissipation of pore pressure, and potential changes in matric suction (especially if drainage is not fully controlled or if there is evaporation).

Researchers have studied that performing UCS tests on soil samples after the application of cyclic loading (post-cyclic UCS tests) may reveal new characteristics. Therefore, it is appropriate to analyze how the post-cyclic UCS results are influenced by the cyclic stress level; e.g., different code procedures, such as the AASHTO and ABNT standards, apply different stresses, confinement stages, and number of cycles in the previous CLTT/RLTT tests. Other influencing factors include the initial soil state (moisture, density, suction) and the possible effects of damage (reduction of strength) versus densification or suction increase effects (increase of strength), referencing again the findings of Puppala et al. (2024).

The rate of permanent deformation (DP Rate) is directly related to the development of

rutting (Rutting Accumulation - RA) on the pavement surface, resulting from the accumulation of plastic deformations in the granular layers and the subgrade. Furthermore, the post-cyclic UCS is directly associated with the ultimate bearing capacity of the subgrade or unbound layers. It is relevant for predicting generalized shear failure under heavy loads, embankment slope instability, and/or localized failures at pavement edges, which depend on the intrinsic strength of the material after being conditioned by traffic and environmental conditions.

A material—whether a natural or recycled mixture—may exhibit an acceptable MR and DP rate, indicating a low risk of premature AC (Asphalt Concrete) fatigue and a low potential for rutting (RA), but displays a significant drop in post-cyclic UCS. This would signal a greater vulnerability to shear failure under heavier occasional loads or during periods of adverse environmental conditions (e.g., increased moisture that reduces suction and, consequently, actual field strength). Measuring post-cyclic UCS thus provides critical information about the potential for shear failure that is complementary and non-redundant with respect to MR and DP data.

For future research, a broad overview should identify the main input parameters derived from laboratory tests (CLTT/RLTT, UCS) that are used in pavement performance prediction models. This should focus on permanent deformation models (e.g., Shakedown theory, mechanistic-empirical models like those of MEPDG, stress/strain-based models) and models related to the bearing capacity and shear failure of the subgrade or granular layers.

Specifically, future studies should attempt to correlate or jointly use the data from the CLTT/RLTT tests (Resilient Modulus, permanent strain accumulation) and the data from the post-cyclic UCS tests. This joint approach aims to estimate parameters of permanent deformation models more accurately, assess the potential for shear failure or residual bearing capacity of the material after cyclic loading, and develop pavement performance indicators that combine information on cyclic stiffness (MR) and residual strength (post-cyclic UCS). Investigating whether the post-cyclic UCS offers additional or complementary information to the Resilient Modulus and permanent strain rate obtained in CLTT/RLTT for performance prediction—especially in relation to different pavement failure mechanisms (e.g., rutting vs. general subgrade failure)—would significantly improve accuracy in the fatigue prediction of pavement layers.

The UCS test results performed in this research are presented in Figures 4.58, 4.59, 4.60, and 4.61.

When comparing static and cyclic loading, the key difference lies in how the soil-OSR mixture behaves under static (UCS) versus cyclic (MR) conditions. OSR enhances the soil's resistance to static failure but may compromise its elastic response and stiffness under repeated loads.

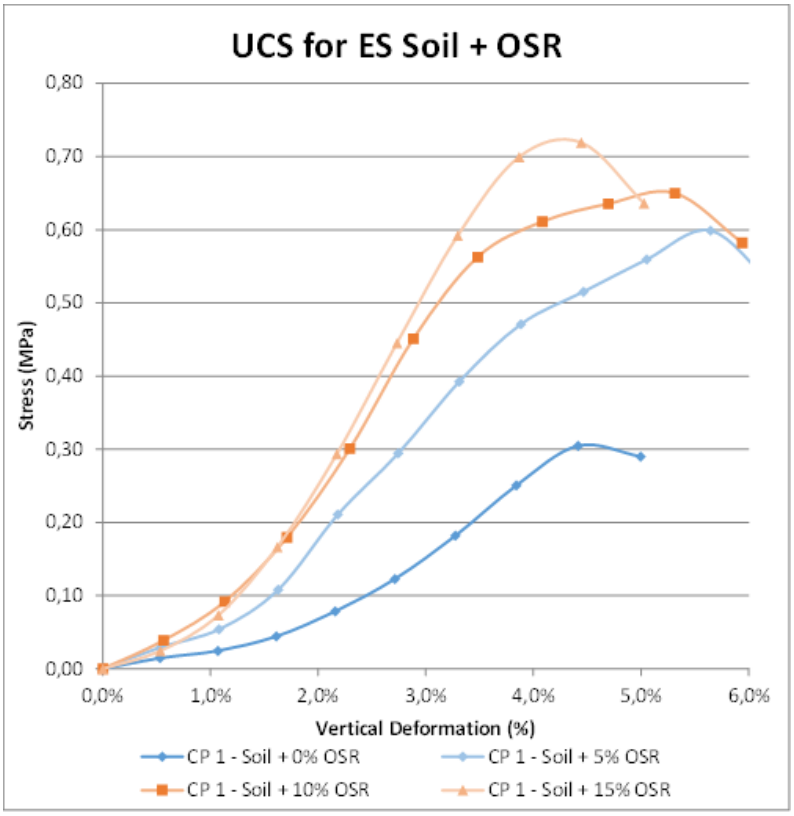


Figure 4.58: Post-cyclic UCS test results for the Vitória soil mixtures (Set 1).

Possible explanations for this behavior rely on several factors:

- **Confining Stress:** The UCS test is an unconfined test (no confining pressure), whereas the MR test is a triaxial test that applies confining stress. The presence of confining stress in the MR test might influence how the OSR affects the soil structure and its subsequent deformation.
- **Particle Arrangement:** This concept may play a significant role. OSR particles, characterized by their angularity and high friction, might contribute to a more interlocked structure that enhances static compressive strength. However, under cyclic loading, this interlocked structure might not be as effective in preventing deformation, or the OSR might even disrupt the soil matrix's ability to respond elastically.
- **Deformation Mechanisms:** These represent another critical aspect to be investigated, considering that the failure mechanism in UCS (shearing and macroscopic collapse) differs fundamentally from the deformation mechanisms in MR (elastic deformation and rebound). Consequently, OSR might influence these distinct mechanisms in fundamentally different ways.

For the Vitória (ES) soil, OSR addition has divergent effects on compressive strength (UCS)—repeating a similar behavior observed in CBR tests—as opposed to its effect on

stiffness (MR). While OSR significantly improves the soil's ability to withstand static compressive loads, it can reduce its stiffness and increase deformation under repeated cyclic loads, especially at higher OSR percentages.

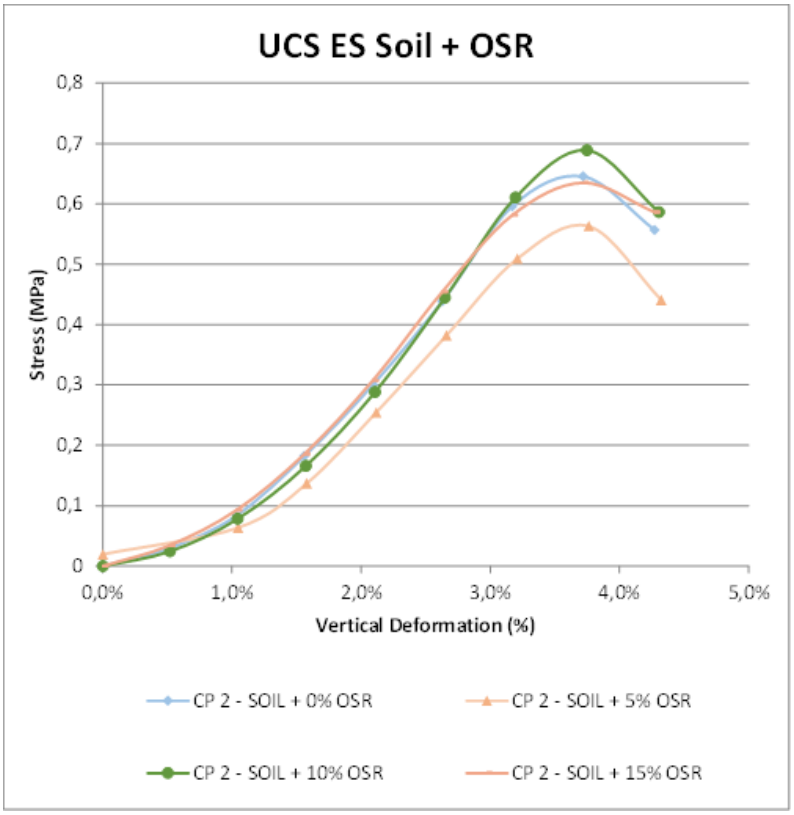


Figure 4.59: Post-cyclic UCS test results for the Vitória soil mixtures (Set 2).

This suggests that while OSR can be highly beneficial for applications where compressive strength is critical, it requires careful consideration in applications where stiffness and resistance to cyclic deformation are paramount, such as pavement subbases, even though the decrease in MR with respect to OSR addition is relatively slight.

As observed in Set 1 of the UCS trends (Figure 4.60) for the Brasília soil, the control specimen (0% OSR) exhibits a baseline UCS of approximately 0.3 MPa. With a 5% OSR addition, the UCS increases significantly, doubling to about 0.6 MPa. For the specimen with 10% OSR, the UCS continues to rise, reaching values around 0.65 MPa. Finally, the specimen with 15% OSR achieves the highest strength, reaching approximately 0.7 MPa. Even though the studied soils are completely different in terms of geology, mineralogy, and other geotechnical aspects, the sequential addition of 5%, 10%, and 15% OSR has shown a unique and consistent sequence of strength improvements.

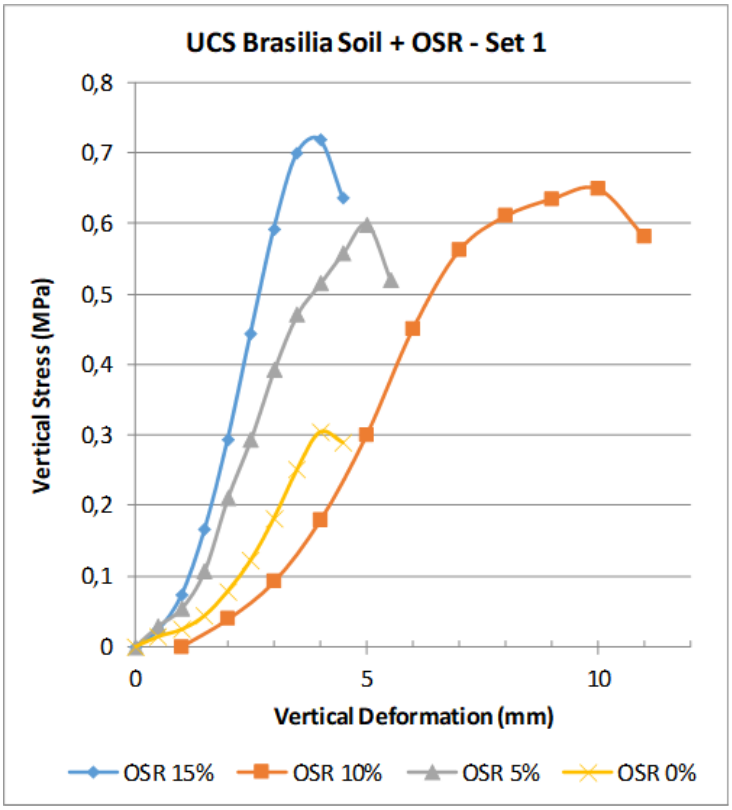


Figure 4.60: Set 1 of post-cyclic UCS trends for the Brasília soil with varying OSR percentages (0%, 5%, 10%, and 15%).

Similarly, Set 2 of the UCS trends (Figure 4.61) for the Brasília soil reveals that the control specimen (0% OSR) maintains the baseline UCS of roughly 0.3 MPa. Upon the addition of 5% OSR, the UCS more than doubles, reaching approximately 0.68 MPa.

The specimen with 10% OSR exhibits a comparable strength gain, plateauing near 0.68 MPa as well. For the 15% OSR mixture, the UCS continues its upward trend, peaking at the highest recorded value of around 0.7 MPa. Despite the Vitória and Brasília soils being completely distinct in their geology, mineralogy, and overall geotechnical behavior, the progressive addition of 5%, 10%, and 15% OSR yields a remarkably consistent sequence of strength enhancements across both materials.

Table 4.4 presents a comprehensive summary of the Unconfined Compressive Strength (UCS) test results for the ES soil specimens blended with varying percentages of OSR. A critical aspect of this experimental phase was the implementation of a rigorous moisture control protocol to ensure the validity, reliability, and repeatability of the mechanical responses. The table meticulously details the optimum water content (W_{ot}), the actual moisture content at the time of specimen molding, and the final moisture content recorded immediately after the testing procedure.

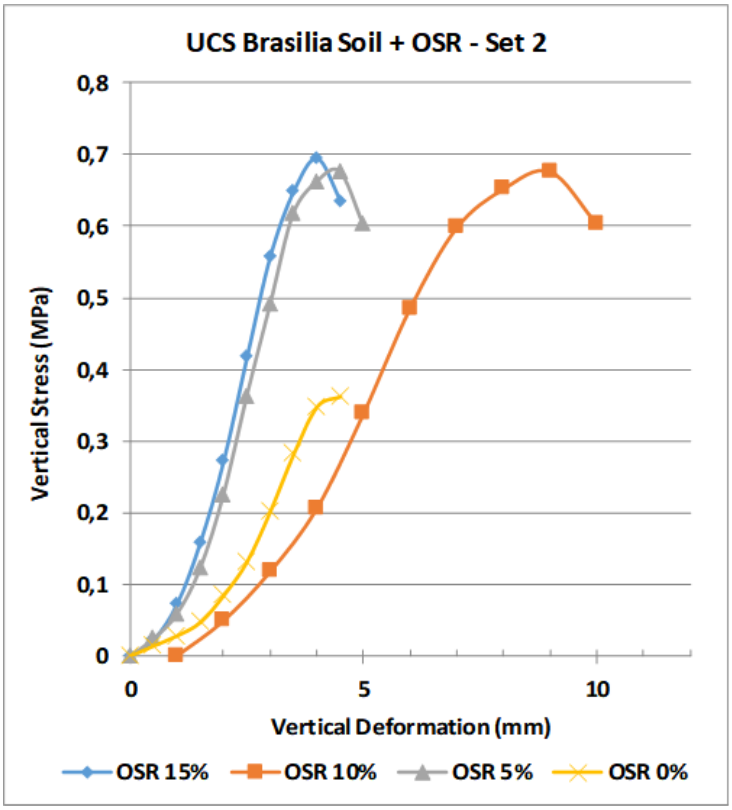


Figure 4.61: Set 2 of post-cyclic UCS trends for the Brasília soil with varying OSR percentages (0%, 5%, 10%, and 15%).

The data demonstrates a tight correlation between the target molding moisture and the actual experimental conditions, with the overall moisture reduction remaining closely monitored and constrained. This strict adherence to moisture tolerances is fundamental; it confirms that the observed variations in the ultimate shear strength (Stress) and corresponding strain at failure (Def) are directly attributable to the geomechanical and microstructural influence of the incorporated residues, rather than spurious moisture fluctuations. Consequently, this high level of preparative control substantiates the structural gains reported for the stabilized mixtures and validates the mechanical characterization of the proposed geomaterials.

This section presents a critical evaluation of the post-cyclic UCS results, considering the fundamental differences between static and cyclic loading protocols and their implications for mechanistic pavement design.The experimental data for both the Vitória (ES) and Brasília (SG-12) soils (Table 4.4) consistently demonstrate a progressive increase in unconfined compressive strength with the addition of Ornamental Stone Residue (OSR) up to 15%. The rigorous moisture control protocol detailed in Table 4.4—where final moisture reductions were tightly constrained—confirms that these strength gains are authentically derived from the microstructural densification and particle interlocking provided by the OSR, rather than spurious moisture fluctuations. However, interpreting these gains within the context of pavement engineering requires a clear distinction between the geomechanical mechanisms

activated in static versus cyclic testing. The UCS test imposes a purely vertical, unconfined stress field, pushing the material to large, irrecoverable macroscopic strains until a complete structural collapse (shear failure) is achieved.

Table 4.4: Unconfined compressive strength test results for the ES Soil

Soil + Residue	OSR	Wot	Molding	Final	Reduction	Stress (MPa)	Def (%)
CP1	0%	22.0%	23.6%	22.2%	6.0%	0.305	0.043
CP2	0%	22.0%	23.6%	22.5%	4.6%	0.645	0.037
CP1	5%	20.0%	20.7%	20.2%	2.4%	0.599	0.043
CP2	5%	20.0%	20.7%	20.3%	1.8%	0.565	0.037
CP1	10%	20.0%	20.6%	20.4%	0.8%	0.650	0.039
CP2	10%	20.0%	20.6%	20.3%	1.3%	0.690	0.038
CP1	15%	19.5%	19.6%	19.4%	1.2%	0.719	0.032
CP2	15%	19.5%	19.6%	19.5%	0.7%	0.640	0.037

In contrast, pavement layers operate under a dynamic, three-dimensional confined stress state, where traffic loads induce micro-strains, and the material's response is governed by its elastic stiffness (Resilient Modulus, MR) and its resistance to the accumulation of micro-plastic deformations over millions of cycles.The apparent discrepancy between the static and cyclic behavior—where OSR substantially improves UCS but can slightly reduce the MR at higher percentages—is a consequence of these differing stress paths. In the UCS test, the angularity and friction of the OSR fines create a highly interlocked skeleton that effectively resists static, unconfined shear failure, doubling the ultimate strength from approximately 0.3 MPa (0% OSR) to 0.7 MPa (15% OSR), despite the higher moiture content higher than the OMC. However, under the rapid, confined cyclic loading of the MR test, this dense, non-plastic packing may lack the necessary cohesion or elastic rebound capacity, leading to microscopic rearrangements and a comparatively lower dynamic stiffness.Therefore, while the post-cyclic UCS test might be a quality control parameter—confirming the physical consistency and macroscopic structural integrity of the stabilized matrix—it does not provide direct, scalable conclusions regarding the material's performance under actual traffic loads. The large strain levels associated with the UCS failure peak (the concave-down portion of the stress-strain curve) are orders of magnitude greater than the micro-strains experienced in a pavement subbase, which remain entirely within the initial, pre-yield convex portion of the loading ramp.To bridge this gap in future research and better correlate large-deformation behavior with confinement effects, monotonic (static) triaxial testing should be considered. By imposing varying levels of confining pressure (σ_3) during static loading, a static triaxial test would provide a more representative evaluation of the material's shear strength parameters (cohesion and friction angle) and its dilatancy under stress states that more closely resemble the operational conditions of a pavement structure.

In conclusion, the overall UCS trend for the Brasília and Espírito Santo soils demonstrates a consistent strength increase with the addition of OSR, yielding substantially and systematically higher compressive strength values compared to the control mixture (0% OSR).

4.3 - ESPÍRITO SANTO KRS-SOIL MIXTURES: ESTABLISHING THE CHEMICAL BASELINE

Following the mechanistic evaluation of OSR on tropical soils, in this stage investigating a typical binary soil-KRS system adopted in Espírito Santo in the last 10 years, with recent mechnistic investigation published by some authors such as Pires et al. (2019). Unlike the lateritic materials typically favored in Brazilian road engineering due to their superior performance, the soil selected for this phase was intentionally chosen for its **non-lateritic behavior**.

The underlying scientific strategy is to evaluate the potential for "upgrading" mechnistic performance of stabilization adopting Kambara Reactor Slag (KRS) mixed in soil, already known for its chemical interaction with clayey soils. Given that literature consistently reports significant relative strength gainsof theses soils with KRS, this research employs a more challenging, marginal soil matrix. The goal is to verify if the KRS-driven stabilization can elevate poor-quality, non-lateritic soils to performance levels comparable to those of stabilized lateritic materials.

4.3.1 - SOIL SELECTION (S1): NON-LATERITIC BEHAVIOR

The natural soil used in this study ($S1$) was collected from a borrow pit located in the Greater Vitória metropolitan area, Espírito Santo, Brazil. This site is geologically situated within the Barreiras Formation, a sedimentary unit that predominates along the entire state coastline. The extraction was performed at Horizon B, found immediately below the root zone at depths ranging from 2 to 20 meters, but typically found up to 5 meters. This layer consists of a leached, yellow clay, a distinct coloration resulting from its high aluminum oxide content. While the overlying layers were avoided due to excess of organic matter, this specific soil horizon represents the typical soil profile of the region.

According to the AASHTO M 145 classification, it is identified as A-7-6; complementary tests indicate that it is a non-lateritic clay Nogami & Villibor (1996). This soil is characterized as high-plasticity clay (CH) according to the USCS. Such characteristics make it poorly suited for earthworks in embankments and as a subgrade for pavement applications without stabilization, according to Brazilian, USA, and other international highway codes.

Figure 4.62 presents the comprehensive grain size distribution (GSD) curves for this $S1$ alongside the stabilizing KRS.

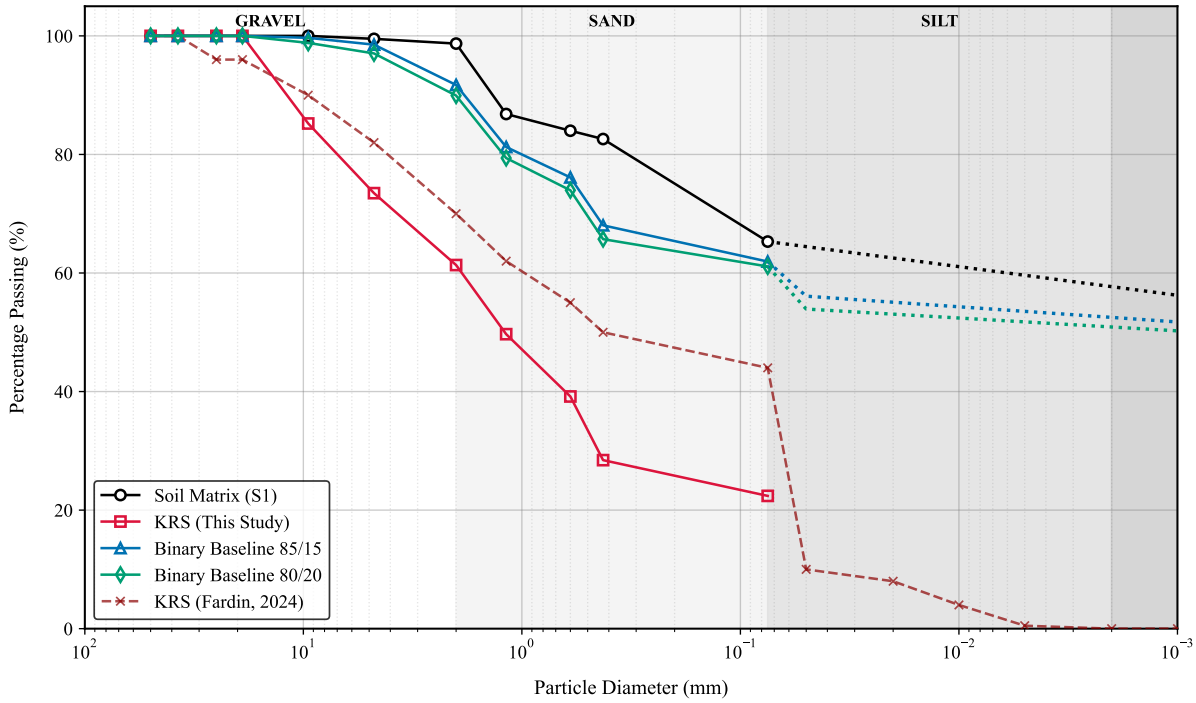


Figure 4.62: Grain size distribution (GSD) curves of the natural soil matrix (S1), the evaluated Steel Slag (KRS), binary baselines (85/15 and 80/20), and the reference KRS from Fardin (2024), highlighting the physical-chemical influence on the sedimentation tails.

4.3.2 - THE KAMBARA REACTOR SLAG (KRS)

TThe KRS utilized in this research was sourced directly from the ArcelorMittal Tubarão steel complex, located in the Greater Vitória industrial hub, Espírito Santo, Brazil. The selection of this stabilizer is driven by its massive industrial availability and the environmental urgency surrounding its management. According to the Statistical Report of the Brazil Steel Institute (IABr, 2024), Brazil produced approximately 25.8 million tons of pig iron in the last 12 months, a process that generated more than 5 million tons of KRS and other slags. While high-value applications are consolidating in Espírito Santo for other slags in the cement industry (such as GBF), other residues such as KRS still face limited use and low added value, since its pozzolanic activity does not reach the requirements to be adopted in Portland cement.

In the Espírito Santo steel hub, the continuous production of this slag results in vast storage piles that represent a significant environmental liability for the steel industry, while simultaneously offering a strategic, low-cost source of material for large-scale infrastructure projects. Characterization was prioritized for physical properties and index parameters directly relevant to soil stabilization. Figure 4.62 presents the GSD curves of this study KRS and the

one from Fardin (2024), indicating a material predominantly within the gravel and sand range, which provides a granular skeleton to enhance the clay's mechanical stability. The material's comprehensive geotechnical properties and its impact on the binary baseline are consolidated in the experimental matrix presented in Table 4.5.

4.3.3 - THE ORNAMENTAL STONE RESIDUE (OSR)

The OSR was incorporated as a granulometric skeleton corrector Prandina & Farias (2026). The OSR of this research was provided by Levantina Natural Stone Ltda., collected at the industrial plant in Serra, state of Espírito Santo (Figure 4.64a). To understand its physical grain size distribution, tests were conducted in two distinct states: with the use of a deflocculating agent to determine the true particle size, and without a deflocculant to observe natural particle aggregation. This dual characterization provides a fundamental observation for predicting how OSR fills the voids within the clay-KRS matrix Prandina & Farias (2025b). Figure 4.63 shows the GSD curves of the OSR collected for this study, and the basic geotechnical properties are presented in Table 4.5.

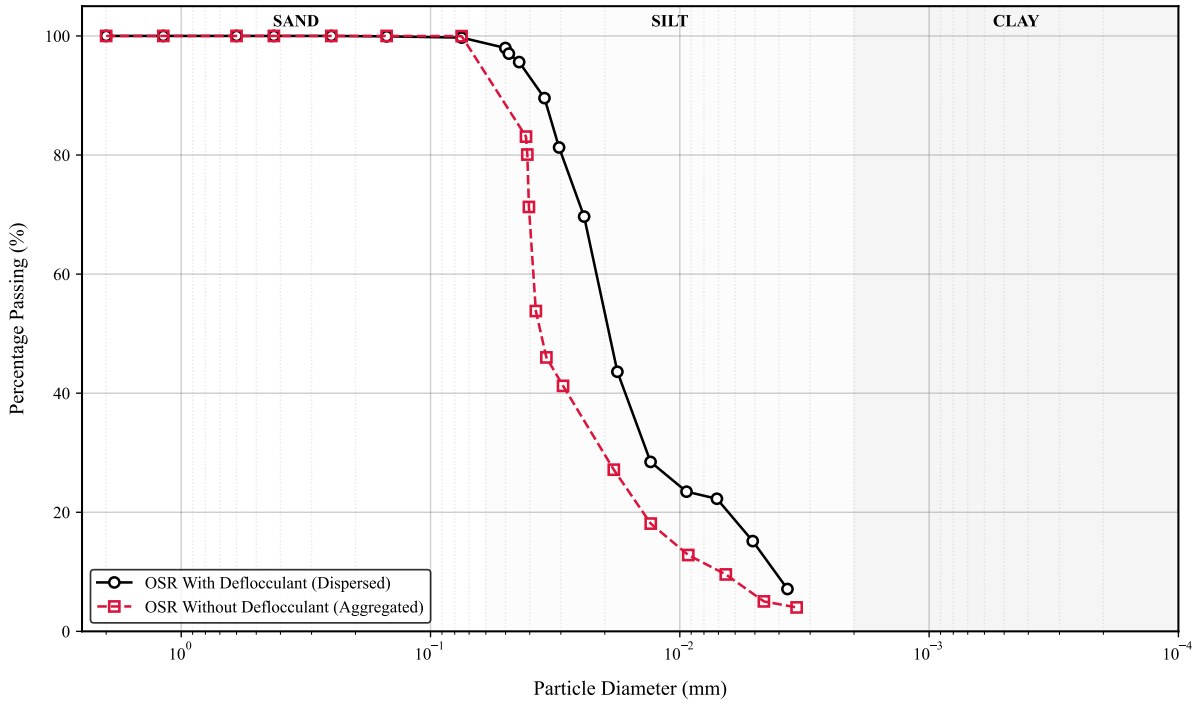


Figure 4.63: Grain size distribution (GSD) comparison of pure OSR: deflocculation sensitivity and particle aggregation analysis.

Analysis of the GSD curves (Figure 4.63) indicates that OSR serves as an effective mineral filler, optimizing particle packing by occupying voids. A distinct change in curvature (kink) was observed between the 200 sieve (0.075 mm) and the initial sedimentation phase (0̃.05



(a) (b)

Figure 4.64: Collection of the Ornamental Stone Residue (OSR) at the industrial plant: (a) general view of the filter press equipment; and (b) detail of the fresh residue discharge.

mm), highlighting a relative scarcity of coarse silt. In the ultra-fine range, the convergence of the curves—with and without the use of a deflocculant—suggests that the clay-sized fraction is not a result of particle aggregation, but rather a characteristic of the parent rock mineralogy (rock flour), which remains chemically inert regardless of the dispersing agent.

Table 4.5 summarizes the massive dataset of index, GSD, and compaction properties for the involved materials, as well as the CBR. The geotechnical characterization presented in Table 4.5 reveals a fundamental phenomenon regarding the chemical kinetics of the investigated mixtures. A primary observation concerns the Atterberg Limits of the binary systems (Soil-KRS). For all soil-slag combinations without the presence of OSR, the cationic exchange was found to be exceptionally aggressive. This "cationic shock" induces immediate flocculation of the clay particles, rendering the matrix Non-Plastic (NP) and Non-Liquid (NL). The reaction is so immediate that it becomes impossible to perform the standard thread-rolling for the Plastic Limit (PL) or to observe liquefaction in the Casagrande cup.

However, a significant and novel scientific finding emerged from the ternary mixtures: the simultaneous incorporation of OSR and KRS restored the feasibility of performing Atterberg tests. It is hypothesized that the OSR, acting as a high-silica and chemically inert filler, functions as a physical buffer that delays the onset of the explosive cationic exchange. This provides a temporal window for characterization, suggesting that the OSR optimizes the workability of the stabilized soil. This mitigation of the immediate chemical reaction by a mineral residue represents a unique contribution of this research, as it has not been previously documented in slag-stabilization literature.

Table 4.5: Comprehensive geotechnical characterization, compaction parameters, and mechanical performance (CBR and Expansion) for raw materials, binary baselines, and ternary mixtures.

Property /	**Raw Materials**			**Binary Baseline (85/15)**			**Binary Baseline (80/20)**			**Ternary Mixtures (4 days)**			
Parameter	**Soil**	**KRS**	**OSR**	**0d**	**4d**	**28d**	**0d**	**4d**	**28d**	**85/15+5%**	**85/15+10%**	**80/20+5%**	**80/20+10%**
GSD (%)													
Gravel ($>$ 2.0 mm)	1.3	38.7	0.3	1.23	1.26	1.96	2.73	2.90	3.24	1.60	2.61	4.22	2.97
Sand (2.0–0.075 mm)	33.4	42.2	5.1	36.23[b]	36.38[b]	37.17[b]	36.64[b]	34.28[b]	36.89[b]	41.26[b]	37.72[b]	40.88[b]	39.10[b]
Silt (0.075–0.002 mm)	22.4	19.1	92.6	28.4[a]	28.4[a]	28.4[a]	26.7[a]	26.7[a]	26.7[a]	3.64[c]	5.17[c]	16.74[c]	21.80[c]
Clay ($<$ 0.002 mm)	42.9	0.0	7.1	36.5[a]	36.5[a]	36.5[a]	34.3[a]	34.3[a]	34.3[a]	53.50[c]	54.50[c]	38.16[c]	36.13[c]
Atterberg Limits (%)													
Liquid Limit (LL)	55.5	NT	29.0	NL	NL	NL	NL	NL	NL	48.1	46.1	45.9	52.2
Plastic Limit (PL)	29.1	NT	26.0	NP	NP	NP	NP	NP	NP	30.9	26.2	29.6	29.3
Plasticity Index (PI)	26.4	NT	3.0	NP	NP	NP	NP	NP	NP	17.2	19.9	16.3	22.8
Classification													
SUCS	CH	GW-GM	ML	ML	ML	ML	ML	ML	ML	ML	CL	ML	MH
TRB (AASHTO)	A-7-6	A-1-a	A-4	A-4	A-4	A-4	A-4	A-4	A-4	A-7-5	A-7-6	A-7-6	A-7-6
Group Index (GI)	15	0	8	6	5	5	5	6	5	8	10	7	11
Compaction (Inter.)													
MDD (g/cm^3)	1.671	NT	1.469	1.771	1.802	1.763	1.746	1.743	1.769	1.747	1.726	1.737	1.741
OMC (%)	20.39	NT	23.47	18.43	19.73	19.04	17.98	19.26	19.55	18.84	19.02	19.05	18.60
Mechanical													
CBR (%)	7.9	NT	12.93	78.15	72.33	72.91	44.77	48.09	52.82	NT	NT	NT	NT
Expansion (%)	0.21	NT	1.32	0.04	0.07	0.05	0.22	0.11	0.19	NT	NT	NT	NT

Note: [a] Estimated based on soil proportion; [b] Sum of sand fractions; [c] Interpolated from sedimentation curve;
NT = Not Tested; NL = Non-Liquid; NP = Non-Plastic.

Regarding the mechanical characterization, all California Bearing Ratio (CBR) tests were performed strictly following the 96-hour soaking protocol. This procedure was adopted as a quality control measure to ensure that all mixtures achieved a consistent compaction performance and to simulate the most critical saturation scenario. Therefore, CBR values for the immediate (0-day) and long-term (28-day) stages of the binary baseline were intentionally kept as an assessment of the quality of the mixtures.

4.4 - PHASE I: BINARY BASELINE ANALYSIS (THE CHEMICAL PHASE)

While Kambara Reactor Slag (KRS) has been identified by previous authors as a high-performance chemical stabilizer, the specific mechanistic evolution and curing kinetics of binary soil-KRS systems remain sparsely documented in the literature. Understanding the temporal maturation of these mixtures was a fundamental prerequisite for defining the overarching research design and the selection of critical testing intervals. Therefore, this phase investigates the specific contribution of curing time—spanning from the immediate state (0 days) to the 28-day pozzolanic milestone. This characterization of the binary system's maturation stands as a novel contribution of this doctoral thesis in its own right, providing the essential framework to evaluate the efficiency of the subsequent ternary stabilization.

The evaluation of time-dependent strength gain is structured around the interaction between the proportions and the curing intervals (Table 4.6). Binary mixtures were evaluated at **0 (immediate), 4, and 28 days** of sealed curing. Ternary mixtures incorporating OSR were evaluated later on **exclusively at the 4-day curing period** to verify if the physical filler effect could immediately outperform the chemical gains observed in the binary baseline.

Table 4.6: Experimental matrix: Curing periods and testing protocols.

Mixture ID	Soil:KRS Ratio	Curing (Days)	Test Performed
85/15-0d	85:15	0	CBR (Immediate) and M_R
85/15-4d	85:15	4	Resilient Modulus (M_R)
85/15-28d	85:15	28	Resilient Modulus (M_R)
80/20-0d	80:20	0	CBR (Immediate) and M_R
80/20-4d	80:20	4	Resilient Modulus (M_R)
80/20-28d	80:20	28	Resilient Modulus (M_R)

4.4.1 - STRUCTURAL BENCHMARK, DATA CURATION, AND CURING PROTOCOL

A preliminary assessment of the empirical bearing capacity, summarized in Table 4.5, immediately highlights the stabilizing potential of the KRS. The natural Barreiras soil (S1) exhibited a California Bearing Ratio (CBR) of merely 7.9%, strictly limiting its use to subgrade

applications. However, the binary stabilization promoted a systematic multiplication of the bearing capacity. Notably, the 85/15 mixture reached CBR values ranging from 72% to 78% across all curing ages, successfully surpassing the 60% minimum threshold required by the Brazilian DNIT guidelines for flexible pavement base layers. While empirical indices validate the mixture's applicability, transitioning to modern mechanistic-empirical design requires a fundamental understanding of how this matrix responds to dynamic stresses over time.

To establish a reliable mechanistic baseline, the Resilient Modulus (M_R) data acquired from the 6 specific test series were subjected to rigorous statistical and technical filtering. Dixon's Q-Test was applied to identify potential outliers among the stiffness intercepts (k_1) using a 90% confidence level ($Q_{crit} = 0.941$ for $n = 3$), exemplified by Figure 4.65 in the set of 3 M_R tests conducted for the 85/15 soil-KRS mixture.

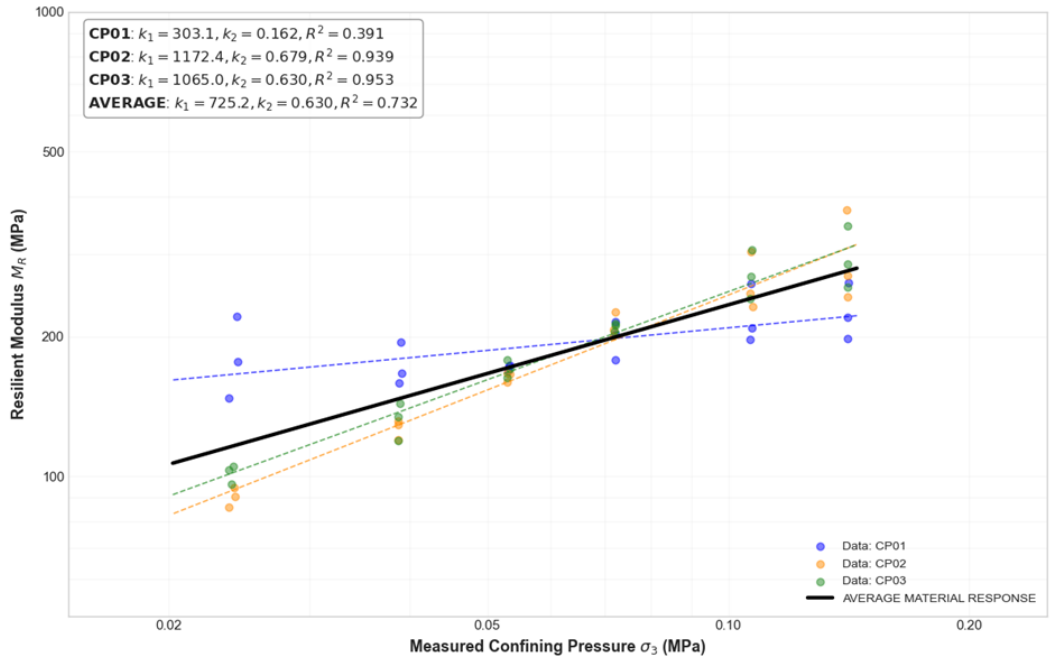


Figure 4.65: Resilient Modulus (M_R) of Binary 85/15 (Soil-KRS) mixture at 0 days of curing (immediate state).

Table 4.7 details the molding parameters and regression constants for each individual specimen tested at age 0. To evaluate the statistical consistency of the structural stiffness within these groups, Dixon's Q-Test was applied to the k_1 (stiffness intercept) parameters. The results of this statistical analysis are presented in Table 4.8, which assesses whether any specific specimen significantly deviates from the sample group using a 90% confidence level. The statistical consistency of the k_1 (stiffness intercept) parameters for each mixture at age 0 was evaluated through Dixon's Q-Test, as summarized in Table 4.8. This analysis identifies whether any specific specimen significantly deviates from the experimental group, employing a 90% confidence level ($Q_{crit} = 0.941$ for $n = 3$).

Table 4.7: Individual specimen molding parameters and regression constants for binary mixtures at 0 days.

Mixture Reference	Specimen (CP)	Molding Dry Density (g/cm^3)	Molding Moisture (%)	k_1	k_2	R^2
Mix 1 (85/15)	CP01	1.785	18.48	303.1	0.162	0.391
	CP02	1.784	19.64	1172.4	0.679	0.939
	CP03	1.779	19.05	1065.0	0.630	0.953
Mix 2 (80/20)	CP01	1.772	17.87	1517.6	0.865	0.952
	CP02	1.739	19.28	1084.5	0.637	0.957
	CP03	1.779	19.54	925.9	0.596	0.944

Table 4.8: Dixon's Q-Test for outlier identification (k_1 values) at a 90% confidence level.

Mixture	Sorted k_1 Values (MPa)	Suspected Outlier	Gap	Range	Q_{calc}	Q_{crit} (90%)	Statistical Result
85/15	303.1, 1065.0, 1172.4	303.1 (CP01)	761.9	869.3	0.876	0.941	Keep Specimen
80/20	925.9, 1084.5, 1517.6	1517.6 (CP01)	433.1	591.7	0.732	0.941	Keep Specimen

Statistical Interpretation and Technical Considerations

- **Statistical Keeping:** For both mixtures, the calculated value (Q_{calc}) is strictly lower than the critical value ($Q_{crit} = 0.941$). Therefore, mathematically, no specimen is identified as an absolute statistical outlier at a 90% confidence level.
- **85/15 Sensitivity and Data Refinement:** Although CP01 from the 85/15 mixture is statistically retained by the Q-Test, its Q_{calc} of 0.876 is perilously close to the critical limit. In the context of mechanistic pavement design, this provides a strong rationale to apply the *Geotechnical Consistency Criteria*. The exclusion of CP01 is therefore justified not purely by statistics, but by its poor regression quality ($R^2 = 0.391$) and severe mechanical inconsistency ($k_2 = 0.162$) when compared to its companion specimens.
- **80/20 Stability:** In contrast, the 80/20 mixture demonstrated high consistency. The Q_{calc} of 0.732 coupled with excellent R^2 values across all three specimens (CP01: 0.952; CP02: 0.957; CP03: 0.944) confirms that this higher-slag matrix is highly stable and that all tested specimens are representative of the material's true behavior.

Based on this critical data curation, Figure 4.66 presents the refined Resilient Modulus (M_R) chart for the 85/15 Binary Mixture, specifically excluding CP01. This refinement provides a more precise representation of the material's mechanical baseline by focusing exclusively on the specimens with superior regression quality ($R^2 > 0.90$) and consistent confining sensitivity. The average trend line is now calculated solely based on the combined data from CP02 and CP03, maintaining the 3% extension logic for visual clarity.

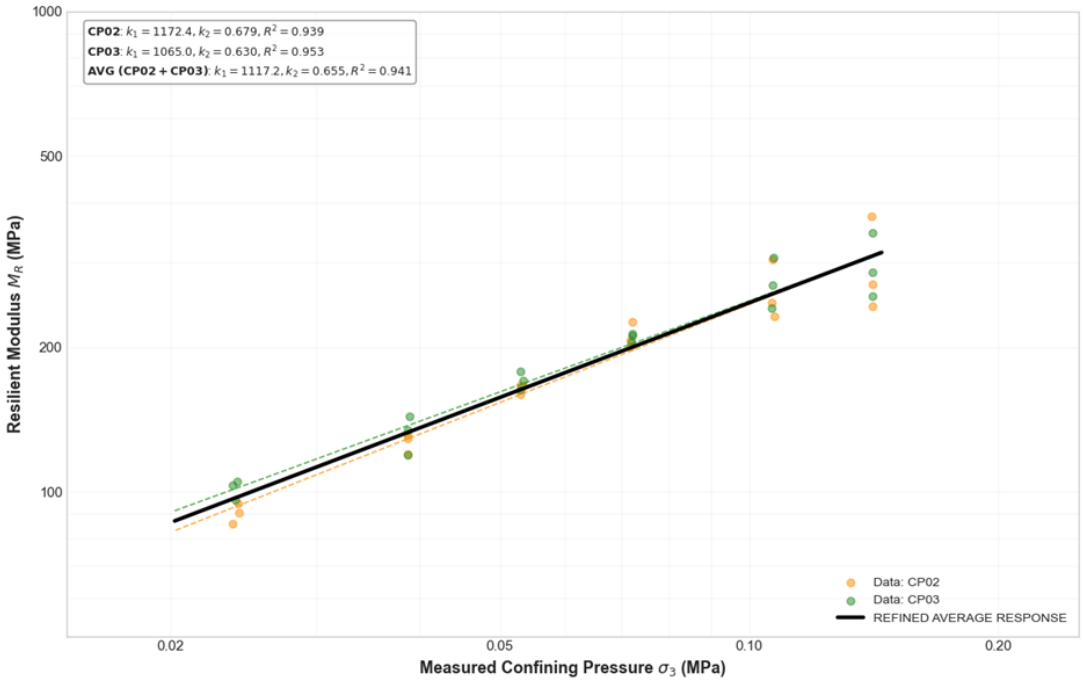


Figure 4.66: Refined Resilient Modulus (M_R) of Binary 85/15 mixture at 0 days. The average trendline is established excluding CP01 based on geotechnical consistency criteria ($R^2 > 0.90$).

Because statistical methods can be overly conservative for small sample sizes, a Geotechnical Consistency Criterion was coupled to the analysis. Specimens were only retained if they demonstrated mechanical logic characteristic of a stabilized matrix, primarily validated by a high coefficient of determination ($R^2 > 0.90$) and consistent confining pressure sensitivity (k_2). Consequently, non-representative specimens—such as CP01 of the 85/15 mixture at 0 days curing period, which displayed severe experimental dispersion ($R^2 = 0.391$)—were systematically excluded from the average calculations.

This curated dataset allowed for the construction of highly accurate predictive models to evaluate the pozzolanic maturation. The structural evolution of the 85/15 and 80/20 binary mixtures over 0, 4, and 28 days of sealed curing is analyzed in the following sections through a multi-scale approach: integrated 2D stress-dependency plots, 3D MeDiNa resilient surfaces at full maturity, and specific stress-state cross-sections.

Interestingly, a comparison between empirical and mechanistic indices reveals a significant discrepancy: the 85/15 mixture exhibited higher CBR values than the 80/20 dosage. This 'CBR Paradox' underscores the limitations of static penetration tests in capturing the true structural potential of stabilized matrices. While CBR measures shear resistance at high strains, it fails to account for the superior elastic stiffness and increasing MR behavior identified in the 80/20 mixture through M_R testing. This finding reinforces the necessity of a mechanistic approach, as relying solely on empirical correlations could lead to an underestimation of the layer's actual resilient performance under cyclic traffic loading.

4.4.2 - EVOLUTION OF CONFINING SENSITIVITY AND EARLY-AGE STRUCTURAL TRANSITION

Figure 4.67 presents the temporal evolution of the resilient modulus as a function of confining pressure (σ_3) for both binary baselines. A meticulous analysis of the power model parameters reveals a critical behavioral shift during the early curing stages. This immediate enhancement at Day 4 is rooted in the "alkaline shock" and subsequent cation exchange. Upon mixing, the high CaO provision of the KRS (typically $> 40\%$) elevates the system's pH to at least 12.4, triggering a rapid displacement of monovalent cations by Ca^{2+} on the clay surfaces. This reduces the diffuse double layer and promotes immediate flocculation, justifying the instantaneous M_R gains observed even before long-term curing begins. Note the rotational shift and slope flattening at 4 days, followed by the pronounced stiffness jump for the 80/20 dosage at advanced maturity (Fig. 4.67).

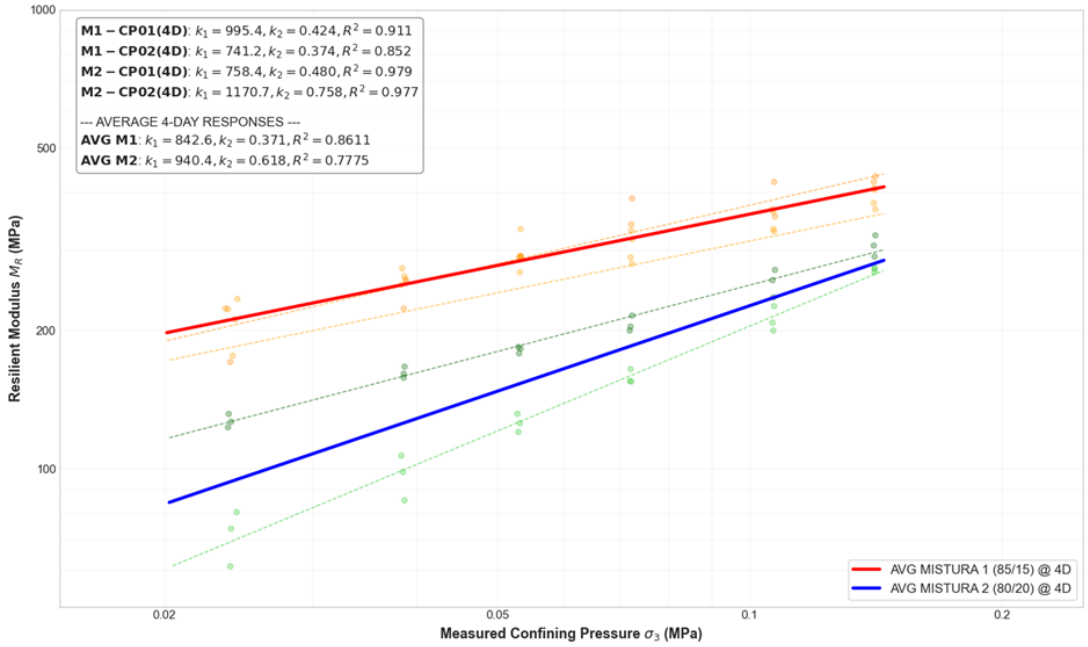


Figure 4.67: Resilient Modulus (M_R) as a function of confining pressure (σ_3) for binary baselines at 4 days: (a) 85/15 mixture; and (b) 80/20 mixture.

4.4.3 - THREE-DIMENSIONAL RESILIENT RESPONSE AND MODEL VALIDATION

To comprehensively visualize the mechanical maturation and validate the predictive models, Figure 4.68 presents the 3D resilient response surfaces for both binary baselines at 0 and at the 28-day curing stage. The dual-curves chart correlates M_R with the full triaxial stress spectrum (σ_3 and σ_d), mapping the empirical data points against the mechanistic surface of the MeDiNa composite model. Additionally, equation coefficients (k1, k2, and k3) of both models, MeDiNa and Universal (MEPDG) are shown in the figures.

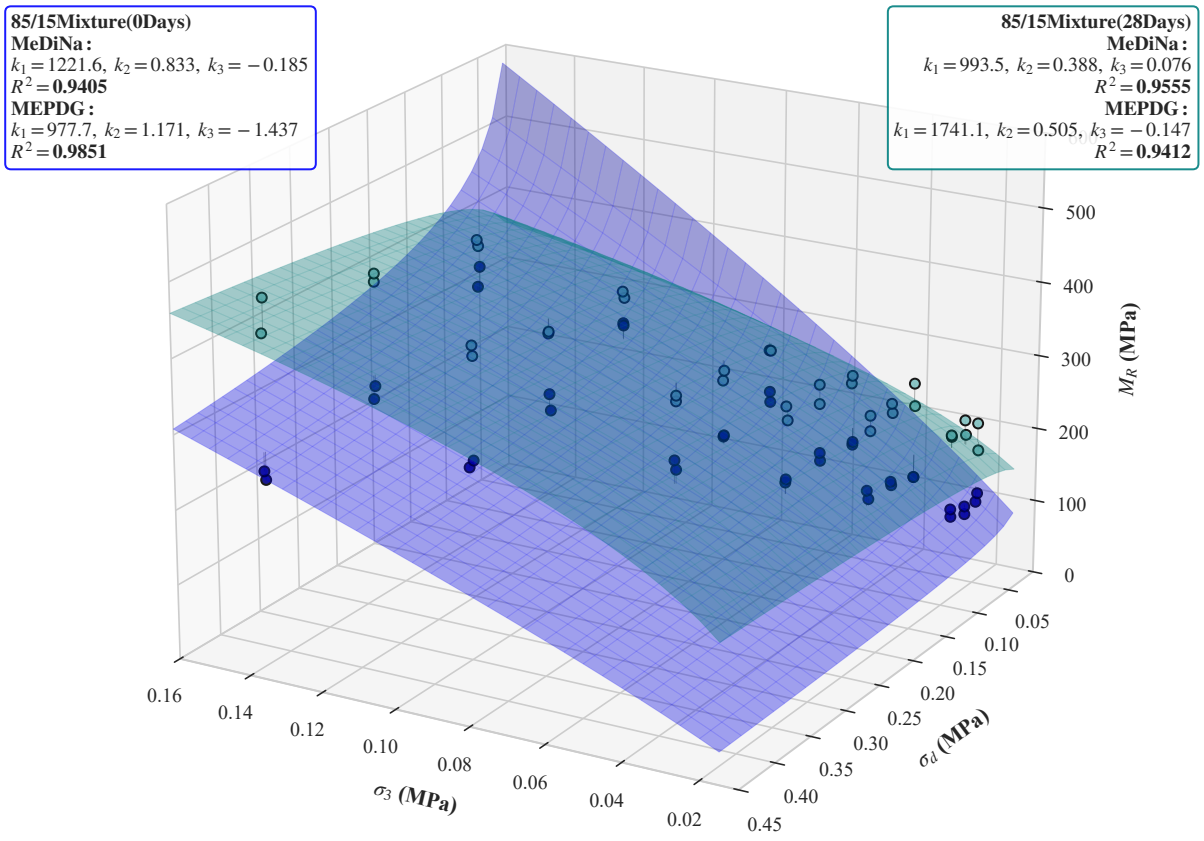


Figure 4.68: Temporal evolution of the 3D Resilient Modulus (M_R) response for the 85/15 Binary Mixture (0 vs. 28 days).

Figure 4.68 presents the 0-day surface was refined by excluding CP01 based on geotechnical consistency criteria. The overlay reveals the structural gain and the attenuation of decreasing stiffness (reduction of MR) behavior (indicated by the k_3 shift) as pozzolanic reactions progress. Model parameters are displayed in lateral boxes for comparative analysis. The 3D surface analysis for the 85/15 dosage reveals the initial stages of chemical structuring. At 0 days, the material exhibits a negative k_3 parameter (-0.185), characterizing the typical decreasing stiffness (reduction of MR) behavior of clayey matrices, where the resilient modulus decreases as deviatoric stress increases.By 28 days, a clear "positive volume" of stiffness gain is formed between the two surfaces. A fundamental inversion in the model's curvature occurs: k_3 transitions to a positive value (+0.076), marking the onset of increasing stiffness (increasing MR). Furthermore, the drastic reduction in the k_2 parameter (from 0.833 to 0.388) indicates that the matrix has become significantly less dependent on confining pressure. This suggests that the pozzolanic cementation has begun to override the purely granular/frictional behavior of the base soil, establishing a more cohesive and stable structure.

In Figure 4.69 the 80/20 soil-KRS dosage mechanistic behavior is presented.

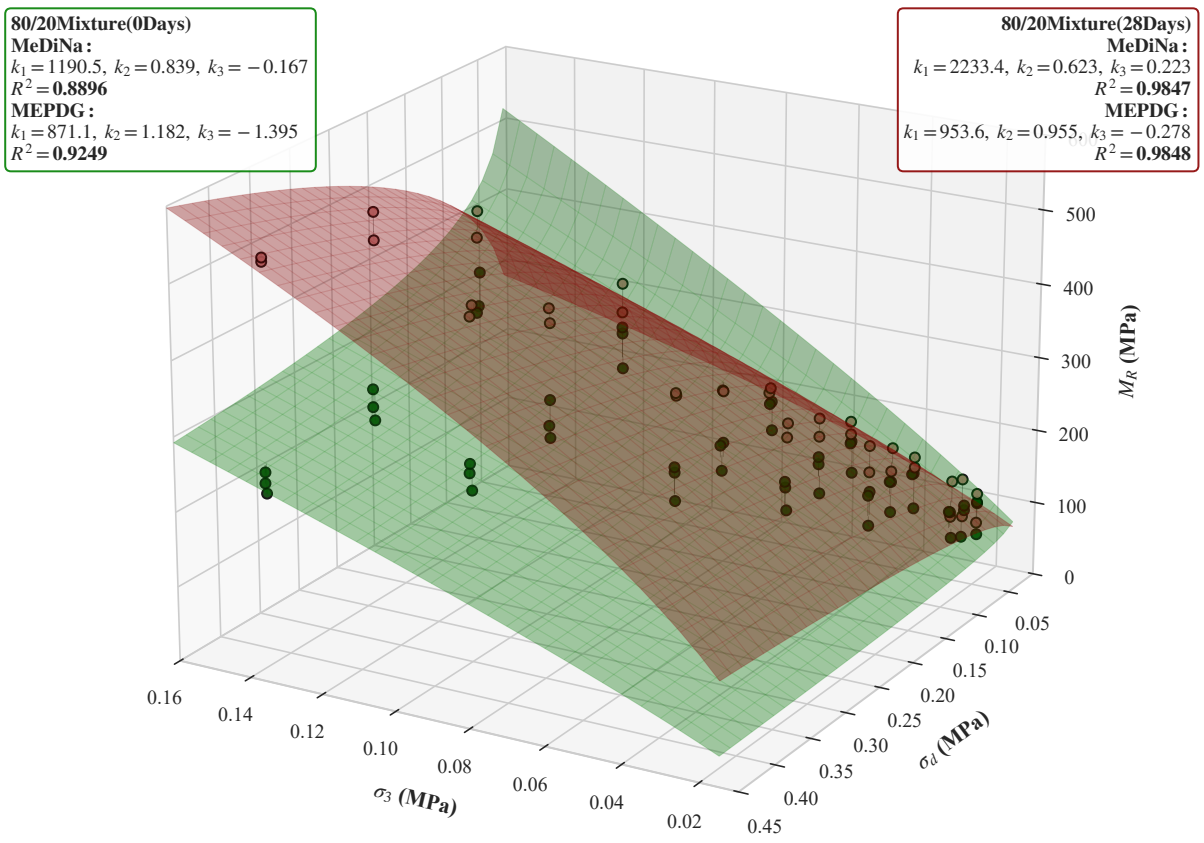


Figure 4.69: Temporal evolution of the 3D Resilient Modulus (M_R) response for the 80/20 Binary Mixture (0 vs. 28 days).

Figure 4.69 shows the comparison highlights a definitive transition from a decreasing stiffness (reduction of MR) regime at early ages ($k_3 = -0.167$) to a increasing stiffness (increasing MR) behavior at 28 days ($k_3 = 0.223$), characteristic of robust cementitious maturation. The high R^2 values for both MeDiNa and MEPDG models validate the consistency of the higher slag dosage. In the 80/20 dosage, the maturation phenomenon is significantly more pronounced. The "volumetric gain" between the 0 and 28-day surfaces is substantially larger than that observed in the 85/15 mixture, representing a massive leap in the global stiffness intercept (k_1), which nearly doubles from 1190.5 to 2233.4 MPa.The behavioral transition is severe: the material shifts from an initial decreasing stiffness (reduction of MR) regime ($k_3 = -0.167$) to a robust increasing stiffness (increasing MR) regime at 28 days, with k_3 surging to +0.223. This "upward slope" of the surface relative to the σ_d axis proves that the higher availability of KRS empowered the cementitious reactions, creating a mineral skeleton that actually stiffens as mechanical demand increases. The widening distance between the surfaces across the entire stress spectrum confirms that, for this dosage, curing time is the primary driver for structural stability and shear resistance.

In Figure 4.70 the 80/20 and 85/15 soil-KRS dosages mechanistic behavior are presented.

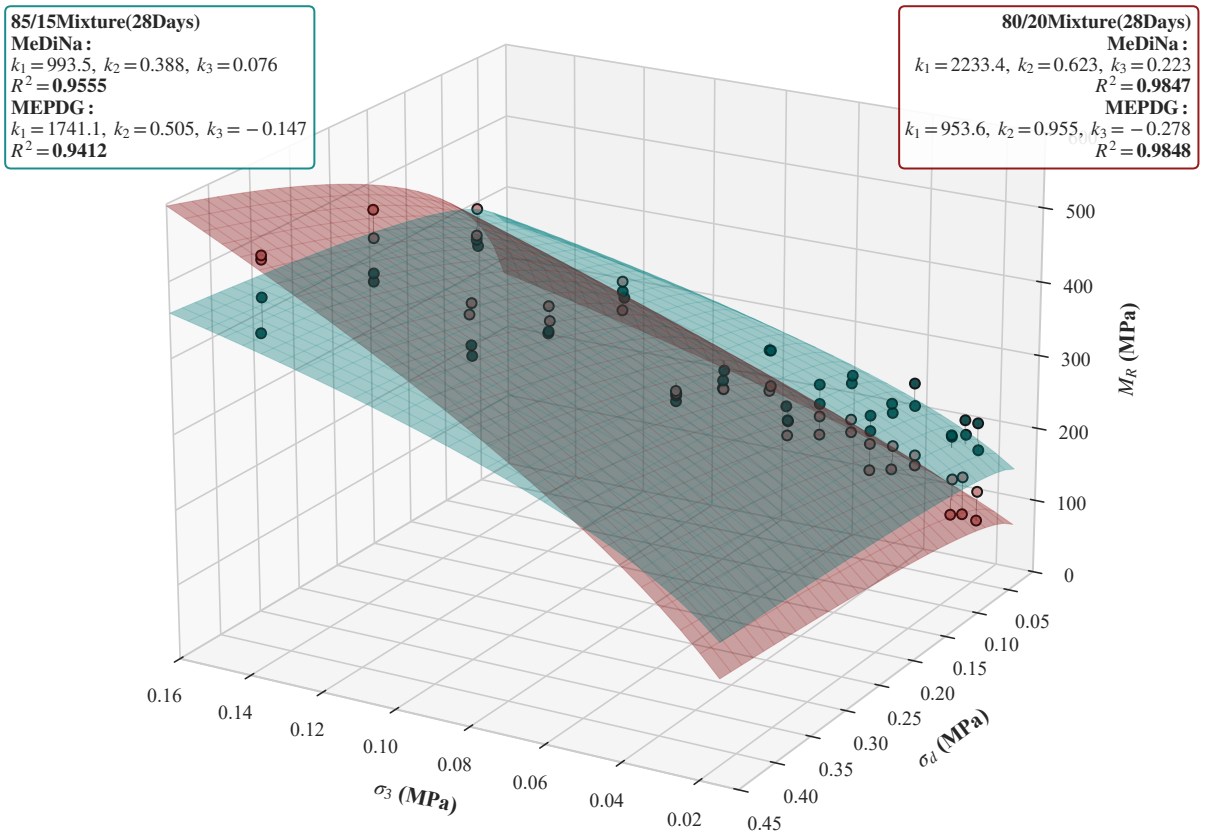


Figure 4.70: 3D Resilient Modulus (M_R) surface comparison between Binary 85/15 and 80/20 mixtures at advanced maturity (28 days).

It can be seen in Figure 4.70 the overlay which illustrates the superior stiffness threshold of the 20% KRS dosage. Individual statistical boxes present the regression constants for both the MeDiNa (Composite) and MEPDG (Universal) models, highlighting the high predictability ($R^2 > 0.95$) of the stabilized non-lateritic matrix. When comparing both dosages at the 28-day mark, the superiority of the 80/20 mixture is evidenced by the steeper inclination and the higher altitude of its surface. Although both mixtures successfully reached an increasing stiffness (increasing MR) behavior (both exhibiting positive k_3 values), the 80/20 surface is significantly sharper and positioned at a much higher global stiffness threshold. The increasing stiffness (increasing MR) phenomenon is more pronounced in the 20% KRS dosage due to a higher densification of the matrix and the formation of a more continuous network of hydration products. While the 85/15 mixture shows a tendency toward modulus stabilization, the 80/20 mixture exhibits an aggressive stiffness increment under higher loads. This divergence between the surfaces translates to the real mechanistic gain provided by the increased chemical activator

dosage, consolidating the non-lateritic soil into a high-performance engineered material suitable for modern pavement design standards.

4.4.4 - COMPARATIVE STRESS-STATE CROSS-SECTIONS

To isolate the dynamic impact of traffic loading from confinement effects, Figure 4.71 extracts 2D cross-sections from the MeDiNa models at fixed confining pressures ($\sigma_3 = 0.02$ and 0.07 MPa). This comparative visualization superimposes the performance of the 85/15 (dashed lines) and 80/20 (solid lines) mixtures, explicitly tracking the transition of their mechanical regimes throughout pozzolanic maturation. Both the 85/15 (gray dashed line) and 80/20 (black solid line) mixtures demonstrate a definitive transition to increasing stiffness (increasing MR) behavior at 28 days (Fig. 4.71).

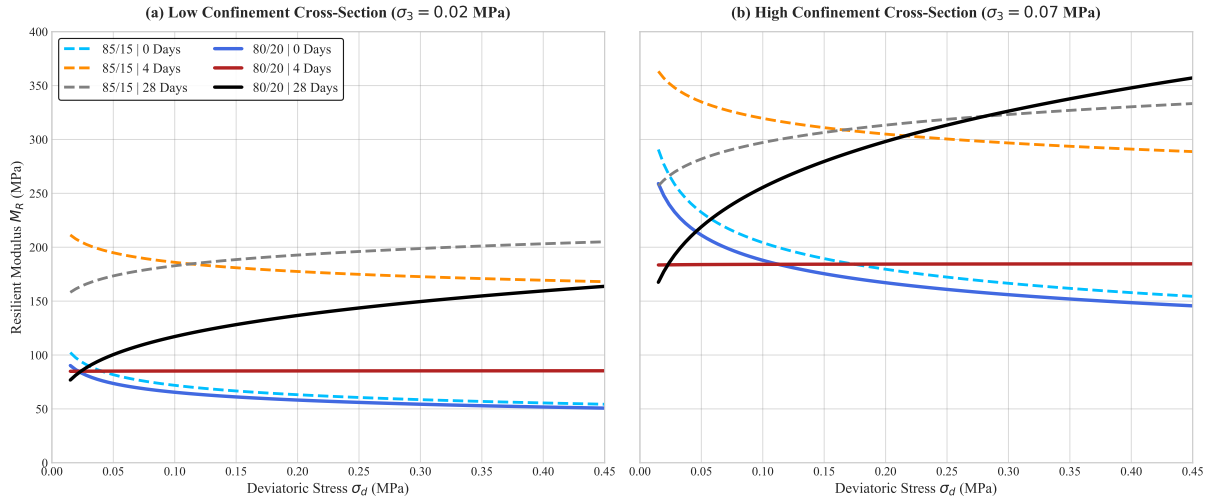


Figure 4.71: Comparative Resilient Modulus cross-sections at fixed confining pressures: (a) $\sigma_3 = 0.02$ MPa and (b) $\sigma_3 = 0.07$ MPa.

At early stages (0 and 4 days), both mixtures exhibit a decreasing stiffness (reduction of MR) behavior (blue and red lines), characterized by a negative slope where stiffness decreases as deviatoric stress increases. However, the 28-day response (gray and black lines) reveals a fundamental structural transformation. In both baselines, the curves transition to a parallel, upward-sloping trajectory, confirming that both mixtures have achieved a increasing stiffness (increasing MR) beahvior ($k_3 > 0$) at full maturity. This parallel development proves that by 28 days, the pozzolanic skeleton is robust enough in both dosages to overcome the natural decreasing stiffness (reduction of MR) of the clay matrix. This generalized increasing stiffness (increasing MR) response is a significant finding, indicating that both binary systems provide a stable and resilient foundation that actively improves its structural support under increased traffic-induced shear stresses.

Figure 4.72 illustrates the temporal evolution of the Resilient Modulus (M_R) as a function of confining pressure (σ_3) for the 85/15 and 80/20 binary blends. The initial "cationic shock" promoted by the high free-lime (CaO) content in the KRS induces immediate soil flocculation. This is physically translated into a rotational shift and slope flattening of the M_R curve at 4 days of curing for both mixtures, indicating an early reduction in the material's sensitivity to stress variations. Note the rotational shift and slope flattening at 4 days, followed by the pronounced stiffness jump for the 80/20 dosage at advanced maturity (Fig. 4.72).

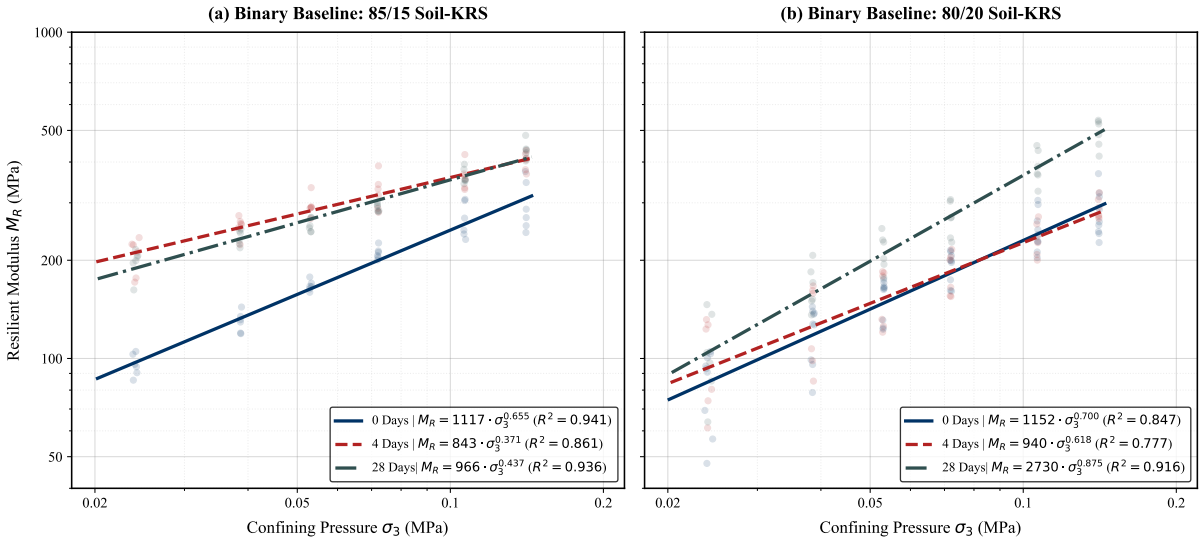


Figure 4.72: Temporal evolution of the Resilient Modulus (M_R) as a function of confining pressure (σ_3) for binary baselines at 0, 4, and 28 days: (a) 85/15 mixture; and (b) 80/20 mixture.

However, the most significant mechanical transformation occurs at advanced maturity (28 days). A pronounced stiffness jump is observed, particularly for the 80/20 dosage (Figure 4.72b), reflecting the consolidation of stable cementitious products (Calcium Silicate Hydrates - CSH, and Calcium Aluminate Hydrates - CAH). This temporal benchmarking confirms that KRS is a highly effective chemical binder, functioning similarly to traditional lime stabilization but requiring longer curing intervals to express its full cementitious potential due to the coarser nature of the slag particles.

At the 4-day mark, early pozzolanic cementation increases the absolute stiffness at low confinement for both mixtures. However, this initial bonding reduces the matrix's responsiveness to confining pressure, evidenced by the flattening of the slopes (lower k_2 values). This transitional instability reflects the microstructural period where the alkaline moisture has disrupted the soil's initial suction-related stability, but the precipitation of Calcium Silicate Hydrate ($C-S-H$) and Calcium Aluminate Hydrate ($C-A-H$) is still in an embryonic, semi-rigid stage. For the 80/20 mixture, this rotational shift is so pronounced that at higher operational stresses, the 4-day curve crosses below the 0-day baseline, exposing a sensitivity gap where the chemical matrix is not yet robust enough to compensate for the lost granular

interlocking under high confinement.

To consolidate the mechanistic evaluation of the binary systems and establish a definitive baseline for the ternary mixtures, a graphical analysis of the temporal evolution of the Resilient Modulus was performed. The 3D response surfaces generated from the MeDiNa composite model allow for a clear visualization of the structural leap provided by the long-term chemical maturation.

Figure 4.73 illustrates the temporal evolution for the 85/15 binary mixture. The lower blue surface represents the immediate mechanical response at 4 days of curing, primarily driven by the initial cationic shock and flocculation. The upper teal surface demonstrates the material's behavior after 28 days. The vertical shift between these surfaces evidences the consolidation of the macroscopic skeleton through slow-reacting pozzolanic activity, elevating the stiffness across all applied stress states. The comparison between 4 days (blue surface) and 28 days (teal surface) highlights the structural gain from pozzolanic maturation (Fig. 4.73).

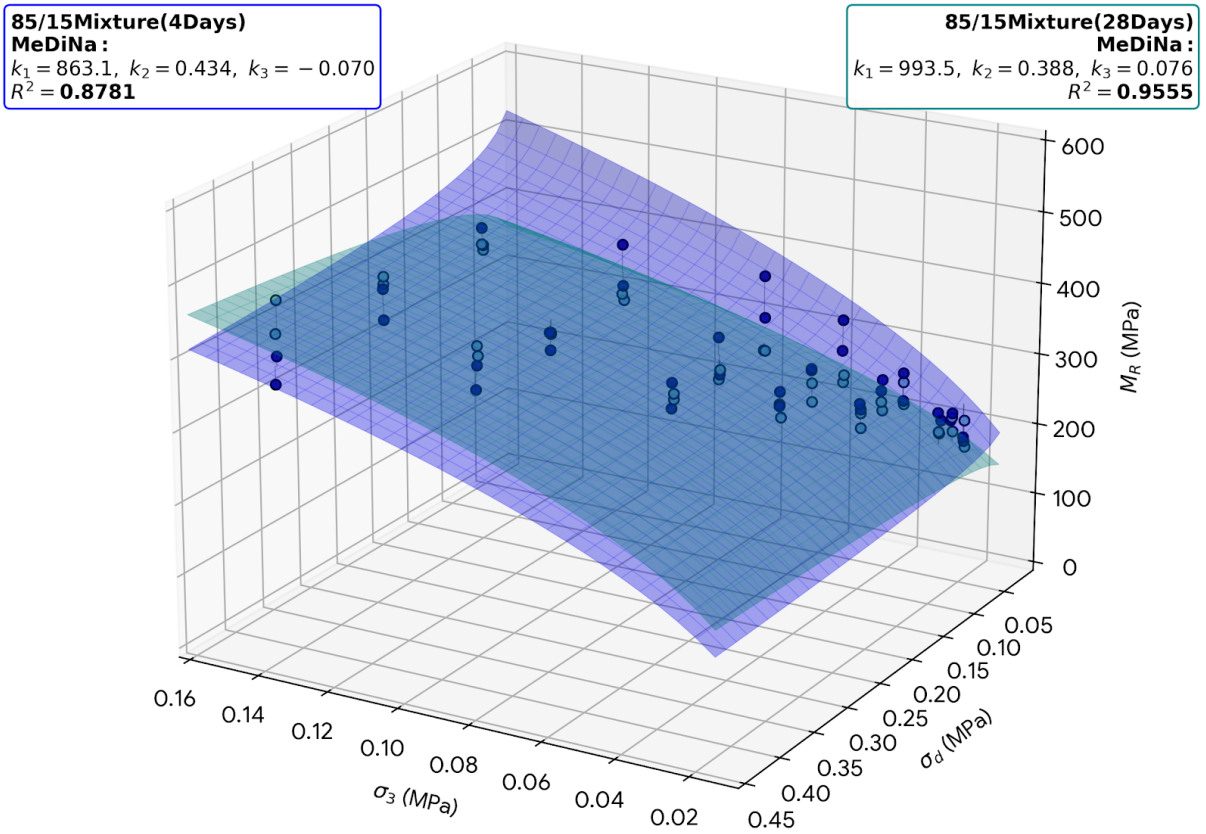


Figure 4.73: Temporal evolution of the 3D Resilient Modulus response for the 85/15 Binary Mixture.

A similar, yet more pronounced, phenomenon is observed for the 80/20 binary mixture,

as presented in Figure 4.74. The initial 4-day stiffness, represented by the green surface, is rapidly overshadowed by the 28-day maturation, depicted by the dark red surface. Due to the higher availability of reactive slag in this dosage, the precipitation of cementitious products is intensified, resulting in a massive leap in dynamic stiffness and establishing a highly rigid, with increasing stiffness (increasing MR) behavior geomaterial. The transition from 4 days (green surface) to 28 days (dark red surface) demonstrates the massive stiffness increment driven by high slag availability (Fig. 4.74).

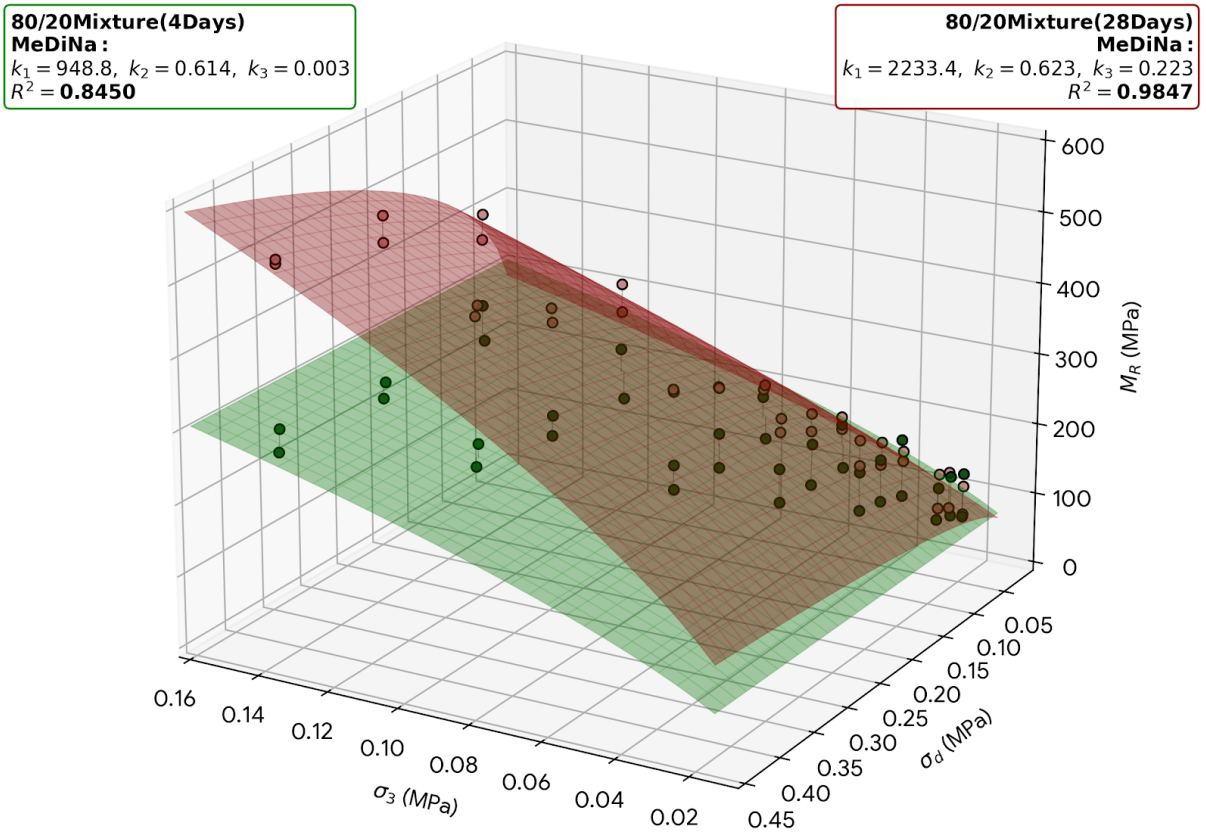


Figure 4.74: Temporal evolution of the 3D Resilient Modulus response for the 80/20 Binary Mixture.

These 28-day surfaces represent the mechanistic gold standard of chemical maturation for the binary systems. However, waiting nearly a month to achieve optimal structural stability poses significant logistical challenges for rapid road construction. This temporal limitation raises a critical engineering question: is it possible to achieve this advanced state of granular equilibrium instantaneously. The following section introduces the ternary system, investigating how the physical packing properties of Ornamental Stone Residue (OSR) can act as a catalyst to bridge this pozzolanic latency period. The evidence for this mechanism is detailed in the forthcoming analysis, where the comparative performance of the ternary systems reveals a

remarkable and superior structural response.

4.5 - TERNARY BASELINE ANALYSIS (PHYSICAL-CHEMICAL SYNERGY)

4.5.1 - EXPERIMENTAL DESIGN, DOSAGES, AND TESTING PROTOCOL

The experimental matrix evaluates four ternary variations across two distinct industrial clusters ($85/15$ and $80/20$ soil-KRS proportions), with OSR additions at 5% and 10% levels. The proportions came from local experience and other studies such as Pires et al. (2019).

Building upon the binary baselines, the KRS was maintained as the chemical activator, and the OSR was incorporated as an **additive percentage** (5% and 10%) over the total dry mass of the pre-established binary mixtures. This additive approach ensures that the Soil:KRS ratio remains constant while the influence of the physical skeleton is isolated (Table 4.9).

Table 4.9: Revised experimental matrix: Soil-KRS binary bases and OSR additive variations.

Mixture Type	Soil:KRS Ratio	OSR Content (%)	Sample ID
Binary (Base 1)	85:15	0%	85/15
Ternary 1a	85:15	5%	85/15 + 5%OSR
Ternary 1b	85:15	10%	85/15 + 10%OSR
Binary (Base 2)	80:20	0%	80/20
Ternary 2a	80:20	5%	80/20 + 5%OSR
Ternary 2b	80:20	10%	80/20 + 10%OSR

4.5.2 - THE FILLER EFFECT AND OSR CONTENT OPTIMIZATION

The incorporation of Ornamental Stone Residue (OSR) into the soil-KRS matrix marks the transition from purely chemical stabilization to a synergistic physical-chemical system. As illustrated in Figure 4.75, the addition of OSR significantly mitigates the 'structural transition' observed in binary mixtures at early ages, providing immediate mechanical stability through a robust mineral filler effect.

For the 85/15 mixture (Figure 4.75a), the optimum residue content (ORC), proposed by Prandina2026, was identified at 5% OSR. At this level, the global stiffness parameter (k_1) reached 1124.7 MPa, representing a significant increase compared to the 4-day binary baseline (863.2 MPa). However, increasing the OSR content to 10% resulted in a stiffness drop to 814.1 MPa. This phenomenon suggests that in leaner slag mixtures, an excess of non-plastic fines may interfere with the continuity of the immature cementitious matrix, acting as a dispersing element rather than a reinforcement.

Conversely, the 80/20 mixture demonstrated a higher capacity to incorporate mineral

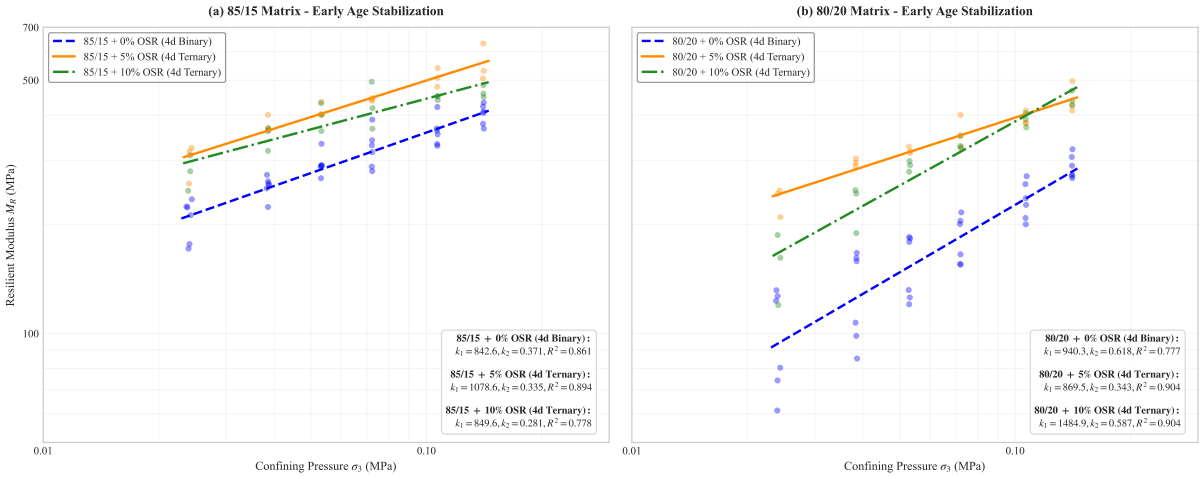


Figure 4.75: Resilient Modulus (M_R) optimization through Ornamental Stone Residue (OSR) addition at 4 days of curing: (a) 85/15 matrix showing an optimum at 5% OSR; and (b) 80/20 matrix achieving peak stiffness at 10% OSR. The dashed blue line represents the reference binary baseline.

fillers, with peak performance achieved at 10% OSR, where k_1 reached 1280.9 MPa. This significant leap indicates that the higher lime/activator content in the 20% KRS blend allows for a more extensive cementitious matrix capable of binding a larger volume of non-plastic OSR fines. Furthermore, the ternary system promotes a more independent structural skeleton, evidenced by the stabilization of the confinement sensitivity (k_2) and the early transition towards a stress-independent behavior, which is critical for minimizing permanent deformations under heavy traffic loads.

4.5.3 - COMPARATIVE ANALYSIS OF RESIDUE-SLAG INTERACTION

The divergent behavior of the optimum residue content (ORC) between the two slag clusters reveals a mandatory correlation between the chemical activator (CaO from KRS) and the physical filler (OSR). In the 85/15 matrix, the threshold for a beneficial filler effect is reached at 5% OSR. Although the 10% dosage in this cluster led to a reduction in absolute stiffness ($k_1 = 814.1$ MPa), it is noteworthy that it promoted the lowest confinement sensitivity ($k_2 = 0.287$) observed in the study. This indicates that while an excess of non-plastic fines might hinder cementitious continuity in leaner mixtures, they continue to densify the mineral skeleton, making the matrix more independent of lateral confining pressures.

In contrast, the 80/20 matrix demonstrates a superior incorporation capacity. The higher dosage of KRS (20%) provides a more robust alkaline environment, which appears sufficient to chemically stabilize and bind a larger volume of non-plastic residue. This synergy is evidenced by the massive surge in stiffness for the 80/20 + 10% OSR mixture, which represents the peak mechanistic performance of the ternary study at early ages.

The stabilization of the k_3 parameter in the 80/20 + 10% OSR mixture ($k_3 = -0.007$) confirms that the ternary system effectively mitigates the structural transition typically observed in binary blends. This early-age reduction of the decreasing stiffness effect, common in untreated clays, proves that the OSR effectively bridges the pozzolanic maturation period of the slag. The physical interlocking provided by the OSR transforms the soil into a stable matrix that tends toward a stress-independent behavior, capable of maintaining its structural integrity under traffic-induced shear stresses as early as 4 days of maturation.

4.5.4 - EVOLUTION OF RESILIENT MODULUS (M_R) AND 3D RESPONSE SURFACES

Ternary mixtures at early ages exhibit superior Resilient Modulus (M_R) values compared to binary baselines, shifting the material to a higher structural performance threshold. The interaction between OSR's physical interlock and KRS's chemical bond creates a significantly more rigid structure, as illustrated by the topological evolution of the surfaces in Figure 4.76.

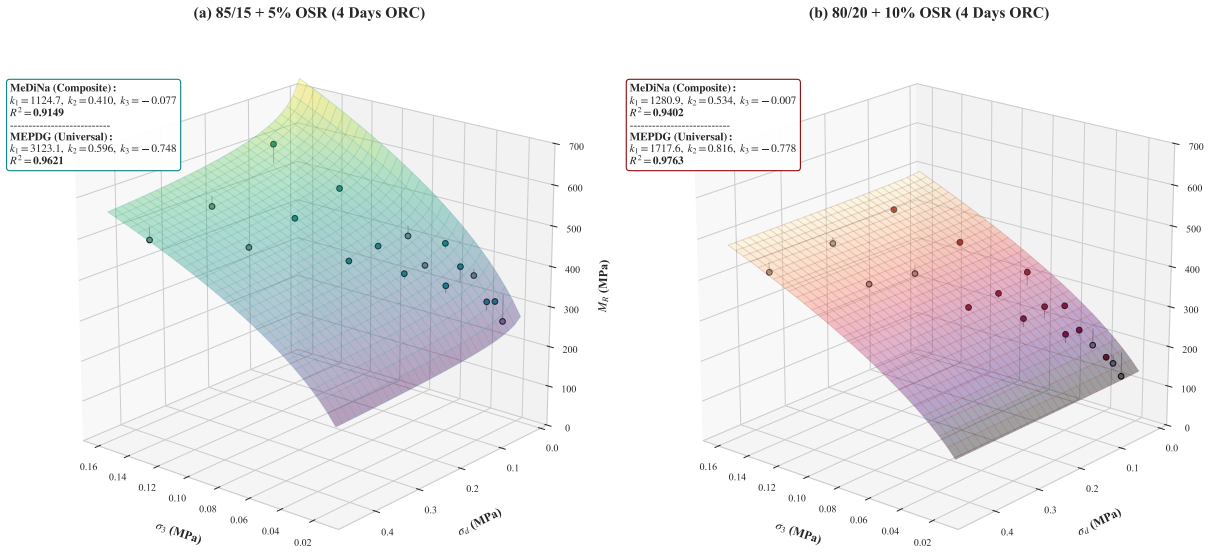


Figure 4.76: 3D Resilient Modulus maturation for Ternary Optimum Residue Content (ORC) at 4 days: (a) 85/15 + 5% OSR matrix; and (b) 80/20 + 10% OSR matrix. Comparison between MeDiNa (Composite) and MEPDG (Universal) models.

A critical finding of this research is the substantial mitigation of the "decreasing stiffness" effect. In high-plasticity clayey soils, stiffness typically decreases drastically as deviatoric stress (σ_d) increases (negative k_3). The ternary systems, however, demonstrate a transition toward a regime of stress-independence or highly attenuated decreasing stiffness (reduction of MR).

For the 85/15 + 5% OSR mixture (Figure 4.76a), while the decreasing stiffness

(reduction of MR) persists, the global stiffness parameter reached a high magnitude ($k_1 = 1124.7$ MPa) and the deviatoric sensitivity was significantly reduced ($k_3 = -0.077$). In the 80/20 + 10% OSR cluster (Figure 4.76b), the stiffness surged to $k_1 = 1280.9$ MPa, with k_3 practically approaching a horizontal plateau (-0.007). This horizontalization suggests that the matrix develops sufficient shear resistance to maintain its modulus nearly constant regardless of the increasing traffic loads.

The topological stability of the M_R surfaces indicates that the mineral filler effect of the OSR provides immediate skeleton densification. The high statistical correlation observed for both the MeDiNa composite model ($R^2 \geq 0.91$) and the Universal MEPDG model ($R^2 \geq 0.96$) confirms that the proposed ternary stabilization provides a predictable and robust mechanistic performance, even before the full pozzolanic maturation of the slag-activated binder.

Table 4.10: Calculated Resilient Modulus (M_R) values for ternary mixtures at 4 days of curing

Mixture	**OSR Content**	σ_3	**Resilient Modulus M_R (MPa)**		
Soil/KRS	**(Model Equation)**	**(MPa)**	$\sigma_d = 0.05$	$\sigma_d = 0.10$	$\sigma_d = 0.15$
85/15	0% (Binary) $M_R = 863.2 \cdot \sigma_3^{0.432} \cdot \sigma_d^{-0.067}$	0.02	194.9	186.0	181.0
		0.05	289.6	276.3	268.9
		0.07	334.9	319.6	311.0
	5% (Ternary) $M_R = 1124.7 \cdot \sigma_3^{0.410} \cdot \sigma_d^{-0.077}$	0.02	284.9	270.0	261.7
		0.05	414.8	393.2	381.1
		0.07	476.2	451.4	437.5
	10% (Ternary) $M_R = 814.1 \cdot \sigma_3^{0.287} \cdot \sigma_d^{-0.030}$	0.02	289.3	283.4	280.0
		0.05	376.4	368.7	364.3
		0.07	414.6	406.1	401.3
80/20	0% (Binary) $M_R = 950.0 \cdot \sigma_3^{0.616} \cdot \sigma_d^{0.002}$	0.02	85.1	85.2	85.2
		0.05	149.5	149.7	149.8
		0.07	183.9	184.1	184.3
	5% (Ternary) $M_R = 917.5 \cdot \sigma_3^{0.437} \cdot \sigma_d^{-0.094}$	0.02	220.2	206.3	198.5
		0.05	328.7	307.9	296.3
		0.07	380.7	356.6	343.2
	10% (Ternary) $M_R = 1280.9 \cdot \sigma_3^{0.534} \cdot \sigma_d^{-0.007}$	0.02	162.0	161.2	160.7
		0.05	264.2	262.9	262.2
		0.07	316.3	314.7	313.8

4.5.5 - MICROSTRUCTURAL DENSIFICATION AND STRESS SENSITIVITY

The cross-sectional analysis of the Resilient Modulus (M_R) at 4 days of curing, presented in Figure 4.77, provides a definitive view of the structural role of Ornamental Stone Residue (OSR) within the soil-KRS matrix. A detailed examination of the curves reveals that the increasing stiffness (increasing MR) effect is not as pronounced as typically observed in long-term

stabilized materials; instead, the inclusion of OSR promotes a significant **horizontalization** of the mechanistic response, particularly in the 80/20 cluster.

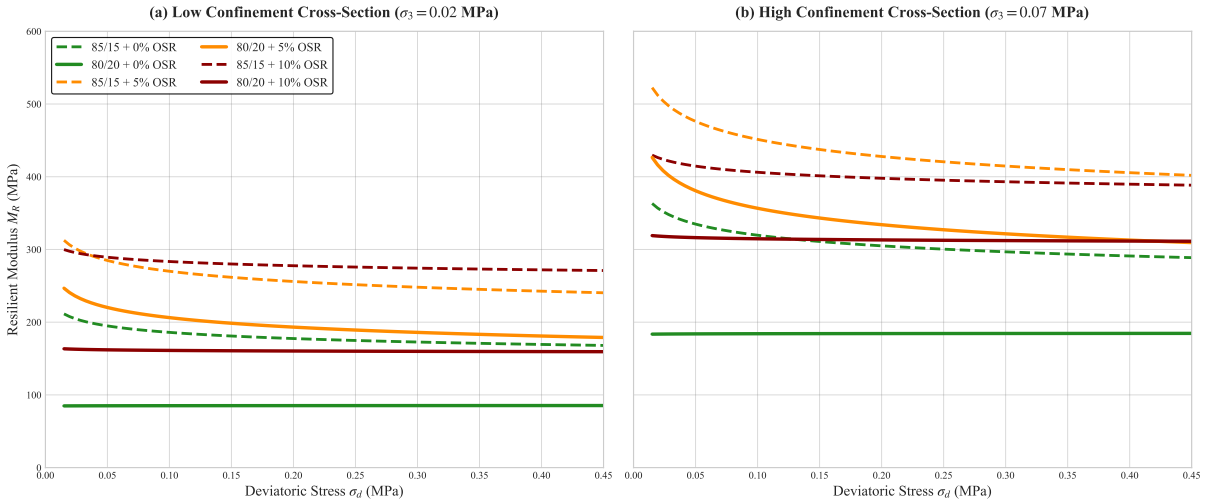


Figure 4.77: Cross-sectional analysis of M_R vs. deviatoric stress (σ_d) at 4 days: (a) low confinement ($\sigma_3 = 0.02$ MPa) and (b) high confinement ($\sigma_3 = 0.07$ MPa). The plots illustrate the stiffness gap and the stress-independence threshold.

The following mechanistic phenomena are highlighted:

- **Transition to Stress Independence:** In the 80/20 + 10% OSR mixture (solid brown line), the M_R curve is equally flatter compared to its binary counterpart (solid green line). This suggests that the microstructural densification provided by the OSR, coupled with the higher KRS content, creates a matrix that—while not explicitly increasing stiffness under load—is as resilient to shear stresses as the mixture without OSR. The material maintains a near-constant modulus even at high deviatoric levels ($\sigma_d > 0.30$ MPa), indicating a transition toward stress-independent behavior.

- **The Stiffness Gap (Structural Gain):** In the 85/15 cluster (dashed lines), the slight decreasing stiffness (reduction of MR) behavior persists across all OSR percentages. However, a consistent "stiffness gap" is observed: the 5% OSR optimum (dashed orange line) maintains a superior stiffness threshold over the binary baseline across the entire stress spectrum. This proves that the mineral filler effect constitutes a permanent structural upgrade; even when the matrix retains the elastic signatures of a fine-grained soil (decreasing stiffness), the magnitude of its support capacity is significantly elevated.

- **Stabilized Support Capacity and Granular Equilibrium:** The horizontal trend in the 80/20 matrix indicates that the material has reached a state of "granular equilibrium." In this state, the physical interlocking of the non-plastic OSR fines effectively compensates for the clay matrix's natural tendency to lose stiffness under shear. This is a robust

argument for the application of ternary mixtures in pavement base layers, where modulus stability is a highly desirable input for fatigue life predictions in the MeDiNa design framework.

To definitively validate the "Double Action Mechanism" of the ternary systems, a comparative 3D graphical analysis was conducted, overlaying the immediate mechanistic performance of the ternary mixtures (4 days of curing) against the long-term chemical maturation of their respective binary baselines (28 days of curing).

Figure 4.78 illustrates the structural evolution of the 85/15 matrix upon the addition of 5% OSR.

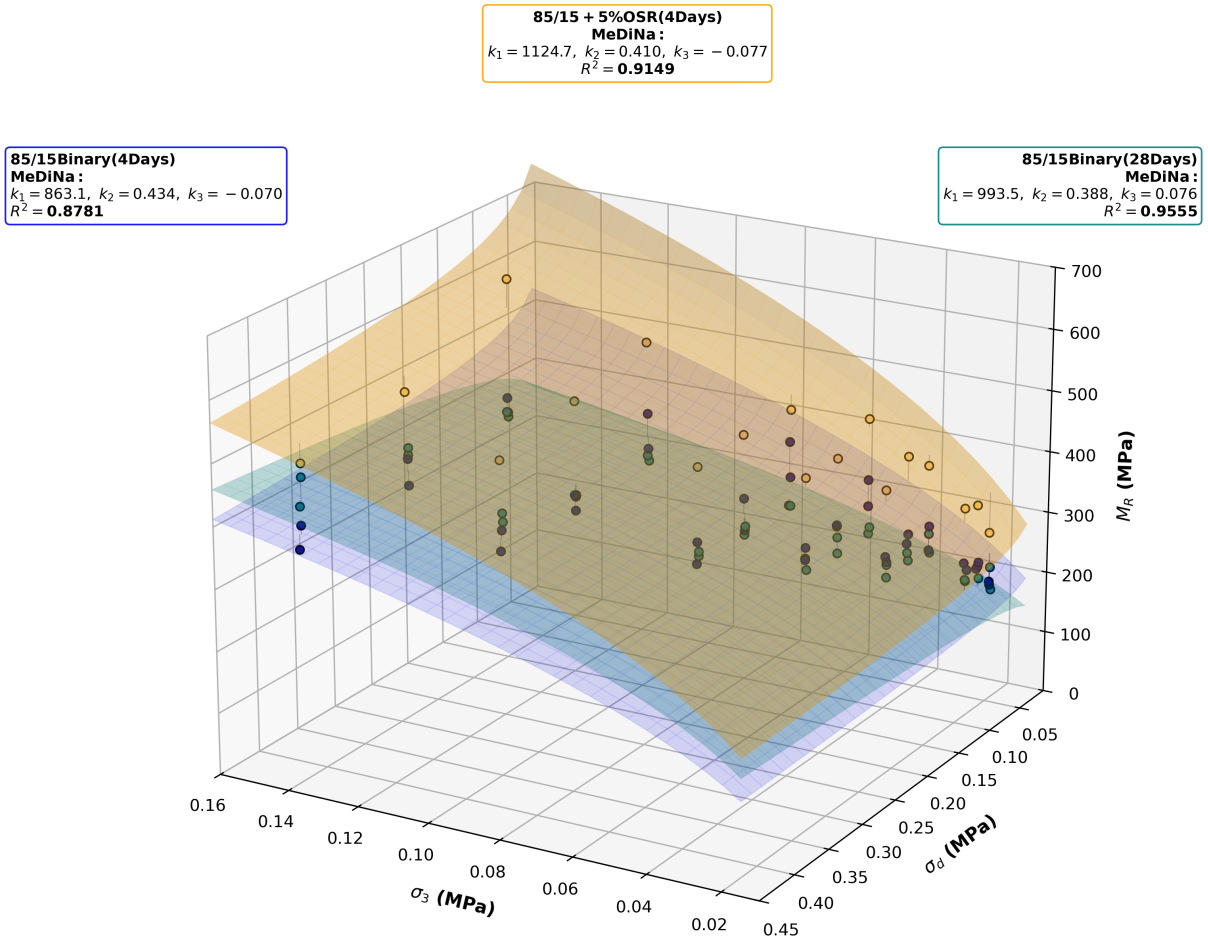


Figure 4.78: Effect of OSR on soil-KRS mixtures: 3D response surfaces comparing the 85/15 binary matrix maturation (4 vs. 28 days) against the immediate structural gain of the ternary mixture with 5% OSR at 4 days.

The blue surface represents the 85/15 binary mixture at 4 days (initial cationic shock), while the teal surface illustrates its performance after 28 days of pozzolanic maturation. The orange surface represents the ternary mixture (85/15 + 5% OSR) with only 4 days of curing.

The visual evidence is striking: the physical packing provided by the OSR instantly elevates the Resilient Modulus (M_R) to such an extent that the 4-day ternary surface not only surpasses its 4-day binary counterpart but also structurally outperforms the 28-day chemically cured binary matrix across the majority of stress states. These results demonstrate the profound structural impact of OSR as a granulometric corrector.

Increasing the OSR content to 10% in the same 85/15 matrix yields a similar, highly efficient response. As shown in Figure 4.79, the green surface representing the 10% OSR ternary mixture at 4 days positions itself remarkably close to, and eventually crosses, the 28-day binary surface (teal). This confirms that a higher dosage of OSR can still effectively bridge the pozzolanic latency period, guaranteeing in mere days the stability that requires nearly a month to develop through pure chemical reactions in the binary system.

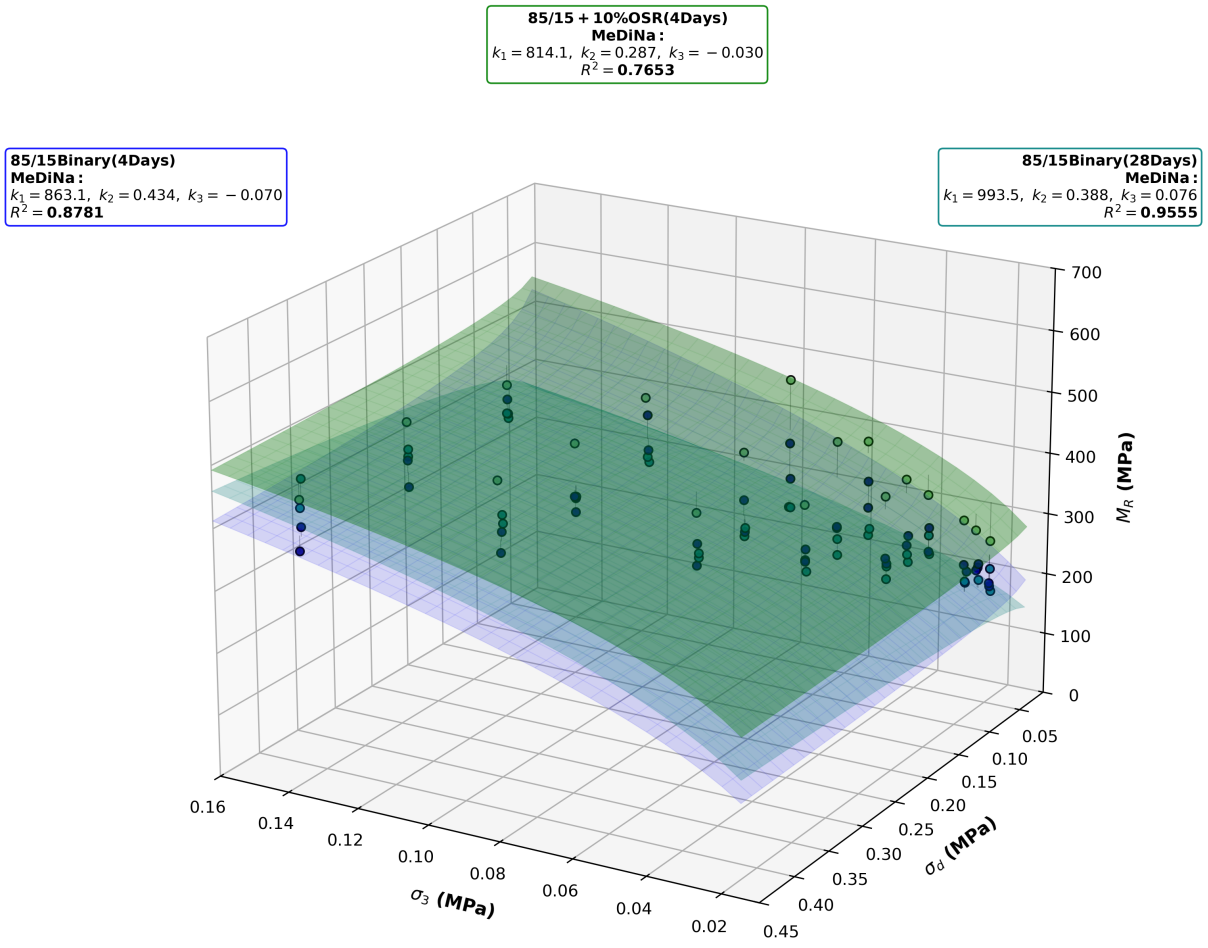


Figure 4.79: Effect of OSR: 3D response surfaces comparing the 85/15 binary matrix maturation against the immediate structural stability of the ternary mixture with 10% OSR at 4 days.

The most compelling demonstration of the Granular Equilibrium concept, however, is observed in the higher-slag 80/20 matrix. Figure 4.80 contrasts the 80/20 binary mixture at 4

days (green surface) and its highly rigid, increasing stiffness (increasing MR) behavior at 28 days (dark red surface) against the ternary mixture with 10% OSR at 4 days (purple surface). Despite the massive pozzolanic gain inherent to the 28-day binary matrix, the 4-day ternary surface intercepts and establishes itself slightly above it within the typical operational stress ranges of a pavement base layer.

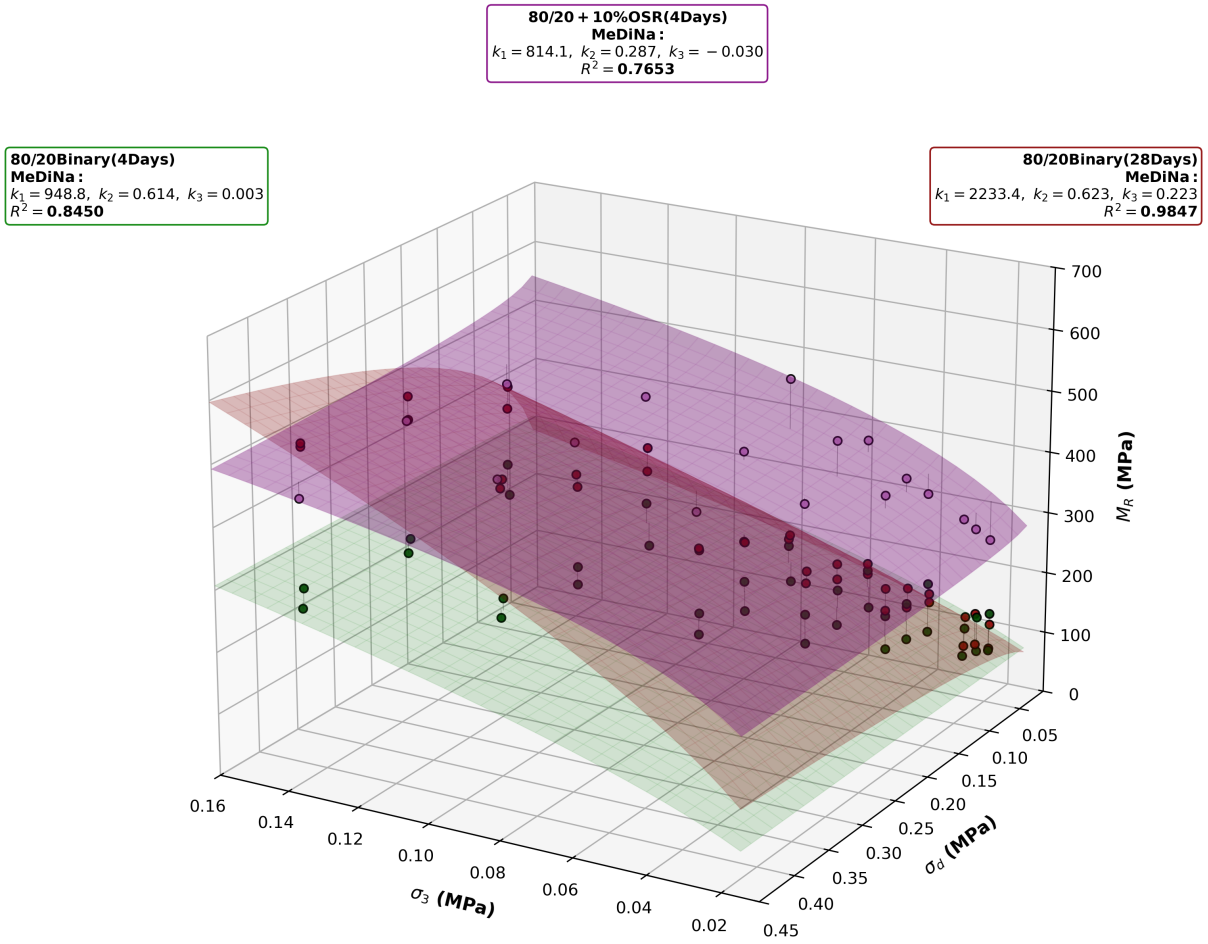


Figure 4.80: Effect of OSR on soil-KRS mixtures: 3D response surfaces comparing the 80/20 binary matrix maturation against the immediate Granular Equilibrium achieved by the ternary mixture with 10% OSR at 4 days.

To isolate the individual effect of a low OSR dosage on a matrix with higher slag content, the 80/20 Soil-KRS mixture was analyzed. The 3D comparative surfaces generated through the MeDiNa composite model provide a definitive visualization of how the filler effect of the Ornamental Stone Residue (OSR) acts as a catalyst, bridging the chemical latency period of the slag (KRS).

Figure 4.81 illustrates this synergistic behavior. The green surface represents the initial state of the 80/20 binary mixture at 4 days, characterized by a lower Resilient Modulus (M_R). The dark red surface illustrates the same binary mixture after 28 days of curing, where

pozzolanic maturation has significantly intensified the skeleton's rigidity.

Notably, the orange surface, which represents the ternary mixture containing 5% OSR with only 4 days of curing, not only vastly outperforms its 4-day binary counterpart but also intercepts and eventually surpasses the 28-day binary surface at specific stress ranges. This observation provides the empirical proof that the physical optimization provided by the residue works in immediate synergy with the initial cationic shock of the KRS, establishing a high-performance geomaterial without the traditional waiting periods associated with slow-reacting pozzolanic binders.

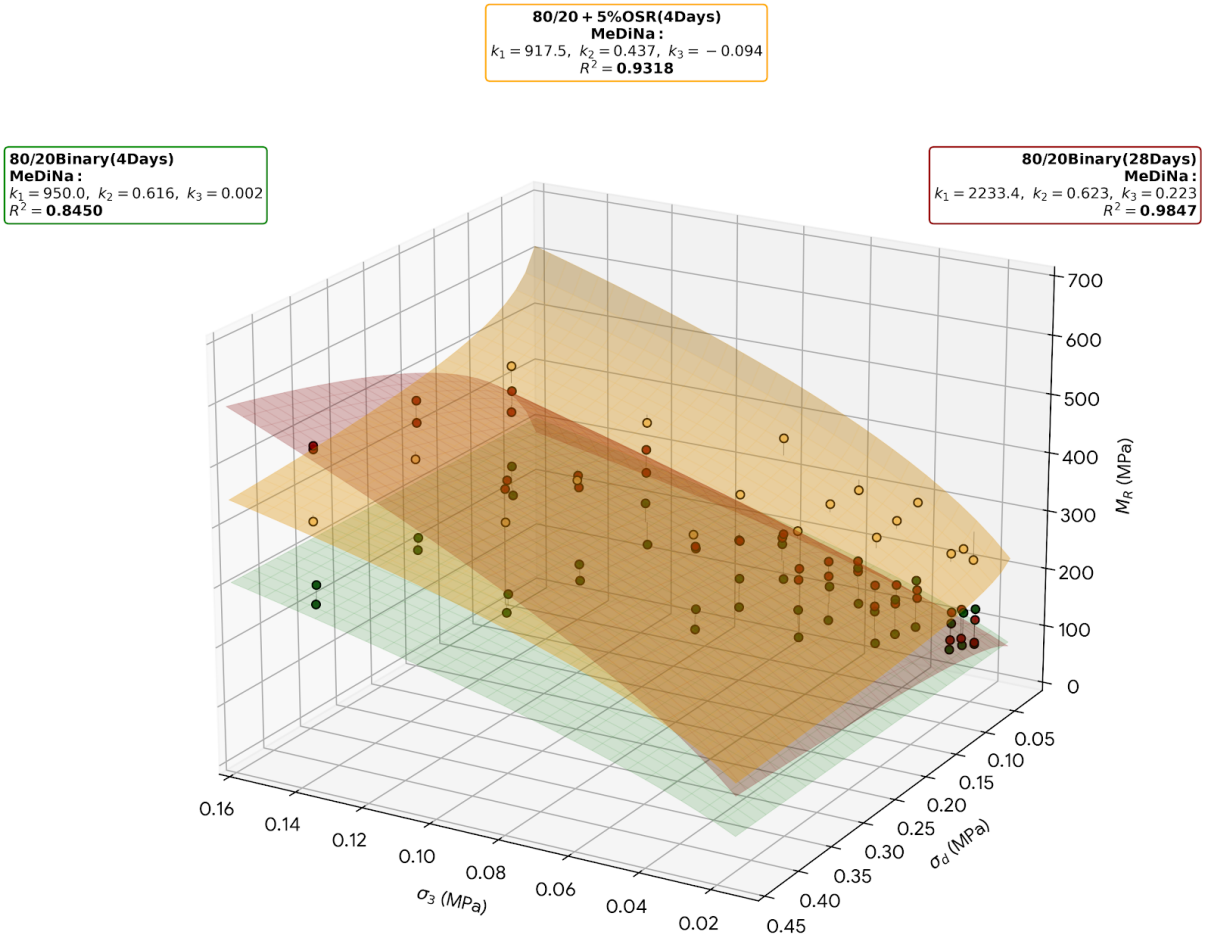


Figure 4.81: The Power of OSR: 3D comparative analysis for the 80/20 matrix. The orange surface (5% OSR ternary at 4 days) rivals the 28-day chemical maturation of the 0% OSR binary baseline (dark red surface).

It is imperative to highlight a methodological limitation of this experimental phase that inherently points to even greater structural potential. The current analysis evaluates the ternary mixtures exclusively at 4 days of curing, proving that the physical OSR-packing mechanism allows these mixtures to match or exceed the 28-day performance of binary systems. However,

the ternary matrices will also undergo long-term pozzolanic maturation. Due to time constraints, the physical evaluation of ternary mixtures at 28 days, or beyond 6 months, was outside the scope of this research.

To illustrate the magnitude of this untapped potential, a numerical projection was conducted based on the experimental data of the 80/20 matrix. Figure 4.82 presents the three previously discussed surfaces—the binary matrix at 4 and 28 days, and the ternary 5% OSR matrix at 4 days—alongside a theoretical fourth surface (gold).

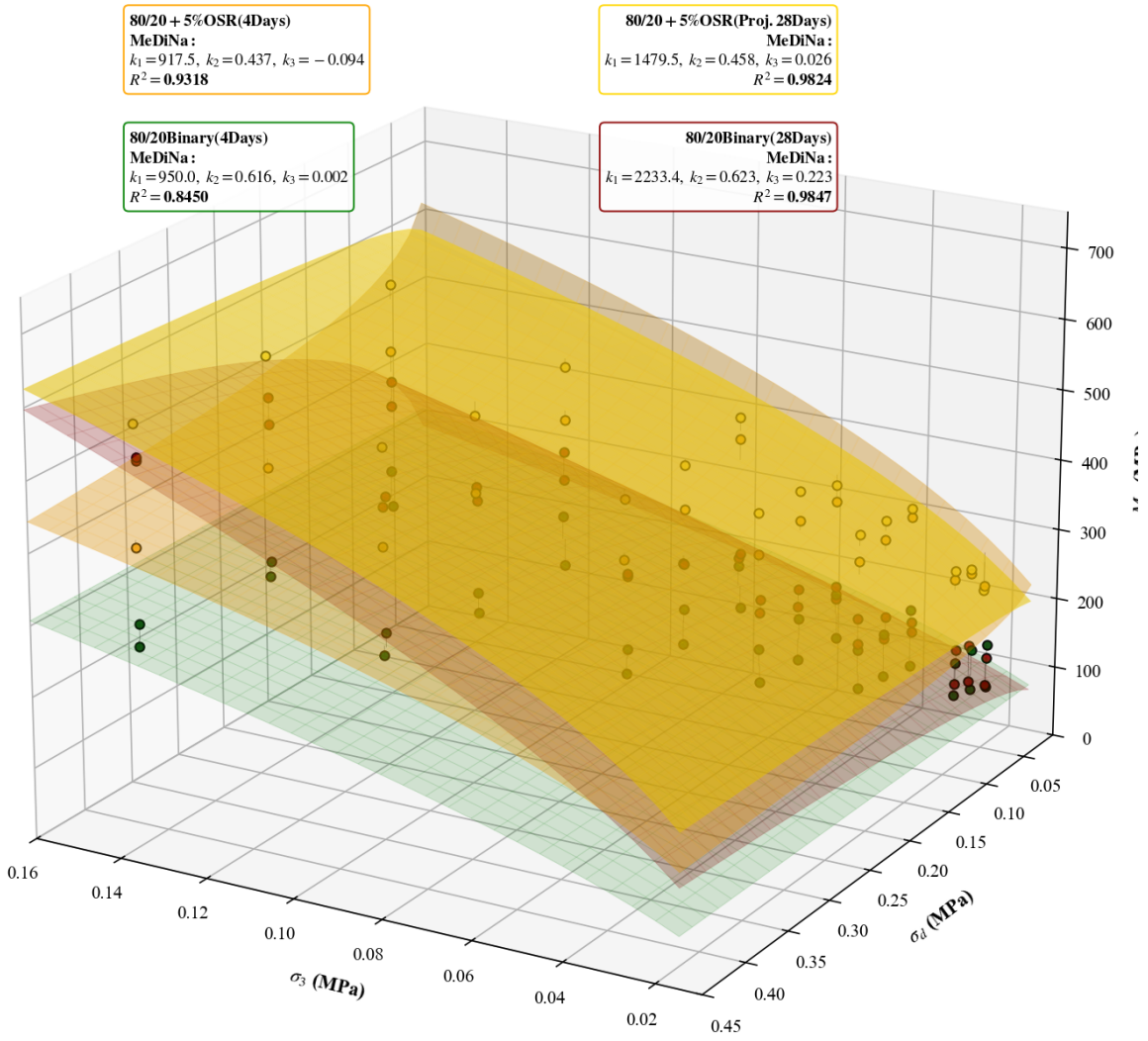


Figure 4.82: Projected maturation of the 80/20 + 5% OSR ternary system.

This projected surface simulates the ternary system at 28 days, assuming it acquires a conservative 70% of the curing gain experienced by the binary mixture over the same period: the gold surface represents the theoretical 28-day response, assuming a proportional 70% gain based on the binary curing curve, reaching resilient moduli above 650 MPa (Fig. 4.82).

The simulation reveals that as the pozzolanic reactions slowly solidify the internal voids already optimized by the OSR filler, the ultimate stiffness of the ternary matrix will likely exceed 610 MPa. This projection suggests that the true capacity of these anthropogenic geomaterials, once fully chemically matured, significantly surpasses the already exceptional thresholds recorded at age 4 days, presenting a critical and promising frontier for future pavement engineering investigations.

These comparative surfaces provide the definitive proof required for modern mechanistic-empirical design: in a properly proportioned ternary system, the physical optimization driven by the fine OSR particles works in perfect synergy with the immediate chemical cationic shock provided by the KRS. This synergy effectively eliminates the critical weakness of slag stabilization—the long pozzolanic latency period—transforming the material into a ready-to-use, high-performance geomaterial.

The inclusion of OSR results in a denser mineral skeleton that maximizes the cementitious efficiency of the KRS binder. By reducing the void volume, the filler ensures that pozzolanic products bridge shorter distances between particles, creating a stable structural plate capable of thriving under traffic loads as early as 4 days of maturation.

4.5.6 - OPTIMUM RESIDUE CONTENT (ORC) AS A PAVEMENT DESIGN CRITERION

While the comparative 3D response surfaces clearly demonstrate the synergistic structural leap achieved by adding Ornamental Stone Residue (OSR), establishing practical limits for this addition is essential for pavement design. The continuous incorporation of non-plastic fines does not yield an infinite increase in stiffness. Instead, the material behavior follows a distinct parabolic trend, governed by the delicate balance between physical packing (void filling) and the disruption of the cementitious matrix.

To quantify this phenomenon and define actionable engineering parameters, the Resilient Modulus (M_R) values for the 85/15 matrix at a representative early-age stress state ($\sigma_3 = 50$ kPa and $\sigma_d = 50$ kPa) were plotted against the OSR content (0%, 5%, and 10%). As depicted in Figure 4.83, a quadratic polynomial fit accurately captures the macroscopic behavior of the ternary system; the parabolic trend defines the Optimum Residue Content (ORC) near the 5% empirical point and establishes the Maximum Residue Content (MRC) intercepting a hypothetical 300 MPa structural target.

The apex of the parabolic trend model suggests the empirical identification of the **Optimum Residue Content (ORC)**. For the 85/15 mixture, the experimental ORC for M_R occurred at the 5% addition level, where the physical interlocking perfectly complements the

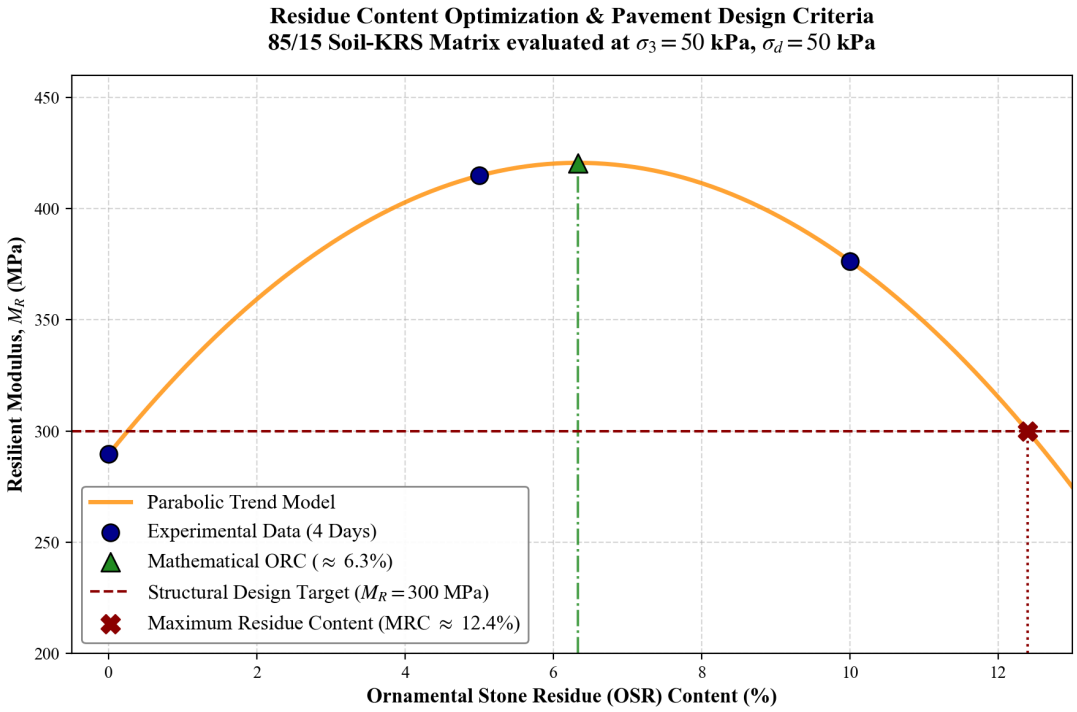


Figure 4.83: Residue Content Optimization and Pavement Design Criteria for the 85/15 Soil-KRS Matrix at 4 days ($\sigma_3 = 50$ kPa, $\sigma_d = 50$ kPa).

available alkaline activator, maximizing the matrix's structural rigidity at 414.8 MPa. However, the quadratic regression indicates that a suggested mathematical ORC lies slightly beyond the experimental point, peaking at approximately 6.3% OSR, suggesting a potential for even finer dosage optimization in future full-scale applications. Beyond this threshold (e.g., at 10% OSR), the surplus of inert filler begins to space apart the reactive soil and slag particles, slightly dampening the early-age cementitious bonds and causing the stiffness to drop to 376.4 MPa.

This parabolic relationship is highly valuable for modern mechanistic-empirical pavement design (such as the MeDiNa framework), as it allows for the definition of the **Maximum Residue Content (MRC)**. While the ORC targets maximum performance, the MRC targets maximum sustainability within safety margins.

For instance, if a pavement project establishes a structural design target of $M_R = 300$ MPa for a high-performance stabilized subbase, the model can project the maximum allowable waste incorporation. As illustrated by the dark red intersection in Figure 4.83, the descending branch of the parabola crosses the 300 MPa target line at approximately 12.4% OSR. This establishes the MRC: the absolute maximum percentage of industrial residue that can be safely incorporated into the matrix while still rigorously fulfilling the structural demands of the engineering project. This approach transforms waste management from an empirical disposal method into a mathematically precise geotechnical solution.

The possible parabolic behavior of the Resilient Modulus (M_R) as a function of the

Ornamental Stone Residue (OSR) content suggests that the physical-chemical stabilization of soils might follow a predictable, non-linear pattern. Based on the experimental curves generated for the 85/15 and 80/20 matrices at $\sigma_3 = 50$ kPa and $\sigma_d = 50$ kPa, it is possible to propose a logical framework for evaluating and optimizing any geotechnical mixture focusing a design criteria chosen, such as best or minimum Resilient Modulus (M_R).

As illustrated in Figure 4.84, plotting multiple stabilization matrices simultaneously reveals profound insights into the material's mechanics; the alignment of the mathematical peaks reveals a "Global Optimization Envelope," defining the ideal physical packing interval regardless of slight variations in the chemical activator content.

The regression models indicate that the mathematical Optimum Residue Content (ORC) for the 85/15 mixture occurs at approximately 6.3%, reaching a peak stiffness of 420.5 MPa. Remarkably, the 80/20 mixture, despite its different chemical proportion, peaks at a nearly identical physical packing threshold of approximately 6.2% (335.6 MPa).

The vertical alignment of these mathematical peaks defines a narrow **Global Optimization Envelope** (highlighted in grey). This finding suggests that the optimal packing density of the soil-residue skeleton is intrinsically linked to the physical characteristics (particle size distribution) of the base soil and the OSR, remaining relatively independent of the activator (KRS) dosage within this studied range.

From an engineering design perspective, this framework might answer the important laboratory question: *How should the testing intervals be established to define the ORC with high precision without excessive costs?* This research proposes a two-tiered testing protocol:

i. **Macro-Screening Phase:** Initial tests should be conducted at wider increments (e.g., 0%, 5%, 10%, 15%) to map the general concavity of the parabola and identify the region where the filler effect transitions into matrix disruption.

ii. **Micro-Optimization Phase:** Once the macro-peak is identified, localized tests with refined increments (e.g., 2% or 2.5% steps) should be performed strictly around the optimal zone. For instance, if the macro-peak occurs at 5%, subsequent tests at 2.5% and 7.5% will provide the resolution needed to mathematically pinpoint the exact ORC with maximum confidence.

Furthermore, mapping multiple matrices simultaneously allows for the definition of the **MRC Operational Window** (highlighted in green). By intersecting the descending branches of the parabolas with a hypothetical structural design target (e.g., $M_R = 300$ MPa), pavement engineers can visualize the safety margins for waste incorporation. In this scenario, while the 80/20 mixture allows for a maximum of 8.9% OSR before dropping below the required stiffness,

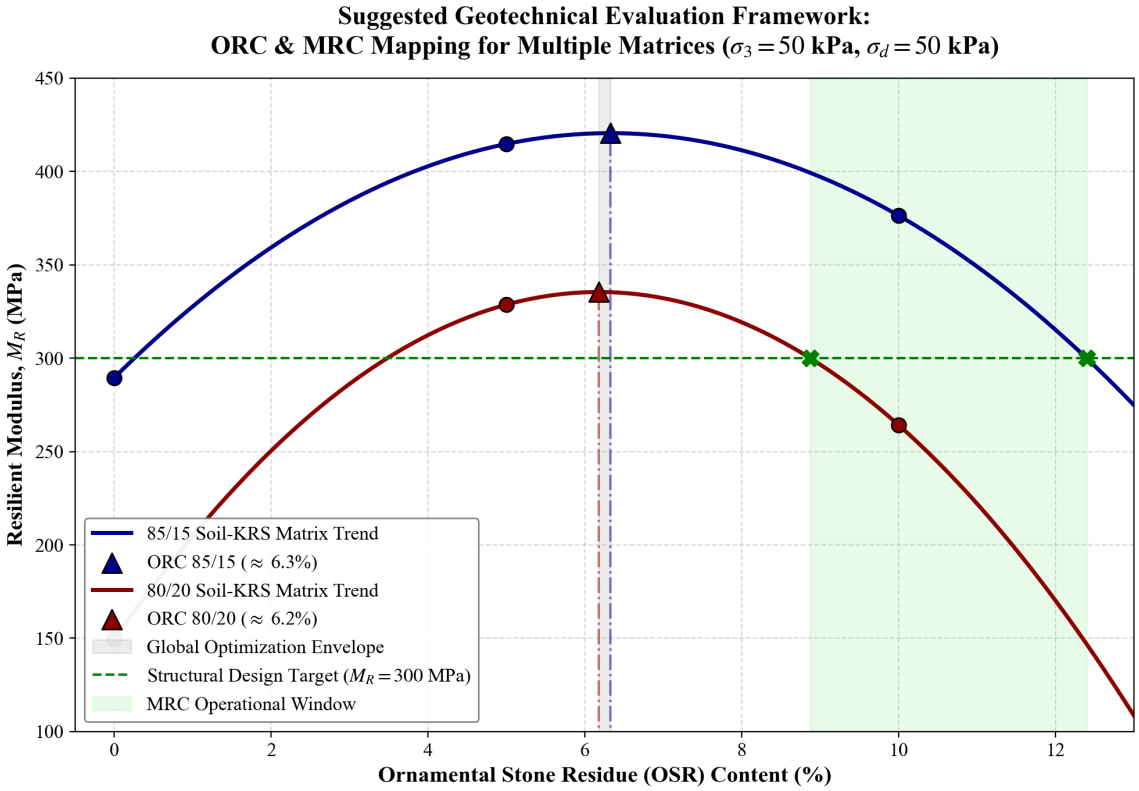


Figure 4.84: Universal Geotechnical Evaluation Framework: ORC and MRC mapping for multiple soil-KRS matrices.

the 85/15 matrix can safely sustain up to 12.4% OSR. This methodology equips engineers with a powerful tool to balance peak mechanical performance (ORC) with maximum environmental sustainability (MRC). All of that for the reference curing time of 4 days.

4.5.7 - PARTIAL CONCLUSIONS ON TERNARY STABILIZATION

The experimental investigation into the ternary stabilization of high-plasticity clayey soils using Kambara Reactor Slag (KRS) and Ornamental Stone Residue (OSR) leads to the following conclusions:

1. **Mechanistic Performance and Temporal Validation:** The research confirms that KRS exerts a substantial impact on the mechanical properties of non-lateritic clay soils. The stabilization is driven by a two-stage chemical maturation: immediate cationic exchange (monitored at 4 days) and long-term pozzolanic maturation (28 days).

2. **Synergy of the Ternary System:** The research successfully validates the synergy between the chemical action of the KRS and the immediate physical reinforcement provided by the OSR. The results prove that OSR acts as a critical granulometric

corrector. By densifying the mineral skeleton, the residue effectively "bridges" the pozzolanic latency period of the slag.

3. **Optimum Residue Content (ORC) and Granular Equilibrium:** The identification of the ORC (5% for 85/15 and 10% for 80/20) promotes a significant horizontalization of the M_R response. This state of "granular equilibrium" ensures that the physical interlocking of the OSR fines compensates for the clay matrix's natural decreasing stiffness (reduction of MR), shifting the material toward a stress-independent behavior.

4. **Final Remarks:** The transition from traditional empirical metrics (CBR) to a mechanistic-empirical protocol (M_R) was essential to reveal the true structural superiority of these ternary systems. The high magnitude of stiffness and the stabilization of the k_3 parameter align these non-traditional mixtures with modern pavement design standards (MeDiNa).

5 - CONCLUSIONS

This research provides a comprehensive geotechnical framework for the sustainable utilization of two importanat industrial byproducts of the Espírito Santo state—specifically Ornamental Stone Residue (OSR) and Kambara Reactor Slag (KRS)—in geotechnical infrastructure, especially embankments and pavements. Through a multi-scale experimental program and mechanistic-empirical analysis, this thesis demonstrates that the controlled combination of these residues with regional tropical soils transforms environmental liabilities into high-performance geotechnical assets. The main conclusions drawn from the literature review, empirical testing, and mechanistic evaluations are structured below.

5.1 - STATE OF THE ART OF OSR UTILIZATION

The comprehensive analysis of OSR confirms its immense potential as a sustainable resource for pavement engineering and earthworks.

- Environmental and Physical Profile: OSR is fundamentally a fine-grained, predominantly silty material, typically classified as ML (USCS) or A-4/A-6 (AASHTO). Its environmental classification as a Class II-B (non-hazardous and inert) residue reinforces its safety profile for large-scale engineering reuse.
- Soil Improvement Mechanisms: When integrated into cohesive soils, OSR acts primarily through physical modification. It consistently reduces Atterberg limits (LL, PL, PI), decreasing the moisture sensitivity and swelling potential of problematic soils while improving workability.
- Mechanical Gains: As a grading corrector, OSR optimizes the particle size distribution of the mixture. This void-filling effect generally increases the Maximum Dry Density (MDD) and decreases the Optimum Moisture Content (OMC), leading to substantial improvements in static load-bearing indicators such as the California Bearing Ratio (CBR) and Unconfined Compressive Strength (UCS).
- Standalone Viability: OSR also shows significant promise as a standalone fill material. Being non-plastic and non-swelling, it possesses high internal friction angles and low cohesion, offering an economically viable alternative that preserves virgin natural resources.
- Efficiency of Milled Slag (KRSP): As highlighted in the literature review, the application

of KRS in powder form (KRSP) demonstrates exceptional efficiency. Small quantities of KRSP, such as 3% to 5%, are capable of matching the mechanistic performance of proportionally much higher volumes of standard granular KRS, revealing the profound impact of specific surface area on reactivity.

5.2 - STATE OF THE ART OF KRS UTILIZATION

The application of steelmaking slags, particularly KRS, represents a highly effective stabilization strategy driven by intense physicochemical reactivity.

- The Four-Model Interaction: The stabilization of soils with KRS is governed by four distinct but simultaneous mechanisms: (1) Chemical Cementation (formation of C-S-H and C-A-H gels), (2) Physicochemical Modification (cation exchange and diffuse double layer reduction), (3) Particle Size Stabilization (packing density optimization), and (4) Granular Reinforcement (interlocked granular skeleton).
- Chronological Maturation: The unified theory of slag stabilization structures these mechanisms into three phases: an immediate phase dominated by cationic shock and improved workability; a short-term phase where initial skeleton interlocking and ettringite nucleation occur; and a long-term phase marked by robust silicate cementation, ensuring lasting structural durability.
- Sustainable Replacement: High calcium oxide (CaO) and silica content confer cementitious and pozzolanic properties to KRS, positioning it as a highly adaptable, low-carbon substitute for traditional commercial binders like Portland cement or lime.

5.3 - MECHANISTIC BEHAVIOR OF OSR IN LATERITIC CLAYS

The application of OSR in high-quality lateritic soils exposes a critical paradox between empirical support capacity and dynamic stiffness.

- Empirical Improvement: The addition of OSR (up to 15%) into lateritic clay matrices enhances traditional compaction characteristics. The residue's contribution to particle interaction and void filling results in increased dry density, elevated CBR values, and higher UCS.
- Mechanistic Nuance: Despite the gains in static resistance, the Resilient Modulus (M_R)—extracted from Cyclic Load Triaxial Tests (CLTT)—exhibits a nuanced response. Increasing OSR content up to 15% yielded either a neutral effect or a slight reduction in dynamic stiffness.

- Paradigm Shift: This divergence demonstrates that while OSR effectively improves a soil's resistance to static penetration (CBR), its impact on elastic response under repeated traffic loading (M_R) is not directly proportional. This conclusion highlights the inadequacy of relying solely on the CBR method and underscores the absolute necessity of mechanistic-empirical evaluations for modern pavement design.

5.4 - MECHANISTIC BEHAVIOR OF KRS IN NON-LATERITIC CLAYS

The incorporation of KRS fundamentally rewrites the mechanical behavior of marginal, non-lateritic cohesive soils.

- Behavioral Transition: High-plasticity, non-lateritic clays inherently exhibit a "decreasing stiffness" behavior, where M_R values degrade under shear stress. The addition of KRS completely reverses this trend, transforming poor-quality clay into a "increasing stiffness" which M_R increases with increasing deviatoric stresses, a type of matrix comparable to premium granular aggregates.
- High-Stiffness Matrices: The aggressive chemical stabilization provided by KRS generates exceptional M_R magnitudes. The resulting geomaterial exhibits mechanical properties that not only meet but frequently exceed the requirements for structural base courses, allowing for significant reductions in the thickness of upper pavement layers.

Influence of Curing Time on the Mechanistic Behavior of KRS Mixtures

The mechanistic performance of KRS-stabilized soils is strictly time-dependent, validating the necessity of temporal benchmarking in geotechnical design.

- Immediate Stage (4 Days): In the early curing stages, the primary driver of stabilization is the "cationic shock." The high availability of free lime (CaO) induces rapid flocculation-agglomeration of clay particles, providing significant early-age stiffness and immediate structural stability to the layer.
- Maturation Stage (28 Days): Long-term performance is dictated by slow-reacting pozzolanic activity. Over 28 days, the continuous dissolution of silica and alumina in the highly alkaline environment precipitates permanent cementitious products. This maturation solidifies the macroscopic skeleton, permanently reducing plastic deformability and maximizing the M_R.

5.5 - INFLUENCE OF OSR ON THE MECHANISTIC BEHAVIOR OF TERNARY MIXTURES (NON-LATERITIC CLAYS AND KRS)

The unprecedented investigation of ternary mixtures (Soil + KRS + OSR) proves that the synergistic combination of physical and chemical agents yields the ultimate infrastructure geomaterial.

- Bridging the Latency Period: While KRS provides immense long-term chemical strength, its coarse granular nature leaves initial voids in the matrix. OSR acts as a highly effective granulometric corrector. The fine OSR particles immediately densify the mineral skeleton, physically bridging the "pozzolanic latency period" of the slag.
- Physics Over Pure Chemistry: The ternary system proves that physical packing is just as critical as chemical reactivity. The OSR filler reinforces the intergranular contacts, ensuring immediate mechanical stability while the KRS slowly develops its cementitious bonds, resulting in a cohesive, ultra-stiff matrix.
- Modulation of Cationic Shock: In ternary systems, OSR acts as a controller of the violence of the cationic shock induced by the KRS. The addition of OSR mitigated the abrupt loss of plasticity, allowing the execution of standard Atterberg limits tests. Since different OSR percentages achieved similar high performances, an optimal OSR content effectively controls the chronology of the chemical reactions, ensuring a more manageable stabilization process.

5.6 - ORC AND MRC CONCEPTS AS DESIGN CRITERIA FOR BINARY AND TERNARY MIXTURES BASED ON RESILIENT MODULUS

The establishment of the Optimum Residue Content (ORC) and Maximum Residue Content (MRC) frameworks represents a definitive transition from trial-and-error empiricism to rational mechanistic engineering.

- Granular Equilibrium (ORC): The ORC is not merely the point of highest strength; it represents a state of "granular equilibrium." At the ORC (e.g., 5% OSR for an 85/15 Soil-KRS base), the physical interlocking of the fines perfectly compensates for the clay matrix's tendency to deform. This manifests as a significant flattening of the 3D M_R response surface, shifting the material toward a highly predictable, stress-independent behavior.
- Sustainability vs. Performance (MRC): The MRC defines the upper limit of waste incorporation before structural degradation occurs. It provides engineers with a crucial

boundary condition when the primary project goal is maximum environmental waste diversion without compromising the minimum mechanistic thresholds required by the MeDiNa method.

- The MeDiNa Alignment: By utilizing ORC and MRC based on Resilient Modulus (M_R) and Permanent Deformation (PD), this research aligns the valorization of industrial residues with the Brazilian National Pavement Design Method (MeDiNa). It supplies the missing constitutive models for these novel anthropogenic geomaterials, empowering designers to confidently specify sustainable, high-performance infrastructure solutions.

5.7 - RECOMMENDATIONS FOR FUTURE RESEARCH

Based on the operational observations and analytical findings of this study, the following areas are strongly recommended for future investigation:

- Field Compaction Window for KRS Mixtures: Given the abrupt loss of plasticity observed within minutes of mixing soil with KRS, comprehensive field and laboratory studies should investigate the exact temporal degradation of workability. Defining strict guidelines regarding maximum allowable wait times (e.g., delays exceeding 24 hours) between mixing, grading, and compaction is essential to prevent structural performance losses in highway projects.

- Granulometric Impact of KRS (Powder vs. Granular): A dedicated comparative analysis is required to evaluate the mechanistic impact of KRS particle size. Considering the high efficiency observed with small dosages of KRSP (powder/milled slag), future research should quantify the performance, economic, and environmental trade-offs between utilizing raw granular KRS versus processed KRSP for pavement stabilization.

- Stockpile Pre-Stabilization with Clay Matrices: Investigate the optimal proportion of cohesive soil required to encapsulate and chemically stabilize raw KRS and OSR directly at the industrial stockpiles. For KRS, research should focus on buffering the high alkalinity and pre-emptively mitigating the expansive potential of free lime before transport. For OSR, the goal is to prevent wind dispersion of fines and control the leaching of residual additives, effectively transforming raw waste into a pre-stabilized, ready-to-use anthropogenic geomaterial at the source.

- Broadening the KRS-Soil Interaction Database: Expand the mechanistic evaluation of KRS by testing its interaction with a wider spectrum of regional and national soils. This should include highly weathered tropical soils, such as porous lateritic clays and varied

saprolites, to verify the universality of the cationic shock and to identify any specific mineralogical incompatibilities that might hinder effective pozzolanic maturation across different pedological profiles.

- Large-Scale Permanent Deformation Analysis: Bridge the gap between laboratory cyclic triaxial testing and real-world field performance by conducting full-scale accelerated pavement testing. This research should focus on the long-term accumulation of permanent deformation under realistic dynamic traffic loads and environmental weathering, physically validating the shakedown behavior and the structural longevity of the optimized binary and ternary mixtures designed via the MeDiNa framework.

- Numerical Modeling of Geochemical Interactions: Transition from empirical observation to predictive numerical modeling. Future studies should develop models coupled with reactive transport modules to simulate the kinetics of the cationic shock and the long-term precipitation of pozzolanic gels. This approach would enable the computational prediction of stiffness evolution over time and the spatial distribution of cementitious bonds within the stabilized matrix, reducing the reliance on extensive laboratory curing periods.

- Comprehensive Life Cycle Assessment (LCA) and Techno-Economic Analysis: While the mechanical superiority of these mixtures has been validated, future research should quantify their macro-environmental impact. Conducting a full LCA would allow for the precise measurement of carbon footprint reduction and energy savings achieved by substituting traditional binders (such as Portland cement or lime) and quarried aggregates with OSR and KRS, solidifying the economic and environmental justification for their large-scale adoption.

- Data-Driven Optimization via Machine Learning: Advanced mineralogical and chemical characterization methods—such as X-ray Fluorescence (XRF) and X-ray Diffraction (XRD)—when systematically cross-analyzed with non-linear geotechnical parameters, generate highly complex, high-dimensional datasets. The manual interpretation of these coupled chemical-physical interactions requires prohibitive time and effort due to the immense variety and subtle interdependencies of the data vectors. Future research should implement machine learning (ML) algorithms not as an autonomous solution, but as a powerful computational tool to handle this multivariate complexity and enhance analytical productivity. By training predictive models on high-resolution chemical signatures (XRF/XRD) alongside structural and physical properties of regional soils and residues, engineers can decode complex patterns to rapidly estimate the Optimum Residue Content (ORC) and Resilient Modulus (M_R). This approach bridges

advanced laboratory characterization and mechanistic design, drastically streamlining mix screening while overcoming the practical constraints of human multi-variable processing.

- Unsaturated Soil Mechanics and Suction Dynamics: Given that pavement layers predominantly operate under unsaturated conditions, it is crucial to understand the hydraulic behavior of the stabilized matrices. Future research should evaluate the Soil-Water Characteristic Curves (SWCC) of ternary mixtures to determine how the void-filling effect of OSR and the cementation of KRS alter water retention, permeability, and matric suction over time, which directly influence the long-term stiffness variations under seasonal climatic changes.

BIBLIOGRAPHY

AASHTO. (1999). Aashto t 307 – 99: Standard method of test for determining the resilient modulus of soils and aggregate materials. (reapproved 2017) [Computer software manual]. Washington, D.C..

Abbas, M. M., & Muntean, R. (2025). Marble powder as a sustainable cement replacement: A review of mechanical properties. *Sustainability*, *17*(2), 736. doi: 10.3390/su17020736

Abdelkader, H. A. M., Ahmed, A. S. A., Hussein, M. M. A., Ye, H., & Zhang, J. (2022). An experimental study on geotechnical properties and micro-structure of expansive soil stabilized with waste granite dust. *Sustainability*, *14*(10), 6218. doi: 10.3390/su14106218

ABIROCHAS. (2021). *The brazilian ornamental stone sector. report 10/2021* (Tech. Rep.). Brasília, Brazil: Associação Brasileira da Indústria de Rochas Ornamentais. ([in Portuguese])

ABIROCHAS. (2024). *Balance of the brazilian ornamental and cladding stone sector in 2023. report 01/2024* (Tech. Rep.). Brasília, Brazil: Associação Brasileira da Indústria de Rochas Ornamentais. ([in Portuguese])

ABNT. (1984). Nbr 6508: Soil grains passing the 4.8 mm sieve – determination of specific gravity [Computer software manual]. Rio de Janeiro, RJ. ([in Portuguese])

ABNT. (2004). Nbr 10007: Sampling of solid waste [Computer software manual]. Rio de Janeiro, Brazil. ([in Portuguese])

ABNT. (2014). Nbr 12653: Pozzolanic materials [Computer software manual]. Rio de Janeiro, Brazil. ([in Portuguese])

ABNT. (2015). Nbr 16364: Execution of granulometrically stabilized sub-base and base with steel aggregate for road paving [Computer software manual]. Rio de Janeiro, Brazil. ([in Portuguese])

ABNT. (2016a). Nbr 7181: Soil – grain size analysis [Computer software manual]. Rio de Janeiro, RJ. ([in Portuguese])

ABNT. (2016b). *Nbr 9895: Soil — california bearing ratio (cbr) — test method* (Tech. Rep.). Rio de Janeiro, Brazil: Brazilian Association of Technical Norms (ABNT). ([in Portuguese])

ABNT. (2016a). Nbr 7181: Soil – grain size analysis [Computer software manual]. Rio de Janeiro, RJ. ([in Portuguese])

ABNT. (2016b). Nbr 7180: Soil – plastic limit determination [Computer software manual]. Rio de Janeiro, RJ. ([in Portuguese])

ABNT. (2016c). Nbr 6459: Soil – liquid limit determination [Computer software manual]. Rio

de Janeiro, RJ. ([in Portuguese])

ABNT. (2016d). Nbr 7182: Soil – compaction test [Computer software manual]. Rio de Janeiro, RJ. ([in Portuguese])

ABNT. (2016e). Nbr 9895: Soil – california bearing ratio (cbr) – test method [Computer software manual]. Rio de Janeiro, RJ. ([in Portuguese])

ABNT. (2021). Nbr 15116: Agregados reciclados para uso em argamassas e concretos de cimento portland – requisitos e métodos de ensaio [Computer software manual]. Rio de Janeiro, RJ. ([in Portuguese])

Aguiar, P. A. (2019). *Avaliação da resistência de um solo do município de paulista-pe estabilizado com cimento portland e resíduo de polimento de rocha ornamental* (Bachelor's thesis). Federal University of Campina Grande.

Akbulut, H., & Gürer, C. (2007). Use of aggregates produced from marble quarry waste in asphalt pavements. *Building and Environment*, *42*, 1921–1930. doi: 10.1016/j.buildenv.2006.03.012

Al-Zboon, K., & Al-Zou'by, J. (2014). Recycling of stone cutting slurry in concrete mixes. *Journal of Material Cycles and Waste Management*, *17*(2), 324–335. doi: 10.1007/s10163-014-0246-x

Alam, M. F., Kumar, A., & Kumar, R. (2023). A review on utilization of industrial wastes and byproducts in highway construction. *American Journal of Science and Learning for Development*, *2*(9).

Aldeed, M., Al-Ameri, M., & Jayasuriya, A. (2020). Stabilization of soft clay using alkali-activated slag. *Materials Today: Proceedings*, *32*, 650–656. doi: 10.1016/j.matpr.2020.03.149

Ally, A. N., Blanche, M. M., Nana, U. J. P., Grâce, M. M., François, N., & Pettang, C. (2021). Recovery of mining wastes in building materials: A review. *Open Journal of Civil Engineering*, *11*, 379–397. doi: 10.4236/ojce.2021.114022

Almeida, R. P. M. (2014). *Evaluation of the hydraulic performance of recycled aggregates from steel slags and c&d waste to water and msw leachate and their comparison with basalt and limestone* (Master's thesis). Nova University Lisbon, Lisbon, Portugal.

Amaral, L. F., Delaqua, G. C. G., Nicolite, M., Marvila, M. T., Azevedo, A. R. G., Alexandre, J., ... Monteiro, S. N. (2020). Eco-friendly mortars with addition of ornamental stone waste - a mathematical model approach for granulometric optimization. *Journal of Cleaner Production*, *248*, 119283. doi: 10.1016/j.jclepro.2019.119283

Amulya, G., Moghal, A. A. B., & Almajed, A. (2023). Sustainable binary blending for low-volume roads—reliability-based design approach and carbon footprint analysis. *Materials*, *16*(5), 2065. doi: 10.3390/ma16052065

Amulya, G., Moghal, A. A. B., & Almajed, A. A. (2021). State-of-the-art review on suitability

of granite dust as a sustainable additive for geotechnical applications. *Crystals*, *11*(12), 1526. doi: 10.3390/cryst11121526

Andrade, C. M. S. (2018). *Evaluation of mechanical and microstructural performance of cement-treated graded crushed stone with the incorporation of kr steelmaking coproduct* (Master's thesis). Federal University of Espírito Santo, Vitória, Brazil.

Anglo American. (2022). *Ferronickel slag is used in roadways.* Brasil Mineral, Belo Horizonte, Brazil. Retrieved from https://brasilmineral.com.br/noticias/escoria-de-ferroniquel-e-usada-em-rodovias ([in Portuguese])

Araújo, M. L. (2018). *Soil stabilization with marble waste addition* (Bachelor's thesis). Federal Rural University of the Semi-Arid.

ArcelorMittal. (2016). Co-product portfolio [Computer software manual]. Serra, Brazil. ([in Portuguese])

ArcelorMittal. (2025). *Relationship with the communities.* Retrieved from https://brasil.arcelormittal.com/sustentabilidade/investimento-social/arcelormittal-tubarao/relacao-com-comunidades (Retrieved June 21, 2025; [in Portuguese])

ASTM. (2002a). Astm d 422 – 63: Standard test method for particle-size analysis of soils. (reapproved 2002) [Computer software manual]. West Conshohocken, PA.

ASTM. (2002b). Astm d 854 – 02: Standard test methods for specific gravity of soil solids by water pycnometer [Computer software manual]. West Conshohocken, PA.

ASTM. (2004). Astm d 3282 – 93: Standard practice for classification of soils and soil-aggregate mixtures for highway construction purposes. (reapproved 2004) [Computer software manual]. West Conshohocken, PA.

ASTM. (2012a). Astm d 698 – 12: Standard test methods for laboratory compaction characteristics of soil using standard effort [Computer software manual]. West Conshohocken, PA.

ASTM. (2012b). Astm d 1557 – 12: Standard test methods for laboratory compaction characteristics of soil using modified effort [Computer software manual]. West Conshohocken, PA.

ASTM. (2017). Astm d 4318 – 17: Standard test methods for liquid limit, plastic limit, and plasticity index of soils [Computer software manual]. West Conshohocken, PA.

Bacarji, E., Toledo Filho, R. D., Koenders, E. A. B., Figueiredo, E. P., & Lopes, J. L. M. P. (2013). Sustainability perspective of marble and granite residues as concrete fillers. *Construction and Building Materials*, *45*, 1–10. doi: 10.1016/j.conbuildmat.2013.03.032

Bahiense, A., de Castro Xavier, G., Rangel Garcez de Azevedo, A., & Montêiro, S. (2021).

Dosage of interlocking paving with ornamental rock waste: An experimental design approach, particle packing and polluting potential. *Case Studies in Construction Materials*, *15*, e00596. doi: 10.1016/j.cscm.2021.e00596

Barksdale, R. D. (1972). Laboratory evaluation of rutting in base course materials. In *Proceedings of the 3rd international conference on the structural design of asphalt pavements* (pp. 161–174). Ann Arbor, MI.

Barrientos, V., Delgado, J., Navarro, V., Juncosa, R., Falcón, I., & Vázquez, A. (2010). Characterization and geochemical–geotechnical properties of granite sawdust produced by the dimension stone industry of o porriño (pontevedra, spain). *Quarterly Journal of Engineering Geology and Hydrogeology*, *43*(4), 403–414. doi: 10.1144/1470-9236/08-098

Bastos, F. C. (2022). *Field and laboratory study of the mechanical behavior of soil stabilized with kr slag* (Master's thesis in Civil Engineering). Federal University of Espírito Santo.

Belihu, J., Teshome, G., Geremew, A., & Fayissa, B. (2025). Experimental study on the stabilization of expansive soil with blended fine cinder gravel and waste marble dust: A case study of jimma town. *Jordan Journal of Civil Engineering*, *19*(1). doi: 10.14525/JJCE.v19i1.10

Ben, L. H. F., Pascoal, P. T., Falcão, P. R., Baroni, M., Specht, L. P., & Neitzke, M. (2023). Deformação permanente de solo argiloso laterítico por meio da metodologia multiestágios. In *Anais da 48 rapv e 25 enacor.* Foz do Iguaçu, PR.

Binici, H., Shah, T., Aksogan, O., & Kaplan, H. (2008). Durability of concrete made with granite and marble as recycle aggregates. *Journal of Materials Processing Technology*, *208*(1-3), 299–308.

Bittencourt, M. C. S. (2023). *Technical study of the application of revsol® mixture with two types of soils from the santa leopoldina-es region in the paving of a low-volume traffic road* (Specialization thesis). Federal Institute of Espírito Santo (IFES), Vitória, Brazil.

Boldrini, B. G., & Pacheco, R. F. R. (2022). Study of the behavior of ld-type steel slag in the base of urban pavements. *Revista Ifesciência*, *8*(1), 01–10. Retrieved from `https://doi.org/10.36524/ric.v8i1.906` ([in Portuguese])

Bona, A. C. D., et al. (2022). Influence of compaction energy on the crushing of barreiras formation soils. *Soils and Rocks*.

Bona, A. C. D., Silveira, V. L., Guimarães, A. C. R., & Azevedo Junior, C. J. d. (2022). Analysis of the expansive effects of steel slag through dynamic tests in a subbase mixture. In *Xx brazilian congress on soil mechanics and geotechnical engineering.* Goiânia, GO, Brazil. ([in Portuguese]) doi: 10.4322/cobramseg.2022.0622

Braz, R. I. F. (2024). *Evaluation of the reduction of expansiveness of soil stabilized with ornamental rock processing residue* (Master's thesis). Universidade Federal do Rio

Grande do Norte, Natal, Brazil.

Bridi, L. O. (2020). *Study of the effect of stabilization with kr desulfurization coproduct on the physical, mechanical, and chemical properties of soils with different fines contents* (Master's thesis). Universidade Federal do Espírito Santo (UFES), Vitória, ES, Brazil.

Brown, S. F. (1996). Soil mechanics in pavement engineering. *Géotechnique*, *46*(3), 383–426.

Buitrago, N. D. T., Oliveira, V. H. S., Ribeiro, L. F. M., & Cavalcante, A. L. B. (2016). Análise da viabilidade do uso de açobrita em pavimentos rodoviários. In *Xviii congresso brasileiro de mecânica dos solos e engenharia geotécnica.* Belo Horizonte, Brazil.

Cabral, W. S. (2021). *Exploration, comparative analysis, and modeling of permanent deformation of granular materials in the mossoró/rn microregion* (Doctoral dissertation). Universidade Federal do Ceará.

Camapum de Carvalho, J., & Mortari, D. (1994). Caracterização geotécnica de solos porosos do distrito federal. In *Anais do 3º simpósio brasileiro de escavações subterrâneas* (pp. 109–122). Brasília, DF: ABMS/ABGE.

Cardoso, A. (2019a). *Mechanical behavior of a soil from the guabirotuba formation with ornamental rock waste addition* (Master's thesis). Federal University of Paraná.

Cardoso, A. (2019b). *Mechanical behavior of a soil from the guabirotuba formation with ornamental rock waste addition* (Master's thesis). Federal Technological University of Paraná, Curitiba, Brazil.

Cardoso, M. D. (2009). *Recycling of electric arc furnace ladle slag into ceramic material* (Master's thesis). University of the Sinos River Valley, São Leopoldo, RS, Brazil.

Carvalho, S. G., Meneguelli, M. R. S., & Sartório, E. A. (2022). *Granulometric soil stabilization with iron mining coproduct for sub-base layer in road pavements* (Specialization thesis). Federal Institute of Espírito Santo (IFES), Vitória, Brazil.

Cavalline, T. L., & Sutter, L. (2024). *Use of industrial byproducts in concrete paving applications* (Tech. Rep. No. FHWA-HIF-24-049). National Concrete Pavement Technology Center, Iowa State University.

CEN. (2004). En 13286-7: Unbound and hydraulically bound mixtures - part 7: Cyclic load triaxial test for unbound mixtures [Computer software manual]. Brussels, Belgium.

Centrorochas. (2025). *Informativo mensal: Exportações de rochas naturais* (Tech. Rep.). Associação Brasileira de Rochas Naturais / Sindirochas. Retrieved from `www.centrorochas.org.br` (Relatório Comparativo de Faturamento e Evolução de Blocos e Chapas (Dados de Janeiro 2025/2026))

Chandra, S., Kumar, P., & Feyissa, B. A. (2002). Use of marble dust in road construction. *Road Materials and Pavement Design*, *3*(3), 317–330.

Chicon, M. C. (2019). *Fine residues from the ornamental rock industry: The deposited and segregated materials* (Master's thesis). Universidade Federal do Espírito Santo (UFES),

Vitória, Brazil.

CNT. (2024). *Pesquisa CNT de rodovias 2024* (Tech. Rep.). Brasília, Brazil: Confederação Nacional do Transporte.

CNT. (2025). *Pesquisa CNT de rodovias 2025* (Tech. Rep.). Brasília, Brazil: Confederação Nacional do Transporte.

Cunha, Y. G. d. (2020). *Avaliação das propriedades ambientais do lixiviado de obras geotécnicas melhoradas com coprodutos siderúrgicos* (Master's thesis). Universidade Federal do Espírito Santo (UFES).

Dawson, A. R., & Wellner, F. (1999). *Plastic behaviour of granular materials* (Research Report). Nottingham, UK: University of Nottingham / Technical University of Dresden. (European Commission COST 337 Project Report)

DER-ES. (2019). *Logistics efficiency program of espírito santo: Environmental and social management plan – esmp – sections 2 and 4 (final version)* (Tech. Rep.). Vitória, Brazil: Department of Buildings and Highways of Espírito Santo (DER-ES) / Inter-American Development Bank (IDB). ([in Portuguese])

Dias, M. B. O. (2024). *Utilization of ornamental rock processing residue (ospr) in pavement layers* (Master's thesis). Federal University of Espírito Santo, Vitória, Brazil.

Dias, T. C. C. C. (2025). *Law project nº 2.159/2021. parecer nº sf/25959.20904-08 de 2025-plen* (Tech. Rep.). Brasília, Brazil: Senado Federal.

Dieguez, A. C. d. O. (2018). *Utilization of kambara reactor slag in the composition of portland cement* (Master's thesis). Federal Institute of Espírito Santo (IFES), Vitória, ES, Brazil. ([in Portuguese])

DNER. (1997). Dner es-303/97 - pavement - granularly stabilized base / paving - granulometrically stabilized base [Computer software manual]. Rio de Janeiro, Brazil.

DNIT. (2005). Highway maintenance manual. 2nd ed. [Computer software manual]. Brasília, Brazil. ([in Portuguese])

DNIT. (2006). Dnit - 031 - 2006 - es – flexible pavements [Computer software manual]. Brasília, Brazil. ([in Portuguese])

DNIT. (2009a). Dnit 108/2009 – es: Earthworks: Embankments - service specification [Computer software manual]. Brasília, DF. ([in Portuguese])

DNIT. (2009b). Earthworks: Embankments - service specification. dnit 108/2009 – es [Computer software manual]. Brasília, Brazil. ([in Portuguese])

DNIT. (2009a). Dnit 113/2009-es: Road paving – artificial aggregate – evaluation of the expansion potential of steel slag [Computer software manual]. Brasília, Brazil. ([in Portuguese])

DNIT. (2009b). Dnit 114/2009-es: Road paving – granulometrically stabilized sub-base with steel slag - acerita® [Computer software manual]. Brasília, Brazil. ([in Portuguese])

DNIT. (2009c). Dnit 115/2009-es: Road paving – granulometrically stabilized base with steel slag - acerita® [Computer software manual]. Brasília, Brazil. ([in Portuguese])

DNIT. (2010). Dnit 139/2010 – es: Paving – granular stabilized sub-base – service specifications [Computer software manual]. Brasília, DF. ([in Portuguese])

DNIT. (2016). *Manual de pavimentação* (3rd ed.; Tech. Rep. No. IPR 719). Rio de Janeiro: Departamento Nacional de Infraestrutura de Transportes.

DNIT. (2017). Dnit 406/2017-es: Road paving – granulometrically stabilized base with açobrita® [Computer software manual]. Brasília, Brazil. ([in Portuguese])

DNIT. (2017b). Dnit 407/2017-es: Road paving – granulometrically stabilized sub-base with açobrita® [Computer software manual]. Brasília, Brazil. ([in Portuguese])

DNIT. (2018). Dnit 179/2018-ie: Pavimentação – solos – determinação da deformação permanente – instrução de ensaio [Computer software manual]. Rio de Janeiro, RJ. ([in Portuguese])

DNIT. (2018a). Dnit 134/2018-me: Pavimentação – solos – determinação do módulo de resiliência – método de ensaio [Computer software manual]. Rio de Janeiro, RJ. ([in Portuguese])

DNIT. (2018b). Dnit 179/2018-ie: Pavimentação – solos – determinação da deformação permanente – instrução de ensaio [Computer software manual]. Rio de Janeiro, RJ. ([in Portuguese])

DNIT. (2020). *IPR - MeDiNa versão 1.1.4.0* (Tech. Rep.). Rio de Janeiro, RJ, Brazil: Departamento Nacional de Infraestrutura de Transportes.

DNIT. (2022). *Resolution no. 5, of april 27, 2022: Provides for the use of the maintenance condition index (ICM) for paved and unpaved highways under the jurisdiction of the national department of transport infrastructure (DNIT)* (Resolution). Brasília, DF, Brazil: National Department of Transport Infrastructure (DNIT). ([in Portuguese])

DNIT. (2023). Dnit 445/2023-es: Earthworks – primary surfacing – service specification [Computer software manual]. Brasília, Brazil. ([in Portuguese])

DNIT. (2025). Dnit 108/2009–es: Terraplenagem – aterros – especificação de serviço (com errata de 2025) [Computer software manual]. Brasília, DF. ([in Portuguese])

DNIT. (2026). *Manual de dimensionamento nacional de pavimentos (MeDiNa)* (Tech. Rep.). Brasília, DF, Brazil: Departamento Nacional de Infraestrutura de Transportes.

Dunlap, W. A. (1963). A report on a mathematical model describing the deformation characteristics of granular materials. *Texas Transportation Institute*.

Eades, J. L., & Grim, R. E. (1960). Reaction of hydrated lime with pure clay minerals in soil stabilization. *Highway Research Board Bulletin*, *262*, 51–63.

Eades, J. L., & Grim, R. E. (1966). A quick test to determine lime requirements for soil stabilization. *Highway Research Record*, *139*, 31–41.

Earland, M. G., & Mayhew, H. C. (1989). Assessing the quality of gravel sub-base. In *Unbound aggregates in roads* (pp. 367–379). Butterworth-Heinemann.

Eighmy, T. T. (2000). Use of recycled materials in highway construction. *Public Roads*, *64*(3). Retrieved from https://www.researchgate.net/publication/291355218

Elghamy, T. T., & Chesner, W. H. (2001). *Framework for evaluating use of recycled materials in the highway environment* (Tech. Rep. No. FHWA-RD-00-140). Federal Highway Administration.

Eltwati, A., Elkaseh, A., & Tarhuni, F. (2020). Potential of granite dust to improve the engineering properties of soft soils for road construction. *Science Proceedings Series*, *2*(1). doi: 10.31580/sps.v2i1.1254

Emmanuel, U. O., Ogbonnaya, I., & Uche, U. B. (2021). Performance evaluation of granite dust, dolerite dust and woodash as additives on the lateritic soil of sagamu-papalanto southwestern nigeria and its implication for road construction. *Global Journal of Science Frontier Research: H Environment & Earth Science*, *21*(1).

Erlingsson, S., Rahman, M. S., & Salour, F. (2017). Characteristics of unbound granular materials from multi-stage cyclic load triaxial tests. *Road Materials and Pavement Design*, *18*(sup2), 327–342. doi: 10.1080/14680629.2017.1304255

Espírito Santo. (2023). *Iema launches statewide online system for solid waste transport manifest.* Retrieved from https://www.es.gov.br/Noticia/iema-lanca-sistema-estadual-on-line-de-manifesto-de-transporte-de-residuos-solidos (Retrieved July 28, 2025; [in Portuguese])

Fardin, H. D. (2024). *Evaluation of kr steelmaking coproduct as a stabilizer for different soil types* (Master's thesis). Universidade Federal do Espírito Santo (UFES), Vitória, ES, Brazil.

Farias, R. R. C., Fernandes, P. G. P. S., & Espíndola, A. C. (2018a). Evaluation of the use of marble and granite processing waste in soil used in the restoration and duplication work of highway al-220. In *32nd congress of research and teaching in transport of anpet.* Gramado, Brazil. ([in Portuguese])

Farias, R. R. C., Fernandes, P. G. P. S., & Espíndola, A. C. (2018b). Evaluation of the use of marble and granite processing waste in soil used in the restoration and duplication work of highway al-220. In *32nd congress of research and teaching in transport of anpet.* Gramado, Brazil. ([in Portuguese])

Freitas, D. P. S. A., & Costa Jr., P. L. D. C. (2024). *Stabilization of silty soils with the use of steel slag for paving* (Undergraduate thesis). São Paulo State University (UNESP), Faculty of Engineering and Sciences, Guaratinguetá, SP, Brazil.

Freitas, J. J. G. (2008). *Inorganic chemical characterization of segregated sawing waste from*

ornamental rocks of espírito santo (Master's thesis). Federal University of Espírito Santo, Vitória, Brazil.

Freitas, J. J. G., Raymundo, V., & Jesus, H. C. (2012). Chemical characteristics of segregated sawing waste from ornamental rocks in the state of espírito santo. *Brazilian Journal of Geology*, *96*(3), 615–624. ([in Portuguese])

Freitas, S. M. A. C. (2018). *Steel slag: Pathways for sustainable management* (Doctoral dissertation). Federal University of Ouro Preto.

Freitas-Silva, F. H., & Campos, J. E. G. (1998). Geologia do distrito federal. *Inventário Hidrogeológico e dos Recursos Hídricos Superficiais do Distrito Federal*, *1*, 1–84.

Furieri, E. C. (2019). *Laboratory and field evaluation of soils stabilized with kr coproduct, cement, and blindasolo chemical stabilizer for pavements* (Master's thesis). Universidade Federal do Espírito Santo (UFES), Vitória, ES, Brazil.

Galetakis, M., & Soultana, A. (2016). A review on the utilisation of quarry and ornamental stone industry fine by-products in the construction sector. *Construction and Building Materials*, *102*, 769–781. doi: 10.1016/j.conbuildmat.2015.10.204

Galindo, J. R. F. (2022). *Stabilization of tropical soils with civil construction waste and steel slag for use in paving* (Doctoral dissertation). Federal University of Viçosa.

Gama, T. B., & Rosa, T. H. O. (2016). *Study of the application of steel aggregate in draining layers for road pavements* (Final Project Monograph). University of Brasília, Department of Civil and Environmental Engineering, Brasília, Brazil.

Gautam, P. K., Kalla, P., Jethoo, A. S., Agrawal, R., & Singh, H. (2018). Sustainable use of waste in flexible pavement: A review. *Construction and Building Materials*, *177*, 239–253. doi: 10.1016/j.conbuildmat.2018.04.067

GEOBASES. (2026). *Sistema integrado de bases geográficas e cartográficas do estado do espírito santo.* Disponível em: <http://www.geobases.es.gov.br>. Vitória, Brazil.

Geotecnia UnB. (2026). *Infraestrutura.* Disponível em: `https://geotecnia.unb.br/index.php/pt/quem-somos/infraestrutura`. (Acesso em: março 2026)

Ghannam, S., Najm, H., & Vasconez, R. (2016). Experimental study of concrete made with granite and iron powders as partial replacement of sand. *Sustainable Materials and Technologies*, *9*, 1–9. doi: 10.1016/j.susmat.2016.06.001

Giri, P. M., & N., B. (2020). Experimental study on usage of industrial waste in road construction. In *Aip conference proceedings* (Vol. 2280, p. 020059). doi: 10.1063/5.0025309

Gomes, G. J. C., Magalhães, A. J., Rocha, F. L. L., & Fonseca, A. (2021). A sustainability-oriented framework for the application of industrial byproducts to the base layers of low-volume roads. *Journal of Cleaner Production*, *295*. doi: 10.1016/j.jclepro.2021.126440

Google LLC. (2026). *Google Earth.* Online Application. (Available at https://earth.google.com. Accessed: May 2026)

Guimarães, A. C. R. (2009). *Um método mecanístico-empírico para a previsão da deformação permanente em solos tropicais constituintes de pavimentos* (Doctoral dissertation). COPPE/UFRJ, Rio de Janeiro, RJ, Brazil.

Haque, M., Ray, S., Karmaker, T., Akter, S., Mita, A. F., & Mozumder, A. (2024). Prediction and optimization of hardened properties of concrete prepared with granite dust and scrapped copper wire using response surface methodology. *Heliyon*, *10*(1), e24705. doi: 10.1016/j.heliyon.2023.e24705

Herzog, A., & Mitchell, J. K. (1963). Reactions accompanying stabilization of clay with cement. *Highway Research Record*, *36*, 146–171.

Hicks, R. G. (1970). *Factors influencing the resilient properties of granular materials* (Doctoral dissertation). University of California, Berkeley, USA.

Hunter, L. W. (1988). Lime-induced heave in sulfate-bearing clay soils. *Journal of Geotechnical Engineering (ASCE)*, *114*(2), 150–167.

IDAF. (2026). *Instituto de defesa agropecuária e florestal do espírito santo: Sistema de consulta de mapas e base de dados geoespaciais.* Disponível em: <http://www.idaf.es.gov.br>. Vitória, Brazil.

IEMA-ES. (2024). *Monthly management report - december/2024: Performance bulletin. control system for waste transport manifests – mtr* (Tech. Rep.). Vitória, Brazil: State Institute of Environment and Water Resources (IEMA-ES). ([in Portuguese])

Ignatius, S. G. (1991). *Proposta de um índice para a classificação de solos tropicais baseada na curva de compactação* (Master's thesis). Escola Politécnica, Universidade de São Paulo, São Paulo, SP.

Instituto Aço Brasil - IAB. (2026, Janeiro). *Estatística mensal* (Tech. Rep. No. Nº 129). Instituto Aço Brasil. Retrieved from www.acobrasil.org.br (Nota Técnica: Dados de dezembro de 2025)

IPR. (1988). *Escórias siderúrgicas: Material de múltiplas aplicações* (Tech. Rep.). Rio de Janeiro, Brazil: Instituto de Pesquisas Rodoviárias – IPR/DNER. ([in Portuguese])

Irakoze, D., Abongo, K., & Waweru, S. (2025). Performance of expansive soil blended with waste marble dust and natural pozzolana for road subgrade. *Engineering, Technology & Applied Science Research*, *15*(2), 21068–21075.

Izoton, S. (2020). *Evaluation of the effects of steel aggregates expansion on the mechanical performance of aged asphalt mixtures containing LD steel slag* (Master's thesis). Universidade Federal do Espírito Santo (UFES).

Jaffar, S. T. A., Muneed Abid, M., Khan, S. Z., Jafri, T., Rehman, Z. U., Tariq, M. A. U. R., & Ng, A. W. M. (2022). Evaluation of conventional and sustainable modifiers to improve

the stiffness behavior of weak sub-grade soil. *Sustainability*, *14*(5), 2493. doi: 10.3390/su14052493

Jha, A. K., Sivapullaiah, P. V., & Reddy, K. R. (2019). Sustainable stabilization of expansive soil using steel slag: Micro-structural and chemo-mechanical investigation. *Geotechnical and Geological Engineering*, *37*(4), 2735–2749. doi: 10.1007/s10706-019-00791-3

Kabeta, W. F., & Lemma, H. (2023). Modeling the application of steel slag in stabilizing expansive soil. *Modeling Earth Systems and Environment*, *9*, 4023–4030.

Kambara, S., et al. (1974). The kambara reactor process for desulfurization of hot metal. *Iron and Steel Engineer*.

Karaca, Z., Pekin, A., & Deliormanlı, A. H. (2012). Classification of dimension stone wastes. *Environmental Science and Pollution Research*, *19*(6), 2354–2362. doi: 10.1007/s11356-012-0745-z

Karas, M., & Terzi, S. (2007). Evaluation of marble waste dust in the mixture of asphaltic concrete. *Construction and Building Materials*, *21*(3), 616–620. doi: 10.1016/j.conbuildmat.2005.12.001

Kaur, L., & Kumar, N. (2021). Study with cement replacement by marble dust in concrete for rigid pavement. *International Journal for Research in Applied Science & Engineering Technology (IJRASET)*, *9*(1).

Kinuthia, J. M., Wild, S., & Jones, G. I. (1999). Effects of lime-slag and lime-pfa blends on the property of sulphate-bearing clay soils. *Engineering Geology*, *52*(1-2), 95–108.

Kuttah, D. (2024). Recycling of industrial and construction waste materials in roads construction. *International Journal of Geotechnical Engineering*, *18*(4), 346–359. doi: 10.1080/19386362.2023.2239684

Lanzellotti, R. F. A., Torem, M. L., & da Luz, A. B. (2005, July). Use of steel slag in flexible pavements of triple surface treatment type. In *60th annual abm congress.* Belo Horizonte, MG, Brazil. ([in Portuguese])

Lekarp, F., Isacsson, U., & Dawson, A. (2000). State of the art ii: Permanent strain response of unbound aggregates. *ASCE Journal of Transportation Engineering*, *126*(1), 76–83.

Lima, C. D. A., Motta, L. M. G., & Aragão, F. T. S. (2021). Ensaios de deformação permanente: efeito do número de ciclos na interpretação do comportamento de solos e britas. *Revista Matéria*, *26*(3).

Little, D. N. (1995). *Handbook for stabilization of pavement subgrades and base courses with lime*. Dubuque, Iowa: Kendall/Hunt Publishing Company.

Lohar, J., & Shrivastava, N. (2025). Beneficial use of dimensional stone industry wastes in geotechnical fills: Geotechnical, environmental and economic perspectives. *Resources Policy*, *101*, 105465. doi: 10.1016/j.resourpol.2025.105465

Lohar, J., Shrivastava, N., & Sharma, A. (2023). Feasibility of granite processing waste as a

fill material in geotechnical applications. *Materials Today: Proceedings*. doi: 10.1016/j.matpr.2023.04.655

Lunz, K. B. (2021). *Evaluation of the geotechnical utilization potential of ornamental rock processing sludge in pavement structural layers* (Master's thesis). Universidade Federal de Viçosa, Viçosa, Brazil.

Magalhães, P., et al. (2020). Cation exchange and double layer reduction in stabilized clays. *Geotecnia*.

Magalhães, A. J., Gomes, G. J. C., & Pires, P. J. M. (2022). Toward improved performance of unpaved roads: laboratory tests and field investigation of a soil-byproduct base layer. *Road Materials and Pavement Design*, *23*(1), 184–198. doi: 10.1080/14680629.2020.1820892

Magalhães, M. A. O., Motta, L. M. G., & Cossio, T. P. (2017). Resilient behavior of a tropical soil-steel slag mixture for pavement bases. *Soils and Rocks*, *40*(3), 291–301.

Manhães, J. P. V. T., & de Holanda, J. N. F. (2008). Caracterização e classificação de resíduo sólido "pó de rocha granítica" gerado na indústria de rochas ornamentais. *Química Nova*, *31*(6), 1301–1304.

Margueron, C., & Mello, E. F. (2005). Estratégias competitivas para empresas de rochas ornamentais na região metropolitana do rio de janeiro / competitive strategies for dimensional stone companies in the rio de janeiro metropolitan area. *Anuário Do Instituto de Geociências - UFRJ*, *28*(2), 71–101.

Marin, A. C. (2022). *Stabilization of low-consistency soil with residue from a flue gas desulfurization plant* (Master's thesis). Federal University of Espírito Santo, Vitória, Brazil.

Marques, L. R., Costa Farias, R. D. J., & Moraes Garcia, L. (2019). Determination of the resistance of the soil-cement mixture with the addition of stone dust for the possible insertion of the base layer for paving. In *Geotechnical engineering in the xxi century: Lessons learned and future challenges* (pp. 1572–1579). IOS Press. ([in Portuguese])

Medeiros, K. P. M. (2019). *Estudo do uso da escória siderúrgica de alto forno e estéril de mineração como alternativa de revestimento primário em estradas não pavimentadas* (Master's thesis). Universidade Federal de Minas Gerais.

Medeiros, W. R. P., Neto, O. D. M. M., Luz, P. M. S. G., de Oliveira, R. K. F., & Guedes, L. R. (2023). Utilizing marble and granite industry waste in asphalt mixtures for enhanced road performance and sustainability. *Journal of Engineering Research*, *11*(2), 293–305. doi: 10.1016/j.jer.2023.01.006

Medina, J., et al. (2025). Environmental life cycle assessment of slag-stabilized pavements. *Sustainability*.

Medina, T. M. (2024). *Life cycle assessment of flexible pavements with sidercal® slag: Case*

studies (Master's thesis). Universidade Federal do Espírito Santo (UFES), Vitória, ES, Brazil.

Mello, H. M. (2019). *Stabilization of pavement subgrade soils with the use of marble and granite cutting residue (mgcr)* (Bachelor's thesis). Federal Institute of Education.

Mendonça, R. L., & Rodrigues, G. L. C. (2010). Primary surfacing on urban and rural roads using steel slag with granulometric control. In *65º congresso abm internacional.* Rio de Janeiro, Brazil. Retrieved from `https://abmproceedings.com.br` ([in Portuguese])

Mendoza, L. E. C. (2023). *Comportamento mecânico de misturas solo-escória de aciaria para uso em pavimentação* (Master's thesis). Universidade Federal do Espírito Santo (UFES), Vitória, ES, Brazil.

Meneguete, D. S. (2018). *Physico-chemical stabilization of sulfidic/sulfated waste with the incorporation of desulfurization slag* (Master's thesis). Federal University of Espírito Santo, Vitória, Brazil.

Meneguete, D. S., Batista, L. C., & Cesconetto Júnior, W. A. (2018). Utilization of waste generated in the cutting of ornamental rocks in asphalt paving for base improvement. *Mosaicum Journal*, *27*. ([in Portuguese])

Mishra, B. (2015). A study on use of industrial wastes in rural road construction. *International Journal of Innovative Research in Science, Engineering and Technology*, *4*(11), 0411009. doi: 10.15680/IJIRSET.2015.0411009

Misra, A. K., Mathur, R., Rao, Y. V., Singh, A. P., & Goel, P. (2010). A new technology of marble slurry waste utilisation in roads. *Journal of Scientific & Industrial Research*, *69*, 67–72.

Monismith, C. L., Inkabi, K., & Freeme, C. R. (1975). Rutting prediction in asphalt concrete pavements. *Transportation Research Record*, *616*, 2–8.

Montani, C. (2021). *Stone sector 2021: Xxi international report on marble and stones*. Carrara, Italy: Aldus Casa di Edizioni.

Moraes, J. M. S., Oliveira, C. F., & Pires, P. J. M. (2018). Characterization of stone slurry waste for reutilization purposes as building construction material. *Journal of Geological Resource and Engineering*, *6*, 45–49. doi: 10.17265/2328-2193/2018.01.007

Moreira, B. C. (2021). *Resíduos da lama de beneficiamento de rochas ornamentais: Potencial de contaminação e possibilidades de uso.* ([Unpublished manuscript])

Moreira, B. C., Neves, M. A., Pinheiro, M. M., Nascimento, W. A. R., Barbosa, J. L. B., & Horn, A. H. (2021). Deposits of dimension stone wastes: Composition, sizing and use for building. *Geociências (São Paulo)*, *40*(2), 525–538. ([in Portuguese]) doi: 10.5016/geociencias.v40i02

Moscon, L. B. P. (2024). *Development of clay mass for red ceramics with the incorporation of*

industrial residues in espírito santo (Master's thesis). Federal Institute of Espírito Santo, Vitória, Brazil.

Motta, M. M., & Portela, R. P. (2023). *Analysis by the igge method of pathological manifestations on a road with primary surfacing using the revsol® mixture and soils in es* (Specialization thesis). Federal Institute of Espírito Santo (IFES), Vitória, Brazil.

Motz, H., & Geiseler, J. (2001). Products of steel slags an opportunity to save natural resources. *Waste Management*, *21*(3), 285–293.

Nascimento, H. D. G. (2019). *Analysis of the mechanical resistance of a soil stabilized with ornamental rock waste* (Bachelor's thesis). Universidade Federal de Campina Grande.

Navarro, V., Barrientos, V., Yustres, , & Delgado, J. (2008). Settlement of embankment fills constructed of granite fines. *Computers & Geosciences*, *34*(8), 978–992.

NCHRP. (2004). *Laboratory determination of resilient modulus for flexible pavement design* (Tech. Rep. No. Project 1-28A). Washington, D.C.: National Cooperative Highway Research Program.

Nepomuceno, D. V. (2019). *Field evaluation of pavement structure incorporating soil stabilized with kr steelmaking coproduct subjected to loading with hvs simulator and comparison with performance predictions according to the new brazilian design method medina* (Master's thesis). Federal University of Espírito Santo, Vitoria, Brazil.

Neves, M. A., Nascimento, W. A. R., & Horn, A. H. (2025). Dimension stone processing sludge at different stages of production: Insights for waste management. *Minerals*, *15*(1), 39. doi: 10.3390/min15010039

Neves, M. A., & Raymundo, V. (2022). Depósitos de resíduos finos do beneficiamento de rochas ornamentais e qualidade do aquífero freático / deposits of fine wastes from dimension stone processing and quality of the phreatic aquifer. *Engenharia Sanitaria e Ambiental*, *27*(2), 257–267. doi: 10.1590/S1413-415220200257

Nogami, J. S., & Villibor, D. F. (1996). Importância e determinação do grau de laterização em geologia de engenharia. In *Anais do viii congresso brasileiro de geologia de engenharia* (pp. 119–122). Rio de Janeiro, Brazil: ABGE.

Nunes, F., et al. (2011). Comportamento geotécnico dos solos da formação barreiras no espírito santo. *Revista Brasileira de Geologia de Engenharia e Ambiental*, *1*, 45–62.

Nunes, N. L. (2024). *Use of powder-type steel coproduct from the kr desulfurization slag particulate capture system and portland cement for stabilization of low-consistency organic soils* (Master's thesis). Federal University of Espírito Santo, Vitória, Brazil.

Oliveira, C. F. (2018). *Use of kambara reactor desulfurization coproduct as a soil stabilizing agent for paving purposes* (Master's thesis). Universidade Federal do Espírito Santo (UFES), Vitória, ES, Brazil.

Oliveira, C. F., Pires, P. J. M., & Teixeira, J. E. S. L. (2019). Physical, mechanical, and

microstructure investigation of tropical clayey soils stabilised with desulfurisation slag for pavement application. *Road Materials and Pavement Design*, *22*(6), 1–12. doi: 10.1080/14680629.2019.1686052

Oliveira, C. F., Ramos, L. B. d. S., Andrade, C. M. S., Picoli, H. C., & Pires, P. J. M. (2017). Stabilization of soils with incorporation of kr desulfurization slag in pavement layers. In *Geocentro 2017.* Goiânia, Brazil. ([in Portuguese])

Oliveira, T. (2015). *Characterization of ornamental rock sawing waste for geotechnical applications* (Master's thesis). Universidade de São Paulo, São Carlos, Brazil.

Oliveira, T., Ribeiro, R. P., & Moreiras, T. F. (2016). Characterization of granite cutting sludge for geotechnical purposes. *Ciência e Engenharia*, *25*(2), 51–57. (EID: 2-s2.0-85037732456 [in Portuguese])

Oliveira, V. H. S. (2016). *Analysis of the feasibility of using steel slag aggregate in road pavements* (Undergraduate thesis). University of Brasília, Faculty of Technology, Department of Civil and Environmental Engineering, Brasília, Brazil.

Ooi, P. S. K., Archilla, A. R., & Sandefur, K. G. (2004). Resilient modulus models for compacted cohesive soils. *Transportation Research Record*, *1874*(1), 115–124.

Ouf, M. E. A. (2017). Stabilization of expansive soil using steel slag. *International Journal of Geo-Engineering*, *8*(1), 1–13. doi: 10.1186/s40703-017-0045-y

Parmar, S. S. (2025). *On-site waste in construction: A two-decade review of global practices, emerging technologies, and policy evolution.* ([Preprint]. Zenodo) doi: 10.5281/zenodo.15208563

PennDOT. (1978). *PTM no. 130/78: Pennsylvania test method* [Test Method]. Harrisburg, PA, USA.

Pequeno, O. T. B. L. (2020). *Incorporation of industrial granite waste in the waterproofing of the base layer of the sanitary landfill in campina grande-pb* (Master's thesis). Universidade Estadual da Paraíba, Campina Grande, Brazil.

Pezo, R. F. (1993). A general method of reporting resilient modulus tests of soils. *Transportation Research Record*, *1406*, 17–24.

Phanikumar, B. R., & Sharma, R. S. (2004). Volume change behavior of fly ash-stabilized clays. *Journal of Geotechnical and Geoenvironmental Engineering*, *130*(7), 762–764.

Picoli, H. C. (2020). *Stabilization of soils with fgd coke oven coproduct and portland cement for use in pavement layers* (Master's thesis). Federal University of Espírito Santo, Vitória, Brazil.

Pinheiro Neto, J. C., Oliveira, F. H. L., & Aguiar, M. F. P. (2015). Review of studies on the application of steel slag in road paving. In *44th annual paving meeting and 18th national road conservation meeting (rapv & enacor).* Foz do Iguaçu, Brazil. ([in Portuguese])

Pinto, P. C. (2010). *Investigation of parameters of roller-compacted concrete with the*

incorporation of granulated blast furnace slag for use as a pavement base (Master's thesis). University of São Paulo, São Paulo, Brazil.

Pires, P. J. M., Teixeira, J. E. S. L., Nepomuceno, D. V., & Furieri, E. C. (2019). Laboratory and field evaluation of KR slag-stabilized soil for paving applications. *Journal of Materials in Civil Engineering*, *31*(9). doi: 10.1061/(ASCE)MT.1943-5533.0002834

Pires-Teixeira, A. S., & Pires, J. P. (2021). Evaluation of steelmaking slag as a soil stabilizer based on the double layer theory. *Construction and Building Materials*.

PMS - Prefeitura Municipal da Serra. (2024). *Polos empresariais.* Serra, Brazil. (Retrieved May 24, 2024, from http://serra.es.gov.br/site/pagina/polos-empresariais)

Poh, H. Y., Ghataora, G. S., & Ghazireh, N. (2016). Soil stabilization using basic oxygen steel slag and ground granulated blast furnace slag. *Journal of Materials in Civil Engineering*, *28*(6), 04016024.

Polese, M. O., Carreiro, G. L., & Silva, M. G. (2006). Caracterização microestrutural da escória de aciaria. *Matéria (Rio de Janeiro)*, *11*(4), 442–452.

Prandina, J. R. R. (2013). *Utilização de resíduo de rochas ornamentais em obras de terra e pavimentação* (Unpublished master's thesis). Universidade Federal do Espírito Santo, Vitória, Brazil.

Prandina, J. R. R. (2018a). *Proof of concept for slag applications in pavements - chief of highway maintenance memorandum* (Technical Memorandum). Vitória, Brazil: National Department of Transport Infrastructure (DNIT). ([in Portuguese])

Prandina, J. R. R. (2018b). *Proposal for the evolution of the maintenance conservation index* (Technical Memorandum No. Memorandum no. 71133/2018/SEMAN-COENGE-ES). Vitória, ES, Brazil: National Department of Transport Infrastructure (DNIT), Regional Superintendency in Espírito Santo (SRE-ES). (SEI/DNIT Process: 1907786; [in Portuguese])

Prandina, J. R. R. (2019). *Analysis of recycled subbase soil mixtures for pavement applications adopting dimension stone sawdust added as industrial residue.* (Unpublished manuscript)

Prandina, J. R. R. (2025). *Racionalidade para sequências de baixa tensão desvio no ensaio de módulo resiliente AASHTO T 307-99 para materiais de base/sub-base* (Research Report). Vitória, Brazil: Universidade Federal do Espírito Santo (UFES).

Prandina, J. R. R., Fall, M., & Sedano, J. A. I. (2017). Chemical and leaching characteristics of ornamental stone residue in pavement application perspective. In *Proceedings of the 70th canadian geotechnical conference (geoottawa 2017).* Ottawa, Canada: The Canadian Geotechnical Society.

Prandina, J. R. R., & Farias, M. M. (2025a). Aplicações geotécnicas notáveis do estado da prática com escórias de aciaria no brasil. *Revista De Geopolítica*, *16*(5), e1107. doi:

10.56238/revgeov16n5-252

Prandina, J. R. R., & Farias, M. M. (2025b). Road infrastructure adopting siderurgical and ornamental stone industrial residues. *Revista Foco*, *18*(7), e9232. doi: 10.54751/revistafoco.v18n7-091

Prandina, J. R. R., & Farias, M. M. d. (2026). Resíduos da indústria de rochas ornamentais em misturas de solos para aplicações geotécnicas: uma revisão de literatura. *Transportes*, *34*, e3155. doi: 10.58922/transportes.v34.e3155

Puppala, A. J., Kadam, R., Biswas, N., Khan, A., & Congress, S. S. C. (2024). Evaluation of resilient moduli and post-cyclic residual strength characterization of stabilized subgrade soils under repeated traffic loading. *Journal of Materials in Civil Engineering*, *36*(4), 04024012. doi: 10.1061/(ASCE)MT.1943-5533.0005120

Rahman, M. S., & Erlingsson, S. (2015). Predicting permanent deformation behaviour of unbound granular materials. *International Journal of Pavement Engineering*, *16*(7), 587–601.

Rahman, M. S., Erlingsson, S., & Ahmed, A. (2023). Modelling the permanent deformation of unbound granular materials in pavements. *Road Materials and Pavement Design*, *24*(8), 1917–1938. doi: 10.1080/14680629.2022.2045953

Rajgor, M. B., & Pitroda, J. (2013). A study of utilization aspect of stone waste in indian context. *International Journal of Global Research Analysis*, *2*(1).

Ramos, F. M., Ramos, C. R., Laó, V. L. d. E. S. T., & Costa, T. R. (2009). Use of steel aggregate (steel slag) in pavement base and surfacing on roads of the rio de janeiro. In *64th annual abm congress.* Belo Horizonte, Brazil. ([in Portuguese])

Ramos, L. B. d. S. (2018). *Study of strength gain and chemical stabilization by the addition of kr coproduct in the improvement of clayey soils* (Master's thesis). Universidade Federal do Espírito Santo (UFES), Vitória, ES, Brazil.

Rao, A. N., & Chittaranjan, M. (2010). Harmful effects of certain industrial wastes on geotechnical properties of soils—a review. *Nature, Environment and Pollution Technology*, *9*(4), 799–804.

Raposo, C. O. L. (2005). *Experimental study of compaction and expansion of an ld steel slag for paving use* (Master's thesis). Federal University of Espírito Santo, Vitória, Brazil.

Reis, A. S., & Tristão, F. A. (2010). Tactile-floor tile hydraulic with addition residue improvement dimension stones. In *Ibracon* (pp. 390–419).

Reng, R. M. (2025). *Assessing the use of marble dust as a mineral filler in asphalt concrete to reduce rutting* (Bachelor's thesis). Uganda Christian University.

Resende, A. D. d. (2010). *Uso de escória de aciaria pura e com adição de argila como camada de base* (Master's thesis). Universidade Federal de Ouro Preto.

Resende, M. H. (1999). *Deformação permanente de materiais granulares* (Doctoral

dissertation). Universidade de São Paulo (EESC-USP), São Carlos, SP, Brazil.

Ribeiro, F. B., Silva, M. A. V. d., Nascimento, F. A. C. d., & Guimarães, A. C. R. (2018). Use of soil-ferrosilicon-manganese slag mixture in road subbase layer. In *9º portuguese roadway congress.* Lisbon, Portugal. ([in Portuguese])

Ribeiro, R. C. d. C., Correia, J. C. G., Seidl, P. R., de Almeida, S. L. M., & de Carvalho, E. A. (2007). *Utilização de rejeitos de rochas ornamentais em misturas asfálticas* (Tech. Rep. No. Série Tecnologia Mineral No. 87). Centro de Tecnologia Mineral (CETEM).

Rith, M., Kim, Y. K., Hong, S. J., & Lee, S. W. (2017). Effect of horizontal loading on RCC-base composite pavement performance at heavy duty area. *Construction and Building Materials*, *131*, 741–745. doi: 10.1016/j.conbuildmat.2016.11.028

Rohde, L. (2002). *Electric arc furnace slag in granular pavement layers - a laboratory study* (Master's thesis). Universidade Federal do Rio Grande do Sul, Porto Alegre, RS, Brazil.

Rohde, L. (2003). *Contribuição ao estudo da resiliência de solos e misturas solo-brita para utilização em camadas de pavimentos* (Unpublished doctoral dissertation). Universidade Federal do Rio Grande do Sul, Porto Alegre, Brazil.

Rombi, J., Coni, M., Portas, S., & Pistis, S. (2013). The use of granite by-products in road asphalt layers. In *12th annual international conference on pavement engineering and infrastructure.* Liverpool, U.K..

Rombi, J., Maltinti, F., & Coni, M. (2022). Sardinia granite scraps application in road pavement layers. In O. Gervasi, B. Murgante, S. Misra, A. M. A. C. Rocha, & C. Garau (Eds.), *Computational science and its applications – iccsa 2022 workshops (lecture notes in computer science, vol. 13382)* (pp. 613–623). Springer, Cham. doi: 10.1007/978-3-031-10592-0_44

Salehi, M., Bayat, M., Saadat, M., & Nasri, M. (2021). Experimental study on mechanical properties of cement-stabilized soil blended with crushed stone waste. *KSCE Journal of Civil Engineering*, *25*(6), 1974–1984.

Sant'Ana, A. P. (2003). *Technological characterization of soil – ground granulated blast furnace slag mixtures for road purposes* (Master's thesis). Universidade Federal de Viçosa, Viçosa, Brazil.

Santos, A., & Leandro, E. (2017). *Study of the application of milled asphalt and ornamental stone residue* (Capstone project). Federal University of Goiás.

Santos, A. S., & Leandro, E. A. (2017). *Study of the application of milled asphalt and ornamental stone residue as base and sub-base for pavements* (Bachelor's thesis). Federal University of Goiás.

Santos, G. P. P. (2013). *A study on the use of ferronickel slag in road pavement* (Master's thesis). Military Institute of Engineering, Rio de Janeiro, RJ, Brazil.

Santos, I. M. (2024). *Stabilization of soils mixed with steel production slag (steelmaking)*

(Undergraduate thesis). São Paulo State University "Júlio de Mesquita Filho", Ilha Solteira, Brazil.

Santos, J. G. S., da Silva, S. S. F., da Silva Nascimento, N. M., Trajano, M. F., & de Mello, V. S. e. M. (2010). *Caracterização da lama abrasiva gerada nos processos de beneficiamento do granito: Um estudo de caso na granfugi localizado em campina grande - pb.* ([Unpublished manuscript])

Sartório, P. D. (2007). *Contribuição ao estudo do comportamento geotécnico de solos da formação barreiras: aplicação ao trecho da rodovia br-101/es* (Doctoral dissertation). Universidade Federal do Rio de Janeiro, COPPE, Rio de Janeiro.

Satvati, S., Cetin, B., Ashlock, J. C., Ceylan, H., & Rutherford, C. (2021). *Use of waste quarry fines as a binding material on unpaved roads* (Tech. Rep.). Iowa Department of Transportation; Iowa Highway Research Board. (IHRB Project TR-747; InTrans Project 18-656)

Scherer, M. R., Knierim, L. D. S., Klamt, R. A., & Mazzutti, E. A. (2023). Verification of the stabilization of a clayey soil with ornamental stone sludge for application in pavement layers. In *Xiii symposium of geotechnical engineering practices of the southern region (geosul 2023).* Foz do Iguaçu, Brazil. ([in Portuguese])

Schiavo, P., et al. (2019). Efeitos da energia de compactação na sucção matricial e rigidez de solos tropicais. *Geotecnia*.

Scottish Government. (2011). *Specification details – spec/gdp/02 granite dust path note* (Tech. Rep.). Scottish Government.

Scottish Government. (2019). *Surfacing guide for path projects.*

Scottish Government. (2022). *New path - unbound surface. rural payments and services.*

Scottish Government. (2025). *Active travel route - montgarrie to alford. rural payments and services.*

SEAG. (2025). *Espírito santo municipalities receive a record amount of revsol in 2023.* Retrieved from `https://seag.es.gov.br/Noticia/municipios-capixabas-recebem-quantidade-recorde-de-revsol-em-2023` ([in Portuguese])

Segui, P., Safhi, A. e. M., Amrani, M., & Benzaazoua, M. (2023). Mining wastes as road construction material: A review. *Minerals*, *13*(1), 90. doi: 10.3390/min13010090

SEINFRA. (2025). *Steel slag is used in the improvement of the unpaved road network in the curvelo region.* Infrastructure Secretariat of Minas Gerais State. Belo Horizonte, Brazil. Retrieved from `http://www.infraestrutura.mg.gov.br` ([in Portuguese])

Shen, P., Wu, H., Zhang, J., & Wang, X. (2019). Mechanical behavior and micro-structure of soft soil stabilized by ld steel slag. *Applied Clay Science*, *170*, 1–10. doi: 10.1016/j.clay.2019.01.015

Silva, A. C. d., Rodrigues, K. H. d. P., Castro, J. C. d., Morais Filho, C. H. d., Melo, B. M. d., & Gravina, A. M. (2022). Use of primary electric arc furnace slag as a tropical soil stabilizing agent. In *Academic integration symposium ufv (sia ufv 2022).* Viçosa, MG, Brazil. ([in Portuguese])

Silva, E. A. d., Coelho, M. A. M., & Silva Júnior, E. A. d. (2007). The use of raw blast furnace slag as a drainage and base layer for asphalt pavements. In *62nd annual abm int. cong.* Vitória, Brazil. ([in Portuguese])

Silva, E. R., Barbosa, L., & Silva, M. M. A. d. (2021). *Use of slag in the base and sub-base of a pavement* (Undergraduate thesis). Centro Universitário de Barra Mansa, Barra Mansa, RJ, Brazil.

Silva, L. A., & Isewaki, N. T. (2018). Utilization of marble and granite waste in soil reinforcement for composition of paved highway subgrade layers. *Perquirere*, *15*(4), 111–129. ([in Portuguese])

Silva, T. B. P. d. (2019). *Comparação entre os resíduos finos recém-gerados e os depositados em aterros da indústria de rochas ornamentais.* ([Unpublished manuscript])

Sivrikaya, O., Kıyıldı, K. R., & Karaca, Z. (2014). Recycling waste from natural stone processing plants to stabilise clayey soil. *Environmental Earth Sciences*, *71*, 4397–4407. doi: 10.1007/s12665-013-2833-x

Song, X., Xu, H., Zhou, D., Yao, K., Tao, F., Jiang, P., & Wang, W. (2021). Mechanical performance and microscopic mechanism of coastal cemented soil modified by iron tailings and nano silica. *Crystals*, *11*, 1331. doi: 10.3390/cryst11111331

Soutsos, M. N., Tang, K., & Millard, S. G. (2011). Use of recycled demolition aggregate in precast products, phase ii: Concrete paving blocks. *Construction and Building Materials*, *25*(7), 3131–3143. doi: 10.1016/j.conbuildmat.2010.12.024

Souza, P. M. d., Oliveira, F. L. d. S. d., Lima, M. V. P. d., & Fernandes Júnior, J. L. (2022). Considerations on the analysis of permanent deformation in the new brazilian asphalt pavement design method. *Transportes*, *30*(2). doi: 10.14295/transportes.v30i2.2731

Souza, R. O., Silva, T. O., Fontes, L. P. T., & Motta, L. M. G. (2017). Uso de escória de aciaria em pavimentação rodoviária: estudo de caso da rodovia mg-232. *Anais da 46 RAPv e 20 ENACOR*. ([in Portuguese])

Souza Júnior, T. F. (2005). *Estudo da aplicabilidade da classificação mct para solos da formação barreiras (espírito santo)* (Master's thesis). Universidade Federal do Espírito Santo, Vitória.

Stroup-Gardiner, M., & Wattenberg-Komas, T. (2013). *Recycled materials and byproducts in highway applications–summary report, volume 1* (Tech. Rep.). National Academies Press. doi: 10.17226/22552

Teixeira, G. B., Bezerra, H., & Borges, P. A. B. (2017b). *Utilization of mixtures of lateritic*

gravel, milled asphalt, and granite powder residue in pavement (Bachelor's thesis). Federal University of Goiás, Goiânia, Brazil.

Teixeira, G. B., Bezerra, H. B., Borges, P. A. B., Rezende, L. R., & Prandina, J. R. R. (2017a). Utilization of mixtures of ornamental rock cutting residue, lateritic gravel, and milled asphalt in pavement. In *Geocentro 2017*. Goiânia, Brazil. ([in Portuguese])

Teixeira, J. E. (2022). *Experts debate the use of steel aggregates during the 6th edition of abm week*. Brazilian Association of Metallurgy, Materials and Mining (ABM). Retrieved from `https://www.abmbrasil.com.br` ([in Portuguese])

Thom, N. H., & Brown, S. F. (1988). The effect of grading and density on the mechanical properties of a crushed dolomitic limestone. In *Proceedings of the 14th arrb conference, part 7* (pp. 94–100).

Thompson, M. R. (1966). Shear strength and elastic properties of lime-soil mixtures. *Highway Research Record*, *139*, 1–14.

Tseng, K. H., & Lytton, R. L. (1989). Prediction of permanent deformation in flexible pavement materials. In *Implication of aggregates in the design, construction, and performance of flexible pavements* (pp. 154–172). ASTM International.

Tutumluer, E., Byun, Y.-H., Feng, B., Qamhia, I., & Moaveni, M. (2018). *Impact of quarry gradation and material properties on base course aggregate testing and rutting model calibration* (Tech. Rep. No. FHWA/NC/2015-23). Urbana-Champaign, IL: University of Illinois at Urbana-Champaign. (NCDOT Project 2015-23)

Uliana, J. G., Bastos, R. S., Calmon, J. L., Tristão, F. A., Vieira, G. L., & Rodrigues, J. A. (2013). Estudo comparativo da caracterização da lama do beneficiamento de rochas ornamentais com e sem granalha de aço. In *Anais do 54º congresso brasileiro do concreto - cbc20* (pp. 13–55). IBRACON.

Umar, I. H., & Lin, H. (2024). Marble powder as a soil stabilizer: An experimental investigation of the geotechnical properties and unconfined compressive strength analysis. *Materials*, *17*(5), 1208. doi: 10.3390/ma17051208

Uzan, J. (1982). Characterization of granular material. *Transportation Research Record*(898), 1–8.

Uzan, J. (1985). Characterization of granular material. *Transportation Research Record*, *1022*, 52–59.

Velten, R. Z., Sant'Ana, A. P., Lima, D. C. d., Silva, C. H. d. C., Carvalho, C. A. B. d., Couto, L. G., & Machado, C. C. (2006). Mechanical characterization of soil–ground granulated blast furnace slag mixtures for forest road applications. *Journal of Forest Investigations - SOIF*, *30*(2), 235–240. ([in Portuguese])

Vieira, V. S., & Menezes, R. G. (Eds.). (2015). *Geologia e recursos minerais do estado do espírito santo: texto explicativo dos mapas geológico e de recursos minerais do estado*

do espírito santo. Belo Horizonte: CPRM. (Org.)

Vikas, K., & Ramana, G. V. (2023). Viability of bulk utilization of granite sludge powder (gsp) to enhance the geotechnical behavior of expansive soil. *Materials Today: Proceedings*. doi: 10.1016/j.matpr.2023.04.574

Wang, H., Zhang, C., Jiang, J., Huang, W., Guo, D., & Sheng, T. (2022). Vibration characteristics and isolation in vibration-sensitive areas under moving vehicle load. *Soil Dynamics and Earthquake Engineering*, *153*, 107077. doi: 10.1016/j.soildyn.2021.107077

Werkmeister, S., Dawson, A. R., & Wellner, F. (2001). Permanent deformation behavior of granular materials and the shakedown concept. *Transportation Research Record: Journal of the Transportation Research Board*, *1757*(1), 75–81. doi: 10.3141/1757-09

Wild, S., Kinuthia, J. M., Jones, G. I., & Higgins, D. D. (1996). Suppression of swelling associated with ettringite formation in lime stabilized sulphate bearing clay soils. *Engineering Geology*, *43*(4), 247–256.

Witczak, M. W., & Uzan, J. (1988). *The universal airport pavement design system, report i of iv: Granular material characterization* (Tech. Rep.). University of Maryland.

Wu, J., Liu, L., Deng, Y., Zhang, G., Zhou, A., & Xiao, H. (2022). Use of recycled gypsum in the cement-based stabilization of very soft clays and its micro-mechanism. *Journal of Rock Mechanics and Geotechnical Engineering*, *14*(3), 909–921. doi: 10.1016/j.jrmge.2021.10.002

Wu, J., Liu, Q., Deng, Y., & Yu, X. (2019). Expansive soil modified by waste steel slag and its application in subbase layer of highways. *Soils and Foundations*, *59*(4), 955–965. doi: 10.1016/j.sandf.2019.03.009

Yadav, V., Rana, M. K., & Kushwaha, P. K. (2024). Review paper on potential use of waste marble fine in construction industries. *International Journal of Research Publication and Reviews*, *5*(1), 5050–5053.

Yi, H., Xu, G., Cheng, H., Wang, J., Wan, Y., & Chen, H. (2012). An overview of utilization of steel slag. *Procedia Environmental Sciences*, *16*, 791–801. doi: 10.1016/j.proenv.2012.10.108

Yildirim, I. Z., & Prezzi, M. (2011). Chemical, mineralogical, and morphological properties of steel slag. *Advances in Civil Engineering*, *2011*, 463638. doi: 10.1155/2011/463638

Yildirim, I. Z., & Prezzi, M. (2015). Geotechnical properties of fresh and aged basic oxygen furnace steel slag. *Journal of Materials in Civil Engineering*, *27*(12), 04015046. doi: 10.1061/(ASCE)MT.1943-5533.0001310

Zhang, F., Jia, M., Kong, L., Sun, Y., Falchetto, A. C., Gao, J., & Wang, W. (2025). Utilizing steelmaking by-products for pavement deicing: A sustainable waste management approach in circular economy. *Waste and Biomass Valorization*. doi: 10.1007/s12649

-025-02917-w

Zheng, S., Chen, J., & Wang, W. (2023). Effects of fines content on durability of high-strength manufactured sand concrete. *Materials*, *16*(2), 522. doi: 10.3390/ma16020522

Zichella, L., Choorackal, E., Airoldi, M., Riviera, P. P., Bellopede, R., & Santagata, E. (2020). Performance-related assessment of the potential use of sawing sludge in cementitious fluidized thermal backfills. *Applied Sciences*, *10*(22), 8243. doi: 10.3390/app10228243

Zumrawi, M. M. E. (2016). Stabilization of expansive soil using bagasse ash and lime. *International Journal of Science and Research*, *5*(10), 611–616.

Zumrawi, M. M. E., & Babikir, A. A.-A. A. (2017). Laboratory study of steel slag used in stabilizing expansive soil. *Asian Engineering Review*, *4*(1), 1–6.

Šernas, O., Strumskys, M., & Skrodenis, D. (2014). Possibility of use of granite fines in asphalt pavements. In *9th international conference "environmental engineering"* (pp. 7–13). Vilnius Gediminas Technical University Press.

ANNEX 1
Raw Data Records of Resilient Modulus Tests

This annex presents the raw data and processed results of the Resilient Modulus (MR) tests conducted on soil samples and OSR (Ornamental Stone Residue) mixtures.

The current set of tests were performed using cyclic load triaxial equipment at the Infrastructure Laboratory (Infralab) of the University of Brasília (UnB), which have been fed in the MR graphs of chapter 4.

It should be highlighted that the methodology adopted for the testing procedures and stress sequences strictly adhered to the AASHTO T 307 protocol. This methodological choice was dictated by the technical and normative context at the time of the experimental campaign (December 2018).

Although the Brazilian standard DNIT 134/2018-ME was published in April 2018, the hardware and software configuration of the triaxial equipment at Infralab was still undergoing the necessary updates and calibrations to comply with the new national standard during that period. Consequently, to ensure the reliability of the results and the integrity of the load and displacement sensors, the AASHTO method was selected, as it was fully operational and consolidated within the laboratory's routine at the time.

The data provided in this annex served as the basis for the non-linear regressions and the generation of the response surfaces discussed throughout this work, applying both the Composite (MeDiNa) and Universal (MEPDG) models.

Table 5.1: Resilient Modulus Test Data - Vitória Soil 0% OSR (CP1)

Seq. AASHTO	**Avg.** σ_3 **(kPa)**	**Avg.** σ_d **(kPa)**	**Avg.** M_R **(MPa)**
1	20.2	21.45	152.6
2	20.4	41.51	229.0
3	34.0	35.17	226.5
4	33.9	69.02	156.3
5	68.4	71.81	135.1
6	68.6	139.99	135.6
7	102.8	5.14	210.5
8	102.9	108.64	170.3
9	137.7	7.25	260.7
10	137.5	145.09	176.3
11	137.0	110.06	182.5
12	136.8	232.93	190.4

Table 5.2: Resilient Modulus Test Data - Vitória Soil 0% OSR (CP2)

Seq. AASHTO	**Avg.** σ_3 **(kPa)**	**Avg.** σ_d **(kPa)**	**Avg.** M_R **(MPa)**
1	20.3	20.37	92.9
2	20.3	41.01	115.2
3	34.2	34.22	135.1
4	34.0	69.71	134.3
5	68.5	71.43	120.1
6	68.3	140.43	147.7
7	102.7	5.23	242.0
8	102.9	109.14	172.8
9	137.7	7.66	238.8
10	137.4	145.56	180.0
11	137.2	108.36	202.2
12	136.6	231.89	214.0

Table 5.3: Full test sequences for Vitória Soil CP1 (0% OSR) - December 2018 Data.

Seq.	M_R **(MPa)**	σ_3 **(kPa)**	σ_d **(kPa)**	**Status**
0	136.36	103.35	92.45	$\sigma_3 > \sigma_d$ (Excluded)
1	314.43	20.51	18.78	$\sigma_3 > \sigma_d$ (Excluded)
2	176.56	20.22	38.15	Valid
3	142.72	20.42	56.35	Valid
4	185.79	34.19	31.11	$\sigma_3 > \sigma_d$ (Excluded)
5	139.97	34.09	61.92	Valid
6	139.54	33.99	92.15	Valid
7	144.78	68.08	61.63	$\sigma_3 > \sigma_d$ (Excluded)
8	130.37	68.47	124.14	Valid
9	146.12	68.67	185.18	Valid
10	117.62	102.86	61.34	$\sigma_3 > \sigma_d$ (Excluded)
11	141.32	102.86	92.45	$\sigma_3 > \sigma_d$ (Excluded)
12	162.91	102.95	185.18	Valid
13	188.57	136.85	93.33	$\sigma_3 > \sigma_d$ (Excluded)
14	180.44	137.73	122.97	$\sigma_3 > \sigma_d$ (Excluded)
15	176.51	137.53	247.40	Valid
16	175.64	137.63	122.97	$\sigma_3 > \sigma_d$ (Excluded)
17	182.46	137.05	247.11	Valid
18	190.39	136.85	369.78	Valid

Table 5.4: Full test sequences for Vitória Soil CP2 (0% OSR) - December 2018 Data.

Seq.	M_R **(MPa)**	σ_3 **(kPa)**	σ_d **(kPa)**	**Status**
0	519.93	103.05	93.33	$\sigma_3 > \sigma_d$ (Excluded)
1	131.12	20.51	18.85	$\sigma_3 > \sigma_d$ (Excluded)
2	354.51	20.32	37.69	Valid
3	452.18	20.32	55.04	Valid
4	354.90	34.09	29.91	$\sigma_3 > \sigma_d$ (Excluded)
5	445.88	34.29	60.43	Valid
6	327.07	34.09	92.14	Valid
7	1112.07	68.77	61.92	$\sigma_3 > \sigma_d$ (Excluded - Anomaly)
8	219.64	68.57	123.55	Valid
9	190.64	68.38	184.57	Valid
10	1120.50	103.15	61.92	$\sigma_3 > \sigma_d$ (Excluded - Anomaly)
11	333.12	102.76	92.44	$\sigma_3 > \sigma_d$ (Excluded)
12	206.81	102.95	186.37	Valid
13	460.99	137.24	92.44	$\sigma_3 > \sigma_d$ (Excluded)
14	315.22	137.73	123.25	$\sigma_3 > \sigma_d$ (Excluded)
15	195.78	137.44	247.09	Valid
16	285.09	137.92	122.65	$\sigma_3 > \sigma_d$ (Excluded)
17	202.15	137.24	245.60	Valid
18	213.99	136.65	368.55	Valid

Table 5.5: M_R Test Results for Vitória Soil CP1 (0% OSR).

Seq.	M_R **(MPa)**	σ_3 **(kPa)**	σ_d **(kPa)**	**Status**
1	314.4	20.5	18.8	$\sigma_3 > \sigma_d$ (Excluded)
2	176.6	20.2	38.2	Valid
3	142.7	20.4	56.3	Valid
4	185.8	34.2	31.1	$\sigma_3 > \sigma_d$ (Excluded)
5	140.0	34.1	61.9	Valid
6	139.5	34.0	92.2	Valid
7	144.8	68.1	61.6	$\sigma_3 > \sigma_d$ (Excluded)
8	130.4	68.5	124.1	Valid
9	146.1	68.7	185.2	Valid
10	117.6	102.9	61.3	$\sigma_3 > \sigma_d$ (Excluded)
11	141.3	102.9	92.4	$\sigma_3 > \sigma_d$ (Excluded)
12	162.9	103.0	185.2	Valid
13	188.6	136.9	93.3	$\sigma_3 > \sigma_d$ (Excluded)
14	180.4	137.7	123.0	$\sigma_3 > \sigma_d$ (Excluded)
15	176.5	137.5	247.4	Valid
16	175.6	137.6	123.0	$\sigma_3 > \sigma_d$ (Excluded)
17	182.5	137.0	247.1	Valid
18	190.4	136.9	369.8	Valid

Table 5.6: M_R Test Results for Vitória Soil CP2 (0% OSR).

Seq.	M_R **(MPa)**	σ_3 **(kPa)**	σ_d **(kPa)**	**Status**
1	131.1	20.5	18.8	$\sigma_3 > \sigma_d$ (Excluded)
2	354.5	20.3	37.7	Valid
3	452.2	20.3	55.0	Valid
4	354.9	34.1	29.9	$\sigma_3 > \sigma_d$ (Excluded)
5	445.9	34.3	60.4	Valid
6	327.1	34.1	92.1	Valid
7	1112.1	68.8	61.9	$\sigma_3 > \sigma_d$ (Excluded - Anomaly)
8	219.6	68.6	123.5	Valid
9	190.6	68.4	184.6	Valid
10	1120.5	103.2	61.9	$\sigma_3 > \sigma_d$ (Excluded - Anomaly)
11	333.1	102.8	92.4	$\sigma_3 > \sigma_d$ (Excluded)
12	206.8	103.0	186.4	Valid
13	461.0	137.2	92.4	$\sigma_3 > \sigma_d$ (Excluded)
14	315.2	137.7	123.2	$\sigma_3 > \sigma_d$ (Excluded)
15	195.8	137.4	247.1	Valid
16	285.1	137.9	122.7	$\sigma_3 > \sigma_d$ (Excluded)
17	202.2	137.2	245.6	Valid
18	214.0	136.7	368.5	Valid

Table 5.7: Resilient Modulus Test Data - Vitória Soil 5% OSR (CP1)

Seq. AASHTO	**Avg.** σ_3 **(kPa)**	**Avg.** σ_d **(kPa)**	**Avg.** M_R **(MPa)**
1	20.22	18.25	146.12
2	20.42	37.08	228.05
3	20.51	55.33	104.92
4	34.19	31.49	165.85
5	34.19	60.93	103.33
6	34.09	92.71	101.90
7	68.08	62.10	107.98
8	68.57	123.62	99.86
9	68.38	184.54	105.81
10	102.86	61.81	115.82
11	102.66	92.12	104.89
12	103.15	185.13	116.52
13	137.44	92.71	116.44
14	137.83	123.62	121.99
15	137.53	246.94	132.99

Table 5.8: Resilient Modulus Test Data - Vitória Soil 5% OSR (CP2)

Seq. AASHTO	**Avg.** σ_3 **(kPa)**	**Avg.** σ_d **(kPa)**	**Avg.** M_R **(MPa)**
1	20.42	18.07	215.85
2	20.51	37.33	142.77
3	20.51	56.59	196.29
4	34.29	30.52	653.02
5	34.09	61.92	224.99
6	34.09	92.44	163.80
7	68.67	62.22	341.00
8	68.47	124.15	152.98
9	68.57	184.89	147.22
10	102.76	61.92	339.26
11	102.95	93.04	226.06
12	102.95	185.18	167.71
13	137.44	92.74	283.76
14	137.53	124.44	252.72
15	137.44	247.40	184.74

Table 5.9: Resilient Modulus Test Data - Vitória Soil 10% OSR (CP1)

Seq. AASHTO	**Avg.** σ_3 **(kPa)**	**Avg.** σ_d **(kPa)**	**Avg.** M_R **(MPa)**
1	20.12	19.24	50.35
2	20.51	37.59	51.72
3	20.51	55.65	62.94
4	34.29	31.08	50.71
5	34.19	60.38	65.39
6	33.80	91.76	81.98
7	68.28	60.98	69.09
8	68.38	123.73	101.22
9	68.38	185.59	120.06
10	103.05	60.98	82.50
11	102.86	92.06	97.82
12	102.56	185.29	123.18
13	137.44	93.24	94.61
14	137.24	123.43	103.40
15	137.24	247.75	138.47

Table 5.10: Resilient Modulus Test Data - Vitória Soil 10% OSR (CP2)

Seq. AASHTO	**Avg.** σ_3 **(kPa)**	**Avg.** σ_d **(kPa)**	**Avg.** M_R **(MPa)**
1	20.42	18.80	349.24
2	20.22	36.72	142.48
3	20.61	54.94	137.38
4	34.09	30.26	95.13
5	34.09	62.29	166.93
6	34.19	92.84	243.12
7	68.77	61.40	288.42
8	68.67	123.98	213.65
9	68.57	185.39	212.29
10	103.05	61.40	1067.85
11	102.86	92.55	356.25
12	102.86	184.80	275.41
13	137.63	91.96	1871.57
14	137.24	123.40	558.40
15	137.53	247.67	242.57

Table 5.11: Resilient Modulus Test Data - Vitória Soil 15% OSR (CP1)

Seq. AASHTO	**Avg.** σ_3 **(kPa)**	**Avg.** σ_d **(kPa)**	**Avg.** M_R **(MPa)**
1	20.51	18.22	200.37
2	20.71	36.73	97.40
3	20.42	54.95	93.67
4	34.09	31.15	80.81
5	34.19	62.00	90.20
6	34.29	92.27	108.36
7	68.67	60.83	90.51
8	68.77	123.71	104.39
9	68.47	185.13	118.78
10	103.25	62.00	126.43
11	102.86	93.15	105.67
12	102.76	185.72	116.94
13	137.44	92.86	93.17
14	137.44	124.01	98.29
15	137.73	248.02	121.98

Table 5.12: Resilient Modulus Test Data - Vitória Soil 15% OSR (CP2)

Seq. AASHTO	**Avg.** σ_3 **(kPa)**	**Avg.** σ_d **(kPa)**	**Avg.** M_R **(MPa)**
1	79.22	16.60	55.01
2	64.08	37.06	138.69
3	20.32	56.03	140.71
4	34.19	30.24	113.73
5	34.09	61.67	134.61
6	34.29	92.20	126.07
7	68.47	62.55	131.45
8	68.57	123.03	123.15
9	68.38	184.70	132.30
10	102.95	61.37	407.76
11	102.95	93.39	205.40
12	103.05	185.29	150.39
13	137.44	92.50	236.43
14	137.44	123.03	205.00
15	137.24	246.96	183.06

Table 5.13: Resilient Modulus Test Data - Vitória Soil 30% OSR (CP2)

Seq. AASHTO	**Avg.** σ_3 **(kPa)**	**Avg.** σ_d **(kPa)**	**Avg.** M_R **(MPa)**
1	0.00	19.06	712.50
2	0.00	37.52	237.39
3	0.00	54.78	153.54
4	0.00	31.26	371.27
5	0.00	62.23	161.15
6	0.00	92.00	121.85
7	0.00	61.63	196.50
8	0.00	124.16	114.86
9	0.00	184.01	107.49
10	0.00	60.14	286.28
11	0.00	92.30	159.59
12	0.00	184.60	126.44
13	0.00	91.41	160.36
14	0.00	122.67	145.92
15	0.00	247.13	143.89

Table 5.14: Resilient Modulus Test Data - Vitória Soil 30% OSR (CP2)

Seq. AASHTO	**Avg.** σ_3 **(kPa)**	**Avg.** σ_d **(kPa)**	**Avg.** M_R **(MPa)**
1	0.00	19.06	712.50
2	0.00	37.52	237.39
3	0.00	54.78	153.54
4	0.00	31.26	371.27
5	0.00	62.23	161.15
6	0.00	92.00	121.85
7	0.00	61.63	196.50
8	0.00	124.16	114.86
9	0.00	184.01	107.49
10	0.00	60.14	286.28
11	0.00	92.30	159.59
12	0.00	184.60	126.44
13	0.00	91.41	160.36
14	0.00	122.67	145.92
15	0.00	247.13	143.89

Table 5.15: Resilient Modulus Test Data - Vitória Soil 30% OSR (CP1 - Retest)

Seq. AASHTO	**Avg.** σ_3 **(kPa)**	**Avg.** σ_d **(kPa)**	**Avg.** M_R **(MPa)**
1	20.51	18.72	47.79
2	20.22	37.14	30.97
3	20.51	55.57	36.82
4	33.99	30.61	32.84
5	34.19	61.81	40.92
6	34.09	92.41	50.28
7	68.38	61.21	38.45
8	68.67	123.32	62.65
9	68.47	186.02	81.50
10	102.66	61.81	52.09
11	103.15	92.71	61.67
12	102.86	184.83	86.16
13	137.24	93.31	65.06
14	137.24	124.21	78.06
15	137.24	246.34	102.52

Table 5.16: Composite Model (DNIT) Parameters for Vitória Soil (VIX) with varying OSR contents

OSR Content (%)	**Specimen**	k_1	k_2	k_3
0%	CP1	157.6	0.050	-0.098
	CP2	361.2	0.391	-0.081
5%	CP1	71.9	-0.052	-0.155
	CP2	170.6	0.510	-0.695
10%	CP1	301.1	0.105	0.395
	CP2	894.4	0.871	-0.483
15%	CP1	84.9	0.029	-0.132
	CP2	533.4	0.452	-0.002
30%	CP1 (Failed)	3134.4	0.173	0.064
	CP2 (Retest)	249.3	0.163	0.423

Table 5.17: Resilient Modulus Test Data - BSB Soil 0% OSR (CP1)

Seq. AASHTO	**Avg.** σ_3 **(kPa)**	**Avg.** σ_d **(kPa)**	**Avg.** M_R **(MPa)**
1	20.51	18.51	134.86
2	20.32	37.03	152.57
3	20.51	55.54	229.01
4	34.29	31.15	205.34
5	34.29	60.83	226.53
6	34.38	92.86	156.28
7	68.57	61.42	251.83
8	68.77	123.71	135.13
9	69.06	186.31	135.59
10	102.76	60.24	344.38
11	103.05	92.56	210.52
12	102.47	184.84	170.33
13	137.05	92.86	395.45
14	137.24	122.83	260.74
15	137.83	246.25	176.29

Table 5.18: Resilient Modulus Test Data - BSB Soil 0% OSR (CP2)

Seq. AASHTO	**Avg.** σ_3 **(kPa)**	**Avg.** σ_d **(kPa)**	**Avg.** M_R **(MPa)**
1	20.32	18.72	225.03
2	20.51	37.44	92.88
3	20.51	56.16	115.17
4	34.19	30.31	92.84
5	33.80	62.70	135.11
6	33.99	92.12	134.32
7	68.77	62.70	169.14
8	68.86	123.32	120.10
9	68.57	184.83	147.66
10	102.47	61.21	297.98
11	103.44	93.01	242.05
12	103.44	185.12	172.84
13	137.63	91.82	308.10
14	137.14	123.02	238.78
15	137.24	246.63	179.97

Table 5.19: Resilient Modulus Test Data - BSB Soil 5% OSR (CP1)

Seq. AASHTO	**Avg.** σ_3 **(kPa)**	**Avg.** σ_d **(kPa)**	**Avg.** M_R **(MPa)**
1	20.32	18.23	431.03
2	20.51	36.75	142.02
3	20.42	55.85	109.49
4	34.09	30.57	194.09
5	34.19	61.44	128.31
6	34.58	92.01	125.83
7	68.77	61.44	177.22
8	68.57	123.76	129.30
9	68.57	185.50	127.67
10	102.08	61.73	155.41
11	103.15	92.31	145.33
12	102.86	185.20	143.26
13	137.63	92.60	152.76
14	136.75	123.17	149.95
15	137.34	247.23	154.96

Table 5.20: Resilient Modulus Test Data - BSB Soil 5% OSR (CP1)

Seq. AASHTO	**Avg.** σ_3 **(kPa)**	**Avg.** σ_d **(kPa)**	**Avg.** M_R **(MPa)**
1*	20.32	18.23	431.03
2	20.51	36.75	142.02
3	20.42	55.85	109.49
4*	34.09	30.57	194.09
5	34.19	61.44	128.31
6	34.58	92.01	125.83
7*	68.77	61.44	177.22
8	68.57	123.76	129.30
9	68.57	185.50	127.67
10*	102.08	61.73	155.41
11*	103.15	92.31	145.33
12	102.86	185.20	143.26
13*	137.63	92.60	152.76
14*	136.75	123.17	149.95
15	137.34	247.23	154.96

Table 5.21: Resilient Modulus Test Data - BSB Soil 5% OSR (CP2)

Seq. AASHTO	**Avg.** σ_3 **(kPa)**	**Avg.** σ_d **(kPa)**	**Avg.** M_R **(MPa)**
1	20.12	18.50	388.16
2	20.42	36.42	271.17
3	20.42	56.39	185.00
4	34.09	30.54	362.99
5	34.38	62.26	256.47
6	34.19	92.51	195.26
7	68.47	60.50	452.15
8	68.28	123.05	191.89
9	68.28	184.43	145.90
10	103.05	62.55	395.72
11	102.86	93.10	231.10
12	103.05	184.73	169.24
13	137.44	92.22	330.59
14	137.53	123.64	249.31
15	137.14	246.99	169.17

Table 5.22: Resilient Modulus Test Data - BSB Soil 5% OSR (CP2)

Seq. AASHTO	**Avg.** σ_3 **(kPa)**	**Avg.** σ_d **(kPa)**	**Avg.** M_R **(MPa)**
1*	20.12	18.50	388.16
2	20.42	36.42	271.17
3	20.42	56.39	185.00
4*	34.09	30.54	362.99
5	34.38	62.26	256.47
6	34.19	92.51	195.26
7*	68.47	60.50	452.15
8	68.28	123.05	191.89
9	68.28	184.43	145.90
10*	103.05	62.55	395.72
11*	102.86	93.10	231.10
12	103.05	184.73	169.24
13*	137.44	92.22	330.59
14*	137.53	123.64	249.31
15	137.14	246.99	169.17

Table 5.23: Integral Resilient Modulus Test Data - BSB Soil 5% OSR (CP3 - Materials Stored for 6 Months)

Sequence	**Avg.** σ_3 **(kPa)**	**Avg.** σ_d **(kPa)**	**Avg.** M_R **(MPa)**
0 (Cond.)	103.05	92.30	140.35
1	20.32	19.35	227.40
2	20.32	36.92	234.66
3	20.42	55.68	147.96
4	33.89	31.56	852.19
5	34.19	61.93	172.15
6	34.19	92.00	130.57
7	68.47	61.63	223.51
8	68.38	125.35	112.94
9	68.18	185.79	116.77
10	102.86	62.23	231.88
11	103.35	93.49	183.28
12	102.95	186.69	140.80
13	137.34	92.60	177.53
14	137.34	122.97	160.50
15	137.53	247.42	136.75
16 (Ext.)	137.34	123.27	147.60
17 (Ext.)	137.44	246.23	139.43
18 (Ext.)	137.34	368.61	153.22

Table 5.24: Resilient Modulus Test Data - BSB Soil 10% OSR (CP1)

Seq. AASHTO	**Avg.** σ_3 **(kPa)**	**Avg.** σ_d **(kPa)**	**Avg.** M_R **(MPa)**
1	20.32	18.51	166.23
2	20.61	36.14	174.00
3	20.12	55.54	148.66
4	34.29	30.27	194.06
5	34.29	62.00	176.71
6	34.09	92.86	128.33
7	68.38	60.53	202.69
8	68.57	124.30	131.11
9	68.38	184.84	109.01
10	102.86	61.42	159.02
11	102.08	92.86	135.80
12	102.86	185.72	117.34
13	137.05	92.27	138.15
14	137.44	123.42	140.20
15	137.44	245.96	122.27

Table 5.25: Resilient Modulus Test Data - BSB Soil 10% OSR (CP2)

Seq. AASHTO	**Avg.** σ_3 **(kPa)**	**Avg.** σ_d **(kPa)**	**Avg.** M_R **(MPa)**
1	20.42	18.98	173.41
2	20.51	37.07	92.70
3	20.42	55.46	74.81
4	33.99	30.85	78.66
5	34.19	61.10	78.33
6	34.29	92.54	86.49
7	68.86	61.69	98.59
8	68.28	123.97	91.45
9	68.47	185.07	96.60
10	102.47	61.10	96.02
11	103.25	91.94	101.30
12	102.76	184.77	107.43
13	137.05	92.24	110.67
14	136.85	123.38	112.31
15	136.95	247.06	120.13

Table 5.26: Integral Resilient Modulus Test Data - BSB Soil 10% OSR (CP3 - Materials Stored for 6 Months)

Sequence	**Avg.** σ_3 **(kPa)**	**Avg.** σ_d **(kPa)**	**Avg.** M_R **(MPa)**
0 (Cond.)*	102.76	91.06	282.87
1*	20.51	18.45	187.96
2*	20.22	35.71	579.41
3	20.22	55.06	178.73
4*	34.19	31.55	1258.14
5	34.29	59.82	440.59
6	34.29	89.87	274.89
7*	68.28	60.41	1699.62
8	68.86	122.61	214.93
9	68.67	183.91	185.80
10*	102.76	61.90	1852.24
11*	102.66	92.25	2110.25
12	102.76	184.51	249.06
13*	137.14	90.77	2287.63
14*	137.34	124.69	676.68
15	137.34	247.90	247.50
16 (Ext.)*	137.14	124.10	1852.93
17 (Ext.)	137.34	245.52	307.46
18 (Ext.)	137.73	369.32	209.02

(*) Points excluded from regression and plots due to Engineering Filter criteria ($\sigma_3 \geq \sigma_d$ or $M_R > 500$ MPa).

Table 5.27: Integral Resilient Modulus Test Data - BSB Soil 15% OSR (Specimen 1)

Sequence	**Avg.** σ_3 **(kPa)**	**Avg.** σ_d **(kPa)**	**Avg.** M_R **(MPa)**
0 (Cond.)	102.08	108.14	108.63
1	20.22	20.28	130.90
2	20.22	40.26	100.08
3	20.12	61.12	94.35
4	33.99	34.68	100.77
5	34.09	69.06	96.37
6	34.09	103.73	98.17
7	68.47	71.99	91.03
8	68.38	140.76	99.86
9	68.57	209.23	117.62
10*	103.15	73.46	93.64
11	102.95	108.73	101.76
12	102.86	211.58	122.18
13*	137.44	111.37	107.42
14	137.34	145.46	114.86
15	137.14	282.69	137.85
16 (Ext.)	137.83	145.46	127.60
17 (Ext.)	137.73	282.10	141.02
18 (Ext.)	137.44	418.75	151.34

(*) Points excluded from plots and regression analysis due to $\sigma_3 \geq \sigma_d$ criterion (transient unloading phase).

Table 5.28: Resilient Modulus Test Data - BSB Soil 15% OSR (CP2)

Seq. AASHTO	**Avg.** σ_3 **(kPa)**	**Avg.** σ_d **(kPa)**	**Avg.** M_R **(MPa)**
1	19.93	17.79	302.47
2	20.32	37.36	420.43
3	20.51	56.33	223.15
4	34.19	31.43	251.23
5	34.19	61.67	185.37
6	34.38	93.09	151.23
7	68.67	61.67	242.78
8	68.57	124.52	136.92
9	68.47	185.29	136.35
10	102.56	61.96	436.76
11	102.17	92.79	214.97
12	102.47	185.29	160.39
13	137.24	92.50	279.66
14	137.34	124.22	232.66
15	137.53	247.26	171.29

Table 5.29: Integral Resilient Modulus Test Data - BSB Soil 15% OSR (Specimen 2)

Sequence	**Avg.** σ_3 **(kPa)**	**Avg.** σ_d **(kPa)**	**Avg.** M_R **(MPa)**
0 (Cond.)	102.76	108.80	149.02
1*	19.93	19.57	302.47
2	20.32	40.91	420.43
3	20.51	61.96	223.15
4	34.19	35.28	251.23
5	34.19	69.37	185.37
6	34.38	103.76	151.23
7	68.67	71.75	242.78
8	68.57	141.12	136.92
9	68.47	209.31	136.35
10*	102.56	74.12	436.76
11	102.17	108.51	214.97
12	102.47	211.98	160.39
13*	137.24	111.47	279.66
14	137.34	145.86	232.66
15	137.53	282.83	171.29
16 (Ext.)	136.75	145.57	272.52
17 (Ext.)	137.73	282.53	178.93
18 (Ext.)	137.34	417.72	175.12

(*) Points excluded from plots and regression analysis due to $\sigma_3 \geq \sigma_d$ criterion (transient unloading phase).

Table 5.30: Integral Resilient Modulus Test Data - BSB Soil 30% OSR (Specimen 1)

Sequence	**Avg.** σ_3 **(kPa)**	**Avg.** σ_d **(kPa)**	**Avg.** M_R **(MPa)**
0 (Cond.)*	103.05	92.55	57.89
1*	20.51	18.15	30.02
2	20.42	37.50	26.21
3	20.22	55.95	35.82
4*	33.99	30.35	31.49
5	34.19	61.01	39.45
6	34.09	93.74	46.37
7*	68.47	61.90	42.28
8	68.47	124.10	54.57
9	68.38	184.81	74.50
10*	102.95	61.30	62.58
11*	102.86	92.55	63.47
12	102.76	185.70	80.96
13*	137.34	93.44	72.19
14*	137.34	123.80	75.08
15	137.44	246.71	94.78
16 (Ext.)*	137.14	122.91	73.21
17 (Ext.)	137.44	246.71	94.86

(*) Points excluded from plots and regression analysis due to $\sigma_3 \geq \sigma_d$ criterion (transient unloading phase).

ANNEX 2
Photographic Report
Selected Research Records

Note: All photographs presented in this report were taken by the author (2018 to 2026).



Figure 5.1: External view of the Infrastructure Laboratory (Infralab) at the University of Brasília (UnB).



Figure 5.2: Espírito Santo (ES) soil specimens wrapped in plastic film for moisture content preservation during the curing period.



Figure 5.3: Detail of soil samples prepared in metallic rings for physical characterization and moisture control tests.



Figure 5.4: Unconfined Compressive Strength (UCS) test setup for a natural Brasília soil specimen (SG-12, 0% OSR).



Figure 5.5: General view of failed specimens after testing, showcasing the contrast between Brasília (SG-12) and Vitória soil matrices with varying OSR dosages.

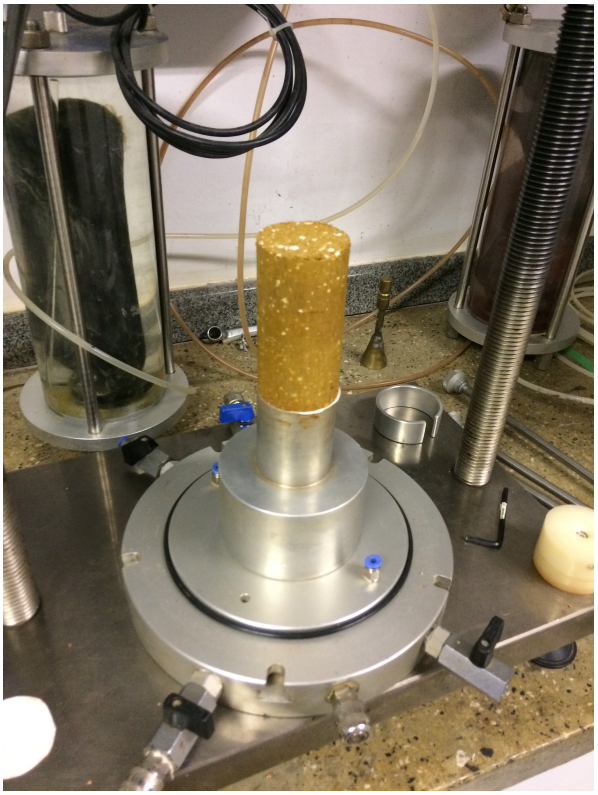


Figure 5.6: Specimen preparation for advanced geotechnical testing (Resilient Modulus) involving 30% OSR content.



Figure 5.7: Identification and storage of stabilized specimens for the study of 5% and 10% OSR mixture maturation.

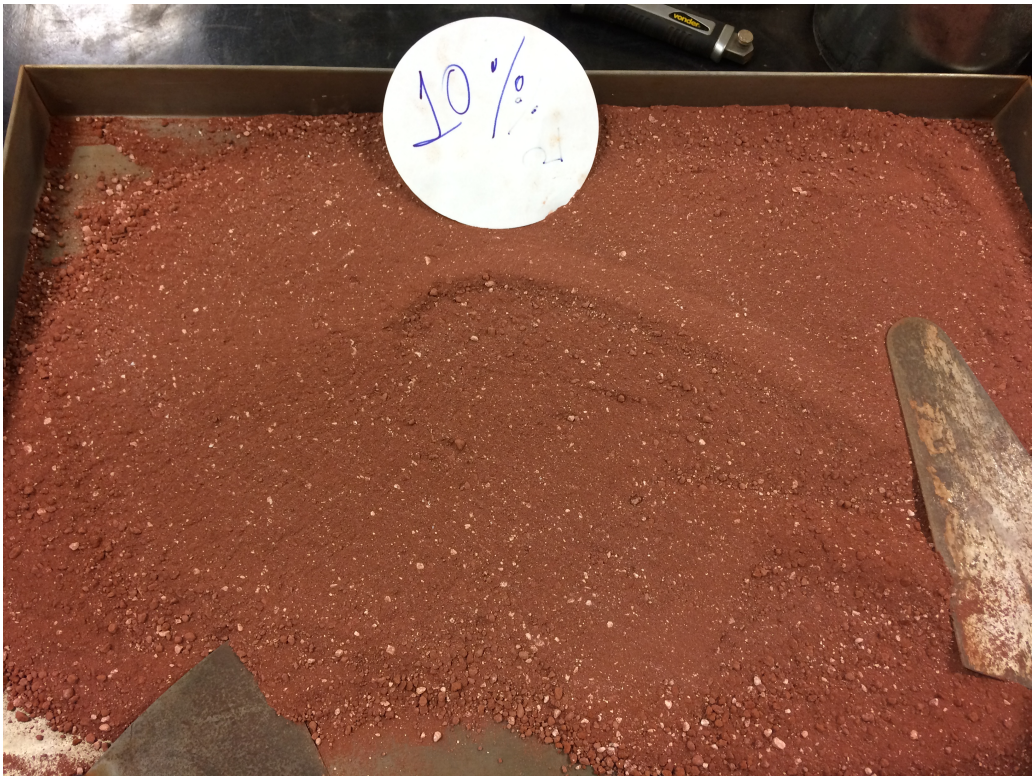


Figure 5.8: Initial stage of manual mixing: Ornamental Stone Residue (white powder) being integrated into the Brasília (SG-12) red soil matrix.



Figure 5.9: Homogenization and moisture adjustment for the 10% OSR-soil mixture in the preparation tray.



Figure 5.10: Specimen molding phase using a Proctor mold for the 30% OSR-SG12 soil mixture.

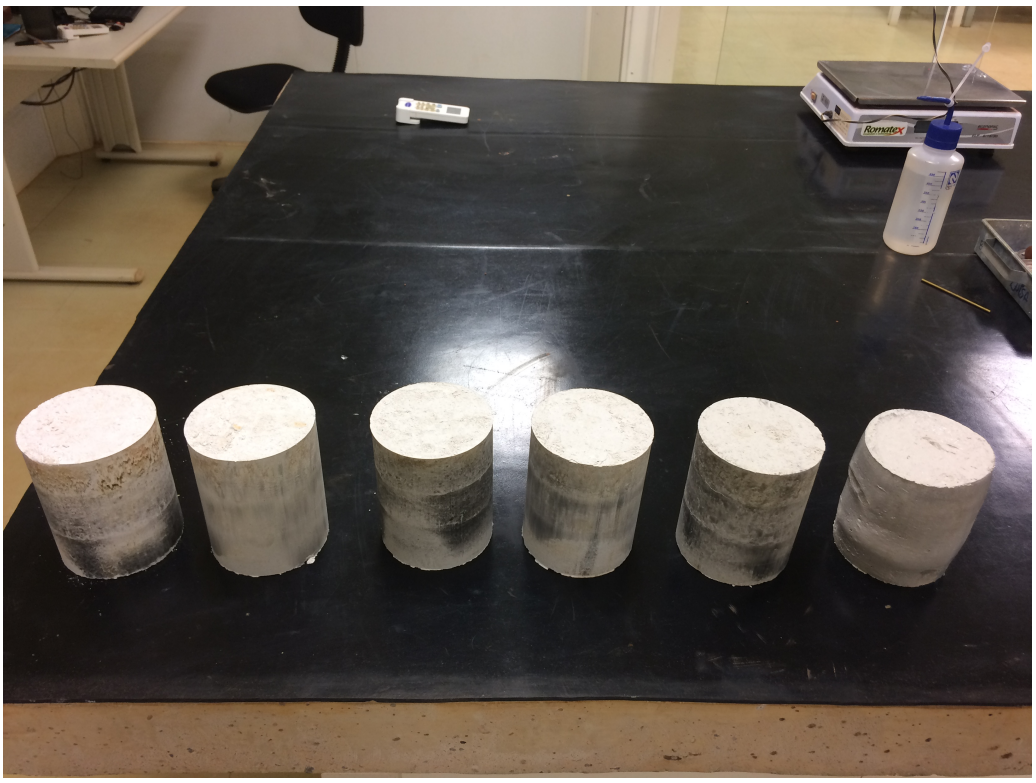


Figure 5.11: Set of cylindrical specimens molded in 2019, ready for basic geotechnical characterization tests.

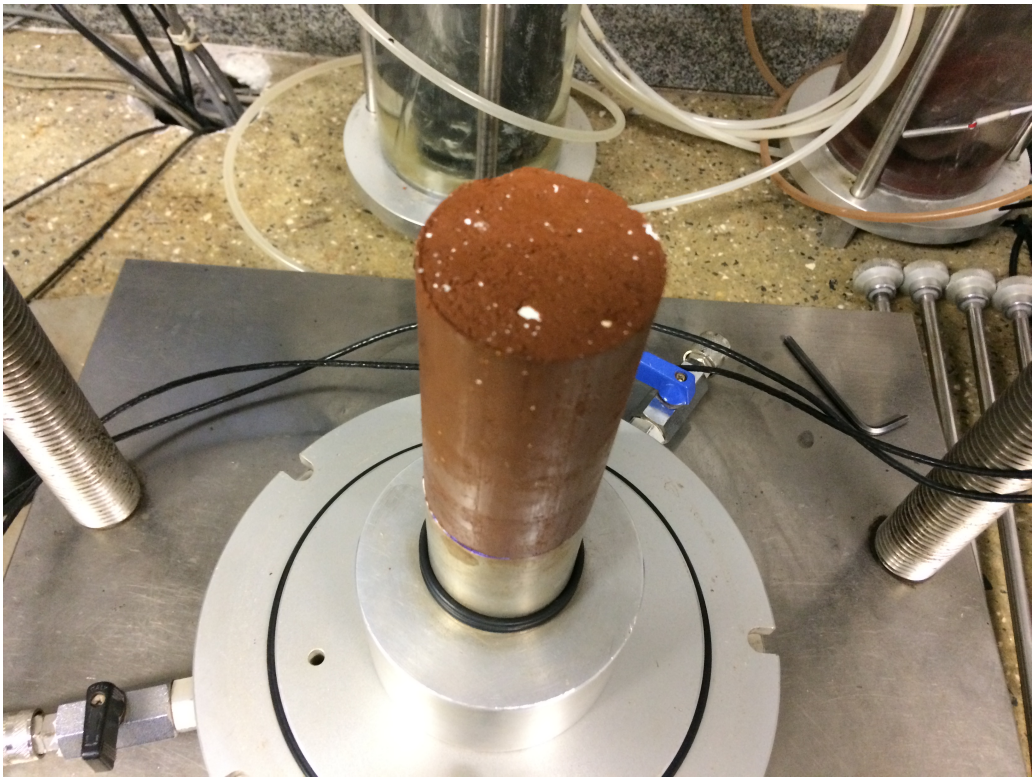


Figure 5.12: Molded specimen (5% OSR-SG12) positioned on the triaxial base for Resilient Modulus (MR) testing.

Table 5.31: Summary of Non-Linear Parameters - Composite Model (MeDiNa/DNIT)

Soil	**% OSR**	**Specimen**	k_1	k_2	k_3	R^2	M_R **(MPa)***
BSB	0%	CP1	128.7	-0.021	-0.100	0.1496	185.1
BSB	0%	CP2	273.8	0.080	0.205	0.7963	112.5
BSB	**0%**	**Average**	**182.2**	**0.049**	**0.006**	**0.0660**	**147.9**
BSB	5%	CP1	197.3	0.342	-0.278	0.6737	113.2
BSB	5%	CP2	151.5	0.480	-0.746	0.9184	189.0
BSB	5%	CP3 (6 mo.)	106.1	0.533	-0.846	0.7966	142.5
BSB	**5%**	**Average**	**144.9**	**0.469**	**-0.661**	**0.8710**	**148.6**
BSB	10%	CP1	98.8	0.276	-0.508	0.8958	140.1
BSB	10%	CP2	162.7	0.342	-0.217	0.4975	78.6
BSB	10%	CP3	108.6	0.142	-0.239	0.6858	122.1
BSB	**10%**	**Average**	**115.7**	**0.267**	**-0.364**	**0.8231**	**113.4**
BSB	15%	CP1	134.4	0.064	0.013	0.1442	100.8
BSB	15%	CP2	85.4	0.049	-0.442	0.5139	239.3
BSB	**15%**	**Average**	**108.9**	**0.454**	**-0.718**	**0.4943**	**141.3**
BSB	**30%**	**Single**	**256.1**	**0.102**	**0.567**	**0.9889**	**34.9**
VIX	0%	CP1	208.8	0.102	-0.006	0.2812	142.5
VIX	0%	CP2	87.1	0.345	-0.075	0.7700	27.9
VIX	**0%**	**Average**	**114.7**	**0.168**	**-0.078**	**0.7008**	**74.0**
VIX	5%	CP1	71.9	-0.052	-0.155	0.2599	136.3
VIX	5%	CP2	170.6	0.510	-0.695	0.4063	163.9
VIX	**5%**	**Average**	**121.3**	**0.229**	**-0.425**	**0.3331**	**163.6**
VIX	10%	CP1	301.1	0.105	0.395	0.9795	65.7
VIX	10%	CP2	894.4	0.871	0.483	0.5491	7.6
VIX	**10%**	**Average**	**577.6**	**0.653**	**0.255**	**0.6120**	**21.9**
VIX	15%	CP1	84.9	0.029	-0.132	0.0768	109.9
VIX	15%	CP2	533.4	0.452	-0.002	0.2293	91.5
VIX	**15%**	**Average**	**288.6**	**0.412**	**-0.144**	**0.4057**	**86.4**
VIX	**30%**	**Single**	**242.4**	**0.135**	**0.469**	**0.9368**	**38.2**

* Reference M_R calculated for typical sub-base stress states: $\sigma_3 = 0.02$ MPa and $\sigma_d = 0.06$ MPa.


UnB